Sterile neutrinos and effective field theory

Zhou, G.

Publication date
2022
Document Version
Final published version

寄蜉蝣于天地，渺沧海之一粟。　　—— 苏轼

We are mayflies enjoying a flicker of life in the world, and as infinitesimal as a grain in the sea.

"I think I can safely say that
nobody understands quantum mechanics"

—— Richard P. Feynman

Sterile Neutrinos and Effective Field Theory

Guanghui Zhou

Sterile Neutrinos and Effective Field Theory

Guanghui Zhou

周光辉

Sterile neutrinos and effective field theory

ACADEMISCH PROEFSCHRIFT

ter verkrijging van de graad van doctor
aan de Universiteit van Amsterdam
op gezag van de Rector Magnificus
prof. dr. ir. P.P.C.C. Verbeek
ten overstaan van een door het College voor Promoties ingestelde commissie,
in het openbaar te verdedigen in de Agnietenkapel
op dinsdag 25 oktober 2022, te 15.00 uur

door Guanghui Zhou
geboren te Henan

Promotiecommissie

Promotor:	prof. dr. E.L.M.P. Laenen	Universiteit van Amsterdam
Copromotor:	dr. J. de Vries	Universiteit van Amsterdam
Overige leden:	prof. dr. R.G.E. Timmermans	Rijksuniversiteit Groningen
	prof. dr. H.K. Dreiner	Rheinische Friedrich-Wilhelms-Universität Bonn
	prof. dr. M.P. Decowski	Universiteit van Amsterdam
	prof. dr. ir. P.J. de Jong	Universiteit van Amsterdam
	dr. W.J. Waalewijn	Universiteit van Amsterdam
	dr. F. de Almeida Dias	Universiteit van Amsterdam

Faculteit der Natuurwetenschappen, Wiskunde en Informatica

This thesis is based on the following publications:

1. W. Dekens, J. de Vries, K. Fuyuto, E. Mereghetti, and G. Zhou
Sterile neutrinos and neutrinoless double beta decay in effective field theory
JHEP 06 (2020) 097.

2. J. de Vries, H. K. Dreiner, J. Y. Günther, Z. S. Wang and G. Zhou
Long-lived sterile neutrinos at the LHC in effective field theory
JHEP 03 (2021) 148.

3. G. Zhou, J. Y. Günther, Z. S. Wang, J. de Vries, and H. K. Dreiner
Long-lived sterile neutrinos at Belle II in effective field theory
JHEP 04 (2022) 057 .

4. G. Zhou
Light sterile neutrinos and lepton-number-violating kaon decays in effective field theory
JHEP 06 (2022) 127.

Author contributions

- In Ref. [1] I was involved in all steps of the development of the effective field theory framework. I sorted out the relevant higher-dimensional operators and matched them to chiral perturbation theory and the resulting $0\nu\beta\beta$ phenomenology. I implemented the various sterile neutrino models to compute the actual rates. I was closely involved with the writing of the paper. The development of hard-neutrino-exchange contributions was mainly done by my co-authors.

- For Refs. [2] and [3], I developed the machinery to systematically compute the production and decay of sterile neutrinos within the νSM-EFT framework. The main simulation code was adapted from an existing code made by my co-author. I rewrote it for the detectors we studied and to implement the phenomenology of sterile neutrinos. I wrote the main part of the papers.

- Ref. [4] is a single-author paper and I thus did all computations and writing.

Contents

Chapter 1

Introduction

1.1 The Standard Model

The Standard Model (SM) of particle physics is described in the framework of quantum field theory and explains nearly all phenomena in particle physics. The SM Lagrangian is symmetric under $SU(3)_c \times SU(2)_L \times U(1)_Y$ gauge symmetries and Lorentz symmetry, which strongly restricts how SM fields can interact. The $SU(2)_L \times U(1)_Y$ group describes the electroweak interaction for three generations of quarks and leptons. The left-handed up-type quarks and left-handed down-type quarks form three $SU(2)_L$ doublets, and the left-handed charged leptons and (left-handed) neutrinos also form three $SU(2)_L$ doublets. We write the doublets as

$$L = \left\{ \begin{pmatrix} \nu_{eL} \\ e_L \end{pmatrix}, \begin{pmatrix} \nu_{\mu L} \\ \mu_L \end{pmatrix}, \begin{pmatrix} \nu_{\tau L} \\ \tau_L \end{pmatrix} \right\}, Q = \left\{ \begin{pmatrix} u_L \\ d_L \end{pmatrix}, \begin{pmatrix} c_L \\ s_L \end{pmatrix}, \begin{pmatrix} t_L \\ b_L \end{pmatrix} \right\}. \tag{1.1}$$

The remaining right-handed quarks and leptons, which are singlets under $SU(2)_L$ group, are given by

$$E_R = \{e_R, \mu_R, \tau_R\}, U_R = \{u_R, c_R, t_R\}, D_R = \{d_R, s_R, b_R\}. \tag{1.2}$$

In the original form of the SM no right-handed neutrino fields were necessary. The strong force is described by the $SU(3)_c$ group, under which quarks transform as triplets and cary a color charge. Apart from these fermions, there are also force carriers, the photon mediating the electromagnetic force, W and Z bosons mediating the weak interaction, and the gluons mediating the strong force. Finally, the Higgs boson is the excitation of the Higgs field that plays a crucial role in giving masses to W and Z bosons and fermions.

The SM has passed a large amount of experimental tests from high-energy collider physics to low-energy precision physics. It has been really successful in explaining the electroweak interactions, the QCD asymptotic freedom, the weak CP violation, etc. Moreover, a new era of particle physics has started since the discovery of a Higgs-like particle at the LHC [1], which verifies the existence of the last particle predicted in the SM. Currently the measurements of the Higgs-like scalar show that it behaves like the SM Higgs boson and no significant deviation from the SM has been found. The SM seems to be the ultimate theory in particle physics. However, there are still some observations the SM can not explain and therefore one can doubt if the SM is valid at all energy scales.

The SM fermions become massive via the Higgs mechanism, where the left-handed particles couple to their corresponding right-handed partner via the Yukawa interactions. After electroweak symmetry breaking (EWSB), the Higgs field gets a vacuum expectation value (VEV) leading to massive fermions. Without right-handed neutrino fields, neutrinos are predicted to

be massless. However, the neutrino oscillation experiments have definitely shown that neutrinos do have masses and this observation requires an extension of the original SM. A second problem of the SM is the nature of dark matter. Evidence from astrophysical and cosmological measurements (galaxy rotation curves, cosmic microwave background, velocity dispersions, etc.) suggest that about 23% of the energy content of the universe is dark matter [2] but no SM particle has the right properties to actually be dark matter. A third problem of the SM is the baryon asymmetry of the universe. There is much more matter than antimatter in the universe. For instance, from Big-Bang Nucleosynthesis (BBN) it is possible to extract the baryon asymmetry of the universe [3]

$$Y_B = \frac{n_B}{s} = (8.59 \pm 0.11) \times 10^{-11}\,, \tag{1.3}$$

where s and n_B are the entropy and baryon density, respectively. This number is defined in such a way that it is invariant during the evolution of the universe. This small Y_B can be roughly understood in a way that, in the early universe, for every 10^{10} antiparticles, there are $(10^{10}+1)$ particles. Sakharov suggested that this asymmetry was dynamically generated through particle physics in the early universe and he listed three necessary conditions for baryogenesis [4]. They are baryon number violation, C and CP violation, and a departure from thermal equilibrium. The SM does not satisfy two of these criteria. Baryon number violation can be induced via sphaleron process [5, 6]. While a strong first-order electroweak phase transition would lead to out-of-equilibrium conditions, it seems that the SM electroweak phase transition is not first order. While the SM contains CP violation, it is not enough to explain the baryon asymmetry [7, 8]. The above problems together imply that there should be physics beyond-the-SM (BSM). Some hints for such BSM physics have actually been accumulating in various precision experiments. Examples are anomalies in the W-boson mass [9], the magnetic dipole moment of the muon [10], and universality of lepton flavor [11–13]. While exciting, these anomalies have not reached the threshold of a discovery and might go away with more data or might be caused by underestimated theoretical or experimental uncertainties.

1.2 Beyond the Standard Model and effective field theories

Motivated by the problems mentioned above, physicists have proposed various BSM models, which usually contain new particles or new interactions. Since no obvious deviations from the SM have been found, the effects of new physics on experiments should be small to avoid being detected. Hence in general the BSM models contain heavy BSM particles, which can not be produced in current experiments, and/or the coupling of the interactions with the SM particles is small.

In the case of heavy BSM particles, it is possible to 'integrate them out' to obtain an effective field theory (EFT). Let us consider the famous Fermi theory as an example. The weak interaction is mediated by the W boson or Z boson and its predictions have been well tested. However it is possible and much easier to describe the weak interaction at low energies in a new theory without the heavy bosons. In many experiments, the typical energy scale lies far below the masses of the heavy electroweak gauge bosons. We can use a simpler theory, called Fermi theory, to describe the weak process by an effective interaction containing four fermions. The effect of heavy bosons is hidden in the coefficient of the four-fermion operator, typically called the Wilson coefficient (in this case, the Fermi constant G_F). There are two different methods to figure out the value of the Wilson coefficient. The first method is to compute the coefficient from a more fundamental theory: we match the SM weak interaction to the Fermi theory and read off the value of G_F in terms of the fundamental SM parameters. In the second method, we do not need to know

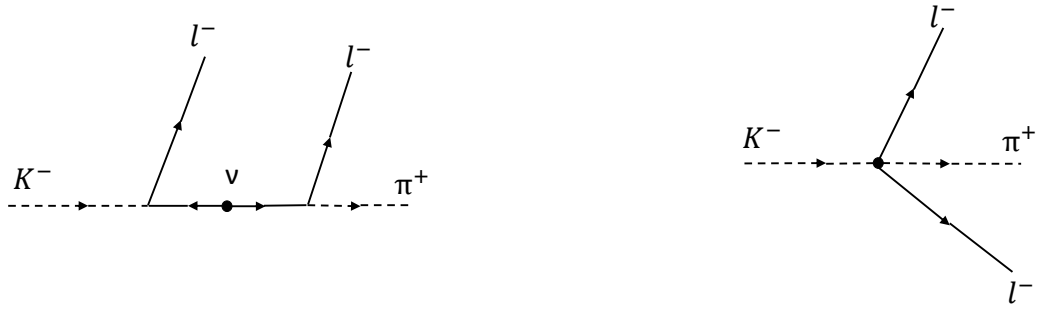

Figure 1.1: Two possible diagrams for the LNV kaon decays. Left panel: the mechanism via the exchange of a light Majorana sterile neutrino; right panel: similar to the left but with a heavy Majorana sterile neutrino.

the SM weak interaction at all, instead we fit the Wilson coefficient to data (this was of course historically how G_F was obtained).

Another example is the lepton-number-violating (LNV) kaon decays, which we will discuss further in this thesis. In this process the kaon K^- decays into two electrons and one pion π^+ through the exchange of a Majorana sterile neutrino (see the first diagram of Fig. 1.1). We can divide this LNV process into two parts. The kaon K^- decays into an electron and a Majorana sterile neutrino, and then the sterile neutrino decays into another electron and a pion π^+. The amplitude is proportional to $\frac{m_\nu}{q^2-m_\nu^2}$, which is induced from the propagator of the mediated neutrino. Here, q is the momentum of the mediated neutrino and m_ν is its mass. Part of the momentum of the kaon transfers to the sterile neutrino and it is of order of hundreds of MeV in the rest-frame of the kaon. If the mass of the sterile neutrino is much larger than the kaon mass, which means $m_\nu \gg q$, the amplitude becomes proportional to $-1/m_\nu$, which does not rely on the momentum q. Then we can describe this LNV decay by a new theory, which is represented in the second diagram of Fig. 1.1. In the new theory, this LNV process is induced by an effective contact interaction without the sterile neutrino and the calculation is much easier than that in the old theory. The effect of the sterile neutrino is hidden in the coefficient of this effective operator, which is proportional to $1/m_\nu$.

The effective theories are based on the idea that physics at different scales can be described separately and independently without having to describe all of them at the same time. At the largest scale, cosmology and astrophysics are described by general relativity. At the scale of a country on the earth, we describe the behavior of human beings by culture, civilization and so on. At the scale of individual person, we describe people by character, habits, morality, etc. The phenomena at the scale of atoms are described by atomic physics and condensed matter physics. Finally at the scale of quarks, we use the SM to describe particle physics. On the one hand, the way to understand the nature by using effective theories has the great advantage that we can describe physics at a particular scale without considering all other scales at the same time: greatly simplifying our computations. On the other hand, it means effective theories are valid only in a limited range. For instance, once the momentum passing through the sterile neutrino is comparable with its mass in LNV kaon decays, we need to include the sterile neutrino to describe this process.

In some BSM models, all the predicted new particles are much heavier than the EW scale, but

the energy of many experiments lies well below the EW scale. Therefore we can use the idea of effective theories to describe the relevant phenomena and the effective theories contain only the SM particles as degree of freedom. The SM is written in the language of quantum field theory, where we use operators to describe the interactions among the SM particles. We do not know which BSM model is the correct one, or what operators we get after integrating out the unknown heavy BSM particles. However, we can write the effective operators based on some principles. First of all, the operators should obey Lorentz invariance to be consistent with special relativity. In addition, the the operators must satisfy some gauge symmetries. In the case for an effective theory above the EW scale, these new operators should satisfy the $SU(3)_c \times SU(2)_L \times U(1)_Y$ gauge group . By using these two principles one can write the effective operators with unknown coefficients. This EFT is called the SM effective field theory (SMEFT). We also can write an effective field theory below the EW scale, which would only satisfy the $SU(3)_c \times U(1)_{em}$ gauge group and contains only light SM fields. This EFT is often called the low-energy effective field theory (LEFT).

An EFT contains all possible interactions to the SM and the effects of different BSM models with heavy particles can be described by the same EFT but with different operators or different strength of the same interactions. An apparent disadvantage of the EFT is that the number of new interactions is infinite. But EFT interactions are suppressed by powers of masses of the integrated heavy particles, and they are thus ordered by their dimension. Interactions with higher dimension are more suppressed compared with those with lower dimension. Thus we only need the first few EFT operators with lowest dimension to actually perform calculations. The operators in EFT start from dimension five, and the first operator one can come up with is the famous Weinberg operator

$$\epsilon_{kl}\epsilon_{mn}(L_k^T\, C L_m)H_l H_n\,, \tag{1.4}$$

which after EWSB contributes to the Majorana mass terms for neutrinos.

Some BSM models might contain a very heavy new particle and a light new particle at the same time. For example, in leptoquark models there can be a heavy leptoquark and a light sterile neutrino simultanously. We can only integrate out the heavy particle and have to keep the light particle as an explicit degree of freedom. We can still can get an EFT above the EW scale by modifying the SMEFT to contain interactions involving the new light particle. In this thesis we focus on the effective theory extended by sterile neutrinos, which is called the neutrino-extended Standard Model effective field theory (νSMEFT).

Even without BSM physics, it can be very advantageous to use EFTs in certain situations. For instance, we can not use a description in terms of quarks and gluons as degrees of freedom below the GeV scale as QCD becomes non-perturbative. Pions and nucleons are degrees of freedom below the GeV scale and we therefore should match QCD to an effective description in terms of these fields. This effective description is called chiral perturbation theory. It is the low-energy EFT of QCD. It contains all interactions that satisfy the chiral and space-time symmetry properties of the underlying theory of QCD and consist of the effective low-energy degrees of freedom.

1.3 Sterile neutrinos

Sterile neutrinos are right-handed neutrinos that are gauge singlets under the SM gauge group. Sterile neutrinos are interesting BSM particles as they provide an excellent candidate to solve several SM problems. Sterile neutrinos can couple to the left-handed neutrino (active neutrino) field and the Higgs field through Yukawa interactions, generating a neutrino Dirac mass term in

m_ν [eV]	Y^ν	M_R [GeV]
$\mathcal{O}(0.1)$	1	$\mathcal{O}(10^{14})$
$\mathcal{O}(0.1)$	10^{-4}	$\mathcal{O}(10^{6})$
$\mathcal{O}(0.1)$	10^{-6}	$\mathcal{O}(10^{2})$
$\mathcal{O}(0.1)$	10^{-7}	$\mathcal{O}(1)$

Table 1.1: The values of M_R needed through the type-I seesaw relation for several choices of Y^ν.

exact analogue to other SM fermions. Furthermore, it is possible to add a Majorana mass term for the sterile neutrino as neither Lorentz invariance nor gauge symmetry forbids this. The most general renormalizable (with dimension four and lower) mass terms for neutrinos are

$$L_{neutrino-mass} = -\bar{L}Y^\nu \tilde{H}\nu_R - \frac{1}{2}\bar{\nu}_R^c M_R \nu_R + \text{h.c.}\,, \tag{1.5}$$

where the first term denotes the Yukawa mass term and the second term is the Majorana mass term.

In the case $M_R \gg vY^\nu$, there exist three light neutrinos with masses $m_\nu \sim \frac{v^2 Y^{\nu 2}}{M_R}$, which is the type-I seesaw mechanism [14–16]. This mechanism can be used to explain the origin of neutrino masses. Assuming the Yukawa coupling Y^ν is of order 1, one can find M_R is of order 10^{15} GeV to explain the small masses of light neutrinos. It is of course not necessary to make Y^ν of order one. In the SM, the electron Yukawa is also much smaller than unity. In Table 1.1 we choose several different values for Y^ν and list their corresponding M_R in the type-I seesaw mechanism. With the Majorana mass term, all neutrino mass eigenstates are Majorana states and if the number of sterile neutrinos we add to the SM is three, we would obtain six neutrino mass eigenstates. Were we to omit the M_R term in Eq. (1.5) and still introduced three right-handed neutrino fields, then neutrinos would have the exact same mass mechanism as the charged leptons and quarks, leading to three neutrino mass eigenstates (all Dirac). However, forbidding the M_R term would require to put in by hand the global symmetry of lepton number, a price we are not willing to pay in this thesis. We thus keep both mass terms. In the mass eigenstates, sterile neutrinos and active neutrinos are mixed together and sterile neutrinos can interact, despite their name, with the SM particles through this mixing. In general the mixing is very small due to the small masses of active neutrinos, and therefore the name sterile is still appropriate.

In addition to explaining the mass origin of neutrinos, light sterile neutrinos could also account for dark matter [17–20], as they are neutral and interact with SM particles weakly. This does require a rather specific mass range for sterile neutrinos at the keV scale. Finally, sterile neutrinos with a broad range of masses can account for the baryon asymmetry of the Universe through leptogenesis [21]. Sterile neutrinos are thus a well-motivated solution to a number of major outstanding issues in particle physics and cosmology. These motivations provide a hint for the existence of sterile neutrinos, but their mass scale and interactions with the SM fields are not clear. A large number of experimental and theoretical works have gone into the search for sterile neutrinos in so-called minimal scenarios, where sterile neutrinos only interact with SM fields through the renormalizable Yukawa interactions in Eq. (1.5).

In this thesis we take a more general approach to study sterile neutrinos and their interactions. In broad classes of BSM models, sterile neutrinos appear sterile at lower energies, but interact at higher energies through the exchange of heavy BSM fields. Examples are left-right symmetric models [16, 22, 23], grand unified theories [24], Z' models [25], or leptoquark models [26]. These models contain new fields that are heavy compared to the electroweak scale. Independent of the details of these models, at low energies the sterile neutrinos can be described in terms of local

effective operators in the framework of νSMEFT [27, 28]. In this thesis we will study the effects of νSMEFT interactions on a wide range of experiments.

1.4 Relevant phenomena

The Majorana mass terms of sterile neutrinos and some higher-dimensional operators in νSMEFT violate the lepton number (L), an accidental symmetry of the SM, by two units. We can verify whether neutrinos are Dirac or Majorana fermions by probing LNV physics such as neutrinoless double-beta decay ($0\nu\beta\beta$) and rare meson decays such as $K^- \to \pi^+ e^- e^-$. If measured, these processes would unambiguously signal LNV but their interpretation in terms of particle physics is not easy. The translation to the fundamental source of LNV involves atomic, nuclear, hadronic, and particle physics taking place at a broad range of energy scales. In this thesis I will systematically describe how to bridge these scales by using a cascade of EFTs.

Experiments looking for $0\nu\beta\beta$ are the most sensitive probes of LNV at present because there are tons of atoms that can decay in these experiments. Current experimental limits on $0\nu\beta\beta$ half lives are at the level of 10^{26} years [29–55] and next-generation ton-scale experiments aim for one or two order-of-magnitude improvements [56–65]. Double-beta decay ($2\nu\beta\beta$) is a nuclear decay, where two neutrons in a nucleus decay into two protons, two electrons and two electron antineutrinos. $0\nu\beta\beta$ is similar to $2\nu\beta\beta$ but without the emission of antineutrinos and we can express it as

$$(A, Z) \to (A, Z + 2) + 2e^- \,, \tag{1.6}$$

where A and Z denote the number of nucleons and the number of protons in the nucleus, respectively. To observe $0\nu\beta\beta$ we should choose those isotopes for which the beta decay is energetically forbidden and double-beta decay is allowed. There are 35 such isotopes in nature and we can use them to probe $0\nu\beta\beta$. The key question once a detection is made, is whether the signal is from $0\nu\beta\beta$ or $2\nu\beta\beta$. In $2\nu\beta\beta$, due to the emitted antineutrinos, the summed energy of the two emitted electrons continually varies from zero to $Q_{\beta\beta}$, which is the energy difference between the intial- and final-state nucleus. While for $0\nu\beta\beta$ all energy is carried away by the electrons and a peak appears at $Q_{\beta\beta}$. We show the spectra for the summed energy of the emitted electrons in Fig. 1.2. The half-life values for $2\nu\beta\beta$ processes have been measured and for ^{136}Xe it is 2.27×10^{21} years [66] much smaller than its half-life value of $0\nu\beta\beta$, which is larger than 2.3×10^{26} [67] years.

$0\nu\beta\beta$ only involves interactions with quarks of the first generation and to study interactions related with quarks of other flavors, we will probe the LNV kaon decays $K^- \to \pi^+ l^- l^-$. In this process the kaon K^- decays into two charged light leptons and one pion π^+ via the exchange of a Majorana neutrino or higher-dimensional LNV operators containing strange and down quarks. Two possible diagrams for final states with two electrons are shown in Fig. 1.1. Now the upper bounds from measurements on the branching ratios of LNV kaon decays are very stringent, 5.3×10^{-11} for $K^- \to \pi^+ e^- e^-$ [68], 4.2×10^{-11} for $K^- \to \pi^+ \mu^- \mu^-$ [69] and 5×10^{-10} for $K^- \to \pi^+ e^- \mu^-$ [70].

In the two LNV processes mentioned above, sterile neutrinos appear in the intermediate state and are virtual particles. In principle light sterile neutrinos might be produced and detected in experiments. If a sterile neutrino is generated at the interaction point of the collider and is long-lived, its decay leads to displaced vertices after propagating for a long distance. We can get a very clean background by putting a detector far from the place where sterile neutrinos are produced. In Fig. 1.3 we present the idea of the displaced-vertex search experiment. There are many existing and proposed experiments (`ALICE`, `ATLAS`,`AL3X`, `SHiP`, `Belle II` and so on) which

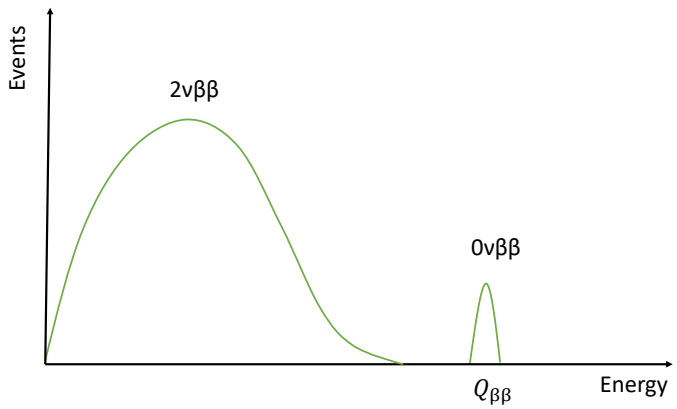

Figure 1.2: Spectra of $0\nu\beta\beta$ and $2\nu\beta\beta$ for illustrative purpose only.

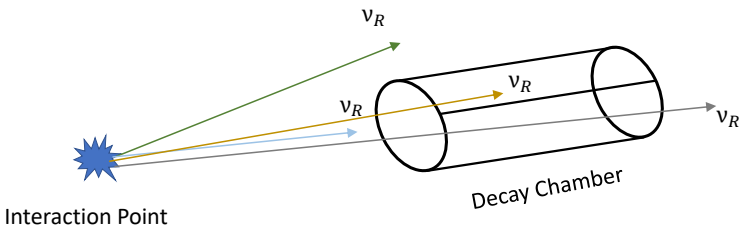

Figure 1.3: Experimental setup in a displaced-vertex search experiment.

can be used to probe long-lived sterile neutrinos. The production and decay of sterile neutrinos can be realized in the minimal model via the mixing between active- and sterile- neutrinos as well as through non-renormalizable interactions in νSMEFT. To study the displaced decays of sterile neutrinos, we will focus on sterile neutrinos of GeV level and work in the framework of νSMEFT. In this case the production of sterile neutrinos via the direct collision at the collider or target is subdominant, instead they are mainly produced via the decay of heavy mesons or τ leptons produced at the interaction points. The produced neutrinos might miss the decay chamber, or decay before reaching it, or just pass through it. These events thus can not be detected and only those, where sterile neutrinos decay into visible particles inside the chamber, are detectable.

1.5 Outline of this thesis

In Chapter 2, we instruct the framework of νSMEFT. We evolve these operators from a BSM energy scale Λ to the electroweak scale and integrate out heavy SM particles. The resulting operators satisfy $SU(3)_c \times U(1)_{em}$ gauge symmetry and consist of only light SM particles and light sterile neutrinos. Then we probe these interactions in a wide range of experiments.

If neutrinos are Majorana particles, they can induce LNV processes. In Chapter 3 and 4 we discuss the LNV process $0\nu\beta\beta$ and LNV kaon decays in the presence of Majorana mass terms and LNV higher-dimensional operators. For $0\nu\beta\beta$ we use the chiral effective field theory to calculate the transition operator by matching the operators containing quarks to those containing nucleons and mesons. We insert the obtained transition operators into many-body nuclear wave functions to get the $0\nu\beta\beta$ rate. In the case of LNV kaon decays, life is easier and we only need the mesonic Lagrangian to calculate the kaon decay rate. By comparing the decay rates with the experimental results, we get limits on the Wilson coefficients of various higher-dimensional operators.

Sterile neutrinos can be produced in experiments if they are light. In Chapter 5 and 6 we discuss long-lived sterile neutrinos at the Large Hadron Collider (LHC) and `Belle II` via displaced vertex search. Sterile neutrinos can be produced at the LHC through the decay of B- and D-type mesons. If they are long-lived, we can detect their decay at a displaced vertex. We mainly consider the case where the sterile neutrino mixes only with the electron neutrino. By calculating the branching ratios of heavy mesons to the sterile neutrino and the branching ratios of the sterile neutrino to visible particles, we develop Monte-Carlo simulations to obtain the sensitivity for various (proposed) experiments at the LHC. We do similar things for the `Belle II` experiment, but in this case, we consider the mixing of sterile neutrinos with tau neutrinos that are produced in the decay of tau leptons, copiously produced at `Belle II`. We summarize and give an outlook in Chapter 7.

Chapter 2

The Lagrangian in νSMEFT up to dimension seven

In this chapter we will present and discuss higher-dimensional operators related with active or sterile neutrinos. We focus on a Lagrangian at the scale of BSM physics $\Lambda \gg v$ that consists of the SM Lagrangian supplemented by a sterile neutrino and higher-dimensional operators up to dimension seven. For convenience, when discussing operators in the νSMEFT, we follow Ref. [71] and denote their dimensions by $\overline{\text{dim-n}}$ with $n = 5, 6, 7$. After EWSB, the resulting operators are only $SU(3)_c \times U(1)_{em}$ invariant and we refer to them, without the overline, as dim-n operators where $n = 3, 6, 7, 9$. The SM Lagrangian satisfies Lorentz and gauge symmetries. The lepton number L and the baryon number B are accidental symmetries of the classical Lagrangian, but only $B - L$ is conserved at the quantum level. The $SU(2)_L$ gauge transformation leaves the SM Lagrangian unchanged but it changes the $B + L$ number by [72]

$$\Delta(B + L) = 2N_f N_{CS}\,, \tag{2.1}$$

where N_f denotes the number of families and N_{CS} indicates the Chern-Simons number. At low temperatures $B+L$ violation is extremely suppressed [73, 74] and has never been observed. Here we focus on baryon-number-conserving operators, which could contribute to $0\nu\beta\beta$ and LNV kaon decays at tree level. The relevant Lagrangian can be written as

$$\begin{aligned}\mathcal{L} \;&=\; \mathcal{L}_{SM} - \left[\frac{1}{2}\bar{\nu}_R^c \bar{M}_R \nu_R + \bar{L}\tilde{H} Y_\nu \nu_R + \text{h.c.}\right] \\ &\quad + \mathcal{L}_{\nu_L}^{(\bar{5})} + \mathcal{L}_{\nu_R}^{(\bar{5})} + \mathcal{L}_{\nu_L}^{(\bar{6})} + \mathcal{L}_{\nu_R}^{(\bar{6})} + \mathcal{L}_{\nu_L}^{(\bar{7})} + \mathcal{L}_{\nu_R}^{(\bar{7})}\,,\end{aligned} \tag{2.2}$$

in terms of the lepton doublet $L = (\nu_L,\, e_L)^T$, while $\tilde{H} = i\tau_2 H^*$ with H the Higgs doublet

$$H = \frac{v}{\sqrt{2}} U(x) \begin{pmatrix} 0 \\ 1 + \frac{h(x)}{v} \end{pmatrix}\,, \tag{2.3}$$

where $v = 246$ GeV is the Higgs vacuum expectation value (vev), $h(x)$ is the Higgs field, and $U(x)$ is a $SU(2)$ matrix encoding the Goldstone modes. ν_R is a column vector of n sterile neutrinos. Y_ν is a $3 \times n$ matrix of Yukawa couplings and $\bar{M}_R$ a general symmetric complex $n \times n$ mass matrix. Without loss of generality we will work in the basis where the charged leptons $e^i_{L,R}$ and quarks $u^i_{L,R}$ and d^i_R are mass eigenstates ($i = 1, 2, 3$). This implies $d^i_L = V^{ij} d^{j,\,\text{mass}}_L$, where V is the CKM matrix. The relation between the mass and weak eigenstates for the neutrinos will be discussed below. We define $\Psi^c = C\bar{\Psi}^T$ for a field Ψ in terms of the charge conjugation matrix

Class 1	$\psi^2 HX$	Class 2	$\psi^2 H^2 D$	Class 3	ψ^4
$\mathcal{O}_{eW}^{(6)}$	$(\bar{L}\sigma^{\mu\nu}e)\tau^I H W^I_{\mu\nu}$	$\mathcal{O}_{HL\,3}^{(6)}$	$(H^\dagger i\overleftrightarrow{D}^I_\mu H)(\bar{L}\tau^I\gamma^\mu L)$	$\mathcal{O}_{LeQu\,1}^{(6)}$	$(\bar{L}^j e)\epsilon_{jk}(\bar{Q}^k u)$
$\mathcal{O}_{uW}^{(6)}$	$(\bar{Q}\sigma^{\mu\nu}u)\tau^I \widetilde{H}\, W^I_{\mu\nu}$	$\mathcal{O}_{HQ\,3}^{(6)}$	$(H^\dagger i\overleftrightarrow{D}^I_\mu H)(\bar{Q}\tau^I\gamma^\mu Q)$	$\mathcal{O}_{Lequ\,3}^{(6)}$	$(\bar{L}^j\sigma_{\mu\nu}e)\epsilon_{jk}(\bar{Q}^k\sigma^{\mu\nu}u)$
$\mathcal{O}_{dW}^{(6)}$	$(\bar{Q}\sigma^{\mu\nu}d)\tau^I H\, W^I_{\mu\nu}$	$\mathcal{O}_{Hud}^{(6)}$	$i(\widetilde{H}^\dagger D_\mu H)(\bar{u}\gamma^\mu d)$	$\mathcal{O}_{LQ\,3}^{(6)}$	$(\bar{L}\gamma^\mu\tau^I L)(\bar{Q}\gamma_\mu\tau^I Q)$
				$\mathcal{O}_{LedQ}^{(6)}$	$(\bar{L}^j e)(\bar{d}Q^j)$

Table 2.1: LNC $\overline{\text{dim-6}}$ operators [75] involving active neutrinos that affect $0\nu\beta\beta$ and LNV kaon decays at tree level.

Class 1	$\psi^2 H^4$	Class 5	$\psi^4 D$
$\mathcal{O}_{LH}^{(7)}$	$\epsilon_{ij}\epsilon_{mn}(L_i^T C L_m)H_j H_n (H^\dagger H)$	$\mathcal{O}_{LL\bar{d}uD\,1}^{(7)}$	$\epsilon_{ij}(\bar{d}\gamma_\mu u)(L_i^T C(D^\mu L)_j)$
Class 2	$\psi^2 H^2 D^2$	Class 6	$\psi^4 H$
$\mathcal{O}_{LHD\,1}^{(7)}$	$\epsilon_{ij}\epsilon_{mn}(L_i^T C(D_\mu L)_j)H_m(D^\mu H)_n$	$\mathcal{O}_{Leu\bar{d}H}^{(7)}$	$\epsilon_{ij}(L_i^T C\gamma_\mu e)(\bar{d}\gamma^\mu u)H_j$
$\mathcal{O}_{LHD\,2}^{(7)}$	$\epsilon_{im}\epsilon_{jn}(L_i^T C(D_\mu L)_j)H_m(D^\mu H)_n$	$\mathcal{O}_{LLQ\bar{d}H\,1}^{(7)}$	$\epsilon_{ij}\epsilon_{mn}(\bar{d}L_i)(Q_j^T C L_m)H_n$
Class 3	$\psi^2 H^3 D$	$\mathcal{O}_{LLQ\bar{d}H\,2}^{(7)}$	$\epsilon_{im}\epsilon_{jn}(\bar{d}L_i)(Q_j^T C L_m)H_n$
$\mathcal{O}_{LHDe}^{(7)}$	$\epsilon_{ij}\epsilon_{mn}(L_i^T C\gamma_\mu e)H_j H_m(D^\mu H)_n$	$\mathcal{O}_{LL\bar{Q}uH}^{(7)}$	$\epsilon_{ij}(\bar{Q}_m u)(L_m^T C L_i)H_j$
Class 4	$\psi^2 H^2 X$		
$\mathcal{O}_{LHW}^{(7)}$	$\epsilon_{ij}(\epsilon\tau^I)_{mn} g(L_i^T C\sigma^{\mu\nu}L_m)H_j H_n W^I_{\mu\nu}$		

Table 2.2: LNV $\overline{\text{dim-7}}$ operators [76] involving active neutrinos that affect $0\nu\beta\beta$ and LNV kaon decays at tree level.

$C = -C^{-1} = -C^T = -C^\dagger$. We use the definition for chiral fields $\Psi^c_{L,R} = (\Psi_{L,R})^c = C\overline{\Psi_{L,R}}^T = P_{R,L}\Psi^c$, with $P_{R,L} = (1 \pm \gamma_5)/2$.

We now consider the higher-dimensional operators and make one truncation of the set of effective operators by focusing on interactions containing just one neutrino field. The only exception are operators that contribute to neutrino masses after EWSB and thus contain two neutrino fields. The $\overline{\text{dim-5}}$ operators satisfying the above criteria are

$$\mathcal{L}^{(\bar{5})}_{\nu_L} = \epsilon_{kl}\epsilon_{mn}(L_k^T\, C^{(5)}\, C L_m)H_l H_n\,, \qquad \mathcal{L}^{(\bar{5})}_{\nu_R} = -\bar{\nu}^c_R\, \bar{M}^{(5)}_R \nu_R H^\dagger H\,, \tag{2.4}$$

which after EWSB contribute to Majorana mass terms for active and sterile neutrinos. For $n \geq 2$ there appears a $\overline{\text{dim-5}}$ transition dipole operator but it does not play an important role in this thesis. The number of operators grows when going to higher dimensions, but the number of operators that match at tree level to $0\nu\beta\beta$ and LNV kaon decays is not that large. In Tables 2.1 and 2.2 we list the operators in $\mathcal{L}^{(\bar{6})}_{\nu_L}$ and $\mathcal{L}^{(\bar{7})}_{\nu_L}$, which involve active left-handed neutrinos and were constructed in Ref. [75] and [76, 77], respectively. The operators appearing in $\mathcal{L}^{(\bar{6})}_{\nu_R}$ and $\mathcal{L}^{(\bar{7})}_{\nu_R}$ involve sterile neutrinos and were first constructed in Ref. [28], they are given in Tables 2.3 and 2.4.

Class 1	$\psi^2 H^3$	Class 4	ψ^4
$\mathcal{O}^{(6)}_{L\nu H}$	$(\bar{L}\nu_R)\tilde{H}(H^\dagger H)$	$\mathcal{O}^{(6)}_{du\nu e}$	$(\bar{d}\gamma^\mu u)(\bar{\nu_R}\gamma_\mu e)$
Class 2	$\psi^2 H^2 D$	$\mathcal{O}^{(6)}_{Qu\nu L}$	$(\bar{Q}u)(\bar{\nu}_R L)$
$\mathcal{O}^{(6)}_{H\nu e}$	$(\bar{\nu}_R\gamma^\mu e)(\tilde{H}^\dagger i D_\mu H)$	$\mathcal{O}^{(6)}_{L\nu Qd}$	$(\bar{L}\nu_R)\epsilon(\bar{Q}d))$
Class 3	$\psi^2 H^3 D$	$\mathcal{O}^{(6)}_{LdQ\nu}$	$(\bar{L}d)\epsilon(\bar{Q}\nu_R)$
$\mathcal{O}^{(6)}_{\nu W}$	$(\bar{L}\sigma_{\mu\nu}\nu_R)\tau^I\tilde{H}W^{I\mu\nu}$		

Table 2.3: LNC $\overline{\text{dim-6}}$ operators [28] involving a sterile neutrino that affect $0\nu\beta\beta$ and LNV kaon decays at tree level.

Class 1	$\psi^2 H^4$	Class 5	$\psi^4 D$
$\mathcal{O}^{(7)}_{\nu H}$	$(\nu_R^T C\nu_R)(H^\dagger H)^2$	$\mathcal{O}^{(7)}_{du\nu eD}$	$(\bar{d}\gamma_\mu u)(\nu_R^T C i D_\mu e)$
Class 2	$\psi^2 H^2 D^2$	$\mathcal{O}^{(7)}_{QL\nu uD}$	$(\bar{Q}\gamma_\mu L)(\nu_R^T C i D_\mu u)$
$\mathcal{O}^{(7)}_{\nu eD}$	$\epsilon_{ij}(\nu_R^T C D_\mu e)(H^i D^\mu H^j)$	$\mathcal{O}^{(7)}_{d\nu QLD}$	$\epsilon_{ij}(\bar{d}\gamma_\mu\nu_R)(Q^i C i D_\mu L^j)$
Class 3	$\psi^2 H^3 D$	Class 6	$\psi^4 H$
$\mathcal{O}^{(7)}_{\nu L1}$	$\epsilon_{ij}(\nu_R^T C\gamma_\mu L^i)(iD^\mu H^j)(H^\dagger H)$	$\mathcal{O}^{(7)}_{Q\nu QLH2}$	$\epsilon_{ij}(\bar{Q}\nu_R)(Q^i C L^j)H$
Class 4	$\psi^2 H^2 X$	$\mathcal{O}^{(7)}_{dL\nu uH}$	$\epsilon_{ij}(\bar{d}L^i)(\nu_R^T C u)\tilde{H}^j$
$\mathcal{O}^{(7)}_{\nu eW}$	$(\epsilon\tau^I)_{ij}(\nu_R^T C\sigma^{\mu\nu}e)(H^i H^j)W^I_{\mu\nu}$	$\mathcal{O}^{(7)}_{dQ\nu eH}$	$\epsilon_{ij}(\bar{d}Q^i)(\nu_R^T C e)H^j$
		$\mathcal{O}^{(7)}_{Qu\nu eH}$	$(\bar{Q}u)(\nu_R^T C e)H$
		$\mathcal{O}^{(7)}_{Qe\nu uH}$	$(\bar{Q}e)(\nu_R^T C u)H$

Table 2.4: LNV $\overline{\text{dim-7}}$ operators [28] involving a sterile neutrino that affect $0\nu\beta\beta$ and LNV kaon decays at tree level.

2.1 Evolution to the electroweak scale

The Wilson coefficients of these higher-dimensional operators might change as the energy scale μ changes. To evolve the higher-dimensional operators from $\mu = \Lambda$ to the electroweak scale, $\mu \simeq m_W$, we need the renormalization group equations (RGEs). We only consider the RGEs due to one-loop QCD effects. Most of the operators in Tables 2.1-2.4 do not undergo QCD renormalization or consist of a quark bilinear and evolve either like a scalar or tensor operator. For these operators the RGEs are rather simple

$$\begin{aligned} \frac{dC_{S,T}}{d\ln\mu} &= \frac{\alpha_s}{4\pi}\gamma_{S,T}C_{S,T}\,, \qquad \gamma_S = -6C_F\,, \qquad \gamma_T = 2C_F\,, \\ C_S &\in \{C^{(6)}_{LeQu1}\,, C^{(6)}_{LedQ}, C^{(7)}_{LLQuH}\}\,, \qquad C_T \in \{C^{(6)}_{uW}\,, C^{(6)}_{dW}, C^{(6)}_{LeQu3}\}\,, \end{aligned} \tag{2.5}$$

where $C_F = (N_c^2-1)/(2N_c)$ for $N_c = 3$, the number of colors, and C_X is the Wilson coefficient of the higher-dimensional operator O_X. In addition, there are several cases for which only combinations of couplings follow a simple RGE

$$\begin{aligned} C^{(1)}_{S,T} &= \mp\frac{1}{2}\left[C^{(7)}_{LLQdH1} \pm \left(C^{(7)}_{LLQdH1}\right)^T\right]\,, \\ C^{(2)}_{S,T} &= \mp\frac{1}{4}\left[C^{(7)}_{LLQdH1} \mp \left(C^{(7)}_{LLQdH1}\right)^T\right] \mp \frac{1}{2}\left[C^{(7)}_{LLQdH2} \mp \left(C^{(7)}_{LLQdH2}\right)^T\right]\,, \\ C^{(3)}_{S} &= -\frac{1}{2}C^{(6)}_{LdQ\nu} + C^{(6)}_{L\nu Qd}\,, \qquad C^{(3)}_{T} = -\frac{1}{8}C^{(6)}_{LdQ\nu}\,, \end{aligned} \tag{2.6}$$

where $C^{(i)}_{S,T}$ follow the same RGEs as $C_{S,T}$ in Eq. (2.5). For some of the operators involving ν_R the linear combinations that run like a scalar or a tensor current are more involved and lead to the following RGEs

$$\begin{aligned}
\frac{d\mathbf{C}_1}{d\ln\mu} &= \frac{\alpha_s}{4\pi}\begin{pmatrix}\gamma_T & 0\\ \frac{\gamma_S-\gamma_T}{2} & \gamma_S\end{pmatrix}\cdot\mathbf{C}_1\,, \qquad \mathbf{C}_1^T = \left(C^{(7)}_{d\nu QLD}\,, C^{(7)}_{dQ\nu eH}/y_e\right)\,,\\
\frac{d\mathbf{C}_2}{d\ln\mu} &= \frac{\alpha_s}{4\pi}\begin{pmatrix}\gamma_T & 0 & 0 & 0 & 0\\ \frac{\gamma_T-\gamma_S}{2} & \gamma_S & 0 & 0 & 0\\ \gamma_S+\gamma_T & 0 & -\gamma_S & 0 & 0\\ 0 & 0 & 0 & \gamma_T & 0\\ \frac{\gamma_S-\gamma_T}{2} & 0 & 0 & \frac{\gamma_T-\gamma_S}{2} & \gamma_S\end{pmatrix}\cdot\mathbf{C}_2\,,\\
\mathbf{C}_2^T &= \left(C^{(7)}_{QL\nu uD}\,, \left(\bar{M}_R^*\right)^{-1} C^{(6)}_{Qu\nu L}\,, C^{(7)}_{dL\nu uH}/y_d\,, C^{(7)}_{Qe\nu uH}/y_e\,, C^{(7)}_{Qu\nu eH}/y_e\right)\,,
\end{aligned} \tag{2.7}$$

where $y_f = \sqrt{2}m_f/v$. The $C^{(7)}_{QL\nu uD}$ and $C^{(7)}_{d\nu QLD}$ couplings induce additional operators that only contribute to neutral currents and are therefore not shown.

2.2 The Lagrangian after EWSB

After EWSB the Higgs field takes its vacuum expectation value and after integrating out heavy SM particles, the νSMEFT operators can be matched to a new EFT. Operators in this EFT are only invariant under $SU(3)_c \times U(1)_{em}$ gauge symmetries and only involve light quarks, charged leptons, neutrinos, photons, and gluons. For purposes of this thesis, operators containing an up-type quark, a down-type quark, and no photons or gluons are the most interesting and we focus on this subset of operators. Below the electroweak scale, the Lagrangian in Eq. (2.2) can be matched to the following effective Lagrangian

$$\begin{aligned}
\mathcal{L} &= L_{SM} - \left[\frac{1}{2}\bar{\nu}_L^c\, M_L \nu_L + \frac{1}{2}\bar{\nu}_R^c\, M_R \nu_R + \bar{\nu}_L M_D \nu_R + \text{h.c.}\right]\\
&\quad + \mathcal{L}^{(6)}_{\Delta L=2} + \mathcal{L}^{(6)}_{\Delta L=0} + \mathcal{L}^{(7)}_{\Delta L=2} + \mathcal{L}^{(7)}_{\Delta L=0} + \mathcal{L}^{(9)}_{\Delta L=2}\,,
\end{aligned} \tag{2.8}$$

where L_{SM} now refers to interactions of dim-4 and lower of light SM fields and Ref. [78] listed the matching conditions. For convenience here we will not give the matching conditions and we refer Ref. [78, 79] for the details. The relevant higher-dimensional operators are written as

$$\begin{aligned}
\mathcal{L}^{(6)}_{\Delta L=2} &= \frac{2G_F}{\sqrt{2}}\Big\{\bar{u}_L\gamma^\mu d_L\left[\bar{e}_R\gamma_\mu C^{(6)}_{\text{VL}}\,\nu_L^c + \bar{e}_L\gamma_\mu \bar{C}^{(6)}_{\text{VL}}\,\nu_R^c\right] + \bar{u}_R\gamma^\mu d_R\left[\bar{e}_R\,\gamma_\mu C^{(6)}_{\text{VR}}\,\nu_L^c + \bar{e}_L\,\gamma_\mu \bar{C}^{(6)}_{\text{VR}}\,\nu_R^c\right]\\
&\quad + \bar{u}_L d_R\left[\bar{e}_L\, C^{(6)}_{\text{SR}}\nu_L^c + \bar{e}_R\,\bar{C}^{(6)}_{\text{SR}}\nu_R^c\right] + \bar{u}_R d_L\left[\bar{e}_L\, C^{(6)}_{\text{SL}}\nu_L^c + \bar{e}_R\,\bar{C}^{(6)}_{\text{SL}}\nu_R^c\right]\\
&\quad + \bar{u}_L\sigma^{\mu\nu} d_R\,\bar{e}_L\sigma_{\mu\nu} C^{(6)}_{\text{T}}\,\nu_L^c + \bar{u}_R\sigma^{\mu\nu} d_L\,\bar{e}_R\sigma_{\mu\nu}\bar{C}^{(6)}_{\text{T}}\,\nu_R^c\Big\} + \text{h.c.}
\end{aligned} \tag{2.9}$$

$$\begin{aligned}
\mathcal{L}^{(6)}_{\Delta L=0} &= \frac{2G_F}{\sqrt{2}}\Big\{\bar{u}_L\gamma^\mu d_L\left[\bar{e}_L\gamma_\mu c^{(6)}_{\text{VL}}\,\nu_L + \bar{e}_R\gamma_\mu \bar{c}^{(6)}_{\text{VL}}\,\nu_R\right] + \bar{u}_R\gamma^\mu d_R\left[\bar{e}_L\,\gamma_\mu c^{(6)}_{\text{VR}}\,\nu_L + \bar{e}_R\,\gamma_\mu \bar{c}^{(6)}_{\text{VR}}\,\nu_R\right]\\
&\quad + \bar{u}_L d_R\left[\bar{e}_R\, c^{(6)}_{\text{SR}}\nu_L + \bar{e}_L\,\bar{c}^{(6)}_{\text{SR}}\nu_R\right] + \bar{u}_R d_L\left[\bar{e}_R\, c^{(6)}_{\text{SL}}\nu_L + \bar{e}_L\,\bar{c}^{(6)}_{\text{SL}}\nu_R\right]\\
&\quad + \bar{u}_R\sigma^{\mu\nu} d_L\,\bar{e}_R\sigma_{\mu\nu} c^{(6)}_{\text{T}}\,\nu_L + \bar{u}_L\sigma^{\mu\nu} d_R\,\bar{e}_L\sigma_{\mu\nu}\bar{c}^{(6)}_{\text{T}}\,\nu_R\Big\} + \text{h.c.}
\end{aligned} \tag{2.10}$$

$$\begin{aligned}\mathcal{L}^{(7)}_{\Delta L=2} &= \frac{2G_F}{\sqrt{2}v}\Big\{\bar{u}_L\gamma^\mu d_L\left[\bar{e}_L\, C^{(7)}_{\rm VL}\, i\overleftrightarrow{D}_\mu\nu^c_L + \bar{e}_R\,\bar{C}^{(7)}_{\rm VL}\, i\overleftrightarrow{D}_\mu\nu^c_R\right]\\ &\quad+\bar{u}_R\gamma^\mu d_R\left[\bar{e}_L\, C^{(7)}_{\rm VR}\, i\overleftrightarrow{D}_\mu\nu^c_L + \bar{e}_R\,\bar{C}^{(7)}_{\rm VR}\, i\overleftrightarrow{D}_\mu\nu^c_R\right]\\ &\quad+\bar{u}_L\sigma^{\mu\nu} d_R\,\bar{e}_L\bar{C}^{(7)}_{\rm TR}\overleftarrow{\partial}_\mu\gamma_\nu\nu^c_R + \bar{u}_R\sigma^{\mu\nu} d_L\,\bar{e}_L\bar{C}^{(7)}_{\rm TL}\gamma_\nu\partial_\mu\nu^c_R\Big\} + \text{h.c.} \qquad (2.11)\end{aligned}$$

$$\begin{aligned}\mathcal{L}^{(7)}_{\Delta L=0} &= \frac{2G_F}{\sqrt{2}v}\Big\{\bar{u}_L\gamma^\mu d_L\left[\bar{e}_R\, c^{(7)}_{\rm VL}\, i\overleftrightarrow{D}_\mu\nu_L + \bar{e}_L\,\bar{c}^{(7)}_{\rm VL}\, i\overleftrightarrow{D}_\mu\nu_R\right]\\ &\quad+\bar{u}_R\gamma^\mu d_R\left[\bar{e}_R\, c^{(7)}_{\rm VR}\, i\overleftrightarrow{D}_\mu\nu_L + \bar{e}_L\,\bar{c}^{(7)}_{\rm VR}\, i\overleftrightarrow{D}_\mu\nu_R\right]\\ &\quad+\bar{u}_L\sigma^{\mu\nu} d_R\,\partial_\mu\left(\bar{e}_L c^{(7)}_{\rm TR}\gamma_\nu\nu_L\right) + \bar{u}_R\sigma^{\mu\nu} d_L\,\partial_\mu\left(\bar{e}_L c^{(7)}_{\rm TL}\gamma_\nu\nu_L\right)\Big\} + \text{h.c.} \qquad (2.12)\end{aligned}$$

where $\overleftrightarrow{D}_\mu = D_\mu - \overleftarrow{D}_\mu$ and each Wilson coefficient carries indices $ijkl$ with $i = u,\, c$ denoting the up-type quarks, $j = d,\, s,\, b$ for the down-type quarks, $k = \{e, \mu\}$ for electron and muon, $l = \{1, 2, 3\}$ for active neutrinos and $l = \{1, \ldots, n\}$ for sterile neutrinos.

Several dim-9 operators are induced as well and we will discuss them in detail later as the dim-9 operators induced in the cases of $0\nu\beta\beta$ and LNV kaon decays are different. To derive the matching contributions, we use the equations of motion of the various fields

$$\begin{aligned} i\not{\partial}\nu_L &= M_D\nu_R + M_L^\dagger\nu_L^c\,, \qquad i\not{\partial}\nu_R = M_D^\dagger\nu_L + M_R^\dagger\nu_R^c\,,\\ i\not{\partial}e_L &= M_e e_R\,, \qquad i\not{\partial}u_L = M_u u_R\,, \qquad i\not{\partial}d_L = M_d d_R\,,\\ W^+_\mu &\simeq -\frac{g}{\sqrt{2}}\frac{1}{m_W^2}\left(\bar{e}_L\gamma_\mu\nu_L + \bar{d}_L\gamma_\mu u_L\right)\,. \end{aligned} \qquad (2.13)$$

Here $M_e = \text{diag}(m_e,\, m_\mu,\, m_\tau)$ which appears in the Lagrangian as $\mathcal{L}_{M_e} = -\bar{e}_L M_e e_R + \text{h.c.}$, while $M_{u,d}$ are the masses of the up-type and down-type quarks.

Besides the charged currents listed above, we also list the SM weak neutral currents that contribute to decay processes of sterile neutrinos

$$\begin{aligned}\mathcal{L}^{(6)}_{\rm neutral} = \frac{-4G_F}{\sqrt{2}}\bar{\nu}^i_L\gamma^\mu\nu^i_L\Big\{&\bar{e}_L\gamma_\mu(-\frac{1}{2}+\sin^2\theta_w)e_L + \bar{e}_R\gamma_\mu(\sin^2\theta_w)e_R\\ &+\bar{u}_L\gamma^\mu(\frac{1}{2}-\frac{2}{3}\sin^2\theta_w)u_L + \bar{u}_R\,\gamma_\mu(-\frac{2}{3}\sin^2\theta_w)u_R\\ &+\bar{d}_L\gamma^\mu(-\frac{1}{2}+\frac{1}{3}\sin^2\theta_w)d_L + \bar{d}_R\,\gamma_\mu(\frac{1}{3}\sin^2\theta_w)d_R\\ &+\frac{1}{4}(2-\delta_{ij})\bar{\nu}^j_L\gamma^\mu\nu^j_L\Big\}\,,\end{aligned} \qquad (2.14)$$

where i, j are the flavor indices of active neutrinos and θ_w is the Weinberg angle. Then we rotate them to the mass basis of the neutrino fields.

2.3 Rotation to the neutrino mass basis

After EWSB the mass terms can be written as

$$\mathcal{L}_m = -\frac{1}{2}\bar{N}^c M_\nu N + \text{h.c.}\,, \qquad M_\nu = \begin{pmatrix} M_L & M_D^* \\ M_D^\dagger & M_R^\dagger \end{pmatrix}\,, \qquad (2.15)$$

where $N = (\nu_L,\, \nu_R^c)^T$ and M_ν is a $\bar{n} \times \bar{n}$ symmetric matrix (since M_L and M_R are symmetric matrices), with $\bar{n} = 3+n$. The mass matrix can be diagonalized by a single $\bar{n}\times\bar{n}$ unitary matrix, U,

$$U^T M_\nu U = m_\nu = \text{diag}(m_1, \ldots, m_{\bar{n}})\,, \qquad N = U N_m\,, \tag{2.16}$$

where U is a unitary mixing matrix. In the general case U contains $\bar{n}(\bar{n}+1)/2$ phases and $\bar{n}(\bar{n}-1)/2$ rotation angles and the $m_1, \ldots, m_{\bar{n}}$ are real and positive. The kinetic and mass terms of the neutrinos can be written as

$$\mathcal{L}_\nu = \frac{1}{2}\bar{\nu} i \not{\partial} \nu - \frac{1}{2}\bar{\nu} m_\nu \nu\,, \tag{2.17}$$

in terms of the Majorana mass eigenstates $\nu = N_m + N_m^c = \nu^c$. The rotation to the mass basis is given by

$$\begin{aligned} \nu_L &= P_L(PU)\nu\,, \qquad & \nu_L^c &= P_R(PU^*)\nu\,, \\ \nu_R &= P_R(P_s U^*)\nu\,, \qquad & \nu_R^c &= P_L(P_s U)\nu\,, \end{aligned} \tag{2.18}$$

where P and P_s are $3\times\bar{n}$ and $n\times\bar{n}$ projector matrices

$$P = \begin{pmatrix} \mathcal{I}_{3\times 3} & 0_{3\times n} \end{pmatrix}\,, \qquad P_s = \begin{pmatrix} 0_{n\times 3} & \mathcal{I}_{n\times n} \end{pmatrix}\,. \tag{2.19}$$

The above rotations lead to the following form for the SM charged and neutral currents,

$$\mathcal{L} = \frac{g}{\sqrt{2}} \bar{e}_L \gamma^\mu PU \nu\, W_\mu^- + \frac{g}{2c_w} \bar{\nu}\gamma^\mu P_L \left(U^\dagger P^T PU\right) \nu\, Z_\mu + \ldots\,. \tag{2.20}$$

Both currents involve the combination PU, which is an $3\times\bar{n}$ non-unitary matrix, implying that the neutral current is no longer necessarily diagonal or universal. In general, the matrix PU contains $(\bar{n}-n)(\bar{n}+n+1)/2$ phases. In the absence of higher-dimensional operators $\bar{n}-n=3$ of these phases can be absorbed by the charged-lepton fields, leading to $(\bar{n}-n)(\bar{n}+n-1)/2 = 3(n+1)$ phases and an equal number of angles [80]. In the case of $\bar{n}=3$ the resulting matrix is the usual PMNS matrix. In the presence of higher-dimensional operators the same re-phasings of the electron fields can still be performed, but will result in redefinitions of the Wilson coefficients of these operators.

After rotating to the neutrino mass basis the operators in $\mathcal{L}^{(6)}_{\Delta L=0}$ and $\mathcal{L}^{(6)}_{\Delta L=2}$, and $\mathcal{L}^{(7)}_{\Delta L=0}$ and $\mathcal{L}^{(7)}_{\Delta L=2}$ can be written in a very compact form. We combine the dim-6 operators into

$$\begin{aligned} \mathcal{L}^{(6)} \;=\; & \frac{2G_F}{\sqrt{2}} \Big\{ \bar{u}_L\gamma^\mu d_L \left[\bar{e}_R\gamma_\mu C^{(6)}_{\text{VLR}}\,\nu + \bar{e}_L\gamma_\mu C^{(6)}_{\text{VLL}}\,\nu\right] + \bar{u}_R\gamma^\mu d_R \left[\bar{e}_R\,\gamma_\mu C^{(6)}_{\text{VRR}}\,\nu + \bar{e}_L\,\gamma_\mu C^{(6)}_{\text{VRL}}\,\nu\right] \\ & + \bar{u}_L d_R \left[\bar{e}_L\, C^{(6)}_{\text{SRR}}\nu + \bar{e}_R\, C^{(6)}_{\text{SRL}}\nu\right] + \bar{u}_R d_L \left[\bar{e}_L\, C^{(6)}_{\text{SLR}}\nu + \bar{e}_R\, C^{(6)}_{\text{SLL}}\nu\right] \\ & + \bar{u}_L\sigma^{\mu\nu} d_R\, \bar{e}_L\sigma_{\mu\nu} C^{(6)}_{\text{TRR}}\,\nu + \bar{u}_R\sigma^{\mu\nu} d_L\, \bar{e}_R\sigma_{\mu\nu} C^{(6)}_{\text{TLL}}\,\nu \Big\} + \text{h.c.}\,, \end{aligned} \tag{2.21}$$

while for the dim-7 operators we get

$$\begin{aligned} \mathcal{L}^{(7)} \;=\; & \frac{2G_F}{\sqrt{2}v} \Big\{ \bar{u}_L\gamma^\mu d_L \left[\bar{e}_L\, C^{(7)}_{\text{VLR}}\, i\overleftrightarrow{D}_\mu \nu + \bar{e}_R\, C^{(7)}_{\text{VLL}}\, i\overleftrightarrow{D}_\mu \nu\right] \\ & + \bar{u}_R\gamma^\mu d_R \left[\bar{e}_L\, C^{(7)}_{\text{VRR}}\, i\overleftrightarrow{D}_\mu \nu + \bar{e}_R\, C^{(7)}_{\text{VRL}}\, i\overleftrightarrow{D}_\mu \nu\right] \\ & + \bar{u}_L\sigma^{\mu\nu} d_R\, \bar{e}_L C^{(7)}_{\text{TR1}} \overleftarrow{D}_\mu \gamma_\nu \nu + \bar{u}_R\sigma^{\mu\nu} d_L\, \bar{e}_L C^{(7)}_{\text{TL1}} \gamma_\nu \partial_\mu \nu \\ & + \bar{u}_L\sigma^{\mu\nu} d_R\, D_\mu \left(\bar{e}_L C^{(7)}_{\text{TR2}}\gamma_\nu \nu\right) + \bar{u}_R\sigma^{\mu\nu} d_L\, D_\mu \left(\bar{e}_L C^{(7)}_{\text{TL2}}\gamma_\nu \nu\right) \Big\} + \text{h.c.}\,. \end{aligned} \tag{2.22}$$

The dim-9 operators contain no neutrino fields and thus are unaffected under the rotation. The dim-6 and -7 operators are now mixtures of LNC and LNV terms, as the ν fields do not have a definite lepton number. The Wilson coefficients of the dim-6 operators are given by

$$\begin{aligned}
C^{(6)}_{\mathrm{VLR}} &= C^{(6)}_{\mathrm{VL}} PU^* + \bar{c}^{(6)}_{\mathrm{VL}} P_s U^* \,, & C^{(6)}_{\mathrm{VRR}} &= C^{(6)}_{\mathrm{VR}} PU^* + \bar{c}^{(6)}_{\mathrm{VR}} P_s U^* \,, \\
C^{(6)}_{\mathrm{VLL}} &= \bar{C}^{(6)}_{\mathrm{VL}} P_s U + c^{(6)}_{\mathrm{VL}} PU \,, & C^{(6)}_{\mathrm{VRL}} &= \bar{C}^{(6)}_{\mathrm{VR}} P_s U + c^{(6)}_{\mathrm{VR}} PU \,, \\
C^{(6)}_{\mathrm{SLR}} &= C^{(6)}_{\mathrm{SL}} PU^* + \bar{c}^{(6)}_{\mathrm{SL}} P_s U^* \,, & C^{(6)}_{\mathrm{SRR}} &= C^{(6)}_{\mathrm{SR}} PU^* + \bar{c}^{(6)}_{\mathrm{SR}} P_s U^* \,, \\
C^{(6)}_{\mathrm{SLL}} &= \bar{C}^{(6)}_{\mathrm{SL}} P_s U + c^{(6)}_{\mathrm{SL}} PU \,, & C^{(6)}_{\mathrm{SRL}} &= \bar{C}^{(6)}_{\mathrm{SR}} P_s U + c^{(6)}_{\mathrm{SR}} PU \,, \\
C^{(6)}_{\mathrm{TLL}} &= \bar{C}^{(6)}_{\mathrm{T}} P_s U + c^{(6)}_{\mathrm{T}} PU \,, & C^{(6)}_{\mathrm{TRR}} &= C^{(6)}_{\mathrm{T}} PU^* + \bar{c}^{(6)}_{\mathrm{T}} P_s U^* \,,
\end{aligned} \tag{2.23}$$

and those of the dim-7 operators become

$$\begin{aligned}
C^{(7)}_{\mathrm{VLL}} &= c^{(7)}_{\mathrm{VL}} PU + \bar{C}^{(7)}_{\mathrm{VL}} P_s U \,, & C^{(7)}_{\mathrm{VRL}} &= c^{(7)}_{\mathrm{VR}} PU + \bar{C}^{(7)}_{\mathrm{VR}} P_s U \,, \\
C^{(7)}_{\mathrm{VLR}} &= C^{(7)}_{\mathrm{VL}} PU^* + \bar{c}^{(7)}_{\mathrm{VL}} P_s U^* \,, & C^{(7)}_{\mathrm{VRR}} &= C^{(7)}_{\mathrm{VR}} PU^* + \bar{c}^{(7)}_{\mathrm{VR}} P_s U^* \,, \\
C^{(7)}_{\mathrm{TL1}} &= \bar{C}^{(7)}_{\mathrm{TL}} P_s U \,, & C^{(7)}_{\mathrm{TL2}} &= c^{(7)}_{\mathrm{TL}} PU \,, \\
C^{(7)}_{\mathrm{TR1}} &= \bar{C}^{(7)}_{\mathrm{TR}} P_s U \,, & C^{(7)}_{\mathrm{TR2}} &= c^{(7)}_{\mathrm{TR}} PU \,.
\end{aligned} \tag{2.24}$$

The coefficients above also carry flavor indices $ijkl$ where $i = u,\, c$ denotes the up-type quarks, $j = d,\, s,\, b$ indicate the down-type quarks, $k = e, \mu$ labels the generation of charged lepton and $l = \{1, ..., \bar{n}\}$ denote neutrinos in the mass basis. The operators involving $\nu^c_{L,R}$ and $\nu_{R,L}$ contribute to the same terms in the mass basis, the only difference results from the flavor indices that are summed over, i.e. whether P or P_s appears.

Below the electroweak scale we again considering the one-loop QCD running of the operators in Eqs. (2.21) and (2.22). The dimension-six and -seven couplings evolve like scalar or tensor currents, as in Eq. (2.5), with

$$C_S \in \{C^{(6)}_{\mathrm{SRR,SRL,SLR,SLL}}\} \,, \qquad C_T \in \{C^{(6)}_{\mathrm{TRR,TLL}},\, C^{(7)}_{\mathrm{TR1,TR2,TL1,TL2}}\} \,. \tag{2.25}$$

2.4 Summary

In this chapter we consider νSMEFT at a very high new physics scale Λ and list higher-dimensional operators up to $\overline{\text{dim-7}}$. Most of them contain one ν_L or ν_R, while several other operators contain no neutrino field and can contribute to LNV process at tree level after EWSB. Those operators which could contribute to neutrino mass are also included. We then evolve them from Λ to the EW scale. The RGEs due to one-loop QCD effects are given in Eqs. (2.5) and (2.7). After EWSB and integrating out heavy SM particles, we are left with operators only invariant under $SU(3)_c \times U(1)_{em}$. For the convenience of calculations, we rotate neutrinos to the mass basis and rewrite the Lagrangian in a very compact form. In the following chapters, we will discuss the applications of the framework developed here on several different phenomena.

Chapter 3

Neutrinoless double beta decay in νSMEFT up to dimension seven

In the process of $0\nu\beta\beta$ two neutrons decay into two protons and two electrons without the emission of neutrinos, and thus violates the lepton number by two units. If sterile neutrinos are heavy with respect to the EW scale $v \simeq 246$ GeV, they can be integrated out and their contributions to LNV processes can be described by local gauge-invariant effective operators that appear in SMEFT. LNV operators have odd dimension [81] and start at dimension five. The effect of SMEFT on $0\nu\beta\beta$ up to dimension seven has been investigated in [82] and in this chapter[1] we focus on sterile neutrinos with masses below the EW scale and study their effect on $0\nu\beta\beta$ in the framework of νSMEFT.

To get calculate the $nn \to ppee$ transintion operator, we use the chiral perturbation theory (χPT) and insert it into many-body nuclear wave functions. Finally we get a so-called 'Master formula' that relates νSMEFT operators to $0\nu\beta\beta$decay rates and the formula expresses $0\nu\beta\beta$ rates in terms of a set of phase-space factors, nuclear matrix elements, hadronic low-energy constants, QCD evolution factors, and the original Wilson coefficients. With this formula, any BSM model with a light sterile neutrino for which the νSMEFT framework is applicable ($\Lambda \gg v$) can be directly connected to $0\nu\beta\beta$ rates.

3.1 The full complete set of dim-9 operators in the case of $0\nu\beta\beta$

Before discussing how to calculate the decay rates, we show the dim-9 operators in this section. After EWSW some dim-9 operators are induced from operators in νSMEFT and they contain two up quarks, two down quarks and two electrons. And more operators are generated if a sterile neutrino with $\Lambda_\chi < m_\nu < m_W$ is integrated out ($\Lambda_\chi \simeq 1$ GeV). We therefore list the complete set

$$\mathcal{L}^{(9)}_{\Delta L=2} = \frac{1}{v^5}\sum_i \left[\left(C^{(9)}_{i\,\mathrm{R}}\, \bar{e}_R C \bar{e}^T_R + C^{(9)}_{i\,\mathrm{L}}\, \bar{e}_L C \bar{e}^T_L \right) O_i + C^{(9)}_i \bar{e}\gamma_\mu\gamma_5 C \bar{e}^T\, O^\mu_i \right], \tag{3.1}$$

[1] This chapter is based on W. Dekens, J. de Vries, K. Fuyuto, E. Mereghetti, and G. Zhou, JHEP 06 (2020) 097.

where O_i and O_i^μ are four-quark operators that are Lorentz scalars and vectors, respectively. The scalar operators have been discussed in Refs. [83,84] and can be written as

$$\begin{aligned}
O_1 &= \bar{q}_L^\alpha \gamma_\mu \tau^+ q_L^\alpha \; \bar{q}_L^\beta \gamma^\mu \tau^+ q_L^\beta \,, & O_1' &= \bar{q}_R^\alpha \gamma_\mu \tau^+ q_R^\alpha \; \bar{q}_R^\beta \gamma^\mu \tau^+ q_R^\beta \,, \\
O_2 &= \bar{q}_R^\alpha \tau^+ q_L^\alpha \; \bar{q}_R^\beta \tau^+ q_L^\beta \,, & O_2' &= \bar{q}_L^\alpha \tau^+ q_R^\alpha \; \bar{q}_L^\beta \tau^+ q_R^\beta \,, \\
O_3 &= \bar{q}_R^\alpha \tau^+ q_L^\beta \; \bar{q}_R^\beta \tau^+ q_L^\alpha \,, & O_3' &= \bar{q}_L^\alpha \tau^+ q_R^\beta \; \bar{q}_L^\beta \tau^+ q_R^\alpha \,, \\
O_4 &= \bar{q}_L^\alpha \gamma_\mu \tau^+ q_L^\alpha \; \bar{q}_R^\beta \gamma^\mu \tau^+ q_R^\beta \,, & & \\
O_5 &= \bar{q}_L^\alpha \gamma_\mu \tau^+ q_L^\beta \; \bar{q}_R^\beta \gamma^\mu \tau^+ q_R^\alpha \,, & &
\end{aligned} \tag{3.2}$$

where $\tau^\pm = (\tau_1 \pm i\tau_2)/2$ with τ_i the Pauli matrices and α, β are color indices and $q = (u, d)^T$ is the doublet of the quark fields. The O_i' operators are related to the O_i by parity. The vector operators are [83]

$$\begin{aligned}
O_6^\mu &= \left(\bar{q}_L \tau^+ \gamma^\mu q_L\right)\left(\bar{q}_L \tau^+ q_R\right) \,, & O_6^{\mu\,\prime} &= \left(\bar{q}_R \tau^+ \gamma^\mu q_R\right)\left(\bar{q}_R \tau^+ q_L\right) \,, \\
O_7^\mu &= \left(\bar{q}_L t^a \tau^+ \gamma^\mu q_L\right)\left(\bar{q}_L t^a \tau^+ q_R\right) \,, & O_7^{\mu\,\prime} &= \left(\bar{q}_R t^a \tau^+ \gamma^\mu q_R\right)\left(\bar{q}_R t^a \tau^+ q_L\right) \,, \\
O_8^\mu &= \left(\bar{q}_L \tau^+ \gamma^\mu q_L\right)\left(\bar{q}_R \tau^+ q_L\right) \,, & O_8^{\mu\,\prime} &= \left(\bar{q}_R \tau^+ \gamma^\mu q_R\right)\left(\bar{q}_L \tau^+ q_R\right) \,, \\
O_9^\mu &= \left(\bar{q}_L t^a \tau^+ \gamma^\mu q_L\right)\left(\bar{q}_R t^a \tau^+ q_L\right) \,, & O_9^{\mu\,\prime} &= \left(\bar{q}_R t^a \tau^+ \gamma^\mu q_R\right)\left(\bar{q}_L t^a \tau^+ q_R\right) \,,
\end{aligned} \tag{3.3}$$

where the second column of operators is related to the first column by a parity transformation. Eqs. (3.2) and (3.3) provide a complete basis of four-quark two-electron operators. Without loss of generality, we work in a basis without operators with tensor structures that can be replaced through Fierz relations in terms of operators involving quark bilinears with uncontracted color indices, for example $O_T = \bar{q}_R^\alpha \sigma_{\mu\nu} \tau^+ q_L^\alpha \; \bar{q}_R^\beta \sigma^{\mu\nu} \tau^+ q_L^\beta = -8O_3 - 4O_2$. The matching conditions for the dim-9 operators, induced from νSMEFT after EWSB, can be taken from Ref. [82,85]

$$\begin{aligned}
\frac{1}{v^3} C_{1L}^{(9)} &= -2V_{ud}^2 \left(C_{LHD\,1}^{(7)} + 4\mathcal{C}_{LHW}\right)^* \,, \\
\frac{1}{v^3} C_{4L}^{(9)} &= -2iV_{ud}\, C_{LL\bar{d}uD}^{(7)*} \,.
\end{aligned} \tag{3.4}$$

In case one or more neutrinos have masses in the range $\Lambda_\chi < m_\nu \leq v$, we should integrate them out before matching onto chiral perturbation theory. We can do so by writing the Lagrangian involving the heavy neutrinos as

$$\mathcal{L}_H = \sum_{i=N-n_H+1}^{N} \left[\frac{1}{2}\bar{\nu}_i i\partial\!\!\!/ \nu_i - \frac{1}{2}\bar{\nu}_i m_{\nu_i} \nu_i + \mathcal{J}_i \nu_i\right], \tag{3.5}$$

where i is a neutrino mass eigenstate index that runs over the heavy neutrinos, i.e. $\Lambda_\chi < m_{\nu_i} \leq v$ for $i \in \{N - n_H + 1,\, N\}$, with n_H the number of heavy neutrinos. Furthermore, $\mathcal{J}_i$ incorporates the interactions of the i-th neutrino that are present in $\mathcal{L}^{(6,7)}$. When integrating out the heavy neutrinos, combinations of the interactions in $\mathcal{L}^{(6,7)}$ will give rise to dimension-nine operators. These can be derived by making use of the equations of motion,

$$\nu_i^T C \simeq \left(\mathcal{J} \bar{m}_\nu^{-1}\right)_i \,, \qquad i \in \{N - n_H + 1,\, N\} \,, \tag{3.6}$$

where $\bar{m}_\nu^{-1}$ is a diagonal $N \times N$ mass matrix for the heavy neutrinos, $\bar{m}_\nu^{-1} = \mathrm{diag}(0, \ldots 0,$ $m_{\nu_{N-n_H+1}}^{-1}, \ldots m_{\nu_N}^{-1})$, and we neglected the kinetic term of the heavy neutrinos, which produces terms that are suppressed by q/m_{ν_i}. Making the same approximation for the interactions in $\mathcal{J}$

allows us to drop the dim-7 terms. Appendix A discusses corrections to this approximation. We obtain

$$\begin{aligned}
\mathcal{J}_i &= J_i + \bar{J}_i \\
J_i &\simeq \frac{1}{v^2}\Big[\bar{u}_L\gamma^\mu d_L\left[\bar{e}_R\gamma_\mu C^{(6)}_{\rm VLR} + \bar{e}_L\gamma_\mu C^{(6)}_{\rm VLL}\right] + \bar{u}_R\gamma^\mu d_R\left[\bar{e}_R\,\gamma_\mu C^{(6)}_{\rm VRR} + \bar{e}_L\,\gamma_\mu C^{(6)}_{\rm VRL}\right] \\
&\quad + \bar{u}_L d_R\left[\bar{e}_L\,C^{(6)}_{\rm SRR} + \bar{e}_R\,C^{(6)}_{\rm SRL}\right] + \bar{u}_R d_L\left[\bar{e}_L\,C^{(6)}_{\rm SLR} + \bar{e}_R\,C^{(6)}_{\rm SLL}\right] \\
&\quad + \bar{u}_L\sigma^{\mu\nu} d_R\,\bar{e}_L\sigma_{\mu\nu}C^{(6)}_{\rm TRR} + \bar{u}_R\sigma^{\mu\nu} d_L\,\bar{e}_R\sigma_{\mu\nu}C^{(6)}_{\rm TLL}\Big]_i\,,
\end{aligned} \tag{3.7}$$

where $\bar{J}_i$ are the interactions that arise from the hermitian conjugate in $\mathcal{L}^{(6,7)}$, i.e. terms involving $e_{L,R}$ instead of $\bar{e}_{L,R}$. This leads to the following effective Lagrangian

$$\mathcal{L}_H \simeq \frac{1}{2}\mathcal{J}\bar{m}_\nu^{-1}C\mathcal{J}^T\,, \tag{3.8}$$

in which the terms of interest for $0\nu\beta^-\beta^-$, namely those that have $L=-2$ (not $L=0,2$), are contained in the $\sim J\bar{m}_\nu^{-1}CJ^T$ part of the above Lagrangian. Instead, the operators with $L=2$, which give rise to $0\nu\beta^+\beta^+$ decays are contained in the $\sim \bar{J}\bar{m}_\nu^{-1}C\bar{J}^T$ term and are given by the hermitian conjugate of the $L=-2$ interactions. This procedure leads to the following matching conditions for the scalar operators

$$\begin{aligned}
C^{(9)}_{1\,R} &= -\frac{v}{2}C^{(6)}_{\rm VLR}\bar{m}_\nu^{-1}C^{(6)\,T}_{\rm VLR}\,, \qquad C^{(9)\prime}_{1\,R} = -\frac{v}{2}C^{(6)}_{\rm VRR}\bar{m}_\nu^{-1}C^{(6)\,T}_{\rm VRR}\,, \\
C^{(9)}_{2\,R} &= \frac{v}{2}C^{(6)}_{\rm SLL}\bar{m}_\nu^{-1}C^{(6)\,T}_{\rm SLL} + 8vC^{(6)}_{\rm TLL}\bar{m}_\nu^{-1}C^{(6)\,T}_{\rm TLL}\,, \qquad C^{(9)\prime}_{2\,R} = \frac{v}{2}C^{(6)}_{\rm SRL}\bar{m}_\nu^{-1}C^{(6)\,T}_{\rm SRL}\,, \\
C^{(9)}_{3\,R} &= 16vC^{(6)}_{\rm TLL}\bar{m}_\nu^{-1}C^{(6)\,T}_{\rm TLL}\,, \qquad C^{(9)\prime}_{3\,R} = 0\,, \\
C^{(9)}_{4\,R} &= -\frac{v}{2}\left[C^{(6)}_{\rm VRR}\bar{m}_\nu^{-1}C^{(6)\,T}_{\rm VLR} + C^{(6)}_{\rm VLR}\bar{m}_\nu^{-1}C^{(6)\,T}_{\rm VRR}\right]\,, \\
C^{(9)}_{5\,R} &= -\frac{v}{4}\left[C^{(6)}_{\rm SRL}\bar{m}_\nu^{-1}C^{(6)\,T}_{\rm SLL} + C^{(6)}_{\rm SLL}\bar{m}_\nu^{-1}C^{(6)\,T}_{\rm SRL}\right]\,.
\end{aligned} \tag{3.9}$$

Analogous matching contributions arise for the $C^{(9)}_{i\,L}$ operators, which can be obtained from the above by replacing

$$\begin{aligned}
C^{(9)}_{i\,R} &\to C^{(9)\prime}_{i\,L}\,, \qquad C^{(9)\prime}_{i\,R} \to C^{(9)}_{i\,L}\,, \qquad C^{(9)}_{4,5\,R} \to C^{(9)}_{4,5\,L} \\
C^{(6)}_{\rm ALL} &\leftrightarrow C^{(6)}_{\rm ARR}\,, \qquad C^{(6)}_{\rm ARL} \leftrightarrow C^{(6)}_{\rm ALR}\,, \qquad A \in \{S,V,T\}\,.
\end{aligned} \tag{3.10}$$

The matching conditions for the vector operators are given by

$$
\begin{aligned}
C_6^{(9)} &= \frac{v}{2}\left[\frac{C_{\mathrm{VLR}}^{(6)}\bar{m}_\nu^{-1}C_{\mathrm{SRR}}^{(6)\,T}+C_{\mathrm{SRR}}^{(6)}\bar{m}_\nu^{-1}C_{\mathrm{VLR}}^{(6)\,T}}{2}-\frac{C_{\mathrm{VLL}}^{(6)}\bar{m}_\nu^{-1}C_{\mathrm{SRL}}^{(6)\,T}+C_{\mathrm{SRL}}^{(6)}\bar{m}_\nu^{-1}C_{\mathrm{VLL}}^{(6)\,T}}{2}\right]\\
&\quad+\frac{1}{4}\left(\frac{2}{N_c}+1\right)C_7^{(9)}\,,\\
C_7^{(9)} &= 8v\left[\frac{C_{\mathrm{VLR}}^{(6)}\bar{m}_\nu^{-1}C_{\mathrm{TRR}}^{(6)\,T}+C_{\mathrm{TRR}}^{(6)}\bar{m}_\nu^{-1}C_{\mathrm{VLR}}^{(6)\,T}}{2}\right],\\
C_8^{(9)} &= \frac{v}{2}\left[\frac{C_{\mathrm{VLR}}^{(6)}\bar{m}_\nu^{-1}C_{\mathrm{SLR}}^{(6)\,T}+C_{\mathrm{SLR}}^{(6)}\bar{m}_\nu^{-1}C_{\mathrm{VLR}}^{(6)\,T}}{2}-\frac{C_{\mathrm{VLL}}^{(6)}\bar{m}_\nu^{-1}C_{\mathrm{SLL}}^{(6)\,T}+C_{\mathrm{SLL}}^{(6)}\bar{m}_\nu^{-1}C_{\mathrm{VLL}}^{(6)\,T}}{2}\right]\\
&\quad+\frac{1}{4}\left(\frac{2}{N_c}+1\right)C_9^{(9)}\,,\\
C_9^{(9)} &= 8v\left[\frac{C_{\mathrm{VLL}}^{(6)}\bar{m}_\nu^{-1}C_{\mathrm{TLL}}^{(6)\,T}+C_{\mathrm{TLL}}^{(6)}\bar{m}_\nu^{-1}C_{\mathrm{VLL}}^{(6)\,T}}{2}\right],\\
C_6^{(9)\prime} &= \frac{v}{2}\left[\frac{C_{\mathrm{VRR}}^{(6)}\bar{m}_\nu^{-1}C_{\mathrm{SLR}}^{(6)\,T}+C_{\mathrm{SLR}}^{(6)}\bar{m}_\nu^{-1}C_{\mathrm{VRR}}^{(6)\,T}}{2}-\frac{C_{\mathrm{VRL}}^{(6)}\bar{m}_\nu^{-1}C_{\mathrm{SLL}}^{(6)\,T}+C_{\mathrm{SLL}}^{(6)}\bar{m}_\nu^{-1}C_{\mathrm{VRL}}^{(6)\,T}}{2}\right]\\
&\quad+\frac{1}{4}\left(\frac{2}{N_c}+1\right)C_7^{(9)\prime}\,,\\
C_7^{(9)\prime} &= -8v\left[\frac{C_{\mathrm{VRL}}^{(6)}\bar{m}_\nu^{-1}C_{\mathrm{TLL}}^{(6)\,T}+C_{\mathrm{TLL}}^{(6)}\bar{m}_\nu^{-1}C_{\mathrm{VRL}}^{(6)\,T}}{2}\right],\\
C_8^{(9)\prime} &= \frac{v}{2}\left[\frac{C_{\mathrm{VRR}}^{(6)}\bar{m}_\nu^{-1}C_{\mathrm{SRR}}^{(6)\,T}+C_{\mathrm{SRR}}^{(6)}\bar{m}_\nu^{-1}C_{\mathrm{VRR}}^{(6)\,T}}{2}-\frac{C_{\mathrm{VRL}}^{(6)}\bar{m}_\nu^{-1}C_{\mathrm{SRL}}^{(6)\,T}+C_{\mathrm{SRL}}^{(6)}\bar{m}_\nu^{-1}C_{\mathrm{VRL}}^{(6)\,T}}{2}\right]\\
&\quad+\frac{1}{4}\left(\frac{2}{N_c}+1\right)C_9^{(9)\prime}\,,\\
C_9^{(9)\prime} &= -8v\left[\frac{C_{\mathrm{VRR}}^{(6)}\bar{m}_\nu^{-1}C_{\mathrm{TRR}}^{(6)\,T}+C_{\mathrm{TRR}}^{(6)}\bar{m}_\nu^{-1}C_{\mathrm{VRR}}^{(6)\,T}}{2}\right].
\end{aligned}
\tag{3.11}
$$

3.2 Chiral perturbation theory with (sterile) neutrinos

Below the GeV scale, a description in terms of quarks and gluons as degrees of freedom breaks down. We need an effective description in terms of pions and nucleons. To keep the connection to QCD and the higher-dimensional operators we apply the framework of chiral perturbation theory (χPT) [86–89]. χPT is the low-energy EFT of QCD and the χPT Lagrangian consists of all interaction among the effective low-energy degrees of freedom consistent with the chiral and space-time symmetry properties of the underlying microscopic theory. In this chapter for $0\nu\beta\beta$, we apply two-flavored χPT in which pions appear as pseudo-Goldstone bosons of the approximate chiral symmetry of QCD. Up to small chiral-symmetry-breaking corrections, pionic interactions involve space-time derivatives. This feature allows for a perturbative expansion in $\epsilon_\chi = p/\Lambda_\chi$ where p is the momentum scale of a process. For $p \sim m_\pi$ only a finite number of interactions need to be considered. Each interaction is proportional to a coupling constant, often called a low-energy constant (LEC), whose value cannot be obtained from symmetry considerations alone. The LECs can be fitted to experimental data, calculated using nonperturbative QCD methods

such as lattice QCD, or estimated based on the power-counting scheme with naive dimensional analysis (NDA) [90].

The extension of χPT to systems with more than one nucleon, as required for our purposes, is often called chiral EFT (χEFT) [91] and has a more complicated power counting. The nuclear scale $p^2/2m_N$ becomes relevant in diagrams in which the intermediate state consists purely of propagating nucleons, which are enhanced with respect to the χPT counting. This leads to the need to resum certain classes of diagrams to all orders, which manifests in the appearance of bound states: atomic nuclei. The need to resum certain nuclear interactions also has important consequences for external currents [92]. Currents that are sandwiched between nuclear interactions that must be resummed can appear at lower order in the power counting than expected based on NDA. For example, the exchange of a light Majorana neutrino between two nucleons leads to a $nn \to pp\,ee$ transition operator whose matrix element between nuclear wave functions diverges [93, 94]. This implies that a counterterm must be present, in the form a short-range $nnppee$ operator, to absorb the associated divergence. We determine the scaling of nucleon-nucleon currents by explicitly enforcing that the $nn \to pp\,ee$ amplitude is renormalized.

The discussion of $0\nu\beta\beta$ mediated by light neutrinos requires the consideration of two more scales: the energy of the outgoing electrons and the neutrino mass. The electron energy is determined by the Q-value of the $0\nu\beta\beta$ reactions. All isotopes of experimental interest have Q-values at the MeV scale $Q \sim \mathcal{O}(\text{MeV})$ which is small compared to the typical momentum exchange between nucleons $q \sim k_F \sim m_\pi$ where k_F is the Fermi momentum of a nucleus. $nn \to pp\,ee$ transition operators that explicitly depend on the lepton momenta therefore give rise to suppressed $0\nu\beta\beta$ amplitudes. To explicitly consider this suppression in the power-counting scheme we assign the counting rule $Q \sim m_e \sim m_\pi \epsilon_\chi^2$ [71]. The electron energy is of similar size as the excitation energy of the nuclear intermediate states, which are related to violation of the so called "closure approximation". In chiral EFT, corrections to closure are associated to the propagation of ultrasoft (usoft) neutrinos, with $q^0 \sim |\mathbf{q}| \sim Q$, and, in the standard mechanism [2], are suppressed by $Q/(4\pi k_F) \sim \epsilon_\chi^3$ [95].

The mass of sterile neutrinos is a varying parameter, which can go from $m_i \ll Q$, similar to the standard mechanism, all the way to $m_i \gg \Lambda_\chi$. For almost massless neutrinos, $m_i \lesssim Q$, the $0\nu\beta\beta$ amplitude receives contributions from "potential" neutrinos, with $(q^0, \mathbf{q}) \sim (0, k_F)$, from hard neutrinos, with $q_0 \sim \mathbf{q} \sim \Lambda_\chi$, and from the usoft regime discussed above. The usoft region is suppressed, unless the LO potential contribution cancels, as happens when the active neutrinos have no Majorana mass, $M_L = 0$, all sterile neutrinos are light, and higher-dimensional operators are turned off. In this case, the potential region is suppressed by m_i^2/k_F^2 [96, 97], while the usoft region is comparatively less suppressed, by m_i^2/Q^2, and the two become similar. In this thesis, we do not include the contributions from the ultrasoft region, which are phenomenologically important only in the narrow region $m_i \lesssim Q$, and very small M_L. In several cases, the hard region gives contributions that are comparable to those from potential neutrinos. We will consider the corresponding chiral Lagrangian in Sect. 3.2.6.

If we increase the neutrino mass to $m_i \sim m_\pi$, the usoft region disappears. In this case, soft neutrinos and pions with $q_0 \sim \mathbf{q} \sim m_\pi$ are explicit degrees of freedom in the theory, but they correct the $0\nu\beta\beta$ transition operator only at loop level, implying a suppression by factors of ϵ_χ [95]. Instead, in the region $m_i \sim \Lambda_\chi$, such loop corrections become large, $\sim m_i/\Lambda_\chi$, making this the most complicated region to describe rigorously. Finally, if $m_i \gg \Lambda_\chi$, the sterile neutrinos can be integrated out in perturbation theory, as discussed in Sect. 3.1.

Within the framework of χEFT, extended with the additional scale considerations mentioned

[2] Throughout this thesis, we refer to the standard mechanism as $0\nu\beta\beta$ induced by three very light, $m_i \ll Q$, Majorana neutrinos.

above, the $nn \to pp\,ee$ transition operators have been derived for several sources of LNV. For example, Refs. [93–95] calculated the transition operator in the standard mechanism up to next-to-next-to-leading order in the ϵ_χ expansion. In this chapter we extend these calculations to contributions from sterile neutrinos.

3.2.1 Chiral building blocks

The construction of the χPT Lagrangian is well documented [87, 89, 98], and the application to $0\nu\beta\beta$ is spelled out in Ref. [82]. For convenience we write the QCD Lagrangian supplemented by the operators in Eqs. (2.21) and (2.22) as

$$\begin{aligned}\mathcal{L}_{qq} &= \bar{q} i\partial\!\!\!/ q + \bar{q}\Big\{ l^\mu \gamma_\mu P_L + r^\mu \gamma_\mu P_R \\ &\quad -(M+s+ip)P_L - (M+s-ip)P_R + t_L^{\mu\nu}\sigma_{\mu\nu}P_L + t_R^{\mu\nu}\sigma_{\mu\nu}P_R\Big\} q\,, \end{aligned} \tag{3.12}$$

with $q = (u\,d)^T$ a doublet of quark fields, and $M = \mathrm{diag}(m_u, m_d)$ is a diagonal matrix of the real quark masses. The external sources s, p, l^μ, r^μ, $t_L^{\mu\nu}$, and $t_R^{\mu\nu}$ can be read from Eqs. (2.21) and (2.22). Neglecting the SM electromagnetic and neutral weak interaction, and focusing on terms that create electrons instead of positrons, we have

$$\begin{aligned} s+ip &= -\frac{2G_F}{\sqrt{2}}\left\{\tau^+\left(\bar{e}_L C^{(6)}_{\mathrm{SLR}}\nu + \bar{e}_R C^{(6)}_{\mathrm{SLL}}\nu\right) + \left(\tau^+\right)^\dagger\left(\bar{e}_L C^{(6)}_{\mathrm{SRR}}\nu + \bar{e}_R C^{(6)}_{\mathrm{SRL}}\nu\right)^\dagger\right\}, \\ s-ip &= (s+ip)^\dagger\,, \\ l^\mu &= \frac{2G_F}{\sqrt{2}v}\tau^+\Big\{ v\,\bar{e}_R\gamma^\mu C^{(6)}_{\mathrm{VLR}}\nu + v\,\bar{e}_L\gamma^\mu C^{(6)}_{\mathrm{VLL}}\nu \\ &\quad + \bar{e}_L\, C^{(7)}_{\mathrm{VLR}}\, i\overleftrightarrow{\partial}^\mu\nu + \bar{e}_R\, C^{(7)}_{\mathrm{VLL}}\, i\overleftrightarrow{\partial}^\mu\nu\Big\} + \mathrm{h.c.}\,, \\ r^\mu &= \frac{2G_F}{\sqrt{2}v}\tau^+\Big\{ v\,\bar{e}_R\gamma^\mu C^{(6)}_{\mathrm{VRR}}\nu + v\,\bar{e}_L\gamma^\mu C^{(6)}_{\mathrm{VRL}}\nu \\ &\quad + \bar{e}_L\, C^{(7)}_{\mathrm{VRR}}\, i\overleftrightarrow{\partial}^\mu\nu + \bar{e}_R\, C^{(7)}_{\mathrm{VRL}}\, i\overleftrightarrow{\partial}^\mu\nu\Big\} + \mathrm{h.c.}\,, \\ t_L^{\mu\nu} &= \frac{2G_F}{\sqrt{2}v}\Big\{\tau^+\left[v\,\bar{e}_R\sigma^{\mu\nu}C^{(6)}_{\mathrm{TLL}}\,\nu + \bar{e}_L C^{(7)}_{\mathrm{TL1}}\gamma^\nu\partial^\mu\nu + \partial^\mu\left(\bar{e}_L C^{(7)}_{\mathrm{TL2}}\gamma^\nu\nu\right)\right] \\ &\quad + \left(\tau^+\right)^\dagger\left[v\,\bar{e}_L\sigma^{\mu\nu}C^{(6)}_{\mathrm{TRR}}\,\nu + \bar{e}_L C^{(7)}_{\mathrm{TR1}}\overleftarrow{\partial}^\mu\gamma^\nu\nu + \partial^\mu\left(\bar{e}_L C^{(7)}_{\mathrm{TR2}}\gamma^\nu\nu\right)\right]^\dagger\Big\}, \\ t_R^{\mu\nu} &= \left(t_L^{\mu\nu}\right)^\dagger\,. \end{aligned} \tag{3.13}$$

The quark-level Lagrangian is formally invariant under local $SU(2)_L \times SU(2)_R$ transformations, $q_L \to Lq_L$ and $q_R \to Rq_R$ with L and R general $SU(2)$ matrices, provided that the spurions transform as

$$\begin{aligned} l_\mu &\to L l_\mu L^\dagger - i\,(\partial_\mu L)\,L^\dagger\,, \qquad r_\mu \to R r_\mu R^\dagger - i\,(\partial_\mu R)\,R^\dagger\,, \\ M+s+ip &\to R(M+s+ip)L^\dagger\,, \qquad t_L^{\mu\nu} \to R t_L^{\mu\nu} L^\dagger\,, \qquad t_R^{\mu\nu} \to L t_R^{\mu\nu} R^\dagger\,. \end{aligned} \tag{3.14}$$

The chiral Lagrangian that describes the exchange of potential neutrinos is then constructed by building the most general interactions that are invariant under these transformations.

3.2.2 The pion sector

In χPT pions are described by

$$U = u^2 = \exp\left(\frac{i\boldsymbol{\pi}\cdot\boldsymbol{\tau}}{F_0}\right), \tag{3.15}$$

in terms of the Pauli matrices $\boldsymbol{\tau}$, the pion triplet $\boldsymbol{\pi}$, and F_0 is the decay constant in the chiral limit. We use $F_\pi = 92.2$ MeV for the physical pion decay constant, and, since we work at lowest order in χPT, we will use $F_\pi = F_0$. Under $SU(2)_L \times SU(2)_R$ transformations the pion field transforms as $U \to LUR^\dagger$. It is convenient to define a covariant derivative that transforms in the same way $D_\mu U \to L(D_\mu U)R^\dagger$ under local transformations, where

$$D_\mu U = \partial_\mu U - i l_\mu U + i U r_\mu \,, \tag{3.16}$$

where l_μ and r_μ are the external source terms given above. Quark masses explicitly break chiral symmetry and their effects are included by the spurion χ that transforms as $\chi \to L\chi R^\dagger$, and explicitly

$$\chi = 2B(M + s - ip)\,, \tag{3.17}$$

where B is a LEC, often called the quark condensate, related to the pion mass via $m_\pi^2 = B(m_u + m_d)$. In mesonic chiral perturbation theory, we can write the most general Lagrangian describing mesons as a list of terms with an increasing number of quark-mass terms and derivatives,

$$\mathcal{L}_{meson} = \mathcal{L}_2 + \mathcal{L}_4 + \mathcal{L}_6 + \cdots\,, \tag{3.18}$$

where we use the subscripts to denote the order in derivative and quark-mass expansion. We count the quark-mass term as two derivatives. For a given Feynman diagram induced by the mesonic interations in Eq. (3.18) we can write its chiral dimension as

$$D = 2 + (n-2)N_L + \sum_{k=1}^{\infty} 2(k-1)N_{2k} \geq 2\,, \tag{3.19}$$

where N_L is the number of independent loops and N_{2k} is the number of interactions from $\mathcal{L}_{2k}$ in Eq. (3.18). For small quark masses and momenta, we only need to consider contributions from small D because the larger D is, the less important its contribution is. The LO chiral Lagrangian consists of the Lorentz- and chiral-invariant terms with the lowest number of derivatives

$$\mathcal{L}_\pi = \frac{F_0^2}{4}\mathrm{Tr}\left[(D_\mu U)^\dagger (D^\mu U)\right] + \frac{F_0^2}{4}\mathrm{Tr}\left[U^\dagger\chi + U\chi^\dagger\right]. \tag{3.20}$$

By expanding the U field, we can immediately read off the interactions between pions, neutrinos, and electrons, that are induced by effective operators containing l^μ, r^μ, s, and p. Contributions from the tensor sources require two additional derivatives and only appear at higher order. For those sources, interactions in the pion-nucleon sector are more relevant. Interactions with more derivatives or insertions of χ also appear at higher order, but will not be necessary for our purposes.

3.2.3 The pion-nucleon sector

We work with non-relativistic heavy-baryon nucleon fields denoted by $N = (p\ n)^T$ characterized by the nucleon velocity $v^\mu = (1, \mathbf{0})$ and spin $S^\mu = (0, \boldsymbol{\sigma}/2)$. Under chiral symmetry the nucleon

field transforms as $N \to KN$ with K an $SU(2)$ matrix, belonging to the diagonal subgroup of $SU(2)_L \times SU(2)_R$. The same matrix appears in the transformation of $u = \sqrt{U} \to LuK^\dagger = KuR^\dagger$. A nucleon covariant derivative can be defined as

$$\mathcal{D}_\mu N = (\partial_\mu + \Gamma_\mu)N\,, \qquad \Gamma_\mu = \frac{1}{2}\left[u^\dagger(\partial_\mu - il_\mu)u + u(\partial_\mu - ir_\mu)u^\dagger\right]\,, \tag{3.21}$$

such that $\mathcal{D}_\mu N \to K\mathcal{D}_\mu N$. It is useful to introduce two more objects with convenient symmetry properties

$$\begin{aligned} u_\mu &= -i\left[u^\dagger(\partial_\mu - il_\mu)u - u(\partial_\mu - ir_\mu)u^\dagger\right]\,, \\ \chi_\pm &= u^\dagger\chi u^\dagger \pm u\chi^\dagger u\,, \end{aligned} \tag{3.22}$$

that transform as $X \to KXK^\dagger$, with $X \in \{\chi_\pm,\, u_\mu\}$. We can write the most general interactions describing mesons and nucleons as a string of terms

$$\mathcal{L}_{\pi N} = \mathcal{L}^{(1)}_{\pi N} + \mathcal{L}^{(2)}_{\pi N} + \mathcal{L}^{(3)}_{\pi N} + \cdots\,, \tag{3.23}$$

where these numbers denote the order of the corresponding interactions. Similar to the mesonic chiral perturbation, only contributions from lower orders dominate. Operators relevant for $0\nu\beta\beta$ with the lowest number of derivatives are given by

$$\mathcal{L}^{(1)}_{\pi N} = i\bar{N}v\cdot\mathcal{D}N + g_A\bar{N}S\cdot uN + c_5\,\bar{N}\hat{\chi}_+N - 2g_T\epsilon_{\mu\nu\alpha\beta}v^\alpha\,\bar{N}S^\beta\left(u^\dagger t_R^{\mu\nu}u^\dagger + ut_L^{\mu\nu}u\right)N\,, \tag{3.24}$$

where $\hat{\chi}_+ = \chi_+ - \mathrm{Tr}(\chi_+)/2$ and c_5 and g_T are two LECs. c_5 is connected to the strong proton-neutron mass splitting $(m_n - m_p)^{\mathrm{str}}$ and to the scalar charge g_S via $c_5 = (m_n - m_p)^{\mathrm{str}}/(4B(m_u - m_d)) = -g_S/(4B)$ [99]. g_T is nowadays known from lattice QCD calculations. The numerical values of all LECs are given in Table 3.1.

For certain LNV sources we also require the NLO corrections. Particularly important are the contributions from the nucleon isovector magnetic moment g_M and the tensor form factor g'_T

$$\mathcal{L}^{(2)}_{\pi N} = -\frac{g_M}{4m_N}\epsilon^{\mu\nu\alpha\beta}v_\alpha\,\bar{N}S_\beta f^+_{\mu\nu}N - \frac{g'_T}{m_N}v_\mu\,\bar{N}\left[(u^\dagger t_R^{\mu\nu}u^\dagger + ut_L^{\mu\nu}u),\,\mathcal{D}_\nu\right]N\,.$$

The m_N in the definitions in Eq. (3.25) is conventional, and do not indicate that the LECs g_M and g'_T are determined by reparameterization invariance. At the same order in the Lagrangian, there arise recoil corrections to the axial, vector and tensor form factors

$$\begin{aligned} \mathcal{L}^{(2)}_{\pi N,\,\mathrm{rec}} &= \frac{1}{2m_N}\left(v^\mu v^\nu - g^{\mu\nu}\right)\left(\bar{N}\mathcal{D}_\mu\mathcal{D}_\nu N\right) - \frac{ig_A}{2m_N}\bar{N}\{S\cdot\mathcal{D}, v\cdot u\}N \\ &\quad -\frac{g_T}{m_N}\epsilon_{\mu\nu\alpha\beta}\,\bar{N}S_\beta\{(u^\dagger t_R^{\mu\nu}u^\dagger + ut_L^{\mu\nu}u),\, i\mathcal{D}_\alpha\}N\,. \end{aligned} \tag{3.25}$$

Notice however that these terms contribute to the neutrino potentials only at N^{2}LO. Before turning towards the nucleon-nucleon sector, we first discuss the single neutron β-decay transition operator, which plays an important role in the descriptions of $0\nu\beta\beta$ induced by sterile neutrinos.

3.2.4 The neutron β-decay transition operator

We use chiral Lagrangians of the pion and pion-nucleon sector to derive the β-decay amplitude of a single neutron. This amplitude provides a building block towards deriving the $0\nu\beta\beta$ transition

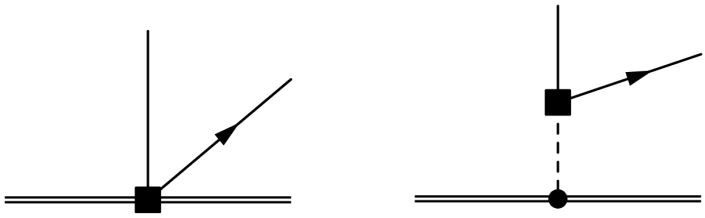

Figure 3.1: Tree-level contributions to $n \to pe^-\nu$, in the presence of non-standard vector, axial, scalar, pseudoscalar, and tensor currents. Nucleons and pions are denoted by double and dashed lines, the electron by a single line with an arrow, while ν, which is a Majorana mass eigenstate, by a single line (with no arrow). The insertion of the non-standard current is denoted by a square, while strong-interaction vertices by a circle. In the case of the vector, scalar, and tensor currents, only the first topology appears because parity forbids the couplings of the current to a single pion. Both diagrams contribute to the axial current at LO, while the pseudoscalar current is dominated by the pion pole in the second diagram.

operators. Not all contributions to $0\nu\beta\beta$ can be included in this way, since LNV interactions such as $\pi\pi ee$, πNee, and $\bar{N}N\bar{N}Nee$ operators, contribute to the $0\nu\beta\beta$ transition operator without the exchange of a neutrino. The long-distance contributions from sterile neutrinos with masses below Λ_χ, however, can be captured by combining two neutron β-decay transition operators that are derived here.

At tree level in χPT, there are two types of diagrams that contribute to beta decay depicted in Fig. 3.1. In the region $m_i \ll \Lambda_\chi$, loop corrections appear at next-to-next-to-leading order and are neglected. The amplitude can be written in compact form

$$\mathcal{A}^{n\to pe^-\nu} = \bar{N}(\mathbf{p}')\left[\frac{l_\mu + r_\mu}{2}J_V^\mu + \frac{l_\mu - r_\mu}{2}J_A^\mu - s\,J_S + ip\,J_P + t_{R\,\mu\nu}\,J_{T_R}^{\mu\nu} + t_{L\,\mu\nu}\,J_{T_L}^{\mu\nu}\right]N(\mathbf{p})\,, \tag{3.26}$$

where $N(\mathbf{p})$ denotes a spinor of a non-relativistic nucleon field with three-momentum $\mathbf{p}$. The sources are given in Eq. (3.13), and include both LNC and LNV terms. Up to NLO in the chiral expansion we obtain

$$\begin{aligned}
J_V^\mu &= g_V(\mathbf{q}^2)\left(v^\mu + \frac{p^\mu + p'^\mu}{2m_N}\right) + \frac{ig_M(\mathbf{q}^2)}{m_N}\varepsilon^{\mu\nu\alpha\beta}v_\alpha S_\beta q_\nu\,,\\
J_A^\mu &= -g_A(\mathbf{q}^2)\left(2S^\mu - \frac{v^\mu}{2m_N}\,2S\cdot(p+p')\right) + \frac{g_P(\mathbf{q}^2)}{2m_N}2q^\mu\,S\cdot q\,,\\
J_S &= g_S(\mathbf{q}^2)\,,\\
J_P &= B\frac{g_P(\mathbf{q}^2)}{m_N}S\cdot q\,,\\
J_{T_R}^{\mu\nu} &= -2g_T(\mathbf{q}^2)\varepsilon^{\mu\nu\alpha\beta}\left(v_\alpha + \frac{p_\alpha + p'_\alpha}{2m_N}\right)S_\beta - i\frac{g'_T(\mathbf{q}^2)}{2m_N}(v^\mu q^\nu - v^\nu q^\mu)\,,\\
J_{T_L}^{\mu\nu} &= J_{T_R}^{\mu\nu}\,,
\end{aligned} \tag{3.27}$$

where p and p' stand for the momenta of the incoming neutron and outgoing proton. $J_{T_L}^{\mu\nu}$ and $J_{T_R}^{\mu\nu}$ start to differ only at higher orders in the chiral expansion. We define $q^\mu = (q^0, \mathbf{q}) = p^\mu - p'^\mu$,

and $\varepsilon^{\mu\nu\alpha\beta}$ is the totally antisymmetric tensor, with $\varepsilon^{0123} = +1$. We have written the currents in terms of form factors that depend on the momentum transfer $\mathbf{q}^2$. Up to the order we work, most form factors are constants with the important exception of $g_P(\mathbf{q}^2)$. Explicitly, we obtain

$$\begin{aligned} g_V(\mathbf{q}^2) &= g_V\,, \qquad g_A(\mathbf{q}^2) = g_A\,, \qquad g_M(\mathbf{q}^2) = g_M\,, \\ g_S(\mathbf{q}^2) &= g_S, \qquad g_P(\mathbf{q}^2) = -\frac{2g_A m_N}{\mathbf{q}^2 + m_\pi^2}\,, \\ g_T(\mathbf{q}^2) &= g_T\,, \qquad g_T'(\mathbf{q}^2) = g_T'\,, \end{aligned} \tag{3.28}$$

and the values of the (combinations of) LECs g_V, g_A, g_M, g_S, g_T, and g_T' are given in Table 3.1. All form factors are $\mathcal{O}(1)$, except for $g_P(\mathbf{q}^2)$ that is enhanced by m_N/m_π. We stress that the form factors $g_P(\mathbf{q}^2)$, $g_M(\mathbf{q}^2)$, and $g_T'(\mathbf{q}^2)$ are associated with an inverted power of m_N in the contributions to the hadronic currents in Eq. (3.27).

3.2.5 Chiral Lagrangian induced by dim-9 operators

The chiral Lagrangian induced by the dim-9 operators in Eqs. (3.2) and (3.3) was discussed in Refs. [71,84]. These operators induce LNV couplings of two pions, two nucleons and one pion, or four nucleons to two electrons. The $\pi\pi$ interactions only get significant contributions from the scalar operators. Neglecting terms with more than two pions, which are only relevant at loop level or in multi-nucleon operators, the pionic Lagrangian can be written as

$$\mathcal{L}_\pi = F_\pi^2 \left[C_L'^{\pi\pi}\, \partial_\mu \pi^- \partial^\mu \pi^- + C_L^{\pi\pi} \pi^- \pi^- \right] \frac{\bar{e}_L C \bar{e}_L^T}{v^5} + (L \leftrightarrow R)\,. \tag{3.29}$$

As we will see in the next subsection, these $\pi\pi$ interactions, as well as the πN and NN interactions discussed below, are not only induced by dim-9 operators, but also receive contributions from the exchange of hard neutrinos. In anticipation of these additional contributions, we will write the above couplings (as well as those to be introduced below) as

$$C_\beta^\alpha = c_\beta^\alpha + \sum_{i=1}^{n_L} C_{i,\beta}^\alpha(m_i)\,, \qquad \alpha \in \{\prime\pi\pi,\, \pi\pi,\, \pi N,\, NN\}\,, \quad \beta \in \{L, R, V\}\,, \tag{3.30}$$

where we use c_β^α to denote the dim-9 contributions, while the remaining terms will be discussed in Sect. 3.2.6. The contributions from the dim-9 operators can then be written as

$$\begin{aligned} c_L'^{\pi\pi} &= \frac{5}{6} g_1^{\pi\pi} \left(C_{1L}^{(9)} + C_{1L}^{(9)\prime} \right)\,, \\ c_L^{\pi\pi} &= \frac{1}{2} \left[g_4^{\pi\pi} C_{4L}^{(9)} + g_5^{\pi\pi} C_{5L}^{(9)} - g_2^{\pi\pi} \left(C_{2L}^{(9)} + C_{2L}^{(9)\prime} \right) - g_3^{\pi\pi} \left(C_{3L}^{(9)} + C_{3L}^{(9)\prime} \right) \right]\,, \end{aligned} \tag{3.31}$$

where the couplings with right-handed electron fields are obtained by the replacement $L \to R$. The LECs, $g_i^{\pi\pi}$, were defined in [71] and their sizes can be estimated using naive dimensional analysis

$$g_1^{\pi\pi} = \mathcal{O}(1)\,, \qquad g_{2,3,4,5}^{\pi\pi} = \mathcal{O}(\Lambda_\chi^2)\,. \tag{3.32}$$

The LECs in Eq. (3.29) were computed in Ref. [100], and are found to be in agreement with these expectations. We write the values of the LECs in Table 3.1.

Pion-nucleon couplings are induced by both scalar and vector operators. For scalar operators, the πN couplings are subleading, with the exception of the operator O_1. For vector operators,

they contribute to the LO $0\nu\beta\beta$ transition operator. Expanding in pion fields, the Lagrangian has the form

$$\begin{aligned}
\mathcal{L}_{\pi N} &= \sqrt{2} g_A F_\pi \left[\bar{p}\, S\cdot(\partial\pi^-) n\right] \left\{ \left[C_L^{\pi N} \frac{\bar{e}_L C \bar{e}_L^T}{v^5} + (L \leftrightarrow R)\right] + C_V^{\pi N} v^\mu \frac{\bar{e}\gamma_\mu\gamma_5 C\bar{e}^T}{v^5} \right\}, \\
c_{L,R}^{\pi N} &= g_1^{\pi N}\left(C_{1L,1R}^{(9)} + C_{1L,1R}^{(9)\prime}\right), \qquad c_V^{\pi N} = g_V^{\pi N} C_V^{(9)} + \tilde{g}_V^{\pi N} \tilde{C}_V^{(9)}, \qquad (3.33)
\end{aligned}$$

where $C_V^{(9)} \equiv C_6^{(9)} + C_8^{(9)} + C_6^{(9)\prime} + C_8^{(9)\prime}$, $\tilde{C}_V^{(9)} \equiv C_7^{(9)} + C_9^{(9)} + C_7^{(9)\prime} + C_9^{(9)\prime}$. The LECs $g_{1,V}^{\pi N}$ and $\tilde{g}_V^{\pi N}$ were defined in Ref. [71], and they are $\mathcal{O}(1)$.

Finally, both scalar and vector operators induce nucleon-nucleon interactions. Following the definitions of Ref. [71] and again expanding in pion fields, we have

$$\begin{aligned}
\mathcal{L}_{NN} &= (\bar{p}n)\,(\bar{p}n) \left\{ \left[C_L^{NN} \frac{\bar{e}_L C \bar{e}_L^T}{v^5} + (L \leftrightarrow R)\right] + C_V^{NN}\, v^\mu \frac{\bar{e}\gamma_\mu\gamma_5 C\bar{e}^T}{v^5} \right\}, \\
c_{L,R}^{NN} &= g_1^{NN}\left(C_{1L,1R}^{(9)} + C_{1L,1R}^{(9)\prime}\right) + g_2^{NN}\left(C_{2L,2R}^{(9)} + C_{2L,2R}^{(9)\prime}\right) + g_3^{NN}\left(C_{3L,3R}^{(9)} + C_{3L,3R}^{(9)\prime}\right) \\
&\quad + g_4^{NN} C_{4L,4R}^{(9)} + g_5^{NN} C_{5L,5R}^{(9)}, \\
c_V^{NN} &= g_6^{NN} C_V^{(9)} + g_7^{NN} \tilde{C}_V^{(9)}. \qquad (3.34)
\end{aligned}$$

The scaling of the nucleon-nucleon couplings follows the NDA expectation for $g_{1,6,7}^{NN}$, while $g_{2,3,4,5}^{NN}$ need to be enhanced with respect to NDA in order to renormalize the $nn \to pp\,ee$ amplitude [71]. Explicitly, we have

$$g_{1,6,7}^{NN} = \mathcal{O}(1), \qquad g_{2,3,4,5}^{NN} = \mathcal{O}\left((4\pi)^2\right). \qquad (3.35)$$

Currently, only NDA estimates are available for the πN and NN LECs.

3.2.6 Chiral Lagrangian from the exchange of hard neutrinos

In addition to the long-range contributions originating from the exchange of potential neutrinos between nucleons, mediated by the currents in Eq. (3.26), the $0\nu\beta\beta$ half-lives receive corrections from short-range operators, induced by the insertions of two currents connected by the exchange of hard, virtual neutrinos. The origin of these contributions can be understood by considering the effective action induced by two insertions of the interactions in Eqs. (2.21) and (2.22)

$$iS_{\text{eff}} = -\frac{1}{2!}\int d^4x\, d^4y\, T\left\{\left[\mathcal{L}^{(6)}(x) + \mathcal{L}^{(7)}(x)\right]\left[\mathcal{L}^{(6)}(y) + \mathcal{L}^{(7)}(y)\right]\right\}. \qquad (3.36)$$

In terms of Eq. (3.36), the long-distance potential, derived in Sects. 3.2.2 and 3.2.3, arises from the region $|\mathbf{x}-\mathbf{y}| \gtrsim 1/k_F$ where factorizing the two interactions is a good approximation. These long-distance contributions do not necessarily capture the region where $|x-y| \lesssim 1/\Lambda_\chi$. In fact, as we will argue below, NDA and renormalization imply that this region contributes at leading order in several cases. In order to correctly describe $0\nu\beta\beta$, the constructed chiral Lagrangian should be able to reproduce the amplitudes that result from inserting S_{eff} between initial and final states. In cases where the $|x-y| \lesssim 1/\Lambda_\chi$ region is important, this implies that additional short-distance interactions, of the same form as those induced by the dim-9 operators, are needed at LO in the chiral Lagrangian.

Before discussing these contributions in generality, let us consider the amplitude $\langle h_f e_1 e_2 | S_{\text{eff}} | h_i\rangle$, where $h_{i,f}$ are hadronic states, for the example of the insertion of two vector operators. Since

we are interested in amplitudes without initial- or final-state neutrinos, the neutrino fields in $\mathcal{L}^{(6,7)}$ will be contracted among each other. Using this fact, and neglecting electron momenta, the Dirac algebra for the leptonic part can be performed, leading to

$$\begin{aligned}\langle h_f e_1 e_2|S_{\text{eff}}|h_i\rangle &= \sum_i \frac{m_i}{2v^4}\int d^4x d^4y \int \frac{d^4q}{(2\pi)^4}\frac{e^{-iq\cdot(x-y)}}{q^2-m_i^2+i\epsilon}\langle e_1 e_2|\bar{e}_R(x)e_R^c(x)|0\rangle \\ &\times\langle h_f|T\Big\{\left(C^{(6)}_{\text{VLR}}\right)^2_{ei}\bar{u}_L\gamma_\mu d_L(x)\,\bar{u}_L\gamma^\mu d_L(y)+\left(C^{(6)}_{\text{VRR}}\right)^2_{ei}\bar{u}_R\gamma_\mu d_R(x)\,\bar{u}_R\gamma^\mu d_R(y) \\ &+2\left(C^{(6)}_{\text{VRR}}\right)_{ei}\left(C^{(6)}_{\text{VLR}}\right)_{ei}\bar{u}_R\gamma_\mu d_R(x)\,\bar{u}_L\gamma^\mu d_L(y)\Big\}|h_i\rangle+(L\leftrightarrow R)+\ldots\end{aligned} \tag{3.37}$$

where the dots stand for terms proportional to other Wilson coefficients, as well as terms that arise from the $\not{q}$ term in the propagator. In this example, we will focus on the terms $\propto m_i$.

As mentioned above, Eq. (3.37) will induce operators of the same form as those induced by the dimension-nine operators. In particular, the $\left(C^{(6)}_{\text{VLR}}\right)^2$, $\left(C^{(6)}_{\text{VRR}}\right)^2$, and $C^{(6)}_{\text{VLR}}C^{(6)}_{\text{VRR}}$ terms transform as the O_1, O_1', and O_4 operators under chiral transformations. As a result, chiral symmetry allows the following non-derivative pionic Lagrangian

$$\mathcal{L}_{\pi\pi} \;=\; 2G_F^2F_\pi^2\sum_i m_i\, g_{\text{LR}}^{\pi\pi}(m_i)\,\text{Tr}[\mathcal{Q}_L\mathcal{Q}_R]\,\bar{e}_R C^{(6)}_{\text{VLR}}\left(C^{(6)}_{\text{VRR}}\right)^T e_R^c+(L\leftrightarrow R)\,, \tag{3.38}$$

where we introduced $\mathcal{Q}_L=u^\dagger\tau^+u$, $\mathcal{Q}_R=u\tau^+u^\dagger$. By NDA the LEC $g_{\text{LR}}^{\pi\pi}(m_i)$ is of order $\mathcal{O}(F_\pi^2)$, and we have explicitly given it a dependence on m_i. With this scaling, $g_{\text{LR}}^{\pi\pi}(m_i)$ contributes at LO to $0\nu\beta\beta$, meaning that the $|x-y|\lesssim 1/\Lambda_\chi$ region in Eq. (3.36) significantly contributes.

Very similar short-distance LECs are generated by the insertions of two electromagnetic currents, where hard virtual photons are exchanged instead of neutrinos. As explained in Refs. [93–95], this analogy can be made precise in the limit $m_i\to 0$, which allows for a relation between $g_{\text{LR}}^{\pi\pi}(0)$ and the pion mass splitting,

$$g_{\text{LR}}^{\pi\pi}(m_i=0)=\frac{m^2_{\pi^\pm}-m^2_{\pi^0}}{2e^2}\simeq 0.8F_\pi^2\,, \tag{3.39}$$

explicitly confirming the NDA expectations. The $\left(C^{(6)}_{\text{VLR,VRR}}\right)^2$ terms in principle give rise to pionic operators involving derivatives, which however induce subleading corrections to the long-distance neutrino potentials. None of the terms in Eq. (3.37) induce πN couplings at leading order and we neglect them here.

Additional interactions appear in the nucleon-nucleon sector. All combinations of couplings in Eq. (3.36) give rise to short-distance nucleon-nucleon couplings, which are expected at N^{2}LO by NDA. However, as discussed in Refs. [71, 93, 94], in the case of the standard mechanism and several dim-9 operators they must appear at LO to guarantee that $nn\to pp\,ee$ amplitudes are

properly renormalized and regulator independent. The chiral Lagrangian is given by

$$\begin{aligned}\mathcal{L}_{NN} &= \frac{1}{2}G_F^2\,\bar{e}_R e_R^c \sum_i m_i \\ &\times\Bigg\{ \left(C^{(6)}_{\text{VLR}}\right)^2_{ei} g_\nu^{\text{NN}}(m_i)\bar{N}\mathcal{Q}_L N\,\bar{N}\mathcal{Q}_L N + \left(C^{(6)}_{\text{VRR}}\right)^2_{ei} g_\nu^{\text{NN}}(m_i)\bar{N}\mathcal{Q}_R N\,\bar{N}\mathcal{Q}_R N \\ &+2\left(C^{(6)}_{\text{VRR}}\right)_{ei}\left(C^{(6)}_{\text{VRL}}\right)_{ei} g_{\text{LR}}^{\text{NN}}(m_i)\left(\bar{N}\mathcal{Q}_L N\,\bar{N}\mathcal{Q}_R N - \frac{1}{6}\text{Tr}(\mathcal{Q}_L\mathcal{Q}_R)\bar{N}\boldsymbol{\tau}N\cdot\bar{N}\boldsymbol{\tau}N\right)\Bigg\} \\ &+(L\leftrightarrow R)\,, \end{aligned} \tag{3.40}$$

where the $\left(C^{(6)}_{\text{VLR,VRR}}\right)^2$ terms are related by parity and therefore come with the same LEC. In addition, we omitted traces that vanish for the form of $\mathcal{Q}_{L,R}$ relevant for $0\nu\beta\beta$, but in principle could be non-zero for other isospin components. From NDA, one finds $g_i^{\text{NN}}(m_i)\sim\Lambda_\chi^{-2}$ which implies the short-range operators contribute at N^{2}LO. To absorb divergences in the scattering amplitudes, however, the scaling needs to be modified into $g_i^{\text{NN}}\sim F_\pi^{-2}$, so that the $g^{\text{NN}}_{\text{LR},\nu}$ operators in $\mathcal{L}_{NN}$ contribute at LO. The coupling g_ν^{NN} was already encountered in Refs. [93, 94], since it also appears in the standard mechanism.

We now discuss the general chiral Lagrangian induced by hard neutrino exchange. This involves other combinations of Wilson coefficients, as well as the terms induced by the $\propto \not{q}$ term in the neutrino propagator, both can be constructed along similar lines. The induced interactions will have the form of the $\pi\pi$, πN, and NN Lagrangians of Sect. 3.2.5 such that all of these effects can be captured by the couplings defined in that section. For the non-derivative pion couplings of Eq. (3.29) we have

$$\begin{aligned} C^{\pi\pi}_{i\,L,R} &= c^{\pi\pi}_{i\,L,R} + \frac{m_i v}{F_\pi^2} c^{\nu\pi\pi}_{i\,L,R}\,, \\ c^{\nu\pi\pi}_{i\,L} &= 2g^{\pi\pi}_{\text{LR}}(m_i)\left(C^{(6)}_{\text{VLL}}\right)_{ei}\left(C^{(6)}_{\text{VRL}}\right)_{ei} - 2g^{\pi\pi}_{\text{S1}}(m_i)\left[\left(C^{(6)}_{\text{SLR}}\right)^2_{ei} + \left(C^{(6)}_{\text{SRR}}\right)^2_{ei}\right] \\ &\quad +4g^{\pi\pi}_{\text{S2}}(m_i)\left(C^{(6)}_{\text{SLR}}\right)_{ei}\left(C^{(6)}_{\text{SRR}}\right)_{ei} - 2g^{\pi\pi}_{\text{TT}}(m_i)\left(C^{(6)}_{\text{TRR}}\right)^2_{ei} + c^{\nu\pi\pi\,7}_{i\,L}\,, \\ c^{\pi\pi}_{i\,L} &= c^{\pi\pi\,7}_{i\,L}, \qquad c^{\pi\pi}_{i\,R} = 0\,. \end{aligned} \tag{3.41}$$

Contributions from dim-7 operators are captured by $c^{(\nu)\pi\pi\,7}_{i\,L}$, which are discussed in Ref. [78], and all LECs scale as $g_i^{\pi\pi}=\mathcal{O}(F_\pi^2)$. The contributions that are explicitly proportional to m_i arise from choosing the $\sim m_i$ part of the neutrino propagator when performing the lepton contractions, as in Eq. (3.37). The remaining terms arise from the $\not{q}$ part of the propagator, but only contribute at the dim-7 level. The right-handed coupling $c^{\nu\pi\pi}_{i\,R}$ can be obtained from $c^{\nu\pi\pi}_{i\,L}$ by interchanging the L,R labels on the Wilson coefficients, $L\leftrightarrow R$, while leaving those on the LECs unchanged, and dropping $c^{\nu\pi\pi\,7}_{i\,L}$.

The derivative $\pi\pi$ couplings are given by

$$\begin{aligned} C'^{\pi\pi}_{i\,L,R} &= \frac{v}{\Lambda_\chi} c'^{\pi\pi}_{i\,L,R} + \frac{m_i}{\Lambda_\chi} c'^{\nu\pi\pi}_{i\,L,R}\,, \\ c'^{\pi\pi}_{i\,L} &= g^{\pi\pi}_{\text{S,VLL}}(m_i)\left[\left(C^{(6)}_{\text{SRR}}\right)_{ei}\left(C^{(6)}_{\text{VLL}}\right)_{ei} + \left(C^{(6)}_{\text{SLR}}\right)_{ei}\left(C^{(6)}_{\text{VRL}}\right)_{ei}\right] \\ &\quad -\frac{g^{\pi\pi}_{\text{T,VLL}}(m_i)}{4}\left(C^{(6)}_{\text{TRR}}\right)_{ei}\left(C^{(6)}_{\text{VLL}}\right)_{ei} + (\text{VLL}\leftrightarrow\text{VRL})\,, \\ c'^{\nu\pi\pi}_{i\,L} &= c'^{\nu\pi\pi\,7}_{i\,L}\,, \qquad c'^{\nu\pi\pi}_{i\,R} = 0\,, \end{aligned} \tag{3.42}$$

where $c'^{\pi\pi}_{i\,R}$ can again be obtained from $c'^{\pi\pi}_{i\,L}$ with the interchange $L \leftrightarrow R$ and $c'^{\nu\pi\pi\,7}_{i\,L}$ is given in Ref. [78]. The LECs related to these derivative couplings scale as $\mathcal{O}(1)$, one of which was already encountered in Ref. [71] where it was called $g_T^{\pi\pi} = \frac{m_N}{\Lambda_\chi} g^{\pi\pi}_{\mathrm{T,VLL}}(0)$. It should be noted that the terms proportional to $g^{\pi\pi}_{\mathrm{S,VLL}}$, $g^{\pi\pi}_{\mathrm{S,VRL}}$, and $g^{\pi\pi}_{\mathrm{S1,S2}}$ are generally suppressed by F_π^2/Λ_χ^2 compared to the long-distance amplitudes in the limit $m_i \to 0$. In this limit these pieces only significantly contribute if the pseudo-scalar and axial couplings, that induce the long-distance contribution, are suppressed compared to the scalar and vector couplings.

The pion-nucleon couplings of (3.33) can be written as,

$$\begin{aligned}
C^{\pi N}_{i\,L,R,V} &= c^{\pi N}_{i\,L,R,V} + \frac{m_i}{\Lambda_\chi} c^{\nu\pi N}_{i\,L,R,V}\,, \\
c^{\pi N}_{i\,L} &= \frac{v}{\Lambda_\chi}\Bigg\{ g^{\pi N}_{\mathrm{S,VLL}}(m_i)\left[\left(C^{(6)}_{\mathrm{SRR}}\right)_{ei}\left(C^{(6)}_{\mathrm{VLL}}\right)_{ei} + \left(C^{(6)}_{\mathrm{SLR}}\right)_{ei}\left(C^{(6)}_{\mathrm{VRL}}\right)_{ei}\right] \\
&\quad - \frac{g^{\pi N}_{\mathrm{T,VLL}}(m_i)}{2}\left(C^{(6)}_{\mathrm{TRR}}\right)_{ei}\left(C^{(6)}_{\mathrm{VLL}}\right)_{ei}\Bigg\} + (\mathrm{VLL} \leftrightarrow \mathrm{VRL})\,, \\
c^{\nu\pi N}_{i\,L} &= c^{\nu\pi N\,7}_{i\,L}\,, \qquad c^{\nu\pi N}_{i\,R} = 0\,, \\
c^{\pi N}_{i\,V} &= -\frac{1}{2}\frac{v}{\Lambda_\chi} g^{\pi N}_{\mathrm{VLL,VLR}}(m_i)\left[\left(C^{(6)}_{\mathrm{VLL}}\right)_{ei}\left(C^{(6)}_{\mathrm{VLR}}\right)_{ei} - (L \leftrightarrow R)\right]\,, \\
c^{\nu\pi N}_{i\,V} &= c^{\nu\pi N\,7}_{i\,V}\,,
\end{aligned} \tag{3.43}$$

where $g^{\pi N}_\alpha = \mathcal{O}(1)$, the right-handed coupling $c^{\pi N}_{i\,R}$ is given by $c^{\pi N}_{i\,L}$ with $L \leftrightarrow R$, and the dimension-7 contributions are again relegated to Ref. [78]. Several of the above LECs are connected to those of Ref. [71], for which we have $g^{\pi N}_{\mathrm{VLL,VLR}}(0) = g^{\pi N}_{\mathrm{VL}} \frac{\Lambda_\chi}{m_N}$ and $g^{\pi N}_{\mathrm{T,VLL}}(0) = g^{\pi N}_{\mathrm{T}} \frac{\Lambda_\chi}{m_N}$.

Finally, the contributions to the nucleon-nucleon couplings in Eq. (3.34) are given by,

$$
\begin{aligned}
C^{\rm NN}_{i\,L,R,V} &= c^{\rm NN}_{i\,L,R,V} + \frac{m_i}{\Lambda_\chi} c^{\nu{\rm NN}}_{i\,L,R,V}\,, \\
c^{NN}_{i\,L} &= \frac{v}{\Lambda_\chi}\Bigg\{ g^{\rm NN}_{\rm S,VLL}(m_i)\left[\left(C^{(6)}_{\rm SRR}\right)_{ei}\left(C^{(6)}_{\rm VLL}\right)_{ei} + \left(C^{(6)}_{\rm SLR}\right)_{ei}\left(C^{(6)}_{\rm VRL}\right)_{ei}\right] \\
&\quad - \frac{g^{\rm NN}_{\rm T,VLL}(m_i)}{2}\left(C^{(6)}_{\rm TRR}\right)_{ei}\left(C^{(6)}_{\rm VLL}\right)_{ei}\Bigg\} + ({\rm VLL}\leftrightarrow{\rm VRL}) + c^{\rm NN\,7}_{i\,L}\,, \\
\frac{c^{\nu NN}_{i\,L}}{v\Lambda_\chi} &= \frac{g^{\rm NN}_{\nu}(m_i)}{4}\left[\left(C^{(6)}_{\rm VLL}\right)^2_{ei} + \left(C^{(6)}_{\rm VRL}\right)^2_{ei}\right] + \frac{g^{\rm NN}_{\rm LR}(m_i)}{2}\left(C^{(6)}_{\rm VLL}\right)_{ei}\left(C^{(6)}_{\rm VRL}\right)_{ei} \\
&\quad + \frac{g^{\rm NN}_{\rm S1}(m_i)}{4}\left[\left(C^{(6)}_{\rm SRR}\right)^2_{ei} + \left(C^{(6)}_{\rm SLR}\right)^2_{ei}\right] - \frac{g^{\rm NN}_{\rm S2}(m_i)}{2}\left(C^{(6)}_{\rm SRR}\right)_{ei}\left(C^{(6)}_{\rm SLR}\right)_{ei} \\
&\quad + \frac{g^{\rm NN}_{\rm TT}(m_i)}{4}\left(C^{(6)}_{\rm TRR}\right)^2_{ei} + \frac{c^{\nu NN\,7}_{i\,L}}{v\Lambda_\chi}\,, \\
c^{NN}_{i\,V} &= -\frac{v}{\Lambda_\chi}\frac{g^{\rm NN}_{\rm VLL,VLR}(m_i)}{2}\left[\left(C^{(6)}_{\rm VLL}\right)_{ei}\left(C^{(6)}_{\rm VLR}\right)_{ei} - (L\leftrightarrow R)\right] \\
&\quad + \frac{v}{\Lambda_\chi} g^{\rm NN}_{\rm T,SRL}(m_i)\left[\left(C^{(6)}_{\rm TRR}\right)_{ei}\left(C^{(6)}_{\rm SRL}\right)_{ei} - (L\leftrightarrow R)\right] \\
&\quad + \frac{v}{\Lambda_\chi} g^{\rm NN}_{\rm T,SLL}(m_i)\left[\left(C^{(6)}_{\rm TRR}\right)_{ei}\left(C^{(6)}_{\rm SLL}\right)_{ei} - (L\leftrightarrow R)\right] + c^{NN\,7}_{i\,V}\,, \\
\frac{c^{\nu{\rm NN}}_{i\,V}}{v\Lambda_\chi} &= g^{\rm NN}_{\rm SLL,VLL}(m_i)\left[\left(C^{(6)}_{\rm SLL} + C^{(6)}_{\rm SRL}\right)_{ei}\left(C^{(6)}_{\rm VLL} + C^{(6)}_{\rm VRL}\right)_{ei} - (L\leftrightarrow R)\right] \\
&\quad + g^{\rm NN}_{\rm TLL,VLL}(m_i)\left[\left(C^{(6)}_{\rm TLL}\right)_{ei}\left(C^{(6)}_{\rm VLL} - C^{(6)}_{\rm VRL}\right)_{ei} - (L\leftrightarrow R)\right] + \frac{c^{\nu{\rm NN}\,7}_{i\,V}}{v\Lambda_\chi}\,. \qquad (3.44)
\end{aligned}
$$

The right-handed couplings $c^{\rm NN,\nu NN}_{i\,R}$ can be obtained from $c^{\rm NN,\nu NN}_{i\,L}$ by interchanging the L, R labels on the Wilson coefficients, $L \leftrightarrow R$, while leaving those on the LECs unchanged, and dropping $c^{\nu NN\,7}_{i\,L}$. By NDA, the LECs related to the $c^{\nu{\rm NN}}_i$ couplings scale as $g^{\rm NN}_i = \mathcal{O}(\Lambda_\chi^{-2})$ while those contributing to the $c^{\rm NN}_i$ couplings follow the scaling $g^{\rm NN}_i = \mathcal{O}(1)$.

3.2.7 Low energy constants

The LECs needed to construct the neutrino potential at LO, and their current determinations, are summarized in Table 3.1. The LECs that enter the neutron β decay operators discussed in Sect. 3.2.4 are well determined, either from experiment, as in the case of $g_{A,M}$, which appear in SM currents, or from lattice QCD, in the case of g_S, g_T and B. The one exception is g'_T, which contributes to the tensor current at recoil order and is not very important in β decays. The evaluation of this LEC could be pursued with the same methods discussed in Refs. [101–103]. The $\pi\pi$ couplings induced by dim-9 operators have been computed in Lattice QCD [100], with uncertainty better than 10%. The $\pi\pi$, πN, and NN couplings induced by dim-6 and dim-7 operators are functions of the neutrino mass. In the case of $g^{\pi\pi}_{\rm LR}$, both the small- and large-m_i behavior are known, allowing us to obtain a reliable interpolation formula, as we will discuss in Sect. 3.6. In several other cases, only the large m_i behavior is known. The calculation of these couplings as a function of m_i could use techniques similar to the Hubbard-Stratanovich transformation proposed in Ref. [104] for the $g^{\pi\pi}_{1,\ldots,5}$ couplings, with the difference that the scalar particle σ introduced in Ref. [104] is kept light. The determination of the pion-nucleon and

$n \to pe\nu$, $\pi \to e\nu$			$\pi\pi \to ee$: $\mathcal{O}^{(9)}$		
g_A	1.271 ± 0.002	[105]	$g_1^{\pi\pi}$	0.36 ± 0.02	[100]
g_S	1.02 ± 0.10	[102, 103]	$g_2^{\pi\pi}$	2.0 ± 0.2 GeV^2	[100]
g_M	4.7	[105]	$g_3^{\pi\pi}$	-0.62 ± 0.06 GeV^2	[100]
g_T	0.99 ± 0.03	[102, 103]	$g_4^{\pi\pi}$	-1.9 ± 0.2 GeV^2	[100]
$\lvert g_T' \rvert$	$\mathcal{O}(1)$		$g_5^{\pi\pi}$	-8.0 ± 0.6 GeV^2	[100]
B	2.7 GeV				
$n \to p\pi ee$: $\mathcal{O}^{(9)}$, $\mathcal{O}^{(6,7)} \otimes \mathcal{O}^{(6,7)}$			$\pi\pi \to ee$: $\mathcal{O}^{(6,7)} \otimes \mathcal{O}^{(6,7)}$		
$\lvert g_i^{\pi N} \rvert$	$\mathcal{O}(1)$		$\lvert g_{\mathrm{T,VLL}}^{\pi\pi} \rvert$, $\lvert g_{\mathrm{S,VLL}}^{\pi\pi} \rvert$, $\lvert g_{\mathrm{T,VRL}}^{\pi\pi} \rvert$, $\lvert g_{\mathrm{S,VRL}}^{\pi\pi} \rvert$	$\mathcal{O}(1)$	
			$\lvert g_{\mathrm{LR}}^{\pi\pi} \rvert$, $\lvert g_{\mathrm{S1,S2}}^{\pi\pi} \rvert$	$\mathcal{O}(F_\pi^2)$	
			$\lvert g_{\mathrm{TT}}^{\pi\pi} \rvert$, $\lvert g_{\mathrm{TL}}^{\pi\pi} \rvert$, $\lvert g_{\mathrm{TL,TR}}^{\pi\pi} \rvert$	$\mathcal{O}(F_\pi^2)$	
$nn \to pp\,ee$: $\mathcal{O}^{(9)}$			$nn \to pp\,ee$: $\mathcal{O}^{(6,7)} \otimes \mathcal{O}^{(6,7)}$		
$\lvert g_{1,6,7}^{NN} \rvert$	$\mathcal{O}(1)$		$\lvert g_{\mathrm{LR}}^{NN} \rvert$, $\lvert g_{\mathrm{S1}}^{NN} \rvert$	$\mathcal{O}(1/F_\pi^2)$	
$\lvert g_{2,3,4,5}^{NN} \rvert$	$\mathcal{O}((4\pi)^2)$		$\lvert g_{\mathrm{S2}}^{NN} \rvert$, $\lvert g_{\mathrm{TT}}^{NN} \rvert$, $\lvert g_{\mathrm{SLL,VLL}}^{NN} \rvert$	$\mathcal{O}(1/F_\pi^2)$	
			$\lvert g_{\mathrm{TLL,VLL}}^{NN} \rvert$, $\lvert g_{\mathrm{TL}}^{NN} \rvert$, $\lvert g_{\mathrm{TL,TR}}^{NN} \rvert$	$\mathcal{O}(1/F_\pi^2)$	
			$\lvert g_{\mathrm{TL,T}}^{NN} \rvert$, $\lvert g_{\mathrm{TR,T}}^{NN} \rvert$	$\mathcal{O}(1/\Lambda_\chi^2)$	
			$\lvert g_{\mathrm{S,VLL}}^{NN} \rvert$, $\lvert g_{\mathrm{T,VLL}}^{NN} \rvert$ $\lvert g_{\mathrm{VLL,VLR}}^{NN} \rvert$	$\mathcal{O}(1)$	
			$\lvert g_{\mathrm{S,VRL}}^{NN} \rvert$, $\lvert g_{\mathrm{T,VRL}}^{NN} \rvert$	$\mathcal{O}(1)$	
			$\lvert g_{\mathrm{T,SRL}}^{NN} \rvert$, $\lvert g_{\mathrm{T,SLL}}^{NN} \rvert$, $\lvert g_{\mathrm{TL,V}}^{NN} \rvert$, $\lvert g_{\mathrm{TR,V}}^{NN} \rvert$	$\mathcal{O}((4\pi)^2)$	
			g_ν^{NN}	-92.5 ± 46.2 GeV^{-2}	[106–108]

Table 3.1: The low-energy constants relevant for the dim-3, dim-6, dim-7, and dim-9 operators. The headings show the type of long-distance ($n \to pe\nu$, $\pi \to e\nu$) or short-distance processes the LECs induce, while the labels $\mathcal{O}^{(9)}$ and $\mathcal{O}^{(6,7)} \otimes \mathcal{O}^{(6,7)}$ indicate whether the corresponding LECs are induced by dim-9 operators or by the insertion of two dim-6(-7) interactions. Whenever known, we quote the values of the LECs at $\mu = 2$ GeV in the $\overline{\text{MS}}$ scheme.

nucleon-nucleon couplings, induced by dim-6, -7 and -9 operators, is much more uncertain. Nearly all the couplings require dedicated Lattice QCD calculations of LNV nucleon-nucleon scattering amplitudes. In the literature, the LECs in Table 3.1 are often estimated using uncontrolled assumptions such as "factorization" of the product of two weak currents. While this might be unavoidable at the moment, we will show that varying the LECs in a range suggested by their NDA scaling introduces uncertainties in the $0\nu\beta\beta$ half-lives that are as large as those in the nuclear matrix elements, and should not be neglected.

3.3 The $nn \to pp\,ee$ transition operator including sterile neutrinos

Now we consider the derivation of the $nn \to pp\,ee$ transition operator. This transition operator will be inserted between nuclear wave functions and is sometimes called the "neutrino potential". The transition operator is not necessarily due to the exchange of a neutrino as other mechanisms exist, for instance via the contact $\pi\pi ee$, $np\pi ee$ and $nnppee$ interactions discussed in Sect. 3.2.5 and 3.2.6. Such mechanisms have been discussed in detail in Ref. [71] and the derivation of the potential in the presence of sterile neutrinos amounts to generalizing the couplings $C^{(\prime)\pi\pi}$, $C^{\pi N}$ and C^{NN} as in Eq. (3.30), to include the contributions of hard-neutrino exchange. We therefore focus here on the neutrino potential arising from the exchange of a light neutrino, with mass below the chiral-breaking scale Λ_χ. In general the induced neutrino potential arises from the

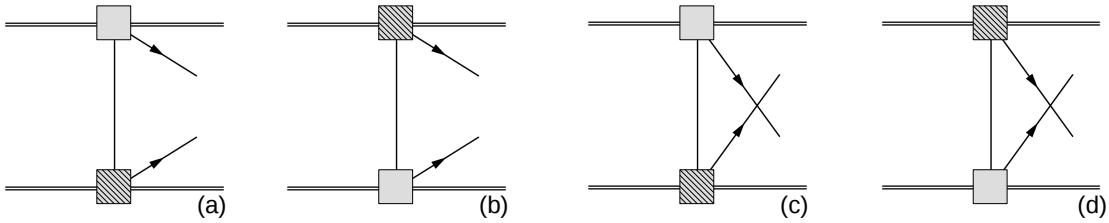

Figure 3.2: Tree-level contributions to the $0\nu\beta\beta$ transition operator arising from the exchange of a light neutrino. The notation for nucleons, electrons, and neutrinos is as in Fig. 3.1. The squares denote the nucleon vector, axial, scalar, pseudoscalar, and tensor form factors, which, at LO in chiral EFT, include one or both diagrams in Fig. 3.1. The currents acting on the two nucleons can be different, which we denoted by hatching one of the two squares. LNV arises from the mass of the neutrinos, which in general are Majorana eigenstates, or from the couplings of the neutrinos to the nucleons, which receive LNV contributions at $\overline{\text{dim-7}}$.

four diagrams in Fig. 3.2, where any combination of hadronic currents can be used. The top (bottom) incoming and outgoing nucleons have momenta p_1 (p_1') and p_2 (p_2'), respectively, and we define $q_{1,2} = p_{1,2} - p_{1,2}'$. The top (bottom) electron has outgoing four-momenta k_1 (k_2). In diagrams (a) and (b) the neutrino then carries momentum $q_{11} = q_1 - k_1 = -q_2 + k_2$. In diagrams (c) and (d) the neutrino carries momentum $q_{12} = q_1 - k_2 = -q_2 + k_1$. In most cases, we can neglect the electron momenta in the neutrino propagators and hadronic currents. In those cases, $q_{11} = q_{12} = q_1 = -q_2 \equiv q$. Finally, we define the notation $J_x(i)$, where $x = \{V, A, S, P, T_R, T_L\}$ and $i = \{1, 2\}$, that implies that the expression in Eq. (3.27) should be evaluated for nucleon i using the momenta p_i, p_i', and q_i.

We begin by studying the so-called standard mechanism of $0\nu\beta\beta$ which is the exchange of a light Majorana neutrino. We review how to derive the well-known form of the neutrino potential appearing in this scenario and how it is affected by the presence of additional sterile neutrinos that interact via left-handed currents. This warm-up calculation provides a useful guide towards obtaining the neutrino potential arising from other interactions. The calculation of the remaining terms is in principle straightforward, however, as it is rather lengthy we have checked our results by use of the MATHEMATICA package FEYNCALC [109, 110].

3.3.1 The standard mechanism with sterile neutrinos

We start by considering the $nn \to pp\,ee$ transition operator arising from potential neutrinos that interact via the $C_{\text{VLL}}^{(6)}$ term in Eq. (2.21). This term includes the SM weak interaction as can be seen from Eq. (2.23). We use the same vertex for the top and bottom nucleon propagators such that diagrams (a) and (b) add coherently and the resulting factor 2 is cancelled by the 1/2! from using the same vertex twice. Diagrams (a) and (b) then sum to

$$\begin{aligned} V_\nu^{(a)+(b)} &= i(\tau_1^+\tau_2^+)\sum_{i=1}^{n_L}\left(\frac{+2iG_F}{\sqrt{2}}C_{\text{VLL}}^{(6)}\right)_{ei}\left(\frac{-2iG_F}{\sqrt{2}}(C_{\text{VLL}}^{(6)})^T\right)_{ie} \times \frac{1}{2}\left[J_V^\mu(1) + J_A^\mu(1)\right] \\ &\quad \times\frac{1}{2}\left[J_V^\nu(2) + J_A^\nu(2)\right] \times \bar{u}(k_1)\gamma_\mu P_L \frac{i(\not{q}_{11} + m_i)}{q_{11}^2 - m_i^2}\gamma_\nu P_R u^c(k_2)\,, \end{aligned} \tag{3.45}$$

where $u(k_i)$ denotes an electron spinor with momenta k_i, and we introduced $n_L = N - n_H$, such that the sum runs over all neutrino eigenstates with masses below Λ_χ. The potential is related to the amplitude via $\mathcal{A} = -V$. This expression can be simplified into

$$\begin{aligned} V_\nu^{(a)+(b)} &= (\tau_1^+\tau_2^+)\frac{G_F^2}{2}\sum_{i=1}^{n_L}\left(C_{\text{VLL}}^{(6)}\right)_{ei}\left(C_{\text{VLL}}^{(6)}\right)_{ie}^T\left[J_V^\mu(1)+J_A^\mu(1)\right]\left[J_V^\nu(2)+J_A^\nu(2)\right] \\ &\quad\times\frac{m_i}{\mathbf{q}^2+m_i^2}\bar{u}(k_1)\gamma_\mu\gamma_\nu P_R u^c(k_2)+\dots\,, \end{aligned} \tag{3.46}$$

where the dots denote corrections proportional to the lepton momenta or nucleon energy which are suppressed by additional powers of ϵ_χ. Similarly, the remaining two diagrams sum to

$$\begin{aligned} V_\nu^{(c)+(d)} &= -(\tau_1^+\tau_2^+)\frac{G_F^2}{2}\sum_{i=1}^{n_L}\left(C_{\text{VLL}}^{(6)}\right)_{ei}\left(C_{\text{VLL}}^{(6)}\right)_{ie}^T\left[J_V^\mu(1)+J_A^\mu(1)\right]\left[J_V^\nu(2)+J_A^\nu(2)\right] \\ &\quad\times\frac{m_i}{\mathbf{q}^2+m_i^2}\bar{u}(k_2)\gamma_\mu\gamma_\nu P_R u^c(k_1)+\dots\,, \end{aligned} \tag{3.47}$$

where the overall sign difference is from exchanging the two electrons. Summing all diagrams then gives

$$\begin{aligned} V_\nu &= (\tau_1^+\tau_2^+)G_F^2\sum_{i=1}^{n_L}\left(C_{\text{VLL}}^{(6)}\right)_{ei}\left(C_{\text{VLL}}^{(6)}\right)_{ie}^T\left[J_V(1)+J_A(1)\right]\cdot\left[J_V(2)+J_A(2)\right] \\ &\quad\times\frac{m_i}{\mathbf{q}^2+m_i^2}\bar{u}(k_1)P_R u^c(k_2)+\dots \end{aligned} \tag{3.48}$$

The product of hadronic currents can be explicitly calculated from Eq. (3.27) and contains parity-even and parity-odd components. As the remaining part of V_ν is an even function of $\mathbf{q}$, only the parity-even parts contribute to the $0^+ \to 0^+$ transitions of experimental interest. The relevant hadronic currents are therefore

$$\begin{aligned} J_V(1)\cdot J_V(2) &= g_V^2(\mathbf{q}^2)-\frac{g_M^2(\mathbf{q})\mathbf{q}^2}{6m_N^2}\left(\boldsymbol{\sigma}_1\cdot\boldsymbol{\sigma}_2+\frac{1}{2}S^{(12)}\right), \\ J_A(1)\cdot J_A(2) &= -g_A^2\Bigg\{\boldsymbol{\sigma}_1\cdot\boldsymbol{\sigma}_2\left(\frac{g_A^2(\mathbf{q}^2)}{g_A^2}+\frac{g_P(\mathbf{q}^2)g_A(\mathbf{q}^2)\mathbf{q}^2}{3g_A^2m_N}+\frac{g_P^2(\mathbf{q}^2)\mathbf{q}^4}{12g_A^2m_N^2}\right) \\ &\quad -S^{(12)}\left(\frac{g_P(\mathbf{q}^2)g_A(\mathbf{q}^2)\mathbf{q}^2}{3g_A^2m_N}+\frac{g_P^2(\mathbf{q}^2)\mathbf{q}^4}{12g_A^2m_N^2}\right)\Bigg\}, \end{aligned} \tag{3.49}$$

where we have defined the tensor operator

$$S^{(12)} = \boldsymbol{\sigma}_1\cdot\boldsymbol{\sigma}_2 - 3\,\boldsymbol{\sigma}_1\cdot\hat{\mathbf{q}}\,\boldsymbol{\sigma}_2\cdot\hat{\mathbf{q}}\,. \tag{3.50}$$

It is useful to split the Fermi (F), Gamow-Teller (GT), and Tensor (T) operators into their separate contributions arising from vector, axial, pseudoscalar, and magnetic currents, as the corresponding nuclear matrix elements are reported in the literature. We define the combinations

$$\begin{aligned} h_{GT}(\mathbf{q}^2) &= h_{GT}^{AA}(\mathbf{q}^2)+h_{GT}^{AP}(\mathbf{q}^2)+h_{GT}^{PP}(\mathbf{q}^2)+h_{GT}^{MM}(\mathbf{q}^2)\,, \\ h_T(\mathbf{q}^2) &= h_T^{AP}(\mathbf{q}^2)+h_T^{PP}(\mathbf{q}^2)+h_T^{MM}(\mathbf{q}^2)\,. \end{aligned} \tag{3.51}$$

For the F, GT, and T functions, we have

$$\begin{aligned} h_F(\mathbf{q}^2) &= \frac{g_V^2(\mathbf{q}^2)}{g_V^2} \qquad h_{GT,T}^{AA}(\mathbf{q}^2) = \frac{g_A^2(\mathbf{q}^2)}{g_A^2}\,, \quad h_{GT}^{AP}(\mathbf{q}^2) = \frac{g_P(\mathbf{q}^2) g_A(\mathbf{q}^2)\mathbf{q}^2}{3 g_A^2 m_N}\,, \\ h_{GT}^{PP}(\mathbf{q}^2) &= \frac{g_P^2(\mathbf{q}^2)\mathbf{q}^4}{12 g_A^2 m_N^2}\,, \qquad h_{GT}^{MM}(\mathbf{q}^2) = \frac{g_M^2(\mathbf{q}^2)\mathbf{q}^2}{6 g_A^2 m_N^2}\,, \end{aligned} \tag{3.52}$$

and $h_T^{AP}(\mathbf{q}^2) = -h_{GT}^{AP}(\mathbf{q}^2)$, $h_T^{PP}(\mathbf{q}^2) = -h_{GT}^{PP}(\mathbf{q}^2)$, and $h_T^{MM}(\mathbf{q}^2) = h_{GT}^{MM}(\mathbf{q}^2)/2$.

We then obtain for the neutrino potential

$$\begin{aligned} V_\nu &= -(\tau_1^+\tau_2^+) g_A^2 G_F^2 \sum_{i=1}^{n_L} \left(C_{\rm VLL}^{(6)}\right)_{ei}^2 \left(\frac{m_i}{\mathbf{q}^2 + m_i^2}\right) \\ &\quad \times \left[-\frac{g_V^2}{g_A^2} h_F(\mathbf{q}^2) + \boldsymbol{\sigma}_1 \cdot \boldsymbol{\sigma}_2\, h_{GT}(\mathbf{q}^2) + S^{(12)}\, h_T(\mathbf{q}^2)\right] \times \bar{u}(k_1) P_R u^c(k_2)\,. \end{aligned} \tag{3.53}$$

This expression reduces to the familiar expression for the neutrino potential for the case of 3 light Majorana neutrinos. We set $n = 0$ and we turn off all higher-dimensional operators except for the active Majorana mass (which is formally a $\overline{\text{dim-5}}$ operator). In this limiting case, $C_{\rm VLL}^{(6)} = -2V_{ud}\, PU$ and

$$\sum_{i=1}^{n_L} \left(C_{\rm VLL}^{(6)}\right)_{ei}^2 \left(\frac{m_i}{\mathbf{q}^2 + m_i^2}\right) \simeq \frac{4V_{ud}^2}{\mathbf{q}^2} \left[PU m_\nu U^T P^T\right]_{ee} = \frac{4V_{ud}^2}{\mathbf{q}^2} (M_L^*)_{ee}\,, \tag{3.54}$$

where we used Eq. (2.16) and used $m_i \ll \mathbf{q}$. The neutrino potential becomes proportional to the Majorana mass of the active neutrinos and agrees with the usual result for the standard mechanism

3.3.2 The general neutrino transition operator with sterile neutrinos

The neutrino potentials arising from the other interactions in Eqs. (2.21) and (2.22) can be obtained in analogous fashion to the calculation in the previous subsection. We give here the results for all combinations of interactions that lead to a non-vanishing potential when the electron mass and momenta are neglected. The limited cases in which the first non-vanishing contribution to the transition operator involves lepton momenta are discussed in Ref. [82].

The neutrino potential can be divided into three separate leptonic structures

$$V = -(\tau_1^+\tau_2^+) g_A^2 G_F^2 \sum_{i=1}^{n_L} \frac{1}{\mathbf{q}^2 + m_i^2}\, \bar{u}(k_1) \left\{V_L\, P_R + V_R\, P_L + V_M\, \gamma^0\gamma^5\right\} u^c(k_2)\,. \tag{3.55}$$

We separate the structures

$$V_{L,R,M} = V_{L,R,M}^{(6)} + \frac{m_\pi}{v} V_{L,R,M}^{(7)} + \frac{\mathbf{q}^2 + m_i^2}{m_\pi^2} V_{L,R,M}^{(sd)}\,, \tag{3.56}$$

into three parts. The part with superscript (6) denotes contributions from the dim-6 operators

in Eq. (2.21) and is given by

$$
\begin{aligned}
V_L^{(6)} &= m_i \left(C_{\mathrm{VLL}}^{(6)} + C_{\mathrm{VRL}}^{(6)}\right)_{ei}^2 \left[-\frac{g_V^2}{g_A^2} h_F + \boldsymbol{\sigma}_1\cdot\boldsymbol{\sigma}_2\, h_{GT}^{MM} + S^{(12)}\, h_T^{MM}\right] \\
&\quad + m_i \left(C_{\mathrm{VLL}}^{(6)} - C_{\mathrm{VRL}}^{(6)}\right)_{ei}^2 \left[\boldsymbol{\sigma}_1\cdot\boldsymbol{\sigma}_2\,(h_{GT}^{AA} + h_{GT}^{AP} + h_{GT}^{PP}) + S^{(12)}\,(h_T^{AP} + h_T^{PP})\right] \\
&\quad + m_i \left(C_{\mathrm{SRR}}^{(6)} + C_{\mathrm{SLR}}^{(6)}\right)_{ei}^2 \frac{g_S^2}{g_A^2} h_F \\
&\quad + m_i \left(C_{\mathrm{SRR}}^{(6)} - C_{\mathrm{SLR}}^{(6)}\right)_{ei}^2 \frac{B^2}{2m_\pi^2} \left[\boldsymbol{\sigma}_1\cdot\boldsymbol{\sigma}_2\,(h_{GT}^{AP} + 2h_{GT}^{PP}) + S^{(12)}\,(h_T^{AP} + 2h_T^{PP})\right] \\
&\quad - m_i \left(C_{\mathrm{TRR}}^{(6)}\right)_{ei}^2 \boldsymbol{\sigma}_1\cdot\boldsymbol{\sigma}_2 \frac{16 g_T^2}{g_A^2} h_{GT}^{AA} \\
&\quad - B \left(C_{\mathrm{VLL}}^{(6)} - C_{\mathrm{VRL}}^{(6)}\right)_{ei} \left(C_{\mathrm{SRR}}^{(6)} - C_{\mathrm{SLR}}^{(6)}\right)_{ei} \left[\boldsymbol{\sigma}_1\cdot\boldsymbol{\sigma}_2\,(h_{GT}^{AP} + 2h_{GT}^{PP}) + S^{(12)}\,(h_T^{AP} + 2h_T^{PP})\right] \\
&\quad + m_N \left(C_{\mathrm{VLL}}^{(6)} + C_{\mathrm{VRL}}^{(6)}\right)_{ei} \left(C_{\mathrm{TRR}}^{(6)}\right)_{ei} \left[\frac{16 g_T}{g_M}\left(\boldsymbol{\sigma}_1\cdot\boldsymbol{\sigma}_2\, h_{GT}^{MM} + S^{(12)}\, h_T^{MM}\right)\right. \\
&\quad \left. - 4\frac{g_T' g_V}{g_A^2}\frac{\mathbf{q}^2}{m_N^2} h_F\right], \qquad (3.57)
\end{aligned}
$$

$$
V_R^{(6)} = V_L^{(6)}\big|_{L\leftrightarrow R}, \qquad (3.58)
$$

$$
\begin{aligned}
V_M^{(6)} &= m_N \left(C_{\mathrm{VLL}}^{(6)} C_{\mathrm{VLR}}^{(6)} - L\leftrightarrow R\right)_{ei} \frac{4 g_A}{g_M} \left[\boldsymbol{\sigma}_1\cdot\boldsymbol{\sigma}_2\, h_{GT}^{MM} + S^{(12)}\, h_T^{MM}\right] \\
&\quad - m_i \left[\left(C_{\mathrm{VLL}}^{(6)} + C_{\mathrm{VRL}}^{(6)}\right)_{ei} \left(C_{\mathrm{SLL}}^{(6)} + C_{\mathrm{SRL}}^{(6)}\right)_{ei} - L\leftrightarrow R\right] \frac{g_S g_V}{g_A^2} h_F \\
&\quad - m_i \left[\left(C_{\mathrm{VLL}}^{(6)} - C_{\mathrm{VRL}}^{(6)}\right)_{ei} \left(C_{\mathrm{TLL}}^{(6)}\right)_{ei} - L\leftrightarrow R\right] \frac{2 g_T}{g_A} \left[\boldsymbol{\sigma}_1\cdot\boldsymbol{\sigma}_2\,(2h_{GT}^{AA} + h_{GT}^{AP}) + S^{(12)}\, h_T^{AP}\right] \\
&\quad + B \left[\left(C_{\mathrm{SRR}}^{(6)} - C_{\mathrm{SLR}}^{(6)}\right)_{ei} \left(C_{\mathrm{TLL}}^{(6)}\right)_{ei} - L\leftrightarrow R\right] \frac{2 g_T}{g_A} \left[\boldsymbol{\sigma}_1\cdot\boldsymbol{\sigma}_2\, h_{GT}^{AP} + S^{(12)}\, h_T^{AP}\right]. \qquad (3.59)
\end{aligned}
$$

Instead, $V_{L,R,M}^{(7)}$ arise from the dim-7 operators in Eq. (2.22). As these terms are parametrically suppressed by a power of m_π/v or Λ_χ/v, we refer to Ref. [78] for details.

Finally, the short-distance part of the potentials, $V_{L,R,M}^{(sd)}$, are induced by dimension-nine operators as well as the exchange of hard neutrinos, see Sects. 3.2.5 and 3.2.6, they are given by,

$$
\begin{aligned}
V_L^{(sd)} &= -4\frac{m_\pi^2}{v}\left\{\left(\frac{C_L^{\pi\pi}}{m_\pi^2} + C_L'^{\pi\pi}\right)\left[\left(\frac{h_{GT}^{AP}}{2} + h_{GT}^{PP}\right)\boldsymbol{\sigma}_1\cdot\boldsymbol{\sigma}_2 + \left(\frac{h_T^{AP}}{2} + h_T^{PP}\right) S^{(12)}\right]\right. \\
&\quad \left. + \frac{C_L^{\pi N} - C_L'^{\pi\pi}}{2}\left(h_{GT}^{AP}\,\boldsymbol{\sigma}_1\cdot\boldsymbol{\sigma}_2 + h_T^{AP} S^{(12)}\right) - \frac{2}{g_A^2} C_L^{NN} h_F\right\}, \\
V_R^{(sd)} &= V_L^{(sd)}\big|_{L\leftrightarrow R}, \\
V_M^{(sd)} &= -4\frac{m_\pi^2}{v}\left\{\frac{C_V^{\pi N}}{2}\left(h_{GT}^{AP}\,\boldsymbol{\sigma}_1\cdot\boldsymbol{\sigma}_2 + h_T^{AP} S^{(12)}\right) - \frac{2}{g_A^2} C_V^{NN} h_F\right\}. \qquad (3.60)
\end{aligned}
$$

[111]	^{76}Ge	^{82}Se	^{130}Te	^{136}Xe
G_{01}	0.22	1.	1.4	1.5
G_{04}	0.19	0.86	1.1	1.2
G_{06}	0.33	1.1	1.7	1.8
G_{09}	0.48	2.	2.8	2.8
Q/MeV [112]	2.04	3.0	2.5	2.5

Table 3.2: Phase space factors in units of 10^{-14} yr^{-1} obtained in Ref. [111]. The last row shows the Q value of $0\nu\beta\beta$ for various isotopes, where $Q = M_i - M_f - 2m_e$.

3.4 The neutrinoless double beta decay master formula including sterile neutrinos

The $nn \to pp\,ee$ amplitude is defined by

$$\mathcal{A} = \langle 0^+ | \sum_{m,n} \int \frac{d^3\mathbf{q}}{(2\pi)^3} e^{i\mathbf{q}\cdot\mathbf{r}} V(\mathbf{q}^2) |0^+\rangle \,, \tag{3.61}$$

where $V(\mathbf{q}^2)$ are the neutrino potentials from the previous section, and the sum extends over all the nucleons in the nucleus. $\mathbf{r} = \mathbf{r}_n - \mathbf{r}_m$ is the distance between nucleons m and n and $|\mathbf{r}| = r$, and the potentials are inserted between the 0^+ initial- and final-state nuclei of experimental interest. The leptonic part of the neutrino potentials can be taken outside of the nuclear wave functions and we define

$$\begin{aligned}
\mathcal{A} = \frac{g_A^2 G_F^2 m_e}{\pi R_A} \quad \times \quad & \left\{ \left[\sum_{i=1}^{n_L} \mathcal{A}_L(m_i) + \sum_{i=n_L+1}^{N} \mathcal{A}_L^{(9)}(m_i) \right] \bar{u}(k_1) P_R u^c(k_2) \right. \\
& + \left[\sum_{i=1}^{n_L} \mathcal{A}_R(m_i) + \sum_{i=n_L+1}^{N} \mathcal{A}_R^{(9)}(m_i) \right] \bar{u}(k_1) P_L u^c(k_2) \\
& \left. + \left[\sum_{i=1}^{n_L} \mathcal{A}_M(m_i) + \sum_{i=n_L+1}^{N} \mathcal{A}_M^{(9)}(m_i) \right] \bar{u}(k_1) \gamma^0 \gamma^5 u^c(k_2) \right\} \\
\equiv \frac{g_A^2 G_F^2 m_e}{\pi R_A} \quad \times \quad & \left[\mathcal{A}_L\, \bar{u}(k_1) P_R u^c(k_2) + \mathcal{A}_R\, \bar{u}(k_1) P_L u^c(k_2) + \mathcal{A}_M\, \bar{u}(k_1) \gamma^0 \gamma^5 u^c(k_2) \right]
\end{aligned} \tag{3.62}$$

where $R_A = 1.2\, A^{1/3}$ fm is the nuclear radius in terms of the atomic number A and $\bar{u}(k_{1,2})$ denote the spinors of the outgoing electrons. This factor is introduced to align the definitions of the NMEs to those in the literature. The subamplitudes $\mathcal{A}_{L,R,M}(m_i)$ and $\mathcal{A}^{(9)}_{L,R,M}(m_i)$ depend on nuclear and hadronic matrix elements, the neutrino masses, and the Wilson coefficients of the higher-dimensional operators. They are discussed in detail below. We have explicitly separated contributions from light neutrinos (with masses $m_i < \Lambda_\chi$) and heavy neutrinos ($m_i > \Lambda_\chi$).

With the definitions of the amplitudes in Eqs. (3.61) and (3.62), we express the inverted half-life for $0^+ \to 0^+$ transitions as

$$\begin{aligned}
\left(T_{1/2}^{0\nu}\right)^{-1} \quad = \quad & g_A^4 \Big\{ G_{01} \left(|\mathcal{A}_L|^2 + |\mathcal{A}_R|^2 \right) - 2(G_{01} - G_{04}) \mathrm{Re} \mathcal{A}_L^* \mathcal{A}_R \\
& + G_{09} \, |\mathcal{A}_M|^2 + G_{06} \, \mathrm{Re} \left[(\mathcal{A}_L - \mathcal{A}_R) \mathcal{A}_M^* \right] \Big\} \,.
\end{aligned} \tag{3.63}$$

Here G_{0j} are electronic phase-space factors given in Table 3.2 that have been calculated in the literature [111, 113, 114].

The subamplitudes depend on a product of Wilson coefficients and hadronic and nuclear matrix elements. To keep the expressions somewhat compact, we list here only the contributions from the standard mechanism and dim-6 interactions. Contributions from dim-7 interactions can be found in Ref. [78]. The amplitude $\mathcal{A}_L$, which includes the standard mechanism, is given by

$$\begin{aligned}\mathcal{A}_L(m_i) &= -\frac{1}{4m_e}\Bigg\{ m_i\mathcal{M}_V(m_i)\left(C^{(6)}_{\mathrm{VLL}}+C^{(6)}_{\mathrm{VRL}}\right)^2_{ei} + m_i\mathcal{M}_A(m_i)\left(C^{(6)}_{\mathrm{VLL}}-C^{(6)}_{\mathrm{VRL}}\right)^2_{ei} \\ &\quad +\mathcal{M}_{PS}(m_i)\left[m_i\frac{B^2}{m_\pi^2}\left(C^{(6)}_{\mathrm{SRR}}-C^{(6)}_{\mathrm{SLR}}\right)_{ei} - 2B\left(C^{(6)}_{\mathrm{VLL}}-C^{(6)}_{\mathrm{VRL}}\right)_{ei}\right]\left(C^{(6)}_{\mathrm{SRR}}-C^{(6)}_{\mathrm{SLR}}\right)_{ei} \\ &\quad +m_i\mathcal{M}_S(m_i)\left(C^{(6)}_{\mathrm{SRR}}+C^{(6)}_{\mathrm{SLR}}\right)^2_{ei} - m_i\mathcal{M}_T(m_i)\left(C^{(6)}_{\mathrm{TRR}}\right)^2_{ei} \\ &\quad +m_N\mathcal{M}_{TV}(m_i)\left(C^{(6)}_{\mathrm{VLL}}+C^{(6)}_{\mathrm{VRL}}\right)_{ei}\left(C^{(6)}_{\mathrm{TRR}}\right)_{ei}\Bigg\} + \mathcal{A}^{(\nu)}_L(m_i)\,, \end{aligned} \tag{3.64}$$

where $\mathcal{M}_i(m_i)$ are combinations of LECs and NMEs defined below and $B=\frac{m_\pi^2}{m_u+m_d}$ is an LEC introduced in Sect. 3.2.2, also see Table 3.1. Most of the terms above describe the long-distance contributions, while $\mathcal{A}^{(\nu)}_L$ is due to the exchange of hard neutrinos and given by

$$\begin{aligned}\mathcal{A}^{(\nu)}_L(m_i) &= \frac{m_\pi^2}{m_e v}\Bigg[\left(\frac{C^{\pi\pi}_{i\,L}}{m_\pi^2}+C'^{\pi\pi}_{i\,L}\right)\mathcal{M}_{PS,sd} + \frac{C^{\pi N}_{i\,L}-C'^{\pi\pi}_{i\,L}}{2}\left(M^{AP}_{GT,\,sd}+M^{AP}_{T,\,sd}\right) \\ &\quad -\frac{2}{g_A^2}C^{NN}_{i\,L}M_{F,\,sd}\Bigg]\,, \end{aligned} \tag{3.65}$$

where the subscript 'sd' on the NMEs refers to their short-distance nature and the combinations of couplings, $C^{\alpha}_{i,\beta}$, are defined in Sect. 3.2.6. The subamplitude for right-handed electrons, which does not appear for the standard mechanism, has a very similar structure. At the dim-6 level, this amplitude can be obtained by exchanging $L\leftrightarrow R$

$$\mathcal{A}_R(m_i) = \mathcal{A}_L(m_i)\big|_{L\leftrightarrow R}\,, \tag{3.66}$$

where $\mathcal{A}^{(\nu)}_R(m_i)$ can be obtained by replacing $C^{\alpha}_{i\,L}\to C^{\alpha}_{i\,R}$ in Eq. (3.65). Once dim-7 operators are included there appear differences between $\mathcal{A}_L(m_i)$ and $\mathcal{A}_R(m_i)$ due to the dim-7 tensor operators. We refer to Ref. [78] for the explicit formulae.

The "magnetic" subamplitude $\mathcal{A}_M$ is given by

$$\begin{aligned}\mathcal{A}_M(m_i) &= \frac{1}{2m_e}\Bigg\{ -m_N\mathcal{M}_{VA}(m_i)\left(C^{(6)}_{\mathrm{VLL}}\right)_{ei}\left(C^{(6)}_{\mathrm{VLR}}\right)_{ei} \\ &\quad +\frac{1}{2}m_i\mathcal{M}_S(m_i)\frac{g_V}{g_S}\left(C^{(6)}_{\mathrm{VLL}}+C^{(6)}_{\mathrm{VRL}}\right)_{ei}\left(C^{(6)}_{\mathrm{SLL}}+C^{(6)}_{\mathrm{SRL}}\right)_{ei} \\ &\quad +m_i\mathcal{M}_{TA}(m_i)\left(C^{(6)}_{\mathrm{VLL}}-C^{(6)}_{\mathrm{VRL}}\right)_{ei}\left(C^{(6)}_{\mathrm{TLL}}\right)_{ei} \\ &\quad +\mathcal{M}_{TP}(m_i)B\left(C^{(6)}_{\mathrm{SLL}}-C^{(6)}_{\mathrm{SRL}}\right)_{ei}\left(C^{(6)}_{\mathrm{TRR}}\right)_{ei} - (L\leftrightarrow R)\Bigg\} + \mathcal{A}^{(\nu)}_M(m_i)\,. \end{aligned} \tag{3.67}$$

Here $\mathcal{A}_M^{(\nu)}(m_i)$ again describes the contributions from hard neutrinos,

$$\mathcal{A}_M^{(\nu)} = \frac{m_\pi^2}{m_e v}\left[-\frac{2}{g_A^2}C_{iV}^{NN}\,M_{F,\,sd} + \frac{1}{2}C_{iV}^{\pi N}\left(M_{GT,\,sd}^{AP} + M_{T,\,sd}^{AP}\right)\right]. \tag{3.68}$$

Finally, we have the subamplitudes related to heavy neutrinos. Since they are induced by the same $\pi\pi$, πN, and NN interactions as those arising from hard-neutrino exchange, the resulting amplitudes are very similar to those mentioned above. In particular, one can obtain the dim-9 amplitudes using the following replacements,

$$\mathcal{A}_{L,R,V}^{(9)} = \mathcal{A}_{L,R,V}^{(\nu)}(m_i)\Big|_{C_{i\,L,R,V}^{\beta}\to c_{L,R,V}^{\beta}}. \tag{3.69}$$

The combinations of couplings c_α^β are defined in Sect. 3.2.5.

In the above expressions we have defined the combinations of NMEs and LECs

$$\begin{aligned}
\mathcal{M}_V(m_i) &= -\frac{g_V^2}{g_A^2}M_F(m_i) + M_{GT}^{MM}(m_i) + M_T^{MM}(m_i)\,,\\
\mathcal{M}_A(m_i) &= M_{GT}^{AA}(m_i) + M_{GT}^{AP}(m_i) + M_{GT}^{PP}(m_i) + M_T^{AP}(m_i) + M_T^{PP}(m_i)\,,\\
\mathcal{M}_{PS}(m_i) &= \frac{1}{2}M_{GT}^{AP}(m_i) + M_{GT}^{PP}(m_i) + \frac{1}{2}M_T^{AP}(m_i) + M_T^{PP}(m_i)\,,\\
\mathcal{M}_{PS,sd} &= \frac{1}{2}M_{GT,\,sd}^{AP}(0) + M_{GT,\,sd}^{PP}(0) + \frac{1}{2}M_{T,\,sd}^{AP}(0) + M_{T,\,sd}^{PP}(0)\,,\\
\mathcal{M}_S(m_i) &= \frac{g_S^2}{g_A^2}M_F(m_i)\,,\\
\mathcal{M}_T(m_i) &= 16\frac{g_T^2}{g_A^2}M_{GT}^{AA}(m_i)\,,
\end{aligned} \tag{3.70}$$

which arise from the insertions of the same currents on the nucleon lines, and the combinations

$$\begin{aligned}
\mathcal{M}_{T\,V}(m_i) &= -4\frac{g_T' g_V}{g_A^2}\frac{m_\pi^2}{m_N^2}M_{F,\,sd}(m_i) + \frac{16 g_T}{g_M}\left[M_{GT}^{MM}(m_i) + M_T^{MM}(m_i)\right]\,,\\
\mathcal{M}_{V\,A}(m_i) &= 2\frac{g_A}{g_M}\left[M_{GT}^{MM}(m_i) + M_T^{MM}(m_i)\right]\,,\\
\mathcal{M}_{V\,S}(m_i) &= \frac{g_V g_S}{g_A^2}M_F(m_i)\,,\\
\mathcal{M}_{T\,A}(m_i) &= \frac{g_T}{g_A}\left[2M_{GT}^{AA}(m_i) + M_{GT}^{AP}(m_i) + M_T^{AP}(m_i)\right]\,,\\
\mathcal{M}_{T\,P}(m_i) &= \frac{g_T}{g_A}\left[M_{GT}^{AP}(m_i) + M_T^{AP}(m_i)\right]\,,
\end{aligned} \tag{3.71}$$

which appear when two different currents interfere. We explicitly denoted the dependence on the neutrino mass in Eqs. (3.70) and (3.71).

3.5 Nuclear matrix elements

While the expressions for the subamplitudes given in the previous section look complex, they actually only depend on a relatively small set of structures. It is useful to introduce the Fourier-

transformed functions in r-space

$$\begin{aligned} h_K^{ab}(r, m_i) &= \frac{2}{\pi} R_A \int_0^\infty d|\mathbf{q}| \frac{\mathbf{q}^2}{\mathbf{q}^2 + m_i^2} h_K^{ab}(\mathbf{q}^2)\, j_\lambda(|\mathbf{q}|r)\,, \\ h_{K,\,sd}^{ab}(r, m_i) &= \frac{2}{\pi} \frac{R_A}{m_\pi^2} \int_0^\infty d|\mathbf{q}| \frac{\mathbf{q}^4}{\mathbf{q}^2 + m_i^2} h_K^{ab}(\mathbf{q}^2)\, j_\lambda(|\mathbf{q}|r)\,, \end{aligned} \tag{3.72}$$

where $j_\lambda(|\mathbf{q}|r)$ are spherical Bessel functions, and the functions $h_K^{ab}(\mathbf{q}^2)$ are defined in Eq. (3.52) for $K = \{F, GT, T\}$, and $ab = \{AA, AP, PP, MM\}$ for $K = GT$, $ab = \{AP, PP, MM\}$ for $K = T$, while for $K = F$ the ab superscript should be ignored. Finally, $\lambda = 0$ for $K = \{F, GT\}$ and $\lambda = 2$ for $K = T$. The factor of R_A in Eq. (3.72) cancels against the $1/R_A$ in Eq. (3.62). Note that the $h_{K,\,sd}^{ij}(r, m_i)$ are normalized using a factor of m_π^{-2} instead of $(m_N m_e)^{-1}$ as was done in Ref. [115]. Apart from this rescaling, these definitions agree with the literature once we neglect the energy of the intermediate states, which is a subleading correction in chiral EFT.

We define the nuclear matrix elements (NMEs) from these functions via

$$\begin{aligned} M_{F,\,(sd)}(m_i) &= \langle 0^+| \sum_{m,n} h_{F,\,(sd)}(r, m_i) \tau^{+(m)} \tau^{+(n)} |0^+\rangle\,, \\ M_{GT,\,(sd)}^{ab}(m_i) &= \langle 0^+| \sum_{m,n} h_{GT,\,(sd)}^{ab}(r, m_i)\, \boldsymbol{\sigma}^{(m)} \cdot \boldsymbol{\sigma}^{(n)}\, \tau^{+(m)} \tau^{+(n)} |0^+\rangle\,, \\ M_{T,\,(sd)}^{ab}(m_i) &= \langle 0^+| \sum_{m,n} h_{T,\,(sd)}^{ab}(r, m_i)\, S^{(mn)}(\hat{\mathbf{r}})\, \tau^{+(m)} \tau^{+(n)} |0^+\rangle\,, \end{aligned} \tag{3.73}$$

where the tensor in coordinate space is defined as

$$S^{(mn)}(\hat{\mathbf{r}}) = -\left(\boldsymbol{\sigma}^{(m)} \cdot \boldsymbol{\sigma}^{(n)} - 3\, \boldsymbol{\sigma}^{(m)} \cdot \hat{\mathbf{r}}\, \boldsymbol{\sigma}^{(n)} \cdot \hat{\mathbf{r}}\right)\,. \tag{3.74}$$

The set of NMEs have been calculated with various nuclear many-body methods and for different isotopes in the limit $m_i \to 0$. We use calculations in the quasi-particle random phase approximation (QRPA) [115], the Shell Model [116], and the interacting boson model [117, 118] and their values are given in Table 3.3. We focus on these particular calculations because, in those works, the results were presented in terms of the different components (i.e. AA, AP, PP, MM) of the F, GT, and T long- and short-distance matrix elements. At leading order in Chiral EFT, not all NMEs are independent. The momentum dependence of $g_V(\mathbf{q}^2)$ and $g_A(\mathbf{q}^2)$ is a higher-order effect in χPT. Neglecting this dependence gives leading-order relations such as

$$M_{GT,\,sd}^{AA}(0) = -3 M_{F,\,sd}(0)\,. \tag{3.75}$$

3.5.1 Interpolation formulae

To calculate $0\nu\beta\beta$ decay rates when sterile neutrinos are present, we require an understanding of the m_i dependence of the NMEs. For certain linear combinations of the NMEs given above, this mass dependence has been explicitly calculated [119, 120], but the results are often not split up as in Table 3.3. Furthermore, in certain cases we also require the derivative of the NMEs with respect to the neutrino masses. Inspired by Ref. [120], we therefore construct an interpolation formula for the m_i dependence of the NMEs. For most NMEs, we know the behavior in the small and large neutrino-mass limits. For instance, for $M_F(m_i)$ we have

$$\lim_{m_i \to 0} M_F(m_i) = M_F\,, \qquad \lim_{m_i \to \infty} M_F(m_i) = \frac{m_\pi^2}{m_i^2} M_{F,\,sd}\,. \tag{3.76}$$

NMEs	^{76}Ge			^{82}Se		^{130}Te		^{136}Xe	
	[115]	[116]	[117, 118]	[115]	[116]	[115]	[116]	[115]	[116]
M_F	-1.74	-0.59	-0.68	-1.29	-0.55	-1.52	-0.67	-0.89	-0.54
M_{GT}^{AA}	5.48	3.15	5.06	3.87	2.97	4.28	2.97	3.16	2.45
M_{GT}^{AP}	-2.02	-0.94	-0.92	-1.46	-0.89	-1.74	-0.97	-1.19	-0.79
M_{GT}^{PP}	0.66	0.30	0.24	0.48	0.28	0.59	0.31	0.39	0.25
M_{GT}^{MM}	0.51	0.22	0.17	0.37	0.20	0.45	0.23	0.31	0.19
M_T^{AA}	–	–	–	–	–	–	–	–	–
M_T^{AP}	-0.35	-0.01	-0.31	-0.27	-0.01	-0.50	0.01	-0.28	0.01
M_T^{PP}	0.10	0.00	0.09	0.08	0.00	0.16	-0.01	0.09	-0.01
M_T^{MM}	-0.04	0.00	-0.04	-0.03	0.00	-0.06	0.00	-0.03	0.00
$M_{F,\,sd}$	-3.46	-1.46	-1.1	-2.53	-1.37	-2.97	-1.61	-1.53	-1.28
$M_{GT,\,sd}^{AA}$	11.1	4.87	3.62	7.98	4.54	10.1	5.31	5.71	4.25
$M_{GT,\,sd}^{AP}$	-5.35	-2.26	-1.37	-3.82	-2.09	-4.94	-2.51	-2.80	-1.99
$M_{GT,\,sd}^{PP}$	1.99	0.82	0.42	1.42	0.77	1.86	0.92	1.06	0.74
$M_{T,\,sd}^{AP}$	-0.85	-0.05	-0.97	-0.65	-0.05	-1.50	0.07	-0.92	0.05
$M_{T,\,sd}^{PP}$	0.32	0.02	0.38	0.24	0.02	0.58	-0.02	0.36	-0.02

Table 3.3: Comparison of NMEs computed in the quasi-particle random phase approximation [115], shell model [116], and interacting boson model [117, 118] for several nuclei of experimental interest. All NMEs are evaluated at $m_i = 0$. The NMEs are defined in Eq. (3.73).

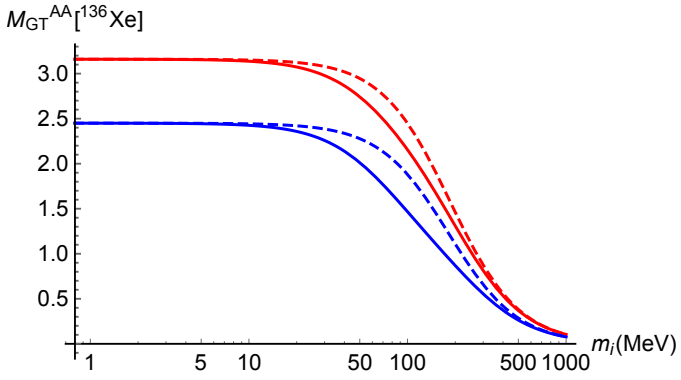

Figure 3.3: The NME $M_{GT}^{AA}(m_i)$ for ^{136}Xe from the interpolation formula in Eq. (3.77) (dashed) and Eq. (3.79) (solid) using the quasi-particle random phase approximation [115] (red) and the Shell Model [116] (blue).

Note that when we give an NME without an (m_i) dependence, it is implied that it is an NME given in Table 3.3 corresponding to $m_i = 0$. We stress that the meaning of an NME becomes ambiguous for $m_i \gtrsim \Lambda_\chi$. For example, in the standard mechanism, the contributions are proportional to the NME $\mathcal{M}_V + \mathcal{M}_A$. However, for large neutrino masses, $m_i \gtrsim \Lambda_\chi$, the neutrino mass eigenstate should be integrated our before matching onto χEFT, which would contribute via the dim-9 operators in Eqs. (3.9)-(3.11), and its effects are no longer captured by $\mathcal{M}_V + \mathcal{M}_A$ alone. This implies that the correct large-m_i limit is not necessarily equivalent to naively taking the $m_i \to \infty$ limit in the NMEs. We discuss this issue in detail in the next section.

To nevertheless capture the m_i dependence of the NMEs in the $m_i \lesssim \Lambda_\chi$ region, we can construct a simple Padé approximation of order $(0, 1)$ that interpolates between the limits in Eq. (3.76)

$$M_{F\,\mathrm{int}}(m_i) = M_{F,\,sd}\frac{m_\pi^2}{m_i^2 + m_\pi^2 \frac{M_{F,\,sd}}{M_F}}\,. \tag{3.77}$$

We can do the same for $M_{GT,T\,\mathrm{int}}^{AA}(m_i)$, $M_{GT,T\,\mathrm{int}}^{AP}(m_i)$, and $M_{GT,T\,\mathrm{int}}^{PP}(m_i)$. The formulae for the tensor NMEs are less reliable due to smallness and large model dependence of the tensor NMEs. The functional form in Eq. (3.77) was used in Ref. [120] and was shown to agree well with the explicit m_i dependence calculated in the interacting boson model.

In case of $M_{GT}^{AA}(m_i)$ we can use additional information to further constrain the interpolation formula

$$\begin{aligned} M_{GT}^{AA}(m_i = m_\pi) &= -\frac{3}{2}M_{GT}^{AP}\,, \\ \frac{\partial}{\partial m_i^2}M_{GT}^{AP}(m_i)\Big|_{m_i=m_\pi} &= \frac{3}{m_\pi^2}\left(M_{GT}^{PP} + \frac{1}{2}M_{GT}^{AP}\right)\,. \end{aligned} \tag{3.78}$$

With additional constraints, we can construct an order $(1, 2)$ Padé approximation

$$M_{\mathrm{int}2}(m_i) = \frac{a_0 + a_1 m_i^2/m_\pi^2}{1 + b_1 m_i^2/m_\pi^2 + b_2 m_i^4/m_\pi^4}\,. \tag{3.79}$$

For an NME, M, with the large m_i behavior of Eq. (3.76), the coefficients are given by

$$\begin{aligned} a_0 &= M(0)\,, \qquad a_1 = M_{sd}\frac{M(m_\pi)^2 - M(0)\,(M(m_\pi) + M'(m_\pi))}{M(m_\pi)^2 + M'(m_\pi)M_{sd}}\,, \\ b_1 &= \frac{a_0 + a_1}{M(m_\pi)} - (b_2 + 1)\,, \qquad b_2 = a_1/M_{sd}\,, \end{aligned} \tag{3.80}$$

where $M'(m_\pi) \equiv \frac{\partial M(m_i)}{\partial \ln m_i^2}\Big|_{m_i = m_\pi}$.

In Fig. 3.3 we plot $M^{AA}_{GT\,\mathrm{int}}(m_i)$ and $M^{AA}_{GT\,\mathrm{int2}}(m_i)$ for neutrino masses between 1 MeV and 1 GeV for ^{136}Xe based on two nuclear many body methods. The two interpolation formulae agree within 25% over the whole range of neutrino masses, and the associated spread is smaller than the spread between different many-body methods. We therefore use Eq. (3.77) for the NMEs where we do not have sufficient information to construct the more accurate approximation in Eq. (3.79).

Armed with these interpolation formulae it is straightforward to obtain the m_i dependence of the remaining NMEs in Table 3.3. For the magnetic GT NME we use

$$M^{MM}_{GT}(m_i) = \frac{g_M^2}{6g_A^2}\left[\frac{m_\pi^2}{m_N^2}M^{AA}_{GT,\,sd} - \frac{m_i^2}{m_N^2}M^{AA}_{GT}(m_i)\right], \tag{3.81}$$

while for the short-distance NMEs we obtain

$$\begin{aligned} M_{F,\,sd}(m_i) &= M_{F,\,sd} - \frac{m_i^2}{m_\pi^2}M_F(m_i)\,, \\ M^{ab}_{GT,\,sd}(m_i) &= M^{ab}_{GT,\,sd} - \frac{m_i^2}{m_\pi^2}M^{ab}_{GT}(m_i)\,, \\ M^{ab}_{T,\,sd}(m_i) &= M^{ab}_{T,\,sd} - \frac{m_i^2}{m_\pi^2}M^{ab}_{T}(m_i)\,. \end{aligned} \tag{3.82}$$

3.5.2 $\mathcal{O}(m_i^2)$ corrections in the small neutrino mass limit

From the functional form of Eqs. (3.77) and (3.79) it is obvious that the NMEs quickly saturate for small neutrino masses, $m_i \ll m_\pi$, and become constant. However, in certain interesting cases it is important to understand how fast the functions become constant. For instance, as observed in Ref. [119], in scenarios with light, $m_i \ll m_\pi$, sterile neutrinos and no additional higher-dimensional operators, i.e. $M_L = 0$, the leading $nn \to pp\,ee$ transition operator is proportional to

$$\sum_{i=1}^{N}\left(C^{(6)}_{\mathrm{VLL}}\right)^2_{ei}\left(\frac{m_i}{\mathbf{q}^2 + m_i^2}\right) \simeq \frac{4V_{ud}^2}{\mathbf{q}^2}\left[PUm_\nu U^T P^T\right]_{ee} = \frac{4V_{ud}^2}{\mathbf{q}^2}(M_L^*)_{ee} = 0\,, \tag{3.83}$$

and vanishes. In this case, the $m_i^2/\mathbf{q}^2$ correction is necessary to get a non-vanishing result. This correction can in principle be estimated from expanding the interpolation formulae in the small m_i^2 limit. We write for $m_i \ll m_\pi$

$$M^{ab}_{\{F,GT,T\}}(m_i) = M^{ab}_{\{F,GT,T\}} + M'^{ab}_{\{F,GT,T\}}\frac{m_i^2}{m_\pi^2}\,. \tag{3.84}$$

Using the interpolation formula in Eq. (3.77), we can directly calculate $M'^{ab}_{\{F,GT,T\}}$ and we give the results in Table 3.4 for ^{136}Xe. We stress that the results for the derivatives for the NMEs

NMEs(^{136}Xe)	[115]	[116]
M'_F	0.52	0.23
M'^{AA}_{GT}	-1.75	-1.41
M'^{AP}_{GT}	0.51	0.31
M'^{PP}_{GT}	-0.14	-0.09
M'^{MM}_{GT}	-0.15	-0.11

Table 3.4: Comparison of the derivative of ^{136}Xe NMEs with respect to m_i^2 in the quasi-particle random phase approximation [115] and shell model [116]. The NMEs are defined in Eq. (3.84).

in the small m_i regime are associated with significant uncertainties even beyond those from the dependence on the nuclear many-body method. By using the interpolation formulae in Eq. (3.79) for $M^{AA}_{GT}(m_i)$ instead of Eq. (3.77) leads to $\mathcal{O}(100\%)$ corrections in M'^{AA}_{GT}. More importantly, for neutrino potentials scaling as $1/\mathbf{q}^4$, contributions from ultrasoft neutrinos can be as important as those from potential neutrinos that are considered here.

3.6 Neutrino mass dependence of subamplitudes

The master formula in Eq. (3.62), combined with the results presented in Ref. [71], describes all possible contributions to $0\nu\beta\beta$ from sterile and active neutrinos, capturing both the regime of heavy sterile neutrinos, $m_i \gg \Lambda_\chi$, and light sterile neutrinos $m_i \ll \Lambda_\chi$. In the former regime, the heavy neutrino is integrated out at the quark level, while in the latter regime it has to be kept as a degree of freedom in chiral EFT. In the region $m_i \sim \Lambda_\chi$, however, both approaches are questionable. Within chiral EFT, diagrams arising at the n-loop level give corrections $\sim (m_i/\Lambda_\chi)^{2n}$ and the loop expansion breaks down. Instead, when integrating out the heavy neutrino at the quark level, operators involving additional derivatives, $\sim \left(\frac{\partial}{m_i}\right)^n \times \mathcal{O}^{(9)}$, cannot be neglected as they induce corrections $\sim (\Lambda_\chi/\, m_i)^n$. This implies the $m_i \sim \Lambda_\chi$ regime is beyond the reach of chiral EFT and of perturbative QCD methods, and it is therefore hard to treat rigorously. In this section we discuss the m_i dependence of the amplitudes in more detail and employ what is known of the amplitudes in the two regimes to suggest approximate interpolation formulae that link the low- and high-mass regions.

Before discussing the interpolation it is useful to consider the two regimes in an example involving one neutrino mass eigenstate with mass m_i which couples to left-handed electrons, and to right- and left-handed quark vector currents. The low-energy amplitudes depend on the neutrino masses in two ways, explicitly through the light neutrino propagator, and implicitly via the mass dependence of the low-energy constants in Eqs. (3.38) and (3.40). The resulting $0\nu\beta\beta$ amplitude, valid in the region $m_i \ll \Lambda_\chi$, can be written as

$$\begin{aligned}\mathcal{A}_L \;=\; -\frac{m_i}{4m_e}\Big\{ & 2C^{(6)}_{\mathrm{VLL}} C^{(6)}_{\mathrm{VRL}} \left(\bar{\mathcal{M}}_V(m_i) - \bar{\mathcal{M}}_A(m_i)\right) \\ & + \left[\left(C^{(6)}_{\mathrm{VLL}}\right)^2 + \left(C^{(6)}_{\mathrm{VRL}}\right)^2\right] \left(\bar{\mathcal{M}}_V(m_i) + \bar{\mathcal{M}}_A(m_i)\right) \Big\},\end{aligned} \tag{3.85}$$

where we include the contributions from the hard neutrino exchange amplitudes, $\mathcal{A}^{(\nu)}_L(m_i)$, in $\bar{\mathcal{M}}_{V,A}(m_i)$. In the limit of large neutrino masses, $\Lambda_\chi \ll m_i$, we can integrate out the neutrino in

perturbation theory, as discussed in Sect. 3.1, and consider the hadronization of the four-fermion operators with coefficients $C_{1\mathrm{L}}^{(9)}$, $C_{1\mathrm{L}}^{(9)\prime}$ and $C_{4\mathrm{L}}^{(9)}$. Using Eq. (3.69), we find

$$\begin{aligned}\mathcal{A}_L^{(9)} &= -\frac{1}{2m_e}\left(C_{\mathrm{VLL}}^{(6)} m_\nu^{-1} C_{\mathrm{VLL}}^{(6)} + C_{\mathrm{VRL}}^{(6)} m_\nu^{-1} C_{\mathrm{VRL}}^{(6)}\right) \\ &\quad \times \left\{\frac{5}{6} m_\pi^2 g_1^{\pi\pi}\left(M_{GT,\,sd}^{PP} + M_{T,\,sd}^{PP}\right) + \frac{m_\pi^2}{2} g_1^{\pi N}\left(M_{GT,\,sd}^{AP} + M_{T,\,sd}^{AP}\right) - \frac{2}{g_A^2} m_\pi^2 g_1^{\mathrm{NN}} M_{F,\,sd}\right\} \\ &\quad -\frac{1}{2m_e}\left(C_{\mathrm{VRL}}^{(6)} m_\nu^{-1} C_{\mathrm{VLL}}^{(6)} + C_{\mathrm{VLL}}^{(6)} m_\nu^{-1} C_{\mathrm{VRL}}^{(6)}\right)\left\{\frac{1}{2} g_4^{\pi\pi}\mathcal{M}_{PS,sd} - \frac{2}{g_A^2} m_\pi^2 g_4^{\mathrm{NN}} M_{F,\,sd}\right\},\end{aligned} \tag{3.86}$$

where $g_4^{\pi\pi} = \mathcal{O}(\Lambda_\chi^2)$ and $g_4^{\mathrm{NN}} = \mathcal{O}(\Lambda_\chi^2/F_\pi^2)$, while $g_1^{\pi\pi,\,\pi\mathrm{N},\,\mathrm{NN}} = \mathcal{O}(1)$.

Although the amplitudes in Eqs. (3.85) and (3.86) look rather different from one another, one can see that they take similar forms in the large-m_i limit. To naively take this limit for the long-range contributions, as discussed in Sect. 3.5.1, we use

$$\lim_{m_i\to\infty} M_K^{(ab)} = \frac{m_\pi^2}{m_i^2} M_{K\,sd}^{(ab)}, \quad \lim_{m_i\to\infty} M_{GT}^{AA} = -3\frac{m_\pi^2}{m_i^2} M_{F,\,sd}\,, \tag{3.87}$$

and neglect the magnetic contributions which lead to short-range derivative operators, subleading in the power counting. Using the above expressions, we obtain naive estimates of the LECs $g_1^{\pi\pi}$, $g_1^{\pi N}$, and g_1^{NN} in Eq. (3.86). By matching terms that depend on the same NMEs in Eqs. (3.85) and (3.86), which is equivalent to matching the $\pi\pi \to ee$ and $nn \to pp\,ee$ amplitudes, we obtain

$$g_1^{\pi\pi} = \frac{3}{5}, \quad g_1^{\pi\mathrm{N}} = 1, \quad g_1^{\mathrm{NN}} = \frac{1}{4}\left(1 + 3g_A^2 - 2m_i^2 g_\nu^{\mathrm{NN}}(m_i)\Big|_{m_i\geq\Lambda_\chi}\right). \tag{3.88}$$

These equations were obtained by setting $\mathcal{A}_L^{(9)} = \mathcal{A}_L$ in the regime $m_i \gg \Lambda_\chi$ where the left-hand side should be reliable, while the right-hand side receives large contributions from loop diagrams that were neglected. This implies that Eq. (3.88) can only give an order-of-magnitude estimate. Nevertheless, neglecting the $g_\nu^{\mathrm{NN}}(m_i)$ contribution, we see that these estimates are consistent with the NDA expectation and coincide with the "factorization" approximation. The value of $g_1^{\pi\pi}$ extracted from the lattice, $g_1^{\pi\pi}(\mu = 2\,\mathrm{GeV}) = 0.36$, is about 40% smaller than Eq. (3.88).

While these estimates are not very accurate, they at least give the right scaling. This is not so clear for the LECs in the third line of Eq. (3.86). For instance, we can obtain

$$g_4^{\mathrm{NN}} = \frac{1}{4}\left(1 - 3g_A^2 - 2m_i^2 g_{\mathrm{LR}}^{\mathrm{NN}}(m_i)\Big|_{m_i\geq\Lambda_\chi}\right), \tag{3.89}$$

where the first two terms on the right-hand side are $\mathcal{O}(1)$, whereas Table 3.1 tells us that $g_4^{\mathrm{NN}} = \mathcal{O}((4\pi)^2)$. In similar fashion, we obtain

$$g_4^{\pi\pi} = -4\frac{m_i^2 g_{\mathrm{LR}}^{\pi\pi}(m_i)}{F_\pi^2}\Big|_{m_i\geq\Lambda_\chi} + \mathcal{O}(m_\pi^2)\,. \tag{3.90}$$

$g_4^{\pi\pi} = \mathcal{O}(\Lambda_\chi^2)$ which is not clear from the right-hand side. Similarly, it is not obvious that the g_ν^{NN} term in Eq. (3.88) scales the same as the left-hand side which is $\mathcal{O}(1)$. In all of these cases, the comparison of the naive limit of Eq. (3.85) with Eq. (3.86) suggests that the hard-neutrino LECs should have a non-trivial m_i dependence. As we will argue below for the case of $g_{\mathrm{LR}}^{\pi\pi}$, it is indeed the m_i-dependence of these LECs which ensures that the matching relations are restored.

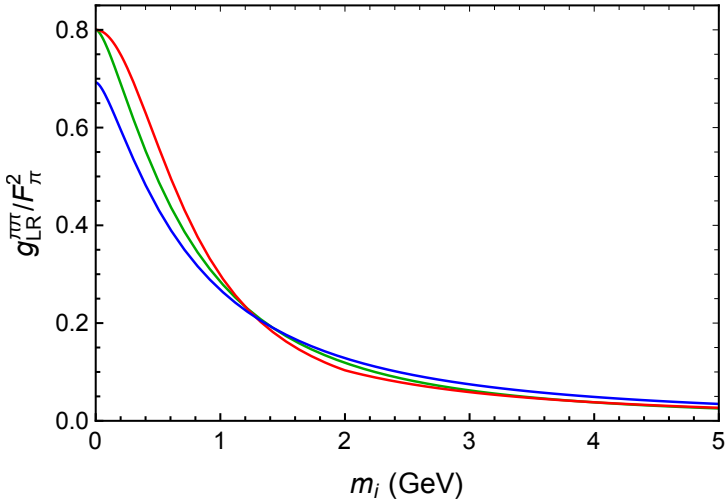

Figure 3.4: The LEC $g_{\rm LR}^{\pi\pi}$ in units of F_π^2 as a function of the neutrino mass m_i. The blue and green lines denote the three- and five-resonance models, while the red line denotes the naive interpolation formula in Eq. (3.93).

3.6.1 A naive interpolation formula

It will prove useful to construct a simpler interpolation formula that can be applied to LECs for which we have less information or where the resonance model is not applicable. We follow a similar strategy as in the start of this section and impose

$$\mathcal{A}_{A\,\rm int}(m_i)\big|_{m_i\gg\Lambda_\chi} \;=\; \mathcal{A}_A^{(9)}(m_i)\,, \tag{3.91}$$

where $\mathcal{A}_{A\,\rm int}(m_i) = \mathcal{A}_A^{(ld)}(m_i) + \bar{\mathcal{A}}_{A\,\rm int}^{(\nu)}(m_i)$ with $A \in \{L,R,V\}$ and $\mathcal{A}_A^{(ld)}(m_i) = \mathcal{A}_A(m_i) - \mathcal{A}_A^{(\nu)}(m_i)$ is the purely long-distance part of the amplitude constructed in Sect. 3.4. Instead, $\bar{\mathcal{A}}_{A\,\rm int}^{(\nu)} = \mathcal{A}_A^{(\nu)}\big|_{g_\alpha\to\bar{g}_\alpha}$ involves 'effective' LECs, $\bar{g}_\alpha(m_i)$, that capture both the hard-neutrino exchange contributions as well as the loop corrections that become large in the $m_i \sim \Lambda_\chi$ regime. In the limit of zero neutrino mass, we have $\bar{g}_\alpha(0) = g_\alpha(0)$. In this way the interpolated amplitude has the correct limiting behavior in both the low- and high-mass regions.

The condition Eq. (3.91) can be used to obtain expressions for these 'effective' hard-neutrino LECs at a scale $m_i \gg \Lambda_\chi$ in terms of LECs arising from dim-nine operators and possible long-distance contributions. To do so, we employ the large-m_i limits of the NMEs, see Eq. (3.87), and demand that the contributions proportional to each NME in Eq. (3.91) match (this is equivalent to demanding that Eq. (3.91) not only holds for the $nn \to pp\,ee$ amplitude, but also for the $\pi\pi \to ee$ and $n \to p\pi\,ee$ subamplitudes). We then construct an interpolation formula

$$g_\alpha(m_i)\big|_{\rm naive} = \frac{g_\alpha(0)}{1 + g_\alpha(0)\left[\theta(m_0 - m_i)\frac{m_0^2}{m_i^2}\bar{g}_\alpha(m_0) + \theta(m_i - m_0)\bar{g}_\alpha(m_i)\right]^{-1}}\,, \tag{3.92}$$

where $m_0 \simeq 2$ GeV is a scale at which the procedure of integrating out the heavy neutrino becomes reliable and we use Eq. (3.91) to obtain expressions for $\bar{g}_\alpha(m_{0,i})$. The 'effective' LECs in the large-m_i region scale as m_i^{-2}, due to the m_i^2 in the denominator of the neutrino propagator. This scaling ensure that $g_\alpha(m_i)\big|_{\rm naive}$ reduces to $\bar{g}_\alpha(m_i)$ for $m_i \to \infty$, while it reproduces $g_\alpha(0)$ in

the opposite, $m_i \to 0$, limit. Using $g_\alpha(m_i)\big|_{\rm naive}$ in the interpolated amplitude, $\mathcal{A}_{A\,\rm int}(m_i)$, then allows us to obtain amplitudes for any value of m_i.

Applying this procedure to the case of $g_{\rm LR}^{\pi\pi}$, we again obtain $\bar{g}_{\rm LR}^{\pi\pi}(m_i)|_{m_i \gg \Lambda_\chi} = -\frac{F_\pi^2}{4m_i^2} g_4^{\pi\pi}(m_i)$ from Eq. (3.91), which, in combination with Eq. (3.92), leads to

$$g_{\rm LR}^{\pi\pi}(m_i)\Big|_{\rm naive} = \frac{g_{\rm LR}^{\pi\pi}(0)}{1 - m_i^2 \frac{4 g_{\rm LR}^{\pi\pi}(0)}{F_\pi^2} \left[\theta(m_0 - m_i) g_4^{\pi\pi}(m_0) + \theta(m_i - m_0) g_4^{\pi\pi}(m_i)\right]^{-1}}\,, \tag{3.93}$$

where on the right-hand-side we use the observed value for $g_{\rm LR}^{\pi\pi}(0) = 0.8 F_\pi^2$ (see Eq. (3.39)). It has the correct logarithmic dependence on m_i in the perturbative QCD regime due to the $\theta(m_i - m_0) g_4^{\pi\pi}(m_i)$ term. This naive interpolation formulae is shown in red in Fig. 3.4, where it is compared to the results from the three- and five-resonance models. The formulae agree over the whole range of m_i within 20%. Based on this success, we will use similar naive interpolation formulae for the other LECs.

It remains to understand the relations in Eqs. (3.88) and (3.89) and the m_i dependence of $g_\nu^{\rm NN}(m_i)$ and $g_{\rm LR}^{\rm NN}(m_i)$. These equations imply that $g_{\rm LR}^{\rm NN}$ is enhanced with respect to $g_\nu^{\rm NN}$ in the $m_i \geq \Lambda_\chi$ region. This can be understood from the different RGEs of these couplings. For $m_i \ll \Lambda_\chi$, the RGE for $g_{\rm LR}^{\rm NN}$ receives contributions from both light neutrino exchange and the $\pi\pi \to e^- e^-$ coupling, while $g_\nu^{\rm NN}$ only from the former

$$\begin{aligned} \frac{d}{d\log\mu}\tilde{g}_\nu^{\rm NN} &= \frac{1}{2}(1 + 2g_A^2)\,, \\ \frac{d}{d\log\mu}\tilde{g}_{\rm LR}^{\rm NN} &= \frac{1}{2}\left(1 - 2g_A^2 + 2g_A^2 \frac{g_{\rm LR}^{\pi\pi}(m_i)}{F_\pi^2}\right), \end{aligned} \tag{3.94}$$

where $g_i^{\rm NN} = (m_N C/4\pi)^2 \tilde{g}_i^{\rm NN} \sim \tilde{g}_i^{\rm NN}/F_\pi^2$. While the first term is independent of m_i, the second term in the RGE of $g_{\rm LR}^{\rm NN}$ scales as Λ_χ^2/m_i^2 for large m_i as can be seen explicitly from Eq. (3.93). It is this behavior which ensures that the left- and right-hand side of Eq. (3.89) match.

We can now construct interpolation formulae for $g_\nu^{\rm NN}(m_i)$ and $g_{\rm LR}^{\rm NN}(m_i)$ similar to Eq. (3.93), by using the matching conditions at large neutrino masses

$$\begin{aligned} \bar{g}_\nu^{\rm NN}(m_i \gg \Lambda_\chi) &= -\frac{2}{m_i^2}\hat{g}_1^{\rm NN}(m_i) = -\frac{2}{m_i^2}\left(g_1^{\rm NN}(m_i) - \frac{1}{4}(1 + 3g_A^2)\right), \\ \bar{g}_{\rm LR}^{\rm NN}(m_i \gg \Lambda_\chi) &= -\frac{2}{m_i^2}\hat{g}_4^{\rm NN}(m_i) = -\frac{2}{m_i^2}\left(g_4^{\rm NN}(m_i) - \frac{1}{4}(1 - 3g_A^2)\right), \end{aligned} \tag{3.95}$$

to obtain

$$\begin{aligned} g_\nu^{\rm NN}(m_i)\Big|_{\rm naive} &= \frac{g_\nu^{\rm NN}(0)}{1 - m_i^2 \frac{g_\nu^{\rm NN}(0)}{2}\left[\theta(m_0 - m_i)\hat{g}_1^{\rm NN}(m_0) + \theta(m_i - m_0)\hat{g}_1^{\rm NN}(m_i)\right]^{-1}}\,, \\ g_{\rm LR}^{\rm NN}(m_i)\Big|_{\rm naive} &= \frac{g_{\rm LR}^{\rm NN}(0)}{1 - m_i^2 \frac{g_{\rm LR}^{\rm NN}(0)}{2}\left[\theta(m_0 - m_i)\hat{g}_4^{\rm NN}(m_0) + \theta(m_i - m_0)\hat{g}_4^{\rm NN}(m_i)\right]^{-1}}\,, \end{aligned} \tag{3.96}$$

where we use the following RGEs to express $g_{1,4}^{\rm NN}(m_i)$ in terms of $g_{1,4}^{\rm NN}(\mu \simeq 2\,\text{GeV})$

$$\begin{aligned} g_1^{\rm NN}(m_i) &= g_1^{\rm NN}(\mu) - \frac{3}{4}\frac{\alpha_s}{\pi}\left(1 - \frac{1}{N_c}\right) g_1^{\rm NN} \log\frac{m_i^2}{\mu^2}\,, \\ g_4^{\rm NN}(m_i) &= g_4^{\rm NN}(\mu) + \frac{3}{4}\frac{\alpha_s}{\pi}\left(g_5^{\rm NN} - \frac{1}{N_c} g_4^{\rm NN}\right) \log\frac{m_i^2}{\mu^2}\,. \end{aligned} \tag{3.97}$$

Armed with the interpolation formulae we are now ready to calculate the $0\nu\beta\beta$ amplitude in Eq. (3.85), starting with the combination of NMEs and LECs $\bar{\mathcal{M}}_V \pm \bar{\mathcal{M}}_A$. The combination $\bar{\mathcal{M}}_V + \bar{\mathcal{M}}_A$, relevant for scenarios without higher-dimensional operators, depends on NMEs such as $M_F(m_i)$ for which we use interpolation formulae of the form in Eq. (3.77). In addition, there is a dependence on $\bar{g}_\nu^{\rm NN}(m_i)$ for which we use Eq. (3.96). Unfortunately, the latter formula depends on two LECs, $g_\nu^{\rm NN}(0)$ and $g_1^{\rm NN}(m_0)$, that have not been determined with nonperturbative methods. For a discussion of the required lattice QCD calculation, as well as recent steps towards such a determination, we refer to Refs. [121–125]. We use two reasonable choices for the LECs to assess the associated uncertainty. We use the estimates from Refs. [106–108]

$$g_\nu^{\rm NN}(0) = -92.5 \pm 46.2 \ \ {\rm GeV}^{-2}\,, \qquad g_1^{\rm NN}(m_0) = \frac{1}{4}(1+3g_A^2)+1\,, \tag{3.98}$$

where the latter choice is guided by the factorization approximation in Eq. (3.88).

Similar interpolation formulae can be derived for the other LECs introduced in Sect. 3.2.6 by matching via Eq. (3.91) and employing the interpolation formula in Eq. (3.92). This procedure allows us to smoothly interpolate between the $m_i \ll \Lambda_\chi$ and $m_i \gg \Lambda_\chi$ limits. In Appendix B we discuss several cases that we require in Sect. 3.7.3.

3.7 Phenomenology

We now turn to applications of the master formula in Eq. (3.63) by investigating several scenarios involving sterile neutrinos. We emphasize that our purpose is not to find phenomenologically viable models of neutrino masses, but mainly to illustrate the use of the framework developed in this chapter. The search for sterile neutrinos is a very rich field with searches in a wide range of experiments, see e.g. Refs. [126–131], of which $0\nu\beta\beta$ is only a small, but crucial, part. The framework presented here can be used directly in future global analyses of sterile neutrinos.

In what follows we study several relatively simple scenarios. We start by considering minimal scenarios in which we extend the SM by one or two sterile neutrinos that are gauge-singlets and do not interact via higher-dimensional interactions. In these so-called $3+1$ and $3+2$ models, $0\nu\beta\beta$ arises solely from the Majorana masses of the sterile neutrinos. We begin by studying whether $0\nu\beta\beta$ can be measured in these minimal models and discuss the m_i dependence of the resulting decay rates. After considering these cases, we turn on several higher-dimensional operators that are induced in BSM scenarios involving leptoquarks and determine the impact of such interactions on the $0\nu\beta\beta$ predictions.

The current experimental bounds on the half-lives of various isotopes are summarized in Table 3.5, where the expected future sensitivities are also shown. In our numerical analyses, we use the limit on $T_{1/2}^{0\nu}(^{136}{\rm Xe})$ obtained by KamLAND-Zen[3], which is the strongest one at present, and take into account the following future prospects

$$T_{1/2}^{0\nu}\left(^{136}{\rm Xe}\right) > 2.0\times10^{27}\ [{\rm yr}] \quad ({\rm KamLAND2-Zen})\,, \tag{3.99}$$

$$T_{1/2}^{0\nu}\left(^{136}{\rm Xe}\right) > 1.0\times10^{28}\ [{\rm yr}] \qquad ({\rm nEXO})\,. \tag{3.100}$$

The prospects for the LEGEND experiment are of high interest as well, with an expected sensitivity of $T_{1/2}^{0\nu}\left(^{76}{\rm Ge}\right) \sim 10^{28}$ yr.

Before we begin analyzing the scenarios with sterile neutrinos mentioned above, we first briefly discuss the scenario of 3 light Majorana eigenstates, that is, the standard mechanism. This case

[3] In the following work we use the old limit 1.06×10^{26} years. The limit was increased to 2.3×10^{26} years right before finalizing this thesis but no major changes of our results will occur.

Isotope	Experiment	Current limit ($\times 10^{25}$yr)		Future sensitivity ($\times 10^{25}$yr)	
^{48}Ca	ELEGANT−IV	5.8×10^{-3}	[30]	–	
	CANDLES	6.2×10^{-3}	[51]	10^{-2}	[56]
	NEMO−3	2.0×10^{-3}	[37]		
^{76}Ge	MAJORANA DEMONSTRATOR	2.7	[50]	–	
	GERDA	9.0	[52]	–	
	LEGEND	–		10^{3}	[57]
^{82}Se	CUPID	3.5×10^{-1}	[53]		
	NEMO−3	2.5×10^{-2}	[48]		
	SuperNEMO	–		10	[58]
^{96}Zr	NEMO−3	9.2×10^{-4}	[31]		
^{100}Mo	NEMO−3	1.1×10^{-1}	[36]		
	CUPID−1T	–		9.2×10^{2}	[65]
	AMoRE	9.5×10^{-3}	[54]	5.0×10	[59]
^{116}Cd	NEMO−3	1.0×10^{-2}	[41]		
^{128}Te	–	1.1×10^{-2}	[29]	–	
^{130}Te	CUORE	3.2	[49]	9.0	[60]
	SNO+	–		1.0×10^{2}	[61]
^{136}Xe	KamLAND-Zen	10.6	[38]	2.0×10^{2}	
	EXO−200	3.5	[55]	10^{3}	[62]
	NEXT	–		2.0×10^{2}	[63]
	PandaX	–		1.0×10^{2}	[64]
^{150}Nd	NEMO−3	2.0×10^{-3}	[40]		

Table 3.5: Current and future experimental limits on $T_{1/2}^{0\nu}$ at 90% C.L.

corresponds to only turning on the LNV operators that generate Majorana masses for the left-handed neutrinos, M_L in Eq. (2.8). We use the standard parametrization and write

$$U = R^{23} W^{13} R^{12} \text{diag}(1, e^{i\lambda_1}, e^{i\lambda_2}) \,, \tag{3.101}$$

in terms of the rotation matrices $\left[W^{ab}(\theta_{ab}, \delta_{ab})\right]_{ij} = \delta_{ij} + (\delta_{ia}\delta_{jb} e^{i\delta_{ab}} - \delta_{ib}\delta_{ja} e^{-i\delta_{ab}}) s_{ab} + (\delta_{ia}\delta_{ja} + \delta_{ib}\delta_{jb})(c_{ab} - 1)$ and $R^{ab}(\theta_{ab}) = W^{ab}(\theta_{ab}, 0)$, so that

$$m_{\beta\beta} = \sum_{i=1}^{3} m_i U_{ei}^2 = m_1 c_{12}^2 c_{13}^2 + m_2 e^{2i\lambda_1} s_{12}^2 c_{13}^2 + m_3 e^{2i(\lambda_2 - \delta_{13})} s_{13}^2 \,, \tag{3.102}$$

in terms of the sines (cosines) of the neutrino mixing angles, s_{ij} (c_{ij}), the Dirac phase δ_{13}, and the Majorana phases, $\lambda_{1,2}$. We set the mixing angles to their central values [132] (see Table 3.6). The relevant subamplitude is $\mathcal{A}_L(m_i)$ that depends on the combination $\bar{\mathcal{M}}_V(m_i) + \bar{\mathcal{M}}_A(m_i)$, but since all mass eigenstates are at the eV scale or below, we actually only require $\bar{\mathcal{M}}_V(0) + \bar{\mathcal{M}}_A(0)$. This combination depends on the unknown LEC $g_\nu^{\rm NN}(0)$ associated with the exchange of hard neutrinos. This contribution is usually not considered in the literature, but as demonstrated in Refs. [93, 94] appears at the same order as the exchange of potential neutrinos. To calculate decay rates we marginalize over the Majorana phases and vary $g_\nu^{\rm NN}(0)$ between -92.5 ± 46.2 GeV^{-2} as discussed below Eq. (3.96).

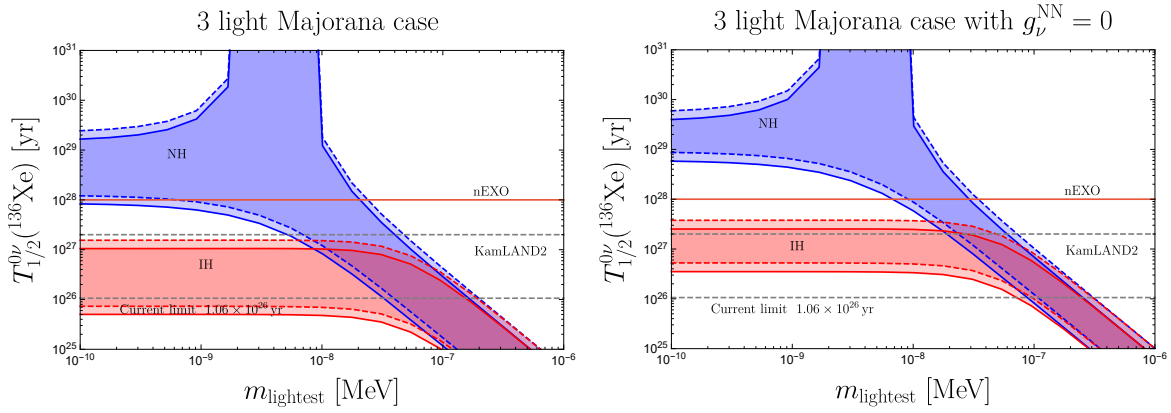

Figure 3.5: $0\nu\beta\beta$ half-life of ^{136}Xe as a function of the lightest neutrino mass in the scenario of 3 light Majorana neutrinos in case of the normal hierarchy (blue) and inverted hierarchy (red). We show results obtained with QRPA (solid) or the Shell Model (dashed) NMEs. In the left panel, the bands reflect the uncertainty due to LECs associated to hard-neutrino exchange and the unknown Majorana phases. In the right panel, we ignore the contributions from hard-neutrino exchange as typically done in the literature and the bands arise solely from varying the unknown Majorana phases. The shaded regions in both panels correspond to the present experimental limit, and expected future limits are depicted by the two dashed lines.

The resulting ^{136}Xe half life is depicted in the left panel of Fig. 3.5 for the normal hierarchy (NH) in blue and inverted hierarchy (IH) in red as a function of the lightest neutrino mass, m. We used two sets of NMEs obtained with the QRPA (solid) and Shell Model (dashed). Around $m = 5 \cdot 10^{-3}$ eV, the usual 'funnel' appears for the NH due to a possible cancellation in $m_{\beta\beta}$. For smaller m, the uncertainty on the half life is roughly two orders of magnitude for both the NH and IH. This uncertainty arises roughly in equal parts from the uncertainties in the LECs and Majorana phases, and in smaller amount from the change in NMEs between the QRPA and Shell Model.

3.7.1 3+1 model

The simplest scenario we investigate is the $3+1$ model where the SM is extended by one gauge-singlet neutrino. That is $n = 1$ and $N = 4$. This model leads to two massless neutrinos and is thus ruled out by the combined atmospheric, $\Delta m^2_{\rm ATM} \simeq 2.4 \cdot 10^{-3}$ eV^2 and solar, $\Delta m^2_{\rm SOL} \simeq 7.5 \cdot 10^{-5}$ eV^2, squared mass differences. Nevertheless, due to its simplicity, the scenario provides a useful toy model. In the flavor basis, we write the neutrino mass matrix as

$$M_\nu = \begin{pmatrix} 0 & 0 & 0 & M^*_{D,1} \\ 0 & 0 & 0 & M^*_{D,2} \\ 0 & 0 & 0 & M^*_{D,3} \\ M^*_{D,1} & M^*_{D,2} & M^*_{D,3} & M_R \end{pmatrix} , \tag{3.103}$$

and we set $M^*_{D,1} = M^*_{D,2} = M^*_{D,3} \equiv M^*_D$. The neutrino mass matrix is then described by just two parameters M^*_D and M_R. Note that in the absence of higher-dimensional operators, $(M_\nu)_{ij} = 0$ for $i, j = 1, 2, 3$ is required by gauge invariance. This simple setup predicts two massless neutrinos, $m_1 = m_2 = 0$, and two massive neutrinos described by

$$m_3 = \frac{1}{2}\left[\sqrt{|M_R|^2 + 12|M_D|^2} - |M_R|\right] , \quad m_4 = \frac{1}{2}\left[\sqrt{|M_R|^2 + 12|M_D|^2} + |M_R|\right] , \tag{3.104}$$

where we assumed $m_3 < m_4$, while the inverted relations are

$$|M_R| = m_4 - m_3\,, \qquad |M_D| = \frac{1}{\sqrt{3}}\sqrt{m_3 m_4}\,. \tag{3.105}$$

It is straightforward to diagonalize the mass matrix to obtain the PMNS matrix, which can be parametrized as [133]

$$\begin{aligned} U &= D_L R^{34} R^{24} R^{23} R^{14} R^{13} W^{12} D_R\,, \\ D_L &= e^{i(\alpha_D+\alpha_R/2)}\mathrm{diag}(1,1,1,e^{-i(\alpha_R+\alpha_D)}) \qquad D_R = \mathrm{diag}(1,1,i,1)\,, \end{aligned} \tag{3.106}$$

where W^{ij} and R^{ij} are defined below Eq. (3.101) and $\alpha_{D,R} = \mathrm{Arg}\, M_{D,R}$. In this fairly simple case nearly all the mixing angles can be expressed in terms of the neutrino masses

$$s_{23} = c_{34}/\sqrt{2}, \qquad s_{34} = t_{24}, \qquad s_{24} = s_{13}\sqrt{m_3/m_4} = t_{14} = \sqrt{\frac{m_3}{2m_3+3m_4}}\,, \tag{3.107}$$

where $t_{ij} = s_{ij}/c_{ij}$, while s_{12} is unconstrained due to the two vanishing neutrino masses. One useful result of the above is

$$U_{e3}^2 = -\frac{m_4}{m_3}U_{e4}^2 = -\frac{1}{3}\frac{m_4}{m_3+m_4}e^{i(2\alpha_D+\alpha_R)}\,. \tag{3.108}$$

As mentioned, this model of neutrino masses is too restrictive to reproduce the oscillation data. To nevertheless investigate the effect a sterile neutrino would have on $0\nu\beta\beta$ in this scenario we approximate $\Delta m^2_{\rm ATM} \simeq 0$, and set $m_3 = \sqrt{\Delta m^2_{31}} \simeq 0.05$ eV. For $m_4 < \Lambda_\chi$ the $0\nu\beta\beta$ half life is then simply given by (Eq. (3.63))

$$\left(T_{1/2}^{0\nu}\right)^{-1} = g_A^4 G_{01}\left|\sum_{i=1}^{4}\mathcal{A}_L(m_i)\right|^2\,, \tag{3.109}$$

where

$$\mathcal{A}_L(m_i) = -\frac{m_i}{4m_e}\left[\bar{\mathcal{M}}_V(m_i) + \bar{\mathcal{M}}_A(m_i)\right](C^{(6)}_{\rm VLL})^2_{ei}\,, \tag{3.110}$$

and

$$C^{(6)}_{\rm VLL} = -2V_{ud}(PU)_{ei} = -2V_{ud}U_{ei}\,. \tag{3.111}$$

All other Wilson coefficients vanish. The combinations of NMEs and LECs $\bar{\mathcal{M}}_{V,A}(m_i)$ are defined in Eq. (3.70), with the inclusion of the short-range pieces in Eq. (3.65), and their dependence on the neutrino masses is discussed in Sects. 3.5.1 and 3.6. For $m_4 > \Lambda_\chi$, instead, the half life becomes

$$\left(T_{1/2}^{0\nu}\right)^{-1} = g_A^4 G_{01}\left|\sum_{i=1}^{3}\mathcal{A}_L(m_i) + \mathcal{A}_L^{(9)}(m_4)\right|^2 \tag{3.112}$$

as the fourth mass eigenstate is integrated out on the quark level. In this case $\mathcal{A}_L^{(9)}(m_4)$ is defined in Eqs. (3.69) and the neutrino mass dependence enters via

$$C^{(9)}_{1L} = -\frac{v}{2m_4}(C^{(6)}_{\rm VLL})^2 = -\frac{2vV_{ud}^2}{m_4}U_{e4}^2\,. \tag{3.113}$$

The interpolation formulae described in Sect. 3.6.1 ensure that the $m_4 \leq \Lambda_\chi$ and $m_4 \geq \Lambda_\chi$ limits smoothly match.

We set $\alpha_{D,R} = 0$ and the result for the $0\nu\beta\beta$ ^{136}Xe rate is depicted in the left panel of Fig. 3.6 as a function of m_4. It can be divided into three regions. For $m_4 \ll m_\pi$ the life time increases as m_4^4 for decreasing neutrino masses. For $m_4 \geq \Lambda_\chi$ the lifetime becomes independent of the neutrino mass. The intermediate region is more complicated and shown in more detail in the right panel of Fig. 3.6. The behavior in the three regions can be understood from the neutrino mass dependence of $\bar{\mathcal{M}}_V(m_i) + \bar{\mathcal{M}}_A(m_i)$ shown in Fig. 3.4. For small neutrino masses $m_4 \ll m_\pi \sim k_F$, the NMEs become almost independent of the neutrino mass. The dominant contribution, however, is proportional to

$$\sum_{i=1}^{4} m_i U_{ei}^2 = 0\,, \tag{3.114}$$

as can be seen explicitly from Eq. (3.108), see also Eq. (3.83) and Ref. [119]. The first non-vanishing contributions in this regime are suppressed by m_i^2/m_π^2 as discussed in Sect. 3.5.2 and the half life is proportional to

$$\left|\sum_{i=1}^{4} m_i^3 U_{ei}^2\right|^2 = \left|M_D^{*2} M_R\right|^2 \sim m_3^2 m_4^4\,, \tag{3.115}$$

in the regime $m_4 \gg m_3$. For large neutrino masses, $m_4 > \Lambda_\chi$, we need to compare the two terms in Eq. (3.112) which are both non-zero. The first term involves the sum over light neutrinos, but only the m_3 contribution is nonzero, and depends on $U_{e3} \simeq -1/\sqrt{3}$ which is constant in the $3+1$ model up to m_3/m_4 corrections, see Eq. (3.108). Similarly, we can see that $m_4 U_{e4}^2$ is roughly independent of m_4 from Eq. (3.108), but in this case the amplitude scales as $\mathcal{A}_L^{(9)}(m_4) \sim C_{1L}^{(9)} \sim U_{e4}^2/m_4 \sim m_4^{-2}$ and thus quickly drops off. In fact, already for $m_4 = 1$ GeV the fourth neutrino only contributes at the 10% level.

From Fig. 3.6 it is clear that for small neutrino masses, the $3+1$ toy model predicts extremely slow $0\nu\beta\beta$ rates, orders of magnitude away from present or projected sensitivities. For $m_4 \geq 1$ GeV, the half lives are roughly $\cdot 10^{27}$ yr. The uncertainty in the half life is at the order-of-magnitude level and mainly due to our poor knowledge of the short-distance LEC $g_\nu^{\rm NN}(m_i)$. Although the uncertainty in the small-m_4 region looks small this is probably unrealistic. In this regime, the amplitudes depend on the derivative of the NMEs with respect to m_i, which we estimated by expanding the interpolation formula. However, as discussed in Sect. 3.5.2, this expression might not be accurate in this region and a realistic uncertainty would likely be at the order-of-magnitude level as well. Since the decay rates are immeasurably small, this uncertainty is not too relevant.

3.7.2 3+2 model

We now consider a minimal $3+2$ model, where we extend the SM with two sterile neutrinos ($n = 2$). This model is more realistic as it can readily accommodate the measured neutrino mass splittings, mixing angles, and CP phase. We closely follow the analysis of Ref. [134] to conveniently parametrize the 5×5 mixing matrix in terms of neutrino masses and PMNS parameters. The original 5×5 mass matrix is given by

$$M_\nu = \begin{pmatrix} 0 & 0 & 0 & M_{D_{14}}^* & M_{D_{15}}^* \\ 0 & 0 & 0 & M_{D_{24}}^* & M_{D_{25}}^* \\ 0 & 0 & 0 & M_{D_{34}}^* & M_{D_{35}}^* \\ M_{D_{14}}^* & M_{D_{24}}^* & M_{D_{34}}^* & M_{R_{44}} & M_{R_{45}} \\ M_{D_{15}}^* & M_{D_{25}}^* & M_{D_{35}}^* & M_{R_{45}} & M_{R_{55}} \end{pmatrix} \tag{3.116}$$

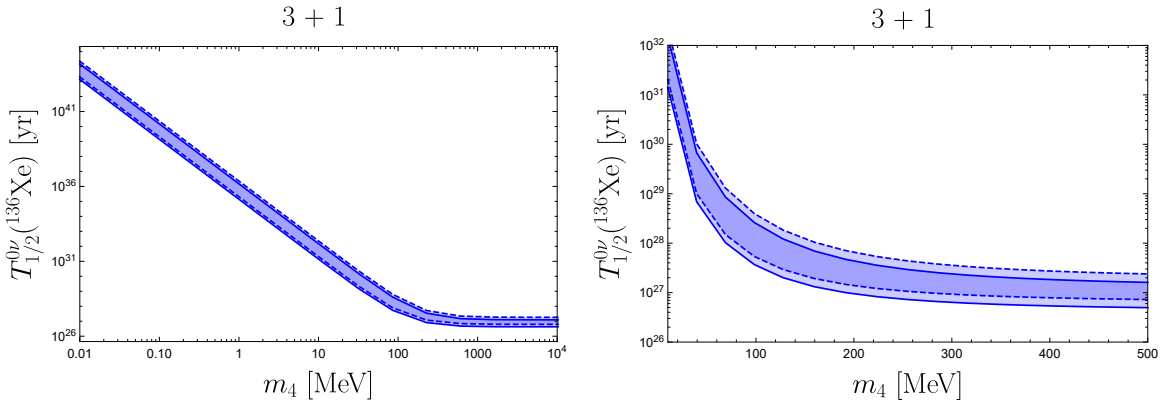

Figure 3.6: $0\nu\beta\beta$ half-life of ^{136}Xe as a function of m_4 in the 3+1 model. We show results obtained with the QRPA (solid) or Shell Model (dashed) NMEs. The bands reflect the uncertainty due to LECs associated with hard-neutrino exchange. Right-panel: same as left panel but for neutrino masses around the pion mass.

This mass matrix leads to one massless and four massive neutrinos and can be diagonalized by a 5×5 unitary matrix U that consists of physical parameters [134]

$$U^T M_\nu U = \mathrm{diag}(m_1, m_2, m_3, m_4, m_5)\,, \qquad U = \begin{pmatrix} U_{aa} & U_{as} \\ U_{sa} & U_{ss} \end{pmatrix}\,, \tag{3.117}$$

where, in the normal hierarchy, we have

$$U_{aa} = U_{\mathrm{PMNS}} \begin{pmatrix} 1 & 0 \\ 0 & H \end{pmatrix}\,, \qquad U_{as} = i U_{\mathrm{PMNS}} \begin{pmatrix} 0 \\ H m_l^{\frac{1}{2}} R^\dagger M_h^{-\frac{1}{2}} \end{pmatrix}\,, \tag{3.118}$$

$$U_{sa} = i \begin{pmatrix} 0 & \overline{H} M_h^{-\frac{1}{2}} R m_l^{1/2} \end{pmatrix}\,, \qquad U_{ss} = \overline{H}\,. \tag{3.119}$$

Here, m_l and M_h are 2×2 mass matrices

$$m_l = \begin{pmatrix} m_2 & 0 \\ 0 & m_3 \end{pmatrix}\,, \quad M_h = \begin{pmatrix} m_4 & 0 \\ 0 & m_5 \end{pmatrix}\,, \tag{3.120}$$

and U_{PMNS} and R are 3×3 and 2×2 matrices

$$U_{\mathrm{PMNS}} = R^{23} W^{13} R^{12}\, \mathrm{diag}(1, 1, e^{i\alpha})\,, \tag{3.121}$$

$$R = \begin{pmatrix} \cos(\theta_{45} + i\gamma_{45}) & \sin(\theta_{45} + i\gamma_{45}) \\ -\sin(\theta_{45} + i\gamma_{45}) & \cos(\theta_{45} + i\gamma_{45}) \end{pmatrix}\,, \tag{3.122}$$

where $\theta_{45} \in [0, \pi/2]$ and $\gamma_{45} \in (-\infty, \infty)$. As the name implies, U_{PMNS} is the usual PMNS matrix consisting of 3 mixing angles, 1 Dirac phase, and 1 Majorana phase (there is only 1 Majorana phase because $m_1 = 0$). The matrices H and $\overline{H}$ are composed of the above mass and rotation matrices

$$H = \left[I + m_l^{\frac{1}{2}} R^\dagger M_h^{-1} R m_l^{\frac{1}{2}} \right]^{-\frac{1}{2}}\,, \quad \overline{H} = \left[I + M_h^{-\frac{1}{2}} R m_l R^\dagger M_h^{-\frac{1}{2}} \right]^{-\frac{1}{2}}\,. \tag{3.123}$$

NH		Δm^2_{21} [eV^2]	Δm^2_{32} [eV^2]	$\lambda_{1,2}$
		$7.39 \cdot 10^{-5}$	$2.449 \cdot 10^{-3}$	0
3σ		$[6.79,\ 8.01] \cdot 10^{-5}$	$[2.358,\ 2.544] \cdot 10^{-3}$	$[0,\ \pi]$
	$\sin^2\theta_{12}$	$\sin^2\theta_{23}$	$\sin^2\theta_{13}$	δ_{13}/π
	$3.10 \cdot 10^{-1}$	$5.58 \cdot 10^{-1}$	$2.241 \cdot 10^{-2}$	1.23
3σ	$[2.75,\ 3.50] \cdot 10^{-1}$	$[4.27,\ 6.09] \cdot 10^{-1}$	$[2.046,\ 2.440] \cdot 10^{-2}$	[0.78, 2.06]
IH		Δm^2_{21} [eV^2]	Δm^2_{32} [eV^2]	$\lambda_{1,2}$
		$7.39 \cdot 10^{-5}$	$-2.509 \cdot 10^{-3}$	0
3σ		$[6.79,\ 8.01] \cdot 10^{-5}$	$[-2.603,\ -2.416] \cdot 10^{-3}$	$[0, \pi]$
	$\sin^2\theta_{12}$	$\sin^2\theta_{23}$	$\sin^2\theta_{13}$	δ_{13}/π
	$3.10 \cdot 10^{-1}$	$5.63 \cdot 10^{-1}$	$2.261 \cdot 10^{-2}$	1.58
3σ	$[2.75,\ 3.50] \cdot 10^{-1}$	$[4.30,\ 6.12] \cdot 10^{-1}$	$[2.066,\ 2.461] \cdot 10^{-2}$	[1.14, 1.97]
3+2	θ_{45}	γ_{45}		
	$\pi/8$	0.5		

Table 3.6: Input parameters used for the analysis of the standard three-light Majorana neutrino scenario, depicted in Fig. 3.5, and the 3+2 model. The values of the light neutrino mass splittings and the PMNS angles are taken from Ref. [132].

The above form of U assumes $m_1 = 0$ making it directly applicable to the case of the NH, while in the case of the IH we instead have $m_3 = 0$. To account for this change we can replace $m_{2,3} \to m_{1,2}$ in the above, leading to a solution of $U^T M_\nu U = \text{diag}(0, m_1, m_2, m_4, m_5)$, after which the mass matrix can be brought into its usual ordering by rearranging the columns of U. Although this procedure leads to a perfectly adequate parametrization of U, it does not lead to the familiar identification of the mixing angles s_{ij} with the solar and reactor angles. To ensure that the usual U_{PMNS} appears as the upper left-hand block in our parametrization of U (in the limit $m_{4,5} \to \infty$) we simply follow the steps of the derivation in Ref. [134], starting from Eq. (3.117) with $m_3 = 0$ instead of $m_1 = 0$. This leads to a form of U which can again be written as in Eq. (3.117), but now

$$\begin{aligned} U_{aa} &= U_{PMNS}\hat{H}\,, \qquad U_{as} = iU_{PMNS}\hat{H}R_3 \begin{pmatrix} 0 \\ m_l^{1/2} R^\dagger M_h^{-1/2} \end{pmatrix}, \\ U_{sa} &= i \begin{pmatrix} 0 & \bar{H} M_h^{-1/2} R m_l^{1/2} \end{pmatrix} R_3^T\,, \qquad U_{ss} = \bar{H}\,, \end{aligned} \tag{3.124}$$

where $m_l = \text{diag}(m_1, m_2)$, while $\hat{H} = R_3 \begin{pmatrix} 1 & 0 \\ 0 & H \end{pmatrix} R_3^T$, with H as in Eq. (3.123) but using $m_l = \text{diag}(m_1, m_2)$, and $R_3 = W^{13}(-\pi/2, 0) W^{23}(\pi/2, 0)$. M_h and $\bar{H}$ are left unchanged. To obtain these expressions we used the relation

$$\text{diag}(m_1, m_2, 0, m_4, m_5) = \begin{pmatrix} R_3 & 0 \\ 0 & 1 \end{pmatrix} \text{diag}(0, m_1, m_2, m_4, m_5) \begin{pmatrix} R_3 & 0 \\ 0 & 1 \end{pmatrix}^T, \tag{3.125}$$

to write Eq. (3.117) in the form of Eq. (2.3) of Ref. [134]. The rest of the derivation then closely follows that of Ref. [134], leading to a similar form of U as in the NH case, but with additional factors of R_3.

We do not wish to perform a fully general analysis of the parameters in the mixing matrix. Instead, we fix all parameters except for m_4 and m_5. We work in the normal hierarchy and set

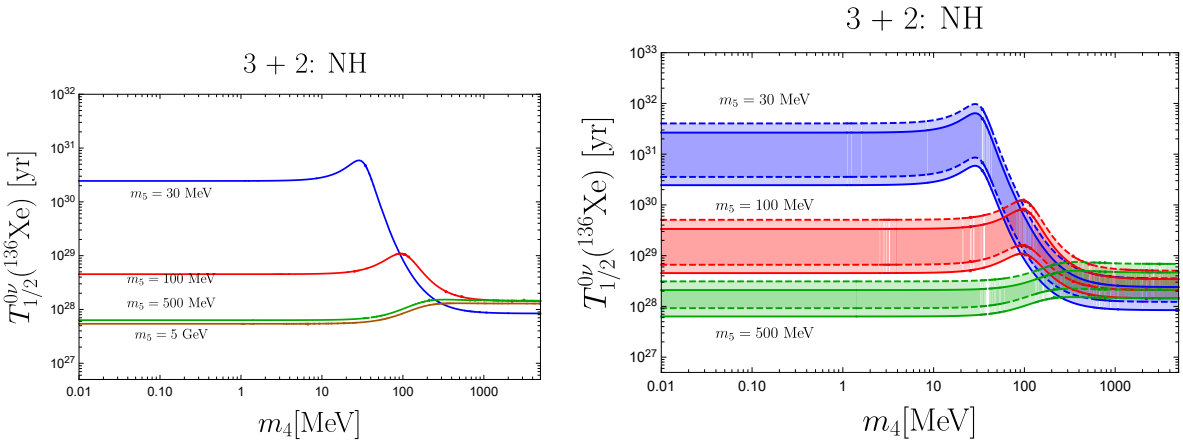

Figure 3.7: Left panel: $0\nu\beta\beta$ half-life of ^{136}Xe as a function of m_4 for $m_5 = 30$ MeV (blue), $m_5 = 100$ MeV (red), $m_5 = 500$ MeV (green), and $m_5 = 5000$ MeV (orange) in the NH. Right panel: Same as left panel but now we included uncertainties from NMEs and LECs. Bands correspond to $m_5 = 30$ MeV (blue), $m_5 = 100$ MeV (red), $m_5 = 500$ MeV (green).

$m_2 = \sqrt{\Delta m^2_{\mathrm{SOL}}} \simeq 8.58 \cdot 10^{-3}$ eV and $m_3 = \sqrt{\Delta m^2_{\mathrm{ATM}}} \simeq 0.05$ eV. We pick the best-fit values for the PMNS mixing angles and Dirac phase [132]. For simplicity we set the Majorana phase to zero, $\alpha = 0$. While the choice of θ_{45} does not affect the unitary matrix drastically, U_{e2} and U_{e3} can deviate from the experimental values if $\gamma_{45} \gtrsim \mathcal{O}(1)$. Taking into account this restriction, we pick moderate values for θ_{45} and γ_{45}. All choices of parameters are given in Table 3.6.

We show the lifetime $T^{0\nu}_{1/2}(^{136}\mathrm{Xe})$ in the case of the NH as a function of m_4 for four different values of m_5 in the left-panel of Fig. 3.7. We use the QRPA NMEs of Ref. [115] and a specific value of the short-distance LECs to not clutter the plots too much. We set

$$g_\nu^{\mathrm{NN}}(0) = -138.7\ \mathrm{GeV}^{-2}\,, \qquad g_1^{\mathrm{NN}}(m_0) = (5 + 3g_A^2)/4\,, \tag{3.126}$$

as discussed in Sect. 3.6.1. We can observe a few things. For small $m_5 < m_\pi$ and $m_4 \ll m_5$ the half life becomes independent of m_4 and scales as m_5^4, similar to the behavior of the 3+1 scenario for small m_4 (the left part of Fig. 3.6). This is the 'cancellation regime', where the NMEs and LECs become m_i independent and

$$\mathcal{A}_L(m_i) \sim \sum_{i=1}^{5} U_{ei}^2 m_i (\bar{\mathcal{M}}_V(m_i) + (\bar{\mathcal{M}}_A(m_i)) \sim \mathcal{O}(U_{ei}^2 m_i^3) \propto m_5^2\,, \tag{3.127}$$

since $U_{e5} \sim \sqrt{m_l/m_5}$. The scaling with m_5^4 breaks down for larger values of m_5, in fact, for $m_5 \geq 500$ MeV and $m_4 \ll m_\pi$ the half life becomes essentially independent of both m_4 and m_5 as can be seen by comparing the left part of the green and orange lines.

For $m_4 \gg m_\pi$ and $m_5 \geq \Lambda_\chi$ (the right part of the green and orange lines), the scenario becomes similar to a standard seesaw scenario with 3 light Majorana neutrinos and 'decoupled' heavy states. The lifetime becomes roughly 10^{28} yr, the predicted lifetime in the NH for a massless lightest neutrino and vanishing Majorana phases. Shorter half lives are possible if one neutrino is heavy while the other is at or below the pion mass. Finally, for almost degenerate m_4 and m_5 there is a cancellation leading to a peak in the half life. In the right panel of

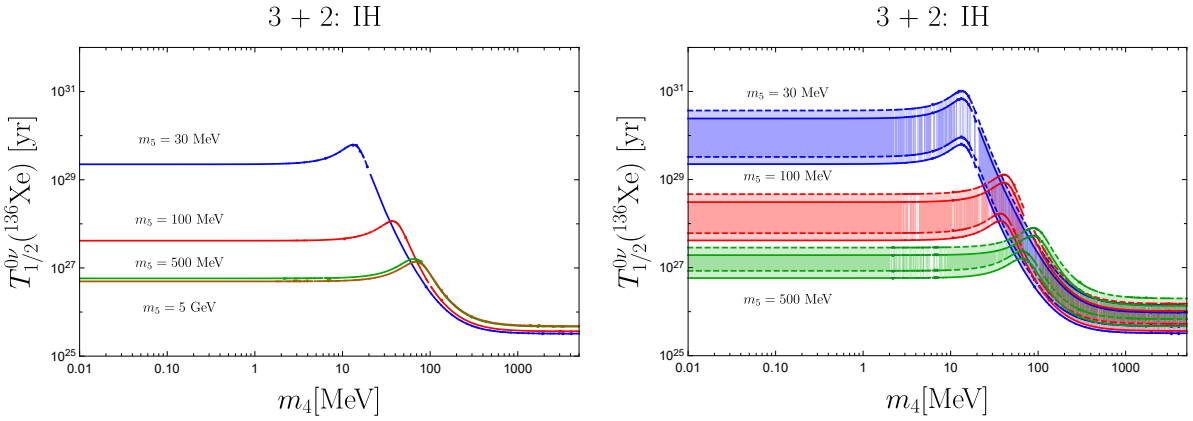

Figure 3.8: Left panel: $0\nu\beta\beta$ half-life of ^{136}Xe as a function of m_4 for $m_5 = 30$ MeV (blue), $m_5 = 100$ MeV (red), $m_5 = 500$ MeV (green), and $m_5 = 5000$ MeV (orange) in the IH. Right panel: Same as left panel but now we included uncertainties from NMEs and LECs. Bands correspond to $m_5 = 30$ MeV (blue), $m_5 = 100$ MeV (red), $m_5 = 500$ MeV (green).

Fig. 3.7, we show the same results for three choices of m_5, now including the uncertainty from the short-distance LECs and we show results for two choices of NMEs. The uncertainties are at the order-of-magnitude level.

The case of the IH is shown in Fig. 3.8, which shows a behavior that is very similar to that of the NH scenario. In particular, at large values of m_5 the half life becomes almost independent of $m_{4,5}$, while, in the small mass region, the scaling $\sim m_5^4$ reappears. We again see a cancellation when $m_4 \sim m_5$, and the half life approximates that of a seesaw scenario with 3 light neutrinos in the large-$m_{4,5}$ region. In contrast, the absolute value of the half life does differ between the scenarios and is roughly an order of magnitude smaller in the IH than in the NH.

It should be mentioned that Figs. 3.7 and 3.8 depend on the choice of mixing angles and phases, for which we used $\alpha = 0$ and the values in Table 3.6. Varying the phases can lead to significantly larger half lives, especially when they are tuned to induce cancellations between the different contributions, while in other parts of parameter space (often milder) enhancements are possible.

3.7.3 A 3+1 scenario with leptoquark interactions

In this section we illustrate the use of the EFT framework by performing the matching in the case of an explicit model of BSM physics. Our main goal is to illustrate the framework and we consider a simple SM extension. We extend the SM with right-handed neutrinos that interact with leptoquarks (LQs). Leptoquarks are hypothetical particles that convert quarks to leptons and vice versa. All possible representations of LQs are summarized in Ref. [26], and among them is a scalar LQ that transforms as an $SU(3)_c$ triplet, an $SU(2)_L$ doublet, and carries nonzero hypercharge: $\tilde{R}\,(\mathbf{3},\ \mathbf{2},\ 1/6)$. The LQ interaction with sterile neutrinos is given by

$$\mathcal{L}_{\mathrm{LQ}} = -y^{RL}_{ab}\bar{d}_{Ra}\tilde{R}^i\epsilon^{ij}L^j_{Lb} + y^{\overline{LR}}_{ab}\bar{Q}^i_{La}\tilde{R}^i\nu_{Rb} + \mathrm{h.c.}\,, \tag{3.128}$$

where a, b and i, j are flavor and $SU(2)$ indices, respectively. In addition to these interactions, we include the right-handed neutrino Majorana mass terms and Yukawa interactions as in Eq. (2.2).

The LQ interactions are LNC so that LNV only arises from the Majorana mass of the sterile neutrinos. Integrating out $\tilde{R}$, one $\overline{\text{dim-6}}$ operator in Table 2.3 is generated

$$\mathcal{L}^{(\bar{6})}_{\nu_R} = \underset{abcd}{C^{(6)}_{LdQ\nu}} \left(\bar{L}^i_a d_b\right) \epsilon^{ij} \left(\bar{Q}^j_c \nu_{Rd}\right) + \text{h.c.}\,, \tag{3.129}$$

where

$$\underset{abcd}{C^{(\bar{6})}_{LdQ\nu}} = \frac{1}{m^2_{\text{LQ}}} y^{\overline{LR}}_{cd} y^{RL*}_{ba}\,, \tag{3.130}$$

with m_{LQ} being the mass of the $\tilde{R}$ LQ. The above operator, as well as $\mathcal{O}_{L\nu Qd}$ generated through the RGEs of Eq. (2.5), induces the dim-6 scalar and tensor operators in Eq. (2.10) below the electroweak scale. We focus on operators involving the first-generation quarks and charged leptons

$$\mathcal{L}^{(6)}_{\Delta L=0} = \frac{2G_F}{\sqrt{2}} \left[\underset{ea}{\bar{c}^{(6)}_{\text{SR}}}\, \bar{u}_L d_R \bar{e}_L \nu_{Ra} + \underset{ea}{\bar{c}^{(6)}_{\text{T}}}\, \bar{u}_L \sigma^{\mu\nu} d_R \bar{e}_L \sigma^{\mu\nu} \nu_{Ra} \right], \tag{3.131}$$

where the subscripts e and a denote the charged-lepton and neutrino flavor, and

$$\underset{ea}{\bar{c}^{(6)}_{\text{SR}}} = 4 \underset{ea}{\bar{c}^{(6)}_{\text{T}}} = \frac{v^2}{2m^2_{\text{LQ}}} y^{\overline{LR}}_{1a} y^{RL*}_{1e}\,, \tag{3.132}$$

where a runs from 1 to n.

Of course, we also have to include the SM weak interactions and together we obtain the following matching to the operators in Eq. (2.23)

$$\left(C^{(6)}_{\text{VLL}}\right)_{ei} = -2V_{ud}U_{ei}\,, \qquad \left(C^{(6)}_{\text{SRR}}\right)_{ei} = 4\left(C^{(6)}_{\text{TRR}}\right)_{ei} = \sum_{a=1}^{n} \underset{ea}{\bar{c}^{(6)}_{\text{SR}}} U^*_{3+a,i}\,. \tag{3.133}$$

With these nonzero Wilson coefficients the $0\nu\beta\beta$ decay rate can be directly read from the master formula in Eq. (3.63). We use the procedure outlined in Sect. 3.6.1 to obtain matching relations for the relevant LECs and we explicitly give the resulting interpolation formulae in Appendix B.

We first consider the $3+1$ scenario, but now with the additional LQ interactions described above. This only provides a simple toy model in which to study the effects of the LQs, as it also leads to two massless neutrinos and cannot explain the observed oscillation data. A more realistic 3+2 scenario is studied in the next subsection, we note, however, that is also possible to explain the neutrino masses in LQ models without introducing sterile neutrinos, see e.g. [135–137]. For simplicity we set the couplings $y^{\overline{LR}}_{11} y^{RL*}_{1e} = 1$ as deviations can be absorbed in m_{LQ}. For the contributions from the standard mechanism we set the unknown LECs as in Eq. (3.126). The LQ interactions induce a large number of contributions to the subamplitude $\mathcal{A}_L$ as given in Eq. (B.4). Unfortunately most of these contributions are associated to LECs we do not control. To simplify the analysis somewhat we only include contributions from purely pionic operators, where lattice results are available that can help constrain the LECs. The missing contributions from pion-nucleon and nucleon-nucleon interactions can be added once more information about the LECs is obtained. The missing contributions appear at the same order as the pionic contributions we do include, and thus correspond to a significant uncertainty. For the pionic operators we require the interpolation formulae discussed in Eq. (B.11) of Appendix B. These depend on $g^{\pi\pi}_{1,2,3,4,5}$ that are known (see Table 3.1) and the unknown couplings $g^{\pi\pi}_{\text{S1}}(0)$, $g^{\pi\pi}_{\text{TT}}(0)$, $g^{\pi\pi}_{\text{S,VLL}}(0)$, $g^{\pi\pi}_{\text{T,VLL}}(0)$. In this section we use the NDA estimates

$$g^{\pi\pi}_{\text{S1}}(0) = -g^{\pi\pi}_{\text{TT}}(0) = \frac{1}{F^2_\pi}\,, \qquad g^{\pi\pi}_{\text{S,VLL}}(0) = g^{\pi\pi}_{\text{T,VLL}}(0) = -1\,, \tag{3.134}$$

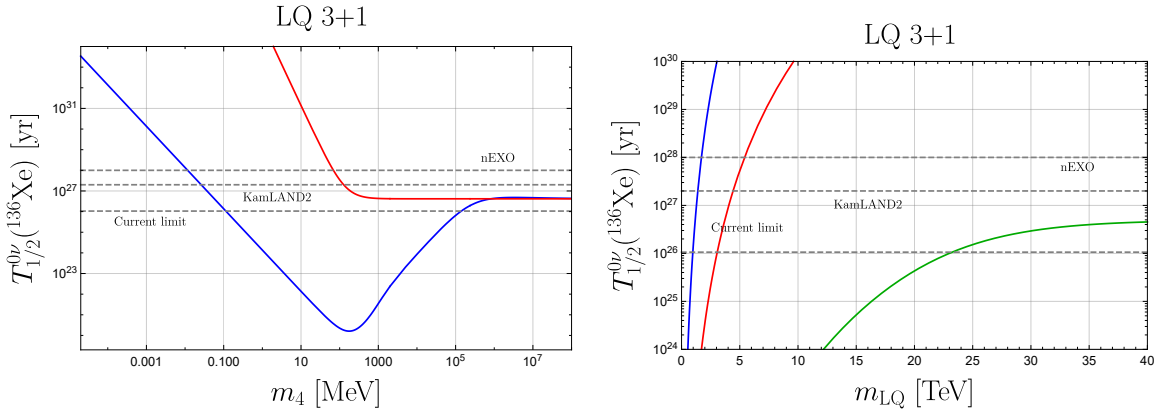

Figure 3.9: Left panel: $T^{0\nu}_{1/2}(^{136}\mathrm{Xe})$ as a function of m_4 in the LQ $3+1$ model. The solid (blue) line is the total half life whereas the dashed (red) line depicts the contribution from just the standard mechanism (exchange of neutrinos interacting via left-handed currents). We have set $y^{\overline{LR}}_{11} y^{RL*}_{12} = 1.0$ and $m_{\mathrm{LQ}} = 10$ TeV. Right panel: Similar but now we fixed $m_4 = 10$ eV (blue), $m_4 = 1$ keV (red), and $m_4 = 5$ GeV (green) and vary m_{LQ}. In both panels the Dirac and Majorana phases were set to zero, $m_3 = \sqrt{\Delta m^2_{\mathrm{ATM}}}$, and the QRPA NMEs were used.

where the signs were chosen in such a way that the LECs do not change sign when varying the neutrino mass.

We plot the resulting $0\nu\beta\beta$ half-life of ^{136}Xe in the left panel of Fig. 3.9 for $m_{\mathrm{LQ}} = 10$ TeV as a function of m_4. The red dashed line denotes the limit of $m_{\mathrm{LQ}} \to \infty$ corresponding the $3+1$ scenario discussed above. We have set the Dirac and Majorana phases to zero, $m_3 = \sqrt{\Delta m^2_{\mathrm{ATM}}}$, and used QRPA NMEs. The theoretical uncertainty due to NMEs and LECs is not shown, but is similar to the $3+1$ and $3+2$ scenarios and thus roughly one-to-two orders of magnitude on the half life. The plot shows that for a light fourth neutrino, $m_4 < 100$ GeV, the LQ interactions completely dominate over the standard mechanism. In fact, the current experiments rule out 10 TeV interactions for $100\,\mathrm{keV} < m_4 < 100$ GeV. In the LQ scenario, $0\nu\beta\beta$ experiments are most constraining at $m_4 \simeq 170$ MeV, where we find $m_{\mathrm{LQ}} > 56$ TeV. Future experiments could push this towards $m_{\mathrm{LQ}} > 150$ TeV.

In the right panel of Fig. 3.9 we show the half life as a function of m_{LQ} for three specific values of m_4. We set $m_4 = 10$ eV, with the eV-scale being motivated by anomalies in neutrino experiments [138–141] (but see Ref. [142] as well), $m_4 = 1$ keV, as motivated by models of sterile neutrino DM [18, 143], and $m_4 = 5$ GeV as motivated by studies of low-scale leptogenesis [144]. For these cases, the limits on m_{LQ} are respectively $m_{\mathrm{LQ}} > 1$ TeV, $m_{\mathrm{LQ}} > 3$ TeV, and $m_{\mathrm{LQ}} > 23$ TeV. While it is difficult for present and future $0\nu\beta\beta$ experiments to probe scenarios with just light sterile neutrinos, these results illustrate that prospects are much better in scenarios where the sterile neutrinos have non-standard interactions.

3.7.4 A 3+2 scenario with leptoquark interactions

We now repeat the analysis in the $3+2$ model. In Sect. 3.7.2 we concluded that detection of $0\nu\beta\beta$ is not possible with the next generation of experiments in the pure $3+2$ model for the NH (see Fig. 3.7). It is interesting to investigate what the scale of BSM physics should be to make

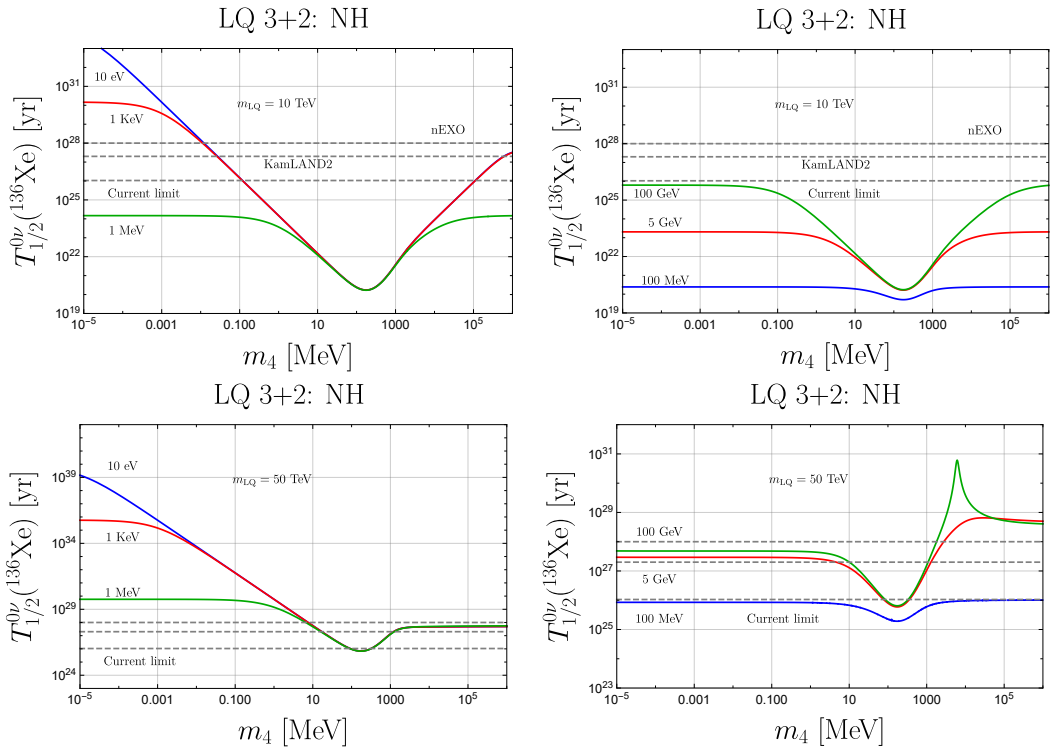

Figure 3.10: Top-left panel: $T^{0\nu}_{1/2}(^{136}\mathrm{Xe})$ as a function of m_4 in the LQ $3+2$ leptoquark model for different choices of $m_5 = 10$ eV (blue), $m_5 = 1$ keV (red), $m_5 = 1$ MeV (green). We consider a leptoquark mass of 10 TeV. Top-right panel: same as top-left but now for $m_5 = 100$ MeV (blue), $m_5 = 5$ GeV (red), $m_5 = 100$ GeV (green). Bottom panels are the same as the top panels but now for a leptoquark mass of 50 TeV. All panels use the same phases, mixing angles, and LECs as in Sect. 3.7.2.

a detection possible. We take the LQ interactions as an example of BSM physics in order to determine the relevant mass of m_{LQ} for different choices of m_4 and m_5. To reduce the number of parameters we set $y_{11}^{\overline{LR}} y_{1e}^{RL*} = y_{12}^{\overline{LR}} y_{1e}^{RL*} = 1$ and use the same phases, angles and LECs as in Sect. 3.7.2. We do not show the dependence on the LQ couplings explicitly, but note that they always appear in the combination $\frac{y_{1a}^{\overline{LR}} y_{1e}^{RL*}}{m_{\mathrm{LQ}}^2}$, so that a shift in the couplings of, for example, $y_{1a}^{\overline{LR}} y_{1e}^{RL*} \to 10^{-2}$, is equivalent to rescaling the LQ mass by a factor of 10.

In the top-left panel of Fig. 3.10, we set $m_{\mathrm{LQ}} = 10$ TeV and $m_5 = 10$ eV (blue), $m_5 = 1$ keV (red), $m_5 = 1$ MeV (green) and vary m_4. Current experiments already rule out such scenarios for a significant range of m_4. For m_5 in the MeV range, the resulting half lives are too short and excluded. For light $m_5 \leq$ keV, the scenario is excluded for $100\,\mathrm{keV} < m_4 < 100\,\mathrm{GeV}$. In the top-right panel, we set $m_5 = 100$ MeV (blue), $m_5 = 5$ GeV (red), $m_5 = 100$ GeV (green) and conclude that such values are ruled out independent of m_4. Of course, the results depend on the scale of BSM physics. In the bottom panels we repeat the analysis but now set $m_{\mathrm{LQ}} = 50$ TeV. The bottom-left panel, corresponding to light m_5, tells us that future experiments are sensitive if $m_4 > 10$ MeV, while scenarios where both m_4 and m_5 are light lead to decay rates that are too slow to observe. The right panel shows that current limits already exclude the scenario for $m_5 = 100$ MeV independent of m_4. For larger m_5, nEXO can observe $0\nu\beta\beta$ events if $m_4 < 1$

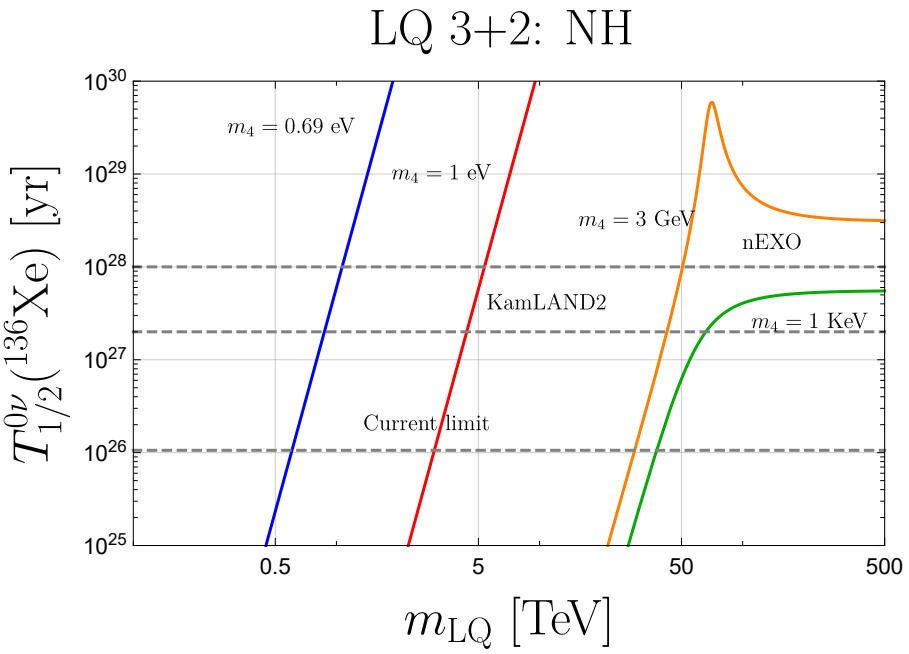

Figure 3.11: $T_{1/2}^{0\nu}(^{136}\mathrm{Xe})$ as a function of m_{LQ} for 4 choices of m_4 and m_5. The blue line corresponds to $m_4 = 0.69$ eV and $m_5 = 1$ eV, the red line to $m_4 = 1$ eV and $m_5 = 1$ keV, the green line to $m_4 = 1$ keV and $m_5 = 1$ GeV, and the orange line to $m_4 = 3$ GeV and $m_4 = 4$ GeV. The same phases, mixing angles, and LECs as in Sect. 3.7.2 were used.

GeV.

Our main goal is not to exhaustively investigate the parameter space of this LQ model. Instead, we wish to highlight that future $0\nu\beta\beta$ experiments are sensitive to a class of BSM models with light sterile neutrinos if they have weak non-standard interactions with SM fields. How weak these interactions can be depends on the exact value of the neutrino masses, but scales of 1-100 TeV can be accessed. We illustrate this in Fig. 3.11. In scenarios with m_4 and m_5 around 1 eV, the ^{136}Xe half life from just the standard mechanism is roughly 10^{60} yr, but nEXO can make a detection for $m_{\mathrm{LQ}} \leq 1$ TeV. In this particular case, LHC experiments already strongly constrain such LQ masses [145, 146], but for heavier neutrinos much higher LQ mass scales can be probed. For instance, for m_4 at the keV scale and m_5 at the GeV scale, next-generation experiments are sensitive to leptoquark masses up to 100 TeV.

This discussion highlights the important role that $0\nu\beta\beta$ experiments can play in understanding the nature and interactions of sterile neutrinos. While a positive $0\nu\beta\beta$ signal alone cannot unambiguously be interpreted as evidence for sterile neutrinos, $0\nu\beta\beta$ experiments, in conjunction with direct observations in laboratory experiments or astrophysical probes, can put severe constraints on the possible interactions of these particles that are very competitive with other low-energy probes and high-energy collider experiments.

3.8 Conclusions

Sterile neutrinos are natural candidates to explain the origin of active neutrino masses via the type-I seesaw mechanism [14–16], which, however, does not definitively point towards a specific

mass scale. While the smallness of neutrino masses can be realized with very massive ν_R, $m_{\nu_R} \sim 10^{15}$ GeV, with $\mathcal{O}(1)$ Yukawa couplings to SM leptons, the sterile neutrino mass scale can be lowered to the TeV scale [16], inducing interesting signals at the Large Hadron Collider [147], or even to the GeV or sub-GeV region [144, 148]. In such scenarios the sterile neutrinos could provide a dark matter candidate and induce the correct matter-antimatter asymmetry in the Universe [19, 20, 144, 148]. While muon, meson, and nuclear β decays constrain the interactions of sterile neutrinos with SM particles to be more feeble than the weak interaction, in generic models ν_R can be charged under new forces, mediated by bosons with masses much larger than the W and Z masses. These interactions, while weak, can leave traces in high-precision experiments, including searches for $0\nu\beta\beta$.

In this chapter, we studied the impact of light sterile neutrinos with mass smaller than the electroweak scale, $m_{\nu_R} < v$, on $0\nu\beta\beta$, in a systematic framework which relies on a tower of EFTs. The contribution of sterile neutrinos to $0\nu\beta\beta$ has been investigated extensively in the literature [97, 119, 120, 149, 150], in the minimal scenario in which ν_R has only renormalizable interactions, namely the Majorana mass term M_R and a Yukawa interaction Y_ν in Eq. (2.2). Here we extend these works in several, significant directions

- We extend the SM by adding a (family) of sterile neutrinos ν_R, which are singlets under the SM gauge group. At scales larger than the electroweak scale, we allow the ν_R to interact with SM degrees of freedom via a dimension-four Yukawa interaction, and the most general set of gauge-invariant higher-dimensional operators up to $\overline{\text{dim-7}}$, in the framework of the sterile-neutrino-extended SMEFT [27, 28, 151]. With the exclusion of the Majorana mass term in Eq. (2.2), we consider operators with at most one ν_R, which are the most relevant for $0\nu\beta\beta$. The $\overline{\text{dim-6}}$ LNC operators with active and sterile neutrinos are listed in Tables 2.1 and 2.3, respectively, while the $\overline{\text{dim-7}}$ LNV operators are given in Tables 2.2 and 2.4. The renormalization-group equations describing the QCD evolution for the coefficients of the $\overline{\text{dim-6}}$ and $\overline{\text{dim-7}}$ operators is given in Eqs. (2.5) and (2.7).

- We match the SMEFT operators onto $SU(3) \times U(1)_{\text{em}}$-invariant operators, by integrating out heavy SM degrees of freedom. For $2\,\text{GeV} \lesssim m_{\nu_R} < v$, the sterile neutrino is also integrated out in this step, and one is left with dim-9 operators in Eqs. (3.2) and (3.3), with coefficients given by Eqs. (3.9), (3.10), and (3.11). If ν_R is lighter, it remains dynamical in chiral EFT. In this case, at the quark level, one finds the generalized LNC and LNV β-decay Lagrangians in Eqs. (2.9), (2.10), (2.11), and (2.12), which involve, vector, axial, scalar, pseudoscalar, and tensor currents as well as derivative operators. Rotating these interactions to the neutrino mass basis gives rise to the operators in Eqs. (2.21) and (2.22), whose coefficients can be expressed in terms of the gauge-invariant operators in Sect. 2.2.

- We systematically construct the chiral Lagrangian in the presence of light sterile neutrinos with non-standard interactions, starting from the quark-level operators in Eqs. (2.21) and (2.22). This Lagrangian includes terms with explicit neutrinos, that couple to pions and nucleons via the vector, axial, scalar, pseudoscalar, and tensor currents. These are constructed in Sects. 3.2.1 and 3.2.4, and the neutron β-decay transition operator is summarized in Eq. (3.26). In addition, the Chiral Lagrangian contains LNV operators that couple pions and nucleons to two leptons, which are induced by the exchange of virtual light neutrinos. In Sect. 3.2.6 we construct, for the first time, these operators in full generality and we show that the $\pi\pi ee$ and $nnppee$ couplings contribute at LO for several higher-dimensional operators. We discuss the dependence of the LECs of these operators

on the neutrino mass, and demonstrate that they are needed to guarantee that the $0\nu\beta\beta$ amplitude has a smooth dependence on the neutrino mass.

- We identify all the chiral EFT low-energy constants required for the derivation of the $0\nu\beta\beta$ operator at LO. They are summarized in Table 3.1. With the exception of the recoil-order LEC appearing in the tensor current, g_T', all LECs in the neutron β-decay operator are well known, either from experiment or Lattice QCD. The $\pi\pi$ couplings induced by dim-9 operators are also well known [100], while $\pi\pi$ couplings induced by hard-neutrino exchange and πN and NN couplings induced by dim-9 operators and hard-neutrino exchange are at the moment mostly undetermined. The ignorance of these LECs causes a sizable hadronization uncertainty in the $0\nu\beta\beta$ half-lives, which, though usually neglected, is often as big as the error from nuclear matrix elements, see for example Figs. 3.5.

- We derive the $0\nu\beta\beta$ transition operator in Sect. 3.3 and the master formula for $0\nu\beta\beta$ in Sect. 3.4. In spite of the large number of operators, we find that the final form of the amplitude and the half-lives, Eqs. (3.62) and (3.63), are rather compact and involve structures that are very similar to those found for the exchange of active neutrinos in Refs. [71, 82]. In particular, they involve the same nuclear matrix elements, with the difference that, for $1\,\text{MeV} < m_\nu < \Lambda_\chi$, the NMEs acquire a non-trivial dependence on the neutrino mass.

- We study the dependence of the $0\nu\beta\beta$ half-lives on the neutrino masses. For neutrino masses below Λ_χ, the dependence arises in two ways, explicitly via the neutrino propagators in the neutrino potentials and implicitly via the LECs induced by hard-neutrino exchange. In contrast, if $m_{\nu_R} \gg \Lambda_\chi$, the mass dependence appears through the matching coefficients of dim-9 operators. We derive interpolation formulae, grounded in QCD and χPT, for both the nuclear matrix elements, in Sect. 3.5.1, and the LECs, in Sect. 3.6. These formulae allow us to smoothly interpolate between the $m_{\nu_R} \ll \Lambda_\chi$ and the $m_{\nu_R} \gg \Lambda_\chi$ regimes, as shown in Figs. 3.9, and to get the correct chiral EFT scaling of the amplitudes. The interpolation formulae for the LECs are partially phenomenological, due to the difficulties to treat the intermediate region $m_\pi \ll m_{\nu_R} \lesssim \Lambda_\chi$ rigorously, but can be systematically improved by calculating pion, nucleon, and two-nucleon LNV matrix elements with nonperturbative methods for different neutrino masses.

- As a consequence of the systematic construction of the chiral Lagrangian and the study of the mass dependence of NMEs and LECs, we can address all sources of theoretical uncertainties on the $0\nu\beta\beta$ half-lives, induced by active and sterile neutrinos. An important finding is that the hadronization uncertainty is very significant. We estimate this uncertainty by conservatively varying the unknown LECs in the range expected on the basis of naive dimensional analysis and internal theoretical consistency. We recommend to include the hadronization uncertainty in future analyses of $0\nu\beta\beta$. As an example, in the left panel of Fig. 3.5 we show the usual inverted and normal hierarchy predictions for the ^{136}Xe half life as a function of the lightest neutrino mass with errors bands that include the hadronization uncertainty. This can be compared with the right panel where this hadronic uncertainty has been neglected.

To illustrate the use of the developed EFT framework, we studied several scenarios with light sterile neutrinos. Scenarios with two additional sterile neutrinos can reproduce all neutrino oscillation data. In the normal hierarchy, a minimal model where sterile neutrinos only interact via mixing, leads to ^{136}Xe half lives that for all choices of m_4 and m_5 are (slightly) above 10^{28} yr, the prospected sensitivity of next-generation experiments. In the inverted hierarchy a

detection will be possible if at least one of the neutrinos has a mass above $\mathcal{O}(500)$ MeV. These conclusions change drastically in the presence of higher-dimensional interactions. For instance, $0\nu\beta\beta$ experiments already exclude scalar interactions at a scale of 10 TeV if one of the neutrinos has a mass around the keV scale and the other at the GeV scale. Such mass ranges appear in scenarios where sterile neutrinos can account for both Dark Matter and the matter-antimatter asymmetry [20], although to account for both at least three sterile neutrinos are necessary. Depending on the exact neutrino masses, next-generation experiments are sensitive to scales up to $\mathcal{O}(100)$ TeV. The framework developed here, and the master formula in (3.63) in particular, can be used directly to assess the impact of $0\nu\beta\beta$ experiments on any BSM scenario with light sterile neutrinos and should prove useful when comparing $0\nu\beta\beta$ with other probes of sterile neutrinos.

Chapter 4

Lepton-number-violating kaon decays in νSMEFT up to dimension seven

In this chapter[1] we study the lepton-number-violating kaon decays $K^{\mp} \to \pi^{\pm} l^{\mp} l^{\mp}$ in the presence of sterile neutrinos. We consider minimal interactions with Standard-Model fields via Yukawa couplings as well as higher-dimensional operators in the framework of νSMEFT up to dimension seven. If neutrinos are heavier than the EW scale, we integrate them out and their low-energy signature is captured by SMEFT operators with odd dimension. Refs. [85,152] have investigated this case in detail. When neutrino masses are below the EW scale, the operators of νSMEFT are evolved to the EW scale and heavy SM particles (top, W, Z, Higgs) are integrated out to match to a Fermi-like EFT extended with ν_R fields that obeys $SU(3)_c \times U(1)_{em}$ gauge symmetry. If the sterile neutrinos are heavier than $\Lambda_\chi \simeq 1$ GeV, they can be integrated out before matching to a chiral EFT Lagrangian. We obtain LNV dimension-9 operators, which involve two up-type quarks, two down-type quarks and two charged leptons as discussed in Sect. 4.1 . These operators induce short-distance LNV contributions and were systematic studied in Refs. [78, 85]. Sterile neutrinos with masses below Λ_χ are active degrees of freedom at hadronic scales. We apply $SU(3)$ chiral EFT extended with sterile neutrinos to describe LNV kaon decays in this mass regime. Such neutrinos can be looked for in many different experiments, ranging from oscillation to beta-decay to collider experiments [130, 153–159].

The current experimental upper bounds on the LNV branching ratios of charged kaons are very stringent (5.3×10^{-11} and 4.2×10^{-11} [68, 69] for $K^- \to \pi^+ e^- e^-$ and $K^- \to \pi^+ \mu^- \mu^-$, respectively). Nevertheless, unlike the case for $0\nu\beta\beta$ these bounds are too weak to set meaningful constraints on the BSM scale Λ for the exchange of virtual sterile neutrinos . However, if a sterile neutrino can be produced on shell, the LNV decay rate is significantly enhanced due to the small width of the sterile neutrino [160]. We apply the narrow-width approximation to modify the decay amplitude and use the resonance to constrain the neutrino mixing angles and the BSM scale. Similar ideas were used for other kinds of LNV decays including D, D_s, B, B_s, B_c, and τ decays, see Refs. [161–167] for discussions on the minimal scenario without higher-dimensional operators and Ref. [168] on the left-right symmetric model.

We present the possible Feynman diagrams relevant with $K^- \to \pi^+ l^- l^-$ in Fig. 4.1. The first three accomplish LNV through the exchange of a light neutrino (long-distance contribution). They can be divided into two parts, one for the leptonic decay of K^- and the other for the leptonic decay of π^-. To get the hadronic operators that induce leptonic decay of mesons, we need quark-level operators involving an up quark, a down (strange) quark, a charged lepton and

[1] This chapter is based on G. Zhou, JHEP 06 (2022) 127.

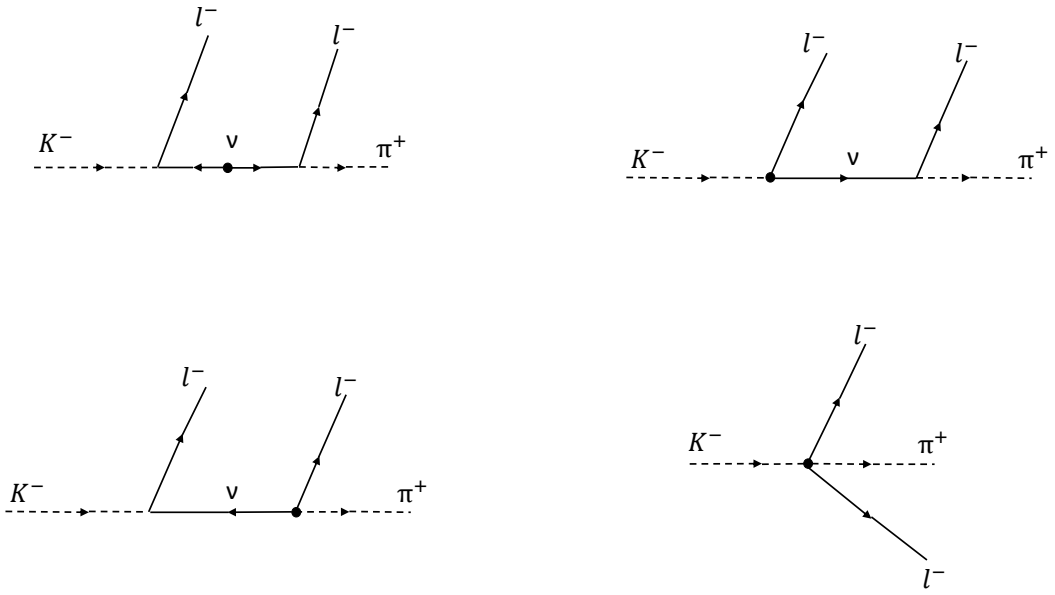

Figure 4.1: Possible Feynman diagrams for $K^- \to \pi^+ l^- l^-$ and the black blob denotes LNV interactions.

a neutrino, which are at least dim-6 after EWSB. The fourth diagram contains no neutrino and we call it the short-distance contribution. It may be induced by integrating heavy neutrinos out or arise from $\overline{\text{dim-7}}$ operators without neutrinos (see Eqs. (4.4) and (4.5)).

The method to study LNV kaon deays is very similar to that of $0\nu\beta\beta$. The relevant operators that contribute to LNV kaon decays are also listed in Tables 2.1-2.4 and after EWSB, the resulting operators are the same as those in Sects 2.2 and 2.3, except the different flavor indices of the Wilson coefficients. The Wilson coefficients of Eqs. (2.21) and (2.22) carry flavor indices $ijkl$ where $i = u$ denotes the up quark, $j = d, s$ indicate the down quark and strange quark, $k = e, \mu$ labels the generation of charged lepton and $l = \{1, ..., \bar{n}\}$ denote neutrinos in the mass basis. In this chapter we focus mainly on the operators in Eq. (2.21) as the operators in Eq. (2.22) are relatively suppressed by m_π/v or v/Λ.

4.1 The full complete set of dim-9 operators in case of LNV kaon decays

Before discussing the calculation details we first list the complete set of dim-9 operators , which contain two up quarks, a down quark, a strange quark, and two electrons or muons. Dim-9 operators are induced at the electroweak scale and, when sterile neutrinos have a mass above the chiral-symmetry-breaking scale Λ_χ, at the sterile neutrino mass threshold. We thus again list all possible $SU(3)_c \times U(1)_{em}$ invariant operators

$$\mathcal{L}^{(9)}_{\Delta L=2} = \frac{1}{v^5} \sum_i \left[\left(C^{(9)}_{i\,\mathrm{R}}\, \bar{l}_R C \bar{l}^T_R + C^{(9)}_{i\,\mathrm{L}}\, \bar{l}_L C \bar{l}^T_L \right) O_i + C^{(9)}_i \bar{l} \gamma_\mu \gamma_5 C \bar{l}^T\, O^\mu_i \right], \tag{4.1}$$

where $l = e\,, \mu$, and O_i (O^μ_i) contain four quarks and they are Lorentz scalars (vectors). In general there should also be Lorentz tensors, but here we only consider the case when both of

the two outgoing leptons are electrons or muons and thus the tensor operators vanish. The scalar operators are [83–85]

$$\begin{aligned}
O_1 &= \bar{u}_L^\alpha \gamma_\mu d_L^\alpha \; \bar{u}_L^\beta \gamma^\mu s_L^\beta , & O_1' &= \bar{u}_R^\alpha \gamma_\mu d_R^\alpha \; \bar{u}_R^\beta \gamma^\mu s_R^\beta , \\
O_2 &= \bar{u}_R^\alpha d_L^\alpha \; \bar{u}_R^\beta s_L^\beta , & O_2' &= \bar{u}_L^\alpha d_R^\alpha \; \bar{u}_L^\beta s_R^\beta , \\
O_3 &= \bar{u}_R^\alpha d_L^\beta \; \bar{u}_R^\beta s_L^\alpha , & O_3' &= \bar{u}_L^\alpha d_R^\beta \; \bar{u}_L^\beta s_R^\alpha , \\
O_4 &= \bar{u}_R^\alpha d_L^\alpha \; \bar{u}_L^\beta s_R^\beta , & O_4' &= \bar{u}_L^\alpha d_R^\alpha \; \bar{u}_R^\beta s_L^\beta , \\
O_5 &= \bar{u}_R^\alpha d_L^\beta \; \bar{u}_L^\beta s_R^\alpha , & O_5' &= \bar{u}_L^\alpha d_R^\beta \; \bar{u}_R^\beta s_L^\alpha ,
\end{aligned} \tag{4.2}$$

where α, β are color indices and a summation over them is implied. We get O_i' by changing the parity of O_i . For the vector operators, we have [83, 85]

$$\begin{aligned}
O^\mu_{6,\text{udus}} &= \bar{u}_L^\alpha \gamma^\mu d_L^\alpha \; \bar{u}_L^\beta s_R^\beta , & O^{\mu\prime}_{6,\text{udus}} &= \bar{u}_R^\alpha \gamma^\mu d_R^\alpha \; \bar{u}_R^\beta s_L^\beta , \\
O^\mu_{6,\text{usud}} &= \bar{u}_L^\alpha \gamma^\mu s_L^\alpha \; \bar{u}_L^\beta d_R^\beta , & O^{\mu\prime}_{6,\text{usud}} &= \bar{u}_R^\alpha \gamma^\mu s_R^\alpha \; \bar{u}_R^\beta d_L^\beta , \\
O^\mu_{7,\text{udus}} &= \bar{u}_L^\alpha \gamma^\mu d_L^\beta \; \bar{u}_L^\beta s_R^\alpha , & O^{\mu\prime}_{7,\text{udus}} &= \bar{u}_R^\alpha \gamma^\mu d_R^\beta \; \bar{u}_R^\beta s_L^\alpha , \\
O^\mu_{7,\text{usud}} &= \bar{u}_L^\alpha \gamma^\mu s_L^\beta \; \bar{u}_L^\beta d_R^\alpha , & O^{\mu\prime}_{7,\text{usud}} &= \bar{u}_R^\alpha \gamma^\mu s_R^\beta \; \bar{u}_R^\beta d_L^\alpha , \\
O^\mu_{8,\text{udus}} &= \bar{u}_L^\alpha \gamma^\mu d_L^\alpha \; \bar{u}_R^\beta s_L^\beta , & O^{\mu\prime}_{8,\text{udus}} &= \bar{u}_R^\alpha \gamma^\mu d_R^\alpha \; \bar{u}_L^\beta s_R^\beta , \\
O^\mu_{8,\text{usud}} &= \bar{u}_L^\alpha \gamma^\mu s_L^\alpha \; \bar{u}_R^\beta d_L^\beta , & O^{\mu\prime}_{8,\text{usud}} &= \bar{u}_R^\alpha \gamma^\mu s_R^\alpha \; \bar{u}_L^\beta d_R^\beta , \\
O^\mu_{9,\text{udus}} &= \bar{u}_L^\alpha \gamma^\mu d_L^\beta \; \bar{u}_R^\beta s_L^\alpha , & O^{\mu\prime}_{9,\text{udus}} &= \bar{u}_R^\alpha \gamma^\mu d_R^\beta \; \bar{u}_L^\beta s_R^\alpha , \\
O^\mu_{9,\text{usud}} &= \bar{u}_L^\alpha \gamma^\mu s_L^\beta \; \bar{u}_R^\beta d_L^\alpha , & O^{\mu\prime}_{9,\text{usud}} &= \bar{u}_R^\alpha \gamma^\mu s_R^\beta \; \bar{u}_L^\beta d_R^\alpha .
\end{aligned} \tag{4.3}$$

The matching conditions for the relevant dim-9 operators are [79]

$$\begin{aligned}
\frac{1}{v^3} C^{(9)}_{1L} &= -4 V_{ud} V_{us} \left(C^{(7)}_{LHD\,1} + 4 \mathcal{C}_{LHW} \right)^* , \\
\frac{1}{v^3} C^{(9)}_{5L} &= 4 i V_{ud} \, C^{(7)*}_{LL\bar{d}uD\,1,us} , \\
\frac{1}{v^3} C^{(9)\prime}_{5L} &= 4 i V_{us} \, C^{(7)*}_{LL\bar{d}uD\,1,ud} .
\end{aligned} \tag{4.4}$$

Note that the notations and basis for dim-9 operators in the cases of LNV kaon decays and $0\nu\beta\beta$ are different because they contain different types of quarks. The higher-dimensional operators are evolved from some BSM scale $\mu = \Lambda$ to the EW scale $\mu = m_W$ and then to the QCD scale Λ_χ.

To integrate out heavy neutrinos above the chiral-symmetry-breaking scale Λ_χ, we again write the Lagrangian containing heavy neutrinos as Eq.(3.5) and by using the equation of motion we integrate out the heavy neutrinos and get the following effective Lagrangian

$$\begin{aligned}
\mathcal{L}_{eff} &\simeq \frac{1}{2m_{\nu_i}^2} \mathcal{J}_i (i\partial\!\!\!/ + m_{\nu_i}) C \mathcal{J}_i^T , \\
\mathcal{J}_i &= J_{ud,i} + J_{us,i} + \bar{J}_{ud,i} + \bar{J}_{us,i} , \\
J_{ud,i} &\simeq \frac{1}{v^2} \Big[\bar{u}_L \gamma^\mu d_L \left[\bar{e}_R \gamma_\mu C^{(6)}_{\text{VLR}} + \bar{e}_L \gamma_\mu C^{(6)}_{\text{VLL}} \right] + \bar{u}_R \gamma^\mu d_R \left[\bar{e}_R \, \gamma_\mu C^{(6)}_{\text{VRR}} + \bar{e}_L \, \gamma_\mu C^{(6)}_{\text{VRL}} \right] \\
&+ \bar{u}_L d_R \left[\bar{e}_L \, C^{(6)}_{\text{SRR}} + \bar{e}_R \, C^{(6)}_{\text{SRL}} \right] + \bar{u}_R d_L \left[\bar{e}_L \, C^{(6)}_{\text{SLR}} + \bar{e}_R \, C^{(6)}_{\text{SLL}} \right] \\
&+ \bar{u}_L \sigma^{\mu\nu} d_R \, \bar{e}_L \sigma_{\mu\nu} C^{(6)}_{\text{TRR}} + \bar{u}_R \sigma^{\mu\nu} d_L \, \bar{e}_R \sigma_{\mu\nu} C^{(6)}_{\text{TLL}} \Big]_i , \\
J_{us,i} &= J_{ud,i}|_{d \to s} ,
\end{aligned} \tag{4.5}$$

where $\bar{J}_i$ is the hermitian conjugate of J_i, a sum over i is implied and by transposing the leptonic part of $\mathcal{J}_i$ we get $\mathcal{J}_i^T$. The interactions relevant with $K^- \to \pi^+ l^- l^-$ are

$$\mathcal{L}_H^{(9)} \simeq \sum_{i=1}^{n_H} \frac{1}{m_{\nu_i}^2} J_{us,i}(i\partial\!\!\!/ + m_{\nu_i}) C J_{ud,i}^T \,, \tag{4.6}$$

which contain two kinds of terms, one proportional to $\frac{1}{m_{\nu_i}}$ and the other proportional to $\frac{1}{m_{\nu_i}^2}$ with an additional derivative. Here we give the matching conditions for terms of the first kind. We find for the scalar dim-9 operators

$$\begin{aligned}
C_{1\,R}^{(9)} &= -vC_{\mathrm{VLR,us}}^{(6)} \bar{m}_\nu^{-1} C_{\mathrm{VLR,ud}}^{(6)\,T} \,, \qquad C_{1\,R}^{(9)\prime} = -vC_{\mathrm{VRR,us}}^{(6)} \bar{m}_\nu^{-1} C_{\mathrm{VRR,ud}}^{(6)\,T} \,, \\
C_{2\,R}^{(9)} &= vC_{\mathrm{SLL,us}}^{(6)} \bar{m}_\nu^{-1} C_{\mathrm{SLL,ud}}^{(6)\,T} - 16vC_{\mathrm{TLL,us}}^{(6)} \bar{m}_\nu^{-1} C_{\mathrm{TLL,ud}}^{(6)\,T} \,, \qquad C_{2\,R}^{(9)\prime} = vC_{\mathrm{SRL,us}}^{(6)} \bar{m}_\nu^{-1} C_{\mathrm{SRL,ud}}^{(6)\,T} \,, \\
C_{3\,R}^{(9)} &= -32vC_{\mathrm{TLL,us}}^{(6)} \bar{m}_\nu^{-1} C_{\mathrm{TLL,ud}}^{(6)\,T} \,, \qquad C_{3\,R}^{(9)\prime} = 0 \,, \\
C_{4\,R}^{(9)} &= vC_{\mathrm{SRL,us}}^{(6)} \bar{m}_\nu^{-1} C_{\mathrm{SLL,ud}}^{(6)\,T} \,, \qquad C_{4\,R}^{(9)\prime} = vC_{\mathrm{SLL,us}}^{(6)} \bar{m}_\nu^{-1} C_{\mathrm{SRL,ud}}^{(6)\,T} \,, \\
C_{5\,R}^{(9)} &= 2vC_{\mathrm{VRR,us}}^{(6)} \bar{m}_\nu^{-1} C_{\mathrm{VLR,ud}}^{(6)\,T} \,, \qquad C_{5\,R}^{(9)\prime} = 2vC_{\mathrm{VLR,us}}^{(6)} \bar{m}_\nu^{-1} C_{\mathrm{VRR,ud}}^{(6)\,T} \,,
\end{aligned} \tag{4.7}$$

where $C_{\mathrm{XXX,us}}^{(6)}$ and $C_{\mathrm{XXX,ud}}^{(6)}$ are the coefficients of dim-6 operators in Eq. (2.21) involving a strange quark and a down quark, respectively. We get the matching conditions for the $C_{i\,L}^{(9)}$ operators via the replacement

$$\begin{aligned}
C_{i\,R}^{(9)} &\to C_{i\,L}^{(9)\prime} \,, \qquad C_{i\,R}^{(9)\prime} \to C_{i\,L}^{(9)} \,, \\
C_{\mathrm{ALL}}^{(6)} &\leftrightarrow C_{\mathrm{ARR}}^{(6)} \,, \qquad C_{\mathrm{ARL}}^{(6)} \leftrightarrow C_{\mathrm{ALR}}^{(6)} \,, \qquad A \in \{S, V, T\} \,.
\end{aligned} \tag{4.8}$$

The matching contributions for the vector dim-9 operators are given by

$$
\begin{aligned}
C^{(9)}_{6,\mathrm{usud}} &= \frac{v}{2}\left(C^{(6)}_{\mathrm{VLR,us}} m^{-1}_{\nu_i} C^{(6)\,T}_{\mathrm{SRR,ud}} - C^{(6)}_{\mathrm{VLL,us}} m^{-1}_{\nu_i} C^{(6)\,T}_{\mathrm{SRL,ud}}\right) \\
&\quad + \frac{1}{2} C^{(9)}_{7,\mathrm{usud}}\,, \\
C^{(9)}_{6,\mathrm{udus}} &= \frac{v}{2}\left(C^{(6)}_{\mathrm{SRR,us}} m^{-1}_{\nu_i} C^{(6)\,T}_{\mathrm{VLR,ud}} - C^{(6)}_{\mathrm{SRL,us}} m^{-1}_{\nu_i} C^{(6)\,T}_{\mathrm{VLL,ud}}\right) \\
&\quad + \frac{1}{2} C^{(9)}_{7,\mathrm{udus}}\,, \\
C^{(9)}_{7,\mathrm{usud}} &= 4v C^{(6)}_{\mathrm{VLR,us}} m^{-1}_{\nu_i} C^{(6)\,T}_{\mathrm{TRR,ud}}\,, \\
C^{(9)}_{7,\mathrm{udus}} &= 4v C^{(6)}_{\mathrm{TRR,us}} m^{-1}_{\nu_i} C^{(6)\,T}_{\mathrm{VLR,ud}}\,, \\
C^{(9)\prime}_{6,\mathrm{usud}} &= \frac{v}{2}\left(C^{(6)}_{\mathrm{VRR,us}} m^{-1}_{\nu_i} C^{(6)\,T}_{\mathrm{SLR,ud}} - C^{(6)}_{\mathrm{VRL,us}} m^{-1}_{\nu_i} C^{(6)\,T}_{\mathrm{SLL,ud}}\right) \\
&\quad + \frac{1}{2} C^{(9)\prime}_{7,\mathrm{usud}}\,, \\
C^{(9)\prime}_{6,\mathrm{udus}} &= \frac{v}{2}\left(C^{(6)}_{\mathrm{SLR,us}} m^{-1}_{\nu_i} C^{(6)\,T}_{\mathrm{VRR,ud}} - C^{(6)}_{\mathrm{SLL,us}} m^{-1}_{\nu_i} C^{(6)\,T}_{\mathrm{VRL,ud}}\right) \\
&\quad + \frac{1}{2} C^{(9)\prime}_{7,\mathrm{udus}}\,, \\
C^{(9)\prime}_{7,\mathrm{usud}} &= -4v C^{(6)}_{\mathrm{VRL,us}} m^{-1}_{\nu_i} C^{(6)\,T}_{\mathrm{TLL,ud}}\,, \\
C^{(9)\prime}_{7,\mathrm{udus}} &= -4v C^{(6)}_{\mathrm{TLL,us}} m^{-1}_{\nu_i} C^{(6)\,T}_{\mathrm{VRL,ud}}\,, \\
C^{(9)}_{8,\mathrm{usud}} &= \frac{v}{2}\left(C^{(6)}_{\mathrm{VLR,us}} m^{-1}_{\nu_i} C^{(6)\,T}_{\mathrm{SLR,ud}} - C^{(6)}_{\mathrm{VLL,us}} m^{-1}_{\nu_i} C^{(6)\,T}_{\mathrm{SLL,ud}}\right) \\
&\quad + \frac{1}{2} C^{(9)}_{9,\mathrm{udus}}\,, \\
C^{(9)}_{8,\mathrm{udus}} &= \frac{v}{2}\left(C^{(6)}_{\mathrm{SLR,us}} m^{-1}_{\nu_i} C^{(6)\,T}_{\mathrm{VLR,ud}} - C^{(6)}_{\mathrm{SLL,us}} m^{-1}_{\nu_i} C^{(6)\,T}_{\mathrm{VLL,ud}}\right) \\
&\quad + \frac{1}{2} C^{(9)}_{9,\mathrm{usud}}\,, \\
C^{(9)}_{9,\mathrm{usud}} &= 4v C^{(6)}_{\mathrm{TLL,us}} m^{-1}_{\nu_i} C^{(6)\,T}_{\mathrm{VLL,ud}}\,, \\
C^{(9)}_{9,\mathrm{udus}} &= 4v C^{(6)}_{\mathrm{VLL,us}} m^{-1}_{\nu_i} C^{(6)\,T}_{\mathrm{TLL,ud}}\,, \\
C^{(9)\prime}_{8,\mathrm{usud}} &= \frac{v}{2}\left(C^{(6)}_{\mathrm{VRR,us}} m^{-1}_{\nu_i} C^{(6)\,T}_{\mathrm{SRR,ud}} - C^{(6)}_{\mathrm{VRL,us}} m^{-1}_{\nu_i} C^{(6)\,T}_{\mathrm{SRL,ud}}\right) \\
&\quad + \frac{1}{2} C^{(9)\prime}_{9,\mathrm{udus}}\,, \\
C^{(9)\prime}_{8,\mathrm{udus}} &= \frac{v}{2}\left(C^{(6)}_{\mathrm{SRR,us}} m^{-1}_{\nu_i} C^{(6)\,T}_{\mathrm{VRR,ud}} - C^{(6)}_{\mathrm{SRL,us}} m^{-1}_{\nu_i} C^{(6)\,T}_{\mathrm{VRL,ud}}\right) \\
&\quad + \frac{1}{2} C^{(9)\prime}_{9,\mathrm{usud}}\,, \\
C^{(9)\prime}_{9,\mathrm{usud}} &= -4v C^{(6)}_{\mathrm{TRR,us}} m^{-1}_{\nu_i} C^{(6)\,T}_{\mathrm{VRR,ud}}\,, \\
C^{(9)\prime}_{9,\mathrm{udus}} &= -4v C^{(6)}_{\mathrm{VRR,us}} m^{-1}_{\nu_i} C^{(6)\,T}_{\mathrm{TRR,ud}}\,.
\end{aligned}
\tag{4.9}
$$

The matching conditions for terms proportional to $\frac{1}{m^2_{\nu_i}}$ are given in Appendix A.

4.2 Amplitudes for LNV kaon decays

4.2.1 The case of light sterile neutrinos

When neutrinos are lighter than Λ_χ, we use chiral perturbation theory to get the amplitudes. Her we still use the external source method as that in Sect. 3.2.1, but now with $q = (u, d, s)^T$, $M = \mathrm{diag}(m_u, m_d, m_s)$ and replace τ^+ with λ_i. $i = d, s$ denote a down quark or a strange quark in the currents. The matrices λ_i are given by

$$\lambda_d = \begin{pmatrix} 0 & 1 & 0 \\ 0 & 0 & 0 \\ 0 & 0 & 0 \end{pmatrix}, \qquad \lambda_s = \begin{pmatrix} 0 & 0 & 1 \\ 0 & 0 & 0 \\ 0 & 0 & 0 \end{pmatrix}. \tag{4.10}$$

In $SU(3)$ chiral perturbation theory $U(x)$ is given by

$$U(x) = \exp\left(\frac{i\sqrt{2}\Pi(x)}{F_0}\right), \qquad \Pi(x) = \begin{pmatrix} \frac{\pi^0}{\sqrt{2}} + \frac{\eta}{\sqrt{6}} & \pi^+ & K^+ \\ \pi^- & -\frac{\pi^0}{\sqrt{2}} + \frac{\eta}{\sqrt{6}} & K^0 \\ K^- & \bar{K}^0 & -\sqrt{\frac{2}{3}}\eta \end{pmatrix}. \tag{4.11}$$

The contribution from tensor sources first appears at $\mathcal{O}(p^4)$ and it can not contribute to $K^- \to \pi^+ l^- l^-$ at tree level. Hence we ignore the tensor sources in this part. While for the remaining sources, we expand $U(x)$ to the leading order and the interactions relevant with the decay $\nu_j \to \pi^+ + e_i^-$ are

$$\begin{aligned} \mathcal{L}_\pi = {} & G_F F_0 \partial^\mu \pi^- \left\{ \bar{e}_{R,i}\gamma^\mu \nu_j (C^{(6)}_{\mathrm{VRR}} - C^{(6)}_{\mathrm{VLR}})_{udij} + \bar{e}_{L,i}\gamma^\mu \nu_j (C^{(6)}_{\mathrm{VRL}} - C^{(6)}_{\mathrm{VLL}})_{udij} \right\} \\ & - iF_0 B G_F \pi^- \left\{ \bar{e}_{L,i}\nu_j (C^{(6)}_{\mathrm{SLR}} - C^{(6)}_{\mathrm{SRR}})_{udij} + \bar{e}_{R,i}\nu_j (C^{(6)}_{\mathrm{SLL}} - C^{(6)}_{\mathrm{SRL}})_{udij} \right\}, \end{aligned} \tag{4.12}$$

where we add indices to denote the generations and we can replace the index d with s and π^- with K^- to get the operators relevant with the decay $K^- \to e_i^- + \nu_j$. By contracting the neutrino in mass basis, we connect the operators containing a π^- with those containing a K^- and get the amplitude. For the process $K^-(k) \to \pi^+(p) l_1^-(p_1) l_2^-(p_2)$ where $l_{1,2}$ is an electron or a muon, there are two types of Feynman diagrams. They are different in the positions of the outgoing charged leptons. For the type where l_1 and K^- share the same vertex, we get the amplitude

$$\begin{aligned} \mathcal{M}_1 = -\frac{iF_0^2 G_F^2}{q^2 - m_i^2} \Big\{ & m_i B^2 \left(C^{(6)}_{\mathrm{SLR}} - C^{(6)}_{\mathrm{SRR}}\right)_{usl_1 i} \left(C^{(6)}_{\mathrm{SLR}} - C^{(6)}_{\mathrm{SRR}}\right)_{udl_2 i} \bar{u}(p_1) P_R u^c(p_2) \\ & + m_i B \left(C^{(6)}_{\mathrm{VLR}} - C^{(6)}_{\mathrm{VRR}}\right)_{usl_1 i} \left(C^{(6)}_{\mathrm{SRR}} - C^{(6)}_{\mathrm{SLR}}\right)_{udl_2 i} \bar{u}(p_1) \not{k} P_R u^c(p_2) \\ & + m_i B \left(C^{(6)}_{\mathrm{SLL}} - C^{(6)}_{\mathrm{SRL}}\right)_{usl_1 i} \left(C^{(6)}_{\mathrm{VRL}} - C^{(6)}_{\mathrm{VLL}}\right)_{udl_2 i} \bar{u}(p_1) \not{p} P_R u^c(p_2) \\ & - B^2 \left(C^{(6)}_{\mathrm{SLL}} - C^{(6)}_{\mathrm{SRL}}\right)_{usl_1 i} \left(C^{(6)}_{\mathrm{SLR}} - C^{(6)}_{\mathrm{SRR}}\right)_{udl_2 i} \bar{u}(p_1) \not{q} P_R u^c(p_2) \\ & + m_i \left(C^{(6)}_{\mathrm{VLL}} - C^{(6)}_{\mathrm{VRL}}\right)_{usl_1 i} \left(C^{(6)}_{\mathrm{VLL}} - C^{(6)}_{\mathrm{VRL}}\right)_{udl_2 i} \bar{u}(p_1) \not{k} \not{p} P_R u^c(p_2) \\ & - B \left(C^{(6)}_{\mathrm{VLL}} - C^{(6)}_{\mathrm{VRL}}\right)_{usl_1 i} \left(C^{(6)}_{\mathrm{SRR}} - C^{(6)}_{\mathrm{SLR}}\right)_{udl_2 i} \bar{u}(p_1) \not{k} \not{q} P_R u^c(p_2) \\ & - B \left(C^{(6)}_{\mathrm{SRR}} - C^{(6)}_{\mathrm{SLR}}\right)_{usl_1 i} \left(C^{(6)}_{\mathrm{VLL}} - C^{(6)}_{\mathrm{VRL}}\right)_{udl_2 i} \bar{u}(p_1) \not{q} \not{p} P_R u^c(p_2) \\ & - \left(C^{(6)}_{\mathrm{VLR}} - C^{(6)}_{\mathrm{VRR}}\right)_{usl_1 i} \left(C^{(6)}_{\mathrm{VLL}} - C^{(6)}_{\mathrm{VRL}}\right)_{udl_2 i} \bar{u}(p_1) \not{k} \not{q} \not{p} P_R u^c(p_2) \\ & + (\text{terms by flipping the chirality of leptons}) \Big\}, \end{aligned} \tag{4.13}$$

where $q = k - p_1$, $l_{1,2}$ can be an electron or a muon, $u(p_{1,2})$ denotes a spinor with momentum $p_{1,2}$, m_i is the Majorana neutrino mass below GeV scale and a summation over i is implied. In the second type of Feynman diagrams l_2 and K^- share the same vertex. To get its amplitude $\mathcal{M}_2$, we only need the replacement $p_1 \leftrightarrow p_2$ and add one minus sign in $\mathcal{M}_1$. The total amplitude is

$$\mathcal{M}_L = \mathcal{M}_1 - \mathcal{M}_1\Big|_{p_1 \leftrightarrow p_2} . \tag{4.14}$$

4.2.2 The case of heavy sterile neutrinos

The chiral Lagrangian induced by the dim-9 operators in Eq. (4.1) has been discussed in Refs. [85]. The most relevant hadronic interactions involve one pion, one kaon and two charged leptons. The mesonic chiral Lagrangian is

$$\begin{aligned}
\mathcal{L}_{\mathcal{S}} =& \frac{F_0^4}{4v^5}\Bigg[\frac{5}{3} g_1^{\pi K} C^{(9)}_{1\,L/R} L^{\mu}_{21} L_{31\,\mu} + (g_2^{\pi K} C^{(9)}_{2\,L/R} + g_3^{\pi K} C^{(9)}_{3\,L/R}) U_{21} U_{31} \\
&+ (g_4^{\pi K} C^{(9)}_{4\,L/R} + g_5^{\pi K} C^{(9)}_{5\,L/R}) U_{21} U^{\dagger}_{31}\Bigg] \bar{e}_{L/R} C \bar{e}^T_{L/R} \\
&+ \frac{F_0^4}{4v^5} \bar{e}\gamma_\mu\gamma_5 C \bar{e}^T \Bigg[(g_6^{\pi K} C^{(9)}_{6,\mathrm{usud}} + g_7^{\pi K} C^{(9)}_{7,\mathrm{usud}}) L^{\mu}_{31} U^{\dagger}_{21} + (g_6^{\pi K\prime} C^{(9)}_{6,\mathrm{udus}} + g_7^{\pi K\prime} C^{(9)}_{7,\mathrm{udus}}) L^{\mu}_{21} U^{\dagger}_{31} \\
&+ g_{8/9}^{\pi K} (C^{(9)}_{8/9,\mathrm{usud}} + C^{(9)}_{8/9,\mathrm{udus}})(L^{\mu}_{31} U_{21} + L^{\mu}_{21} U_{31}) \\
&+ g_{8/9}^{\pi K\prime} (C^{(9)}_{8/9,\mathrm{usud}} - C^{(9)}_{8/9,\mathrm{udus}})(L^{\mu}_{31} U_{21} - L^{\mu}_{21} U_{31})\Bigg] \\
&+ (C_i^{(9)} \to C_i^{(9)\prime}) ,
\end{aligned} \tag{4.15}$$

where $L_\mu = iUD_\mu U^\dagger$ and the parity invariance of QCD implies that the hadronic operators induced by O_i are the same as those induced by O_i' and they share the same LECs. Then we expand the U matrix and get operators involving two mesons and two leptons [85]

$$\begin{aligned}
\mathcal{L}_{\mathcal{S}} =& \frac{1}{v^5} K^- \pi^- \left[c_1 \bar{e}_L C \bar{e}^T_L + c_2 \bar{e}_R C \bar{e}^T_R\right] + \frac{1}{v^5}\left[c_3 \partial^\mu K^- \pi^- + c_4 \partial^\mu \pi^- K^-\right] \bar{e}\gamma_\mu\gamma_5 C \bar{e}^T \\
&+ \frac{1}{v^5} \partial^\mu K^- \partial_\mu \pi^- \left[c_5 \bar{e} C P_L \bar{e}^T + c_6 \bar{e} C P_R \bar{e}^T\right] ,
\end{aligned} \tag{4.16}$$

where the parameters c_i are

$$\begin{aligned}
c_1 &= -\frac{1}{2}F_0^2[g_2^{\pi K}(C_{2\,L}^{(9)}+C_{2\,L}^{(9)\prime})+g_3^{\pi K}(C_{3\,L}^{(9)}+C_{3\,L}^{(9)\prime})\\
&\quad -g_4^{\pi K}(C_{4\,L}^{(9)}+C_{4\,L}^{(9)\prime})-g_5^{\pi K}(C_{5\,L}^{(9)}+C_{5\,L}^{(9)\prime})]\,,\\
c_2 &= c_1\Big|_{L\to R}\,,\\
c_3 &= -\frac{i}{2}F_0^2[g_6^{\pi K}(C_{6,usud}^{(9)}+C_{6,usud}^{(9)\prime})+g_7^{\pi K}(C_{7,usud}^{(9)}+C_{7,usud}^{(9)\prime})\\
&\quad -g_{8/9}^{\pi K}(C_{8/9,usud}^{(9)}+C_{8/9,usud}^{(9)\prime}+C_{8/9,udus}^{(9)}+C_{8/9,udus}^{(9)\prime})\\
&\quad -g_{8/9}^{\pi K\prime}(C_{8/9,usud}^{(9)}+C_{8/9,usud}^{(9)\prime}-C_{8/9,udus}^{(9)}-C_{8/9,udus}^{(9)\prime})]\,,\\
c_4 &= -\frac{i}{2}F_0^2[g_6^{\pi K\prime}(C_{6,udus}^{(9)}+C_{6,udus}^{(9)\prime})+g_7^{\pi K\prime}(C_{7,udus}^{(9)}+C_{7,udus}^{(9)\prime})\\
&\quad -g_{8/9}^{\pi K}(C_{8/9,usud}^{(9)}+C_{8/9,usud}^{(9)\prime}+C_{8/9,udus}^{(9)}+C_{8/9,udus}^{(9)\prime})\\
&\quad +g_{8/9}^{\pi K\prime}(C_{8/9,usud}^{(9)}+C_{8/9,usud}^{(9)\prime}-C_{8/9,udus}^{(9)}-C_{8/9,udus}^{(9)\prime})]\,,\\
c_5 &= \frac{5}{6}F_0^2 g_1^{\pi K}(C_{1\,L}^{(9)}+C_{1\,L}^{(9)\prime})\,,\\
c_6 &= c_5\Big|_{L\to R}\,.
\end{aligned} \tag{4.17}$$

The LECs, $g_i^{\pi K}$, can be estimated by using naive dimensional analysis (NDA)

$$g_1^{\pi K}=\mathcal{O}(1)\,,\qquad g_{2,3,4,5}^{\pi K}=\mathcal{O}(\Lambda_\chi^2)\,,\qquad g_{6,7,8,9}^{\pi K(\prime)}=\mathcal{O}(\Lambda_\chi)\,. \tag{4.18}$$

We can also relate $g_i^{\pi K}$ with the LECs appearing in $K^0\to\bar{K}^0$ [169], $K^\pm\to\pi^\pm\pi^0$ [170] and $\pi^-\to\pi^+$ [169], some of which have been computed by several lattice QCD groups [171–177]. Finally the tree-level amplitude for $K^-(k)\to\pi^+(p)l^-(p_1)l^-(p_2)$ can be read off directly

$$\begin{aligned}
\mathcal{M}_S &= -i\frac{1}{v^5}\Big[2c_1\bar{u}(p_1)P_R u^c(p_2)+2c_2\bar{u}(p_1)P_L u^c(p_2)-2ic_3\bar{u}(p_1)\not{k}\gamma_5 u^c(p_2)\\
&+ 2ic_4\bar{u}(p_1)\not{p}\gamma_5 u^c(p_2)+2k\cdot p[c_5\bar{u}(p_1)P_R u^c(p_2)+c_6\bar{u}(p_1)P_L u^c(p_2)]\Big]\,.
\end{aligned} \tag{4.19}$$

4.3 Phase space integral

The momentum products in the amplitude square $|\mathcal{M}|^2$ of the decay $K^-(k)\to\pi^+(p)l_1^-(p_1)l_2^-(p_2)$ have two independent terms, $(k-p_1)^2=q^2$ and $k\cdot p_2$, and all the other products can be expressed in terms of these two products and particle masses. To simplify the integral further, we write [152]

$$(k-p_1)^2=a\,,\qquad k\cdot p_2=\frac{1}{4a}(m_K^2+a-m_{l_1}^2)(a+m_{l_2}^2-m_\pi^2)+\frac{1}{\sqrt{a}}m_K|\mathbf{q}||\mathbf{p}_2|\cos\theta\,, \tag{4.20}$$

where $|\mathbf{q}|=\frac{\lambda^{\frac{1}{2}}(m_K,\sqrt{a},m_{l_1})}{2m_K}$, $|\mathbf{p}_2|=\frac{\lambda^{\frac{1}{2}}(m_\pi,\sqrt{a},m_{l_2})}{2\sqrt{a}}$ with $\lambda(a,b,c)=a^4+b^4+c^4-2a^2b^2-2a^2c^2-2b^2c^2$ and m_{l_i} is the mass of lepton l_i. The decay rate becomes

$$\Gamma=(2-\delta_{l_1l_2})\frac{1}{2!}\frac{1}{2m_K^2}\frac{1}{64\pi^3}\int da\int d\cos\theta\,|\mathbf{q}|\frac{|\mathbf{p}_2|}{\sqrt{a}}|\mathcal{M}|^2(a,\,k\cdot p_2)\,, \tag{4.21}$$

and the integration domains are given by

$$a \in [(m_{l_2} + m_\pi)^2\,,\,(m_K - m_{l_1})^2]\,, \qquad \cos\theta \in \quad [-1\,,\,1]\,. \tag{4.22}$$

If the mass of neutrino is in the range $[m_{l_{1,2}} + m_\pi\,,\, m_K - m_{l_{2,1}}]$, the exchanged neutrino can go on shell. Near the pole, we modify the propagator

$$\frac{1}{q^2 - m_i^2 + i\epsilon} \longrightarrow \frac{1}{q^2 - m_i^2 + i m_i \Gamma_i}\,, \tag{4.23}$$

where Γ_i is the total decay width of ν_i in the mass basis. When the mass of sterile neutrino is much larger than its decay rate, we use the narrow width approximation

$$\frac{1}{(q^2 - m_i^2)^2 + m_i^2\Gamma_i^2} \longrightarrow \frac{\pi}{m_i\Gamma_i}\delta(q^2 - m_i^2)\,, \tag{4.24}$$

to simplify the phase space. The resulting m_i/Γ_i enhancement is typically large enough that other contributions can be neglected.

4.4 Phenomenology

The EFT approach to the long-distance contributions without a sterile neutrino and the short-distance contributions has been discussed in Refs. [85,152], which considered $\overline{\text{dim-7}}$ LNV operators in SMEFT and matched them onto dim-9 operators ($C^{(9)}_{5\,L}$, $C^{(9)\prime}_{5\,L}$ and $C^{(9)}_{1\,L}$), and the resulting $C_i^{(9)}$ are proportional to $\frac{v^3}{\Lambda^3}$ given that the WCs of $\overline{\text{dim-n}}$ operators are proportional to $\frac{1}{\Lambda^n}$. Using the current experimental limit, they obtained a relatively weak bound on $\Lambda > \mathcal{O}(10)$ GeV. This scale is too low for the SMEFT approach to be valid. However, this is not the case when we work in the framework of νSMEFT.

In the presence of a sterile neutrino with mass $m_N > \Lambda_\chi$, where the same $C_i^{(9)}$ are induced, the bound on Λ can be slightly improved. For instance, let us consider a dim-9 operator, $C^{(9)}_{5\,R}$, which could receive a contribution from two dim-6 operators $C^{(6)}_{\text{VRR,us}} \times C^{(6)}_{\text{VLR,ud}}$, or equivalently from two $\overline{\text{dim-6}}$ operators $\mathcal{O}^{(6)}_{du\nu e} \times \mathcal{O}^{(6)}_{H\nu e}$. $C^{(9)}_{5\,R}$ is thus proportional to $v^5/(m_N\Lambda^4)$. Due to the enhancement by v/m_N it is possible to get a more stringent bound.For instance, for $m_N = 1$ GeV, we get a better lower limit on Λ with $\Lambda > \mathcal{O}(100)$ GeV based on current experimental limits, which improves the result in Ref. [85] by one order. Nevertheless, it is clear that for sterile neutrinos with masses above a GeV or so, the resulting limits are rather weak and it is unclear whether the use of the SMEFT or νSMEFT frameworks are justified.

If a sterile neutrino exists with a mass inside the resonance range $[m_l + m_\pi, m_K - m_l]$, the decay rate is significantly enhanced [160] and we can get much stronger constraints on Λ and neutrino mixing angles. From now on we ignore sterile neutrinos with mass outside the resonance range and discuss two scenarios, the minimal scenario and the leptoquark scenario, and show their effects on the decay rates of $K^-(k) \to \pi^+(p)l^-(p_1)l^-(p_2)$. Finally we give constraints on the energy scale of operators in Table 2.3.

4.4.1 The minimal scenario

In the minimal scenario, we add a sterile neutrino ν_R with mass m_N in the resonance region and it can only interact with the SM particles via the mixing with active neutrinos. We get the

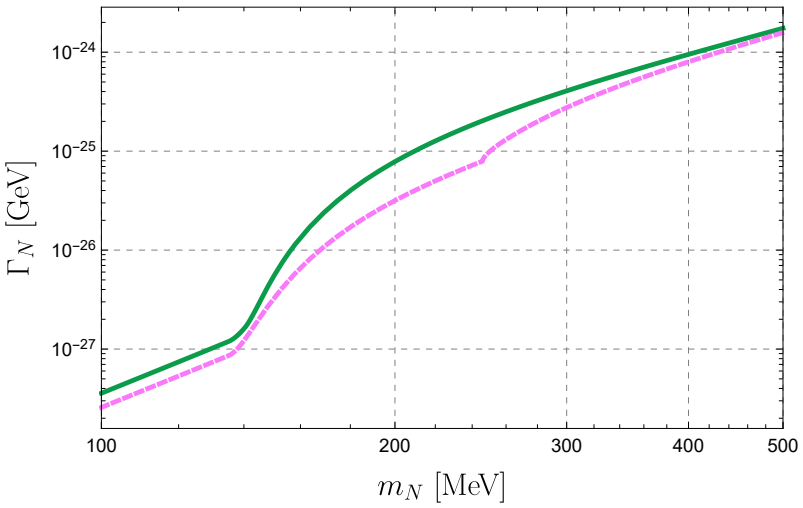

Figure 4.2: Decay rates of the sterile neutrino in the minimal scenario for cases $U_{e4} \neq 0$ (green solid) and $U_{\mu 4} \neq 0$ (pink dashed). The kinks at $m_N \approx 140$ and 240 MeV are due to threshold of decay channels $N \to \pi^0 + \nu_e/\nu_\mu$ and $\pi^\pm + e^\mp/\mu^\mp$.

Lagrangian by setting the WCs of operators from Tables 2.1-2.4 to zero and writing the active neutrino ν_α in the weak interaction in terms of the neutrino mass eigenstates ν_i

$$\nu_\alpha = U_{\alpha i}\nu_i \,, \tag{4.25}$$

where $\alpha = e, \mu$ and $i = 1, 2, 3, 4$. We also assume the sterile neutrino mixes only with the electron neutrino ν_e in $K^- \to \pi^+ e^- e^-$ or with the muon neutrino ν_μ in $K^- \to \pi^+ \mu^- \mu^-$. Due to the small mixing angles between the sterile- and active- neutrinos, ν_R is approximately equivalent to ν_4.

We can calculate the rates of sterile neutrinos by expanding Eq. (3.20) to the leading order in $SU(3)$ framework. We show the decay rates Γ_N of the sterile neutrino in Fig. 4.2. In Fig. 4.3 we plot the branching ratios of kaons as a function of m_N for the case of final-state electrons (left panel) and muons (right panel). When calculating the decay rates, the mixing angles $|U_{e4}|$ and $|U_{\mu 4}|$ are set to the see-saw prediction $\sqrt{0.05 \text{ eV}/\text{m}_\text{N}}$. It is clear that $m_N/\Gamma_N \gg 1$ and it is safe to use the narrow-width approximation. The two branching ratios are slightly above the current limit around 300 MeV. Hence either there is no such a sterile neutrino with a Majorana mass around 300 MeV, or the mixing angle $|U_{l4}|$ ($l = e\,, \mu$) is smaller than the see-saw relation.

In Fig. 4.4 we show the limits on $|U_{e4}|^2$ and $|U_{\mu 4}|^2$ as functions of m_N. The limits are quite close to the black curve indicating the type-I seesaw relation. The constraints on $|U_{e4}|^2$ and $|U_{\mu 4}|^2$ could reach $\mathcal{O}(10^{-10})$. The limits on the mixing angles detoriate quickly near the boundaries of resonance regions due to the phase space suppression.

4.4.2 The leptoquark scenario

In this section we neglect the interactions of the minimal scenario and the SM is extended only by interactions with leptoquarks (LQs), which can convert quarks to leptons and vice versa. Ref. [26] summarized all the possible representations of LQs and we focus again on the scalar

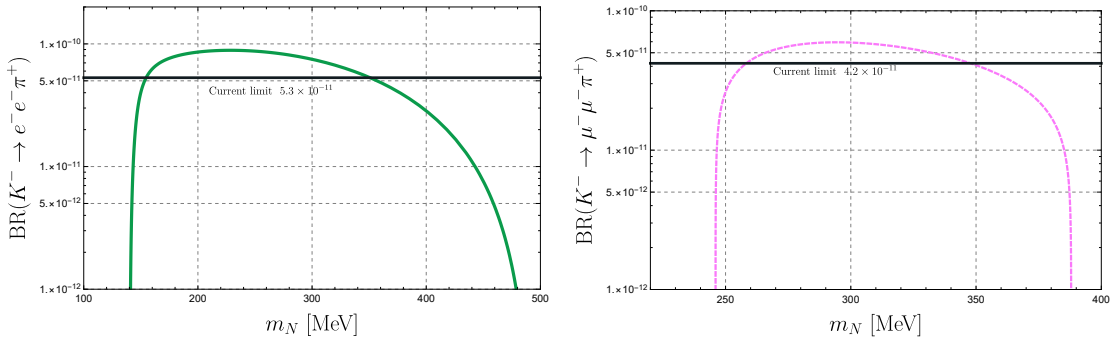

Figure 4.3: Branching ratios of $K^- \to \pi^+ e^- e^-$ (left panel) and $K^- \to \pi^+ \mu^- \mu^-$ (right panel) as functions of the sterile neutrino mass m_N in the minimal scenario.

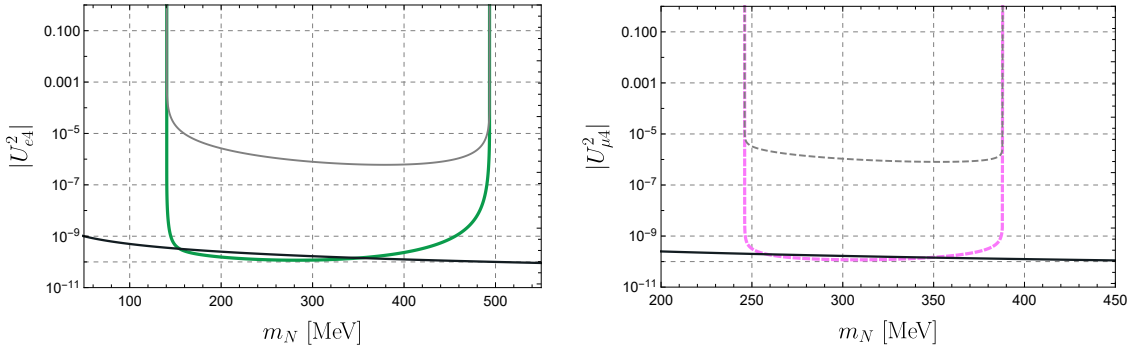

Figure 4.4: The excluded parameter space above the curves for $|U_{e4}|^2$ (left panel) and $|U_{\mu 4}|^2$ (right panel) from the limits on branching ratios of $K^- \to \pi^+ l^- l^-$. The two black lines correspond to the type-I seesaw relation $\{|U_{e4}|^2, |U_{\mu 4}|^2\} = 0.05$ eV/m$_{\rm N}$. The gray (dashed) lines are the modified limits when including the finite detector size effect.

LQ: $\tilde{R}\,(\mathbf{3},\ \mathbf{2},\ 1/6)$. Its interactions with quarks and leptons are given in Eq. (3.128). After integrating the LQ we get the following $\overline{\text{dim-6}}$ operator

$$\mathcal{L}_{\nu_R}^{(\bar{6})} = C_{LdQ\nu,ijkl}^{(6)} \left(\bar{L}_i^a d_j\right) \epsilon^{ab} \left(\bar{Q}_k^b \nu_{Rl}\right) + \text{h.c.}\,, \tag{4.26}$$

where

$$C_{LdQ\nu,ijkl}^{(\bar{6})} = \frac{1}{m_{\rm LQ}^2} y_{kl}^{\overline{LR}} y_{ji}^{RL*}\,, \tag{4.27}$$

and $m_{\rm LQ}$ is the mass of the LQ. Below the electroweak scale, four operators are induced

$$\begin{aligned}\mathcal{L}_{\Delta L=0}^{(6)} = \frac{2G_F}{\sqrt{2}} \Big[& \bar{c}_{{\rm SR},ijkl}^{(6)}\ \bar{u}_{L,i} d_{R,j} \bar{e}_{L,k} \nu_{R,l} + \bar{c}_{{\rm T},ijkl}^{(6)}\ \bar{u}_{L,i} \sigma^{\mu\nu} d_{R,j} \bar{e}_{L,k} \sigma^{\mu\nu} \nu_{R,l} \\ & + \bar{c}_{{\rm NSR},ijkl}^{(6)}\ \bar{d}_{L,i} d_{R,j} \bar{\nu}_{L,k} \nu_{R,l} + \bar{c}_{{\rm NT},ijkl}^{(6)}\ \bar{d}_{L,i} \sigma^{\mu\nu} d_{R,j} \bar{\nu}_{L,k} \sigma^{\mu\nu} \nu_{R,l} \Big] + \text{h.c.}\,,\end{aligned} \tag{4.28}$$

where the two neutral currents contribute to the decay width of the sterile neutrino and thus affect LNV decay process in the resonance region, and the coefficients satisfy

$$\bar{c}^{(6)}_{\mathrm{SR},ijkl} = 4\bar{c}^{(6)}_{\mathrm{T},ijkl} = \frac{v^2}{2m^2_{\mathrm{LQ}}} y^{\overline{LR}}_{il} y^{RL*}_{jk} \,, \tag{4.29}$$

$$\bar{c}^{(6)}_{\mathrm{NSR},ijkl} = 4\bar{c}^{(6)}_{\mathrm{NT},ijkl} = \frac{v^2}{2m^2_{\mathrm{LQ}}} y^{\overline{LR}}_{ml} y^{RL*}_{jk} V^*_{mi} \,. \tag{4.30}$$

The matching to the operators in Eq. (2.21) is

$$C^{(6)}_{\mathrm{SRR},ijkl} = 4C^{(6)}_{\mathrm{TRR},ijkl} = \sum_{l=1}^{n} \bar{c}^{(6)}_{\mathrm{SR},ijkl} U^*_{3+l,i} \,, \tag{4.31}$$

where n is the number of sterile neutrinos and here we consider only one sterile neutrino. Since we focus on the resonance region, the contributions from other light neutrinos can be safely ignored and the mixing angle $|U_{44}| \approx 1$.

In order to induce the decay $K^- \to \pi^+ e^- e^-$, we set $y^{\overline{LR}}_{u1} y^{RL*}_{de} = y^{\overline{LR}}_{u1} y^{RL*}_{se}$ to one and all other indices configurations to zero. Similarly for $K^- \to \pi^+ \mu^- \mu^-$ we assume $y^{\overline{LR}}_{u1} y^{RL*}_{d\mu} = y^{\overline{LR}}_{u1} y^{RL*}_{s\mu} = 1$ with all others being zero. Then the decay rates are a function of the leptoquark mass m_{LQ} and the sterile neutrino mass m_N. One can check the decay rate of the sterile neutrino is much smaller than its mass and thus the narrow width approximation is still valid. In Fig. 4.5, we show the limits on m_{LQ} by varying m_N. The regions below the two colorful curves are excluded, and the green curve ($K^- \to \pi^+ e^- e^-$) reaches an energy scale around 300 TeV while the pink curve ($K^- \to \pi^+ \mu^- \mu^-$) could reach 250 TeV. Due to the same reason as that in the minimal scenario, m_{LQ} approaches 0 near the resonance boundaries.

4.5 Limits on $\overline{\text{dim-6}}$ operators with a sterile neutrino

In principle by using the current limit on $K^- \to \pi^+ l^- l^-$ in the resonance region we can make a limit plot for every operator from Tables 2.1-2.4. The strongest limits arise from (part of) the operators in Table 2.3, because contributions from the operators in the other tables are suppressed by either the small mixing angles $|U_{e/\mu 4}|$ for those containing a left-handed neutrino or Λ for the $\overline{\text{dim-7}}$ operators. Not all νSMEFT dimension-six operators contribute equally. For instance, $\mathcal{O}^{(6)}_{L\nu H}$ has no direct effect on the LNV kaon decay and is ignored here. $\mathcal{O}^{(6)}_{\nu W}$ can induce the decay $N \to \nu\gamma$, which is relatively fast and decreases the LNV kaon decay rates in the resonance region. $\mathcal{O}^{(6)}_{\nu W}$ is strictly constrained because it generates neutrino dipole moments at one-loop [178, 179] and it is also ignored. We are then left with four operators ($\mathcal{O}^{(9)}_{LdQ\nu}$ has been discussed in previous subsection) in Table 2.3. These operators can easily be obtained in models with Z' bosons ($\mathcal{O}^{(9)}_{Qu\nu L}$, $\mathcal{O}^{(9)}_{L\nu Qd}$), and left-right symmetric models ($\mathcal{O}^{(9)}_{H\nu e}$). We refrain from introducing specific models and focus on giving the limits on the WCs of these four operators directly.

To induce the LNV kaon decay, we turn on a single operator with specific flavor configurations at a time and ignore the minimal interactions. For $\mathcal{O}^{(9)}_{Qu\nu L}$ and $\mathcal{O}^{(9)}_{H\nu e}$ we only need to turn on one flavor configuration to induce LNV kaon decay. We set $C^{(9)}_{H\nu e,11} = \frac{1}{\Lambda^2}$ to induce $K^- \to \pi^+ e^- e^-$ with all other indices configurations being zero. Then we can get limits on Λ as a function the sterile neutrino mass m_N. Because the left handed down-type quarks are not in mass eigenstates, $K^- \to \pi^+ e^- e^-$ can also be realized via $C^{(9)}_{Qu\nu L,1111} = \frac{1}{\Lambda^2}$. The remaining two operators are special

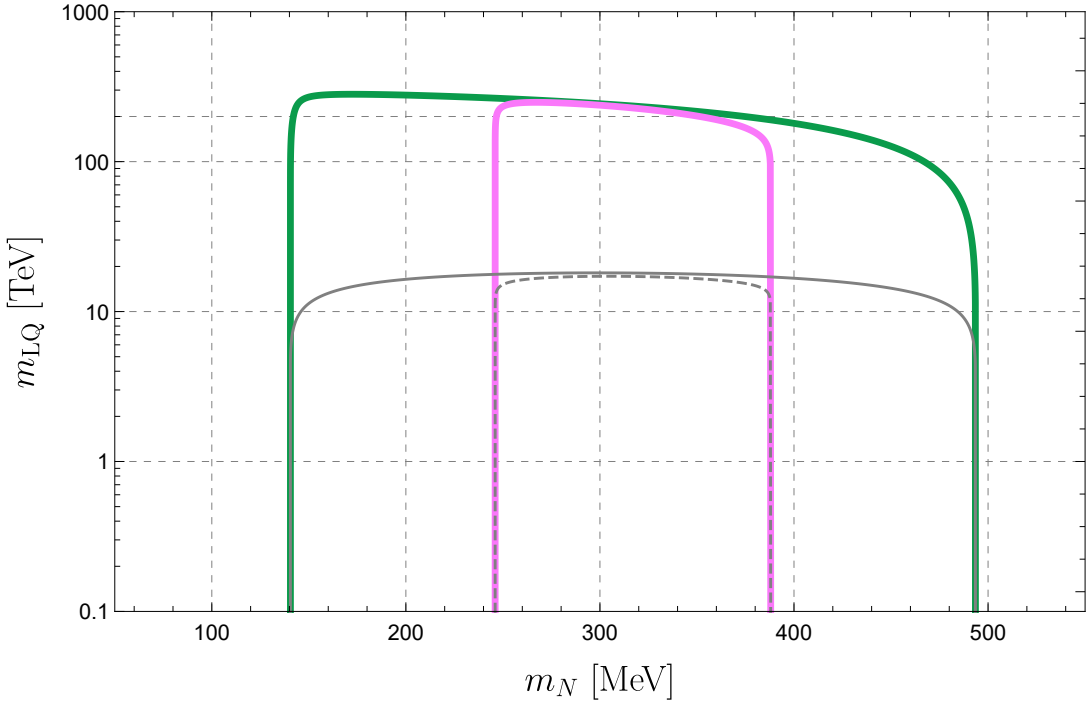

Figure 4.5: Limits on the leptoquark mass $m_{\rm LQ}$ versus the sterile neutrino mass m_N in the resonance region. The green curve is based on current limit for $K^- \to \pi^+ e^- e^-$ and similarly the pink one for $K^- \to \pi^+ \mu^- \mu^-$. The gray (dashed) lines include the finite detector size effect.

in the sense that we need to turn on two flavor configurations to induce LNV kaon decays. For convenience we assume $C^{(9)}_{du\nu e,1111} = C^{(9)}_{du\nu e,2111} = \frac{1}{\Lambda^2}$ or $C^{(9)}_{L\nu Qd,1111} = C^{(9)}_{L\nu Qd,1112} = \frac{1}{\Lambda^2}$ to induce $K^- \to \pi^+ e^- e^-$. Similarly, we set $C^{(9)}_{H\nu e,12}$, $C^{(9)}_{Qu\nu L,1112}$, $C^{(9)}_{du\nu e,1112} = C^{(9)}_{du\nu e,2112}$ and $C^{(9)}_{L\nu Qd,2111} = C^{(9)}_{L\nu Qd,2112}$ to $\frac{1}{\Lambda^2}$ to induce $K^- \to \pi^+ \mu^- \mu^-$.

We show the limits on Λ for these four operators in Fig. 4.6. The two scalar-type operators give stronger limits than the two vector-type operators, because the decay rates from the latter are relatively suppressed by m_π^2/B^2. The contributions to the LNV kaon decay rate from $\mathcal{O}^{(9)}_{H\nu e}$ and $\mathcal{O}^{(9)}_{Qu\nu L}$ are further suppressed by $|V_{us}|^2$. Note that near the threshold $m_N = m_l + m_\pi$ for the plot of $\mathcal{O}^{(9)}_{du\nu e}$, the decay rates of the sterile neutrino and the $|\mathbf{p}_2|$ in Eq. (4.21) approach to zero at the same speed. Hence the two curves for Λ approach to some fixed values instead of going down straightly around $m_N = m_l + m_\pi$. While for the plots from other three operators, the decay rates of the sterile neutrino are not zero around $m_N = m_l + m_\pi$ as the sterile neutrino can still decay into light particles, e.g. $\pi^0 + \nu_e$. We refer to Ref. [180, 181] for a more detailed discussion and calculation on the decay modes of the sterile neutrino for various $\overline{\text{dim-6}}$ operators.

4.5.1 Finite detector size effect

In the resonance region where a sterile neutrino could be produced on-shell, we consider the intermediate neutrino as a real particle and it propagates for some distance before decaying into a pion and a charged lepton. In the case when sterile neutrinos decay outside the detector, we can

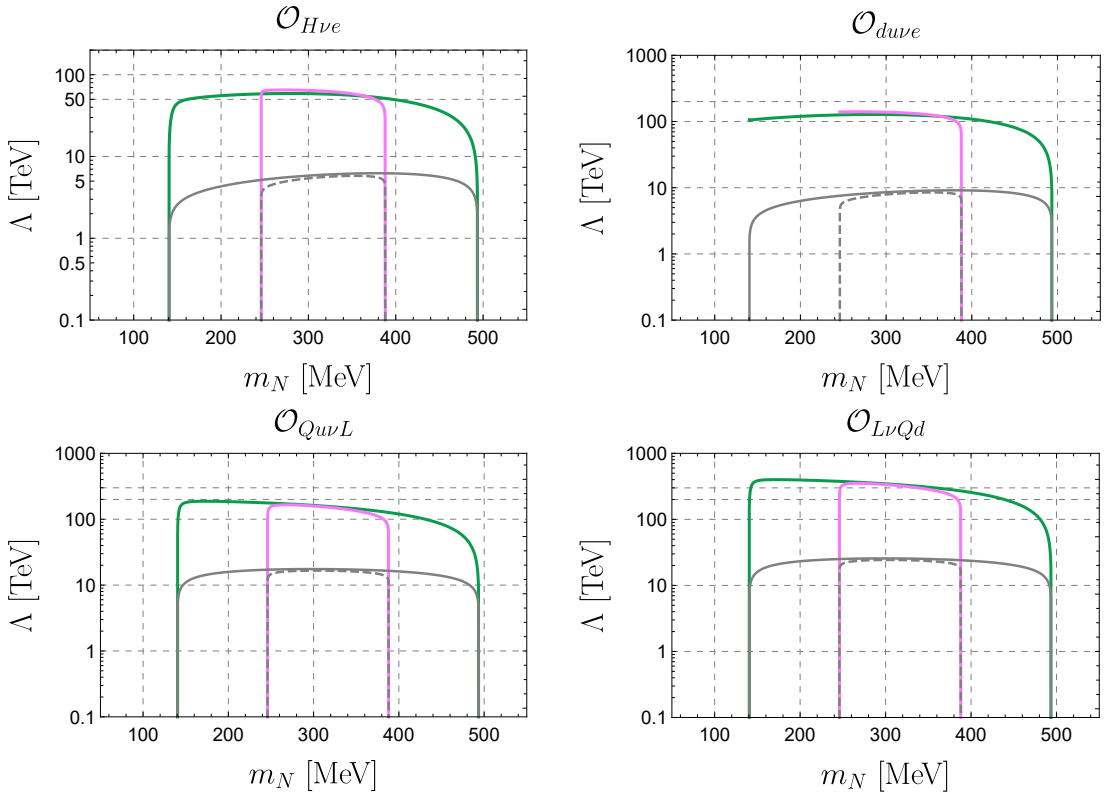

Figure 4.6: Same as Fig. 4.5 but now we present limits on the BSM scale Λ associated to various dim-6 operators.

not reconstruct the LNV process and thus get no valuable bound on the mixing angles or energy scales of the higher-dimensional operators. The observed branching ratio is suppressed due to the fact that some neutrinos decay outside the detector. Refs. [166, 182–186] have discussed this effect. Here we follow the method used in Ref. [183] to make a rough estimate. We include the finite size detector effect by a probability factor P_N, which is the probability of ν_R to decay within the detector. We write P_N as

$$P_N = 1 - e^{-\frac{L_D}{L_N}}\,, \tag{4.32}$$

where L_D denotes the typical detector length and $L_N = \frac{p_N}{m_N \Gamma_N}$ with p_N the momentum of ν_R. In the rest frame of K^-, the momentum of the sterile neutrino is given by

$$p_N^\star = \frac{\lambda^{\frac{1}{2}}(m_l\,, m_K\,, m_N)}{2m_K}\,. \tag{4.33}$$

We can relate the energy E_N of ν_R in the lab frame with those quantities in the rest frame of K^- by the relation

$$E_N = E_N^\star(\gamma + \frac{p_N^\star}{E_N^\star}\sqrt{\gamma^2 - 1}\cos\theta_N^\star)\,, \tag{4.34}$$

where $\gamma = \frac{E_K}{m_K}$ denoting the boost factor of K^-, $E_N^\star$ is the energy of ν_R in the rest frame of K^- and $\theta_N^\star$ is the emission angle of ν_R relative to the velocity direction of K^- in the rest frame of

K^-. The energy of ν_R lies in the range $E_N^- < E_N < E_N^+$ with $E_N^\pm = \gamma E_N^\star \pm p_N^\star \sqrt{\gamma^2 - 1}$ and obeys a flat distribution.

We then can get the total number of LNV kaon decays inside the detector by integrating neutrino energy E_ν

$$\begin{aligned} N_{\text{event}} &= N_{K^-} \int_{E_N^-}^{E_N^+} dE_N \frac{\text{BR}(K^- \to l^- l^- \pi^+)}{E_N^+ - E_N^-} P_N \,, \\ &\approx N_{K^-} \int_{E_N^-}^{E_N^+} dE_N \frac{\text{BR}(K^- \to l^- \nu_R)}{E_N^+ - E_N^-} \frac{\Gamma(\nu_R \to l^- \pi^+)}{\Gamma_N} P_N \,, \end{aligned} \tag{4.35}$$

where N_{K^-} is the number of K^-. In NA62 experiment, 400 GeV protons collide the target and produce a large number of K^+ mesons, which carry a momentum of 75 GeV. Assuming three years of running, the expected number of K^+ decays in the fiducial volume is $N_{K^+} = 1.35 \times 10^{13}$. Following Refs. [183, 187], we assume zero background events and $L_D \approx 65$ m.

By requiring the signal events to be $N_{\text{event}} = 3.09$ we get bound on the mixing angle or new physics energy scale Λ as a function of sterile neutrino mass m_N. We show our results in Figs. 4.4-4.6, where we use the gray lines to denote the sensitivity for $K^- \to \pi^+ e^- e^-$ and gray dashed lines for $K^- \to \pi^+ \mu^- \mu^-$. Through the gray (dashed) lines, we find the limits on $|U_{l4}^2|$ are of the order 10^{-6}, and the limits on Λ are 5 - 30 TeV.

4.6 Conclusions

In this chapter, we used a systematic framework to study the effect of light sterile neutrinos with mass smaller than the electroweak scale, $m_\nu < v$, on the lepton-number-violating decays $K^- \to \pi^+ l^- l^-$. We find the presence of a sterile neutrino and the non-standard interactions have a dramatic impact on the LNV kaon decay phenomenology. In the case of a sterile neutrino with mass $\Lambda_\chi < m_\nu < v$, the new physics scale probed by the dim-9 operators is improved by one order compared to the case without a sterile neutrino [85]. Nevertheless, the BSM physics scale that can be probed is of order $\mathcal{O}(100)$ GeV which is still too low to make the νSMEFT approaches valid. The limits are also much weaker than the corresponding $0\nu\beta\beta$ decay limits for similar operators with different generation indices because of the relatively small data samples of kaon experiments. However, very stringent bounds on the EFT operators emerge if the sterile neutrino mass lies in the resonance region $(m_\pi + m_l, m_K - m_l)$. The resulting lepton-number-violating decay rate are highly enhanced and we obtain strong limits on the neutrino mixing angles $|U_{e4}^2|$ and $|U_{\mu 4}^2|$ at the level of 10^{-9}-10^{-10}, close to seesaw predictions, and on the BSM scales Λ, up to $\mathcal{O}(300)$ TeV, for various higher-dimensional operators. After considering the finite detector size effect, we find the limits on mixing angle $|U_{l4}^2|$ become at the level of 10^{-6} and the BSM scales Λ are weakened to $\mathcal{O}(30)$ TeV. These limits obtained this way are very strong though only in a narrow window of sterile neutrino masses with 150 MeV$< m_\nu <$490 MeV. The framework we developed in this work can be readily extended to probe BSM physics in other types of decays, e.g. the LNV decays of charm and bottom mesons, or τ leptons.

Chapter 5

Long-lived sterile neutrinos at the LHC in νSMEFT

In this chapter[1], we study relatively light GeV-scale sterile neutrinos. Sterile neutrinos can be produced either via direct production with parton collisions, or via rare decays of mesons that are copiously produced at the LHC interaction points [188, 189]. For sterile neutrino masses below the B-meson threshold the primary production mode is through rare decays of mesons with subleading contributions from partonic processes, which we estimated using MadGraph5 3.0.2 [190] to be less than 10%. The latter become more important and even dominant for heavier sterile neutrinos. We choose to focus on the mass range below about 5 GeV and hence on the rare meson decays. If the sterile neutrinos are relatively long-lived, their decays lead to displaced vertices that can be reconstructed in LHC detectors. We consider a broad range of (proposed) LHC experiments: `ATLAS` [191]/`CMS` [192], `CODEX-b` [193], `FASER` [194, 195], `MATHUSLA` [196–198], `AL3X` [199], `ANUBIS` [200], `MoEDAL-MAPP` [201, 202], as well as the proposed CERN SPS experiment `SHiP` [203–205], and discuss their potential in probing νSMEFT operators. We calculate νSMEFT corrections to sterile neutrino production and decay processes and perform simulations for the various detectors, to estimate their search sensitivities. Our simulations show that the experimental reach is strong, probing dimension-six operators associated to BSM scales up to a hundred TeV. In a simple $3+1$ model, adding just one sterile neutrino field, we compare our results to existing $0\nu\beta\beta$ decay limits, showing that these experiments are complementary.

5.1 The effective neutrino Lagrangian

We are interested in the production and decay of sterile neutrinos at the LHC. In particular, we investigate the production of sterile neutrinos in the decay of mesons containing a single b or c quark, as these are copiously produced and are sufficiently massive to produce GeV sterile neutrinos. This is an interesting mass range that appears in scenarios of low-scale leptogenesis [144, 148, 206–210]. In this chapter we only consider the operators of Table 2.3, which involve a single right-handed neutrino[2] and lead to hadronic processes at tree level. After EWSB and

[1] This chapter is based on J. de Vries, H. K. Dreiner, J. Y. Günther, Z. S. Wang and G. Zhou JHEP 03 (2021) 148.

[2] Operators with a left-handed neutrino also contribute to the same observables we discuss here, but the contributions are suppressed by small heavy-light neutrino mixing angles.

rotating to the neutrino mass basis, we can only get part of the operators in Eqs. (2.21-2.22)

$$\begin{aligned}\mathcal{L}^{(6,7)}_{\text{mass}} \;=\; & \frac{2G_F}{\sqrt{2}}\Big\{\bar{u}_L\gamma^\mu d_L\left[\bar{e}_L\gamma_\mu C^{(6)}_{\text{VLL}}\,\nu+\bar{e}_R\gamma_\mu C^{(6)}_{\text{VLR}}\,\nu\right]+\bar{u}_R\gamma^\mu d_R\,\bar{e}_R\,\gamma_\mu C^{(6)}_{\text{VRR}}\,\nu \\ & \bar{u}_L d_R\,\bar{e}_L\,C^{(6)}_{\text{SRR}}\nu+\bar{u}_R d_L\,\bar{e}_L\,C^{(6)}_{\text{SLR}}\nu+\bar{u}_L\sigma^{\mu\nu}d_R\,\bar{e}_L\sigma_{\mu\nu}C^{(6)}_{\text{TRR}}\nu \\ & +\frac{1}{v}\bar{u}_L\gamma^\mu d_L\,\bar{e}_L\,C^{(7)}_{\text{VLR}}\,i\overleftrightarrow{D}_\mu\nu\Big\}+\text{h.c.}\,. \end{aligned} \tag{5.1}$$

For convenience we use a new notation for the flavor indices in this chapter. Each Wilson coefficient carries four flavor indices $ijkl$ where $i,j=\{1,2,3\}$ indicate the generation of the involved up-type quark and down-type quark, respectively. $k=e$ denotes the electron and l now is for the particular neutrino mass eigenstate and runs from 1 to $\bar{n}$.

5.2 Production of sterile neutrinos

In this section we discuss the production of sterile neutrinos at collider and fixed-target experiments. For concreteness we consider the case where the sterile neutrinos are Majorana particles. We consider the production through the decay of mesons, produced at the interaction points, containing a single charm or bottom quark. We neglect the subdominant contribution from B_c, J/Ψ, and Υ mesons although they would allow to probe a larger neutrino mass range. Production via the decay of pseudoscalar mesons dominates over the contribution from vector mesons of the same quark composition, due to the much shorter lifetime of the latter. Sterile neutrino production via direct decays of W-, Z-, and Higgs bosons is subdominant for $\mathcal{O}(\text{GeV})$ neutrinos, mainly because of their smaller production cross sections [128, 197, 211].

5.2.1 Sterile neutrino production in minimal models

We begin by discussing sterile neutrino production in minimal models where sterile neutrinos interact with SM fields only via mixing. For simplicity, we consider a single sterile neutrino with mass m_N and set $n=1$ ($\overline{n}=4$). The production then arises solely from the first term in Eq. (5.1) with $(C^{(6)}_{\text{VLL}})_{ijk4}=-2V_{ij}\,U_{k4}$, where V is the CKM matrix and U the lepton mixing matrix. A broad range of processes are relevant. Naively one might think that leptonic meson decays $M^\pm_{ij}\to N+l^\pm_k$ would dominate because of phase space suppression associated to semi-leptonic decays, but CKM factors and powers of meson/neutrino masses in the amplitude expressions change this picture. To calculate the production rate, we require the number of mesons produced at the various experiments and the branching ratio to final states including a sterile neutrino. The former is discussed below, while here we calculate the latter. For minimal models, these branching ratios have been calculated in the literature, see Refs. [212, 213] for recent discussions, and here we confirm (most of) these results.

We consider leptonic and semi-leptonic decays of $D^\pm$, D^0, D_s, $B^\pm$, B^0, and B_s mesons. For semi-leptonic decays, we consider final-state pseudoscalar and vector mesons. The decay rate formulae and the associated decay constants and form factors are given in the Appendix. In the left and right panels of Fig. 5.1 we depict a selection of branching ratios for decay processes of D^-, D_s, and B^-, B_s mesons, respectively. Branching ratios for analogous decays of neutral D^0 or B^0 are similar and not shown to not clutter the plots too much. For these examples we considered a final-state electron and set $U_{e4}=1$. All branching ratios are in excellent agreement with Ref. [212]. From the plots it is clear that, depending on the mass m_N, both leptonic (solid

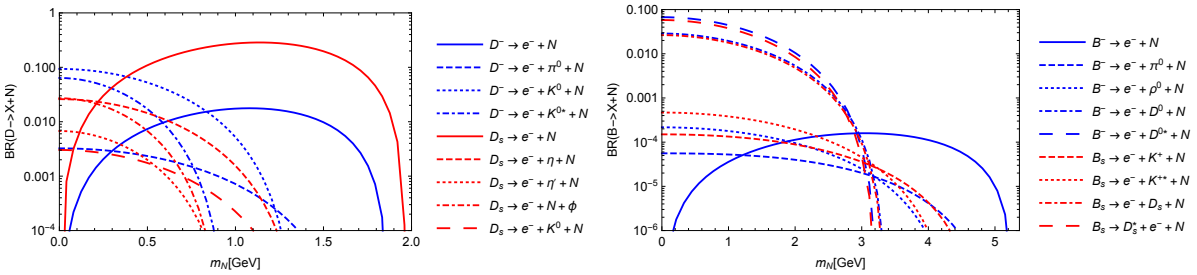

Figure 5.1: Branching ratios of sterile neutrino production channels through D (left figure) or B (right figure) mesons in the minimal scenario for final-state electrons and $U_{e4} = 1$.

lines) and semi-leptonic processes (dashed, dotted, and dot-dashed lines) must be included and the latter involve both final-state pseudoscalar and vector mesons.

5.2.2 Sterile neutrino production from higher-dimensional operators

For higher-dimensional operators the quark flavor structure of the Wilson coefficients is unknown in contrast to the minimal case where the CKM matrix provides the relation between processes involving different quarks. As such, each flavor structure is independent unless model assumptions are used. This leads to a large number of possible cases corresponding to several flavor structures for each effective operator in Eq. (5.1). All branching ratios can be calculated from the expressions given in the appendices.

Here we discuss a few cases only. We consider the operators with Wilson coefficients $C^{(6)}_{\mathrm{SRR}}$, $C^{(6)}_{\mathrm{TRR}}$, and $C^{(6)}_{\mathrm{VLR}}$. We consider the flavor structures $\{ijkl\} = 13e4$ and $\{ijkl\} = 21e4$ that allow for leptonic decays $B \to N + e$ and $D \to N + e$, respectively, if the Lorentz structure permits this. These choices also allow for semi-leptonic decays of the form $B \to N + e + X$ and $D \to N + e + X$ where X is a pseudoscalar or vector meson consisting of just up, down, and strange quarks (strange quarks only if the decaying meson contains a strange quark as is the case for B_s and D_s mesons). For the plots in this section, we assume the weak interaction is turned off and consider only one non-zero EFT operator at a time. The results are depicted in Fig. 5.2.

The three chosen operators correspond to quark bilinears with different Lorentz structures (scalar, tensor, and vector, respectively). In the scalar case, leptonic decays are allowed and these dominate over semi-leptonic decay modes for all considered values of the sterile neutrino mass. For the tensor operator, however, the leptonic decay mode is forbidden and a final-state meson must be produced. In these cases, the dominant decay modes are those with a final-state vector meson. Finally, the $C^{(6)}_{\mathrm{VLR}}$ vector operator has a similar Lorentz structure as the SM charged weak current, but with different flavor structure. As was the case in Fig. 5.1, depending on the sterile neutrino mass, either leptonic (solid lines) or semi-leptonic processes (dashed, dotted, and dot-dashed lines) can dominate the production of sterile neutrinos, and must all be included.

5.3 Decay of sterile neutrinos

5.3.1 Sterile neutrino decays in minimal models

We begin by considering the minimal scenario, where we assume that the only non-zero term in Eq. (5.1) is $(C^{(6)}_{\mathrm{VLL}})_{ijk4} = -2V_{ij}\,U_{k4}$. For concreteness we consider decays of Majorana sterile

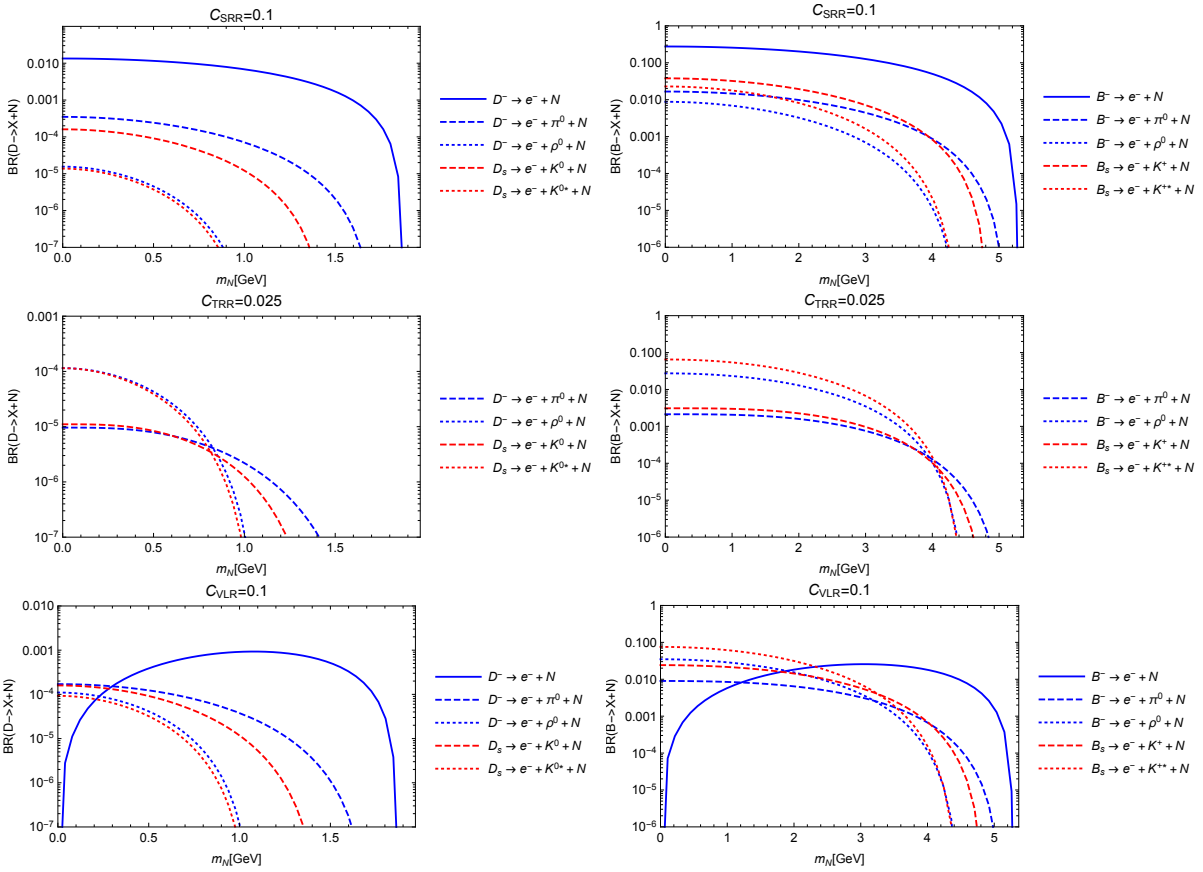

Figure 5.2: Branching ratios of D and B mesons in the left and right panels, respectively. Left: from top to bottom the figures correspond to $(C^{(6)}_{\rm SRR})_{21e4} = 0.1$, $(C^{(6)}_{\rm TRR})_{21e4} = 0.025$ and $(C^{(6)}_{\rm VLR})_{21e4} = 0.1$, respectively. Right: from top to bottom the figures correspond to $(C^{(6)}_{\rm SRR})_{13e4} = 0.1$, $(C^{(6)}_{\rm TRR})_{13e4} = 0.025$ and $(C^{(6)}_{\rm VLR})_{13e4} = 0.1$, respectively

.

neutrinos into final-state electrons and set $U_{e4} \neq 0$ and $U_{\mu 4} = U_{\tau 4} = 0$. In addition, we consider the SM weak neutral current (see Eq. (2.14)), which leads to $N \to \nu + f + \bar{f}$ decays where f denotes any SM fermion that is kinematically allowed (in case of quarks, we consider a final-state neutral meson). These decay rates have all been calculated in the literature, see *e.g.* Refs. [162, 164, 212–215]. Most results agree with each other and with our findings given in the Appendix, with the exception for decay processes into final-state neutral mesons where some differences appear. For these cases, our results agree with Ref. [213].

We consider $N \to$ leptons through both charged and neutral weak currents. The latter leads to the invisible three-neutrino decay mode. We include decays into a single pseudoscalar (π, K, η, η', D, D_s, η_c) and vector meson (ρ, ω, K^*, ϕ, D^*, D_s^*, J/Ψ). This effectively also takes into account decay modes into two pions through the intermediate decays of ρ mesons [212], assuming $m_N > m_\rho$. For heavier sterile neutrinos other multi-meson final states become relevant and summing exclusive channels becomes impractical. Instead we follow Refs. [212] and estimate the total hadronic decay width by calculating the decay width to spectator quarks times appropriate

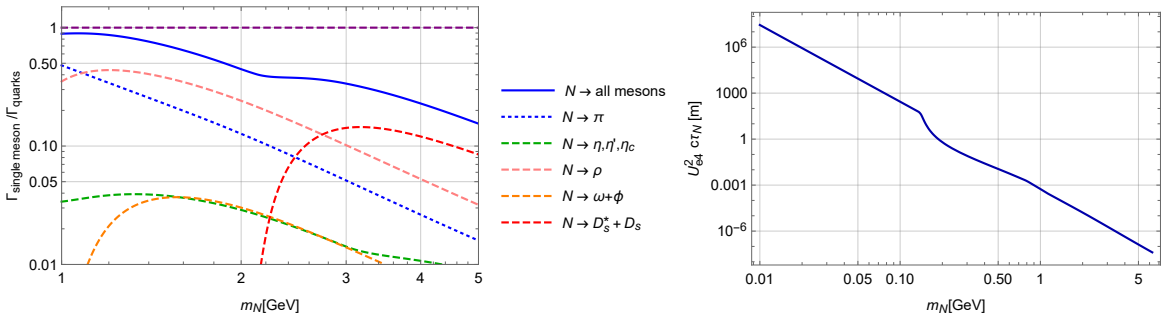

Figure 5.3: Left: Comparison of branching ratios to individual mesons divided by the inclusive hadronic branching ratio calculated via Eq. (5.4). Right: Decay length of the sterile neutrino in minimal scenarios.

.

loop corrections. The loop corrections are taken from a comparison to hadronic τ decays

$$1 + \Delta_{QCD}(m_\tau) \equiv \frac{\Gamma(\tau \to \nu_e + \text{hadrons})}{\Gamma_{\text{tree}}(\tau \to \nu_\tau + \bar{u} + D))}\,, \tag{5.2}$$

where D denotes a down or strange quark and

$$\Delta_{QCD} = \frac{\alpha_s}{\pi} + 5.2\frac{\alpha_s^2}{\pi^2} + \dots\,, \tag{5.3}$$

where dots denote higher-order corrections. This gives a good description of the inclusive hadronic τ decay rate and we assume this to hold for sterile neutrino decays in the minimal scenario as well. That is, we use

$$1 + \Delta_{QCD}(m_N) \equiv \frac{\Gamma(N \to e^-/\nu_e + \text{hadrons})}{\Gamma_{\text{tree}}(N \to e^-/\nu_e + \bar{q}q)}\,, \tag{5.4}$$

to calculate the inclusive hadronic sterile neutrino decay rate through both charged and neutral weak currents.

We find that single meson channels dominate for $m_N \lesssim 1$ GeV, while the decay to quarks become relevant for larger masses, indicating that multi-meson final states become significant. We demonstrate this in the left plot of Fig. 5.3, which shows branching ratios to individual mesons, compared to the sum of all single-meson final states, and compared to quarks, for $m_N \gtrsim 1$ GeV. At $m_N = 5\,\text{GeV}$, the single meson final states make up roughly 20% of the hadronic decay rate. Our results are in good agreement with Ref. [212], apart from decays to neutral vector mesons, which only play a small role.

We write the total decay rate as

$$\begin{aligned}\Gamma_N \;=\; & \theta(1\,\text{GeV} - m_N)\Gamma_{N\to\text{single meson}} + \theta(m_N - 1\,\text{GeV})\left[1 + \Delta_{QCD}(m_N)\right]\Gamma_{N\to\bar{q}q} \\ & + \Gamma_{N\to\text{leptons}}\,.\end{aligned} \tag{5.5}$$

In the right panel of Fig. 5.3, we show a plot of the scaled proper decay length, $U_{e4}^2 c\tau_N$, as a function of m_N in the minimal scenario, where c is the speed of light and τ_N is the proper lifetime of N. The branching ratios to individual mesons, leptons, and three neutrinos (invisible) for $m_N < 1\,\text{GeV}$ are shown in the left panel of Fig. 5.4 while the branching ratios to quarks, leptons, and invisible for $m_N > 1$ GeV are shown in the right panel of the same figure.

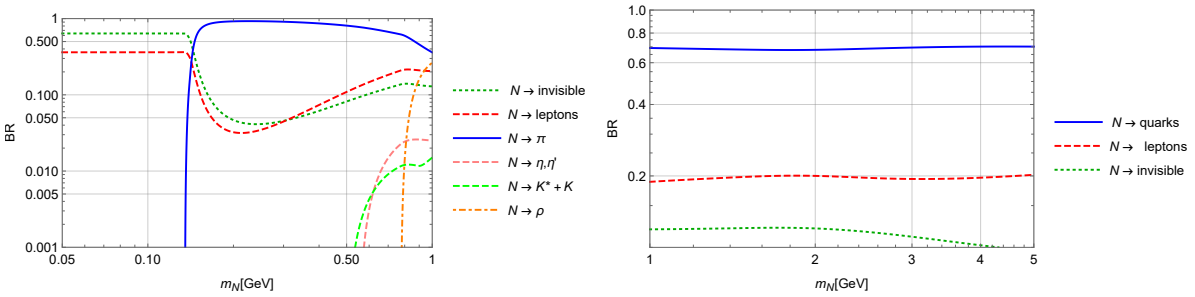

Figure 5.4: Branching ratios in the minimal scenario for $U_{e4} = 1$ and $U_{\mu 4} = U_{\tau 4} = 0$. Left: $m_N < 1\,\text{GeV}$ with decays to individual mesons. Right: $m_N > 1$ GeV and the decays to quarks correspond to the total hadronic branching ratio.

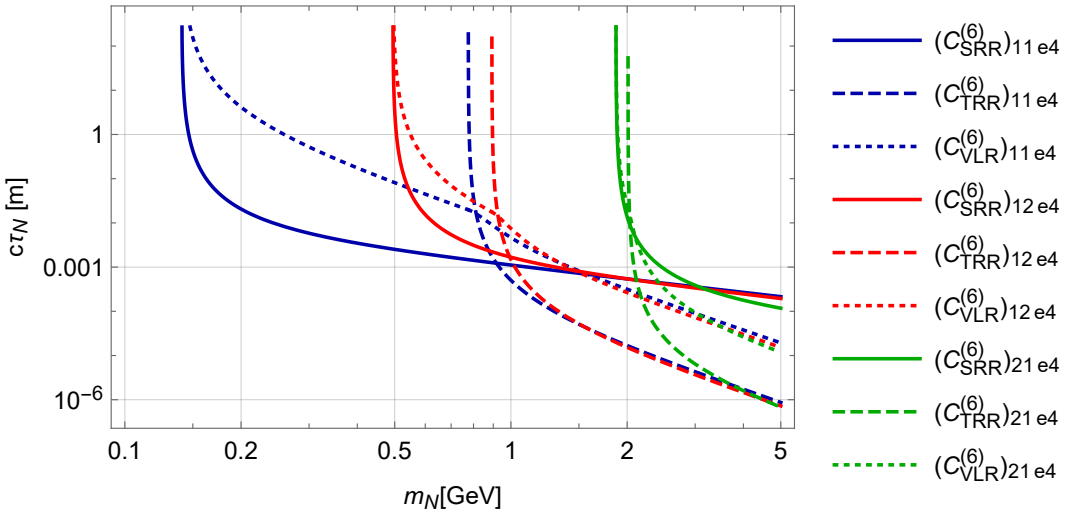

Figure 5.5: Proper decay length of sterile neutrinos for various choices of EFT operators and flavor assignments. The Wilson coefficients are set to unity and the minimal active-sterile mixing is turned off.

5.3.2 Sterile neutrino decays from higher-dimensional operators

The EFT operators in Eq. (5.1) involve two quarks and a charged lepton and induce new channels for sterile neutrinos to decay into hadrons. Depending on the flavor structure of the operators, typically only one or two single-meson decay modes are relevant. For instance for an operator $(C^{(6)}_{\text{VLR}})_{ije4}$ with $ij = 11$ we consider decays into a single charged pion or ρ meson, while for $(C^{(6)}_{\text{SRR}})_{11e4}$ only pions are relevant. As is the case for the minimal scenario, one can imagine multi-meson states to become relevant for larger sterile neutrino masses (for this flavor choice, such states would be three- or more pions). We do not include such states here, although we find that decays to quarks become dominant around $m_N \gtrsim 2\,\text{GeV}$ for scalar operators, as we do not have the benchmark of hadronic τ decays to verify our results for non-SM currents. We only consider decays into individual mesons. This leads to a potential underestimate of the sterile neutrino decay width and consequently renders our sensitivity limits for future experiments conservative in the large decay length regime. As all our results below are given on log scales, we do not expect significant deviations from our findings. In Fig. 5.5 we plot the proper decay length of N, $c\tau_N$, against its mass for various choices of Wilson coefficients and flavor assignments. We

consider one effective coupling at the time, turn off minimal mixing, and the Wilson coefficients are set to unity.

5.4 Theoretical scenarios

We focus on the production of sterile neutrinos through the decays of B and D mesons. We consider three classes of scenarios that are representative of the effective Lagrangian in Eq. (5.1). We always consider the case of a single sterile neutrino which is mixed with the active electron neutrino. The three classes of scenarios are listed below:

1. Here we consider the minimal scenario without higher-dimensional operators and 1 sterile neutrino (a $3+1$ model). Because of minimal sterile-active mixing, the sterile neutrino only interacts through charged and neutral SM weak interactions. In the $3+1$ minimal seesaw model, the mixing angle is related to the ratio of active and sterile neutrino masses $|U_{e4}|^2 \sim m_\nu/m_N$, but we treat the mixing angle as a free parameter. We stress that the minimal 3+1 model leads to two massless active neutrinos and is thus ruled out by neutrino oscillation experiments, but with its simplicity it provides a useful benchmark.

2. In this scenario we extend the minimal $3+1$ model by interactions generated by the exchange of leptoquarks. We again focus on the representation $\tilde{R}\,(\mathbf{3},\ \mathbf{2},\ 1/6)$ and the coefficients satisfy

$$\bar{c}^{(6)}_{\mathrm{SR}} = 4\bar{c}^{(6)}_{\mathrm{T}} = \frac{v^2}{2} C^{(6)}_{LdQ\nu}\,. \tag{5.6}$$

   Finally, going to the neutrino mass basis and focusing on the couplings to electrons and sterile neutrinos, we obtain the matching contributions to the effective operators in Eq. (5.1)

$$\left(C^{(6)}_{\mathrm{VLL}}\right)_{ije4} = -2V_{ij}U_{e4}\,, \qquad \left(C^{(6)}_{\mathrm{SRR}}\right)_{ije4} = 4\left(C^{(6)}_{\mathrm{TRR}}\right)_{ije4} = \left(\bar{c}^{(6)}_{\mathrm{SR}}\right)_{ije1} U^*_{44}\,, \tag{5.7}$$

   where i and j denote the up- and down-quark generation, respectively, and V_{ij} elements of the CKM matrix. In this scenario, we have contributions from minimal mixing proportional to the mixing angle U_{e4} and from leptoquark interactions proportional to U^*_{44}. We will use the canonical see-saw relations

$$U_{e4} \simeq \sqrt{\frac{m_\nu}{m_N}}\,, \qquad U_{44} = 1\,, \tag{5.8}$$

   and set $m_\nu = 0.05$ eV as representative for the active neutrino masses. For a specific quark flavor choice of i and j, this reduces the effective number of free parameters to two: the sterile neutrino mass m_N and the combination of the LQ couplings and mass $y^{\overline{LR}}_{i1} y^{RL*}_{je}/m^2_{LQ}$.

3. The final scenario we consider is inspired by models, such as left-right symmetric models, with right-handed charged gauge bosons, which can mix with $W^\pm$. Instead of implementing the full left-right symmetric model, we take a simplified scenario and consider the effects of a nonzero $C^{(6)}_{\mathrm{VLR}}$ in Eq. (5.1) in combination with the SM left-handed weak interactions. That is, we consider

$$\left(C^{(6)}_{\mathrm{VLL}}\right)_{ije4} = -2V_{ij}U_{e4}\,, \qquad \left(C^{(6)}_{\mathrm{VLR}}\right)_{ije4} > 0\,. \tag{5.9}$$

In left-right symmetric scenarios nonzero $C^{(6)}_{\mathrm{VRR}}$ and $C^{(6)}_{\mathrm{VRL}}$ are generally induced as well. The resulting phenomenology is very similar to $C^{(6)}_{\mathrm{VLL}}$ and $C^{(6)}_{\mathrm{VLR}}$ and for simplicity we do not consider these effective operators here. They can be easily added to the analysis if so required. For the active-sterile neutrino mixing parameter, we follow the leptoquark scenario and set $U_{e4} = \sqrt{m_\nu/m_N}$. In minimal left-right symmetric models with exact P or C symmetry, the dependence of the effective operators on the quark flavor indices ij can be calculated. We do not consider this here and consider one particular choice of ij at a time. It is straightforward to generalize this choice.

5.5 Collider and fixed-target analysis

We proceed to explore the search possibilities for the above scenarios at the LHC, considering both existing and proposed experiments, as well as the proposed fixed-target experiment SHiP at the CERN SPS [203–205]. Currently at the LHC we have the operational experiments ALICE [216, 217], ATLAS [191], CMS [192], and LHCb [218, 219]. Of these we shall focus on the search sensitivity for long-lived sterile neutrinos at ATLAS, which is the largest experiment in detector volume, and can thus in principle explore the largest decay lengths. Beyond this, a series of new experiments has recently been proposed at various locations near the LHC interaction points (IPs), namely in alphabetical order: AL3X [199], ANUBIS [200], CODEX-b [193], FASER and FASER2 [194,195], MATHUSLA [196–198], and MoEDAL-MAPP1 and MoEDAL-MAPP2 of the MoEDAL collaboration [201, 202]. These latter experiments, including SHiP, are all designed to specifically look for neutral long-lived particles (LLPs). We shall discuss the search potential of all the above-mentioned experiments specifically for sterile neutrinos.

In this section, we review briefly the setup of the beam and detector geometries for each experiment and introduce the Monte Carlo (MC) simulation procedure for the event simulation. We focus on the production via the rare decay of B- and D-mesons. This can proceed via either purely leptonic two-body decays, or semi-leptonic three-body decays, as discussed in Sect. 5.2. Similarly, for the displaced decay of sterile neutrinos, we consider both the two-body decay into a charged lepton and a charged meson, and decays into multiple hadronic states plus a lepton, as explained in Sect. 5.3. It is worth mentioning that the heavy meson M_1 that is to decay into a sterile neutrino, is produced in the process $pp \to M_1 + X$ and decays promptly into *e.g.* a sterile neutrino (X denotes the remaining decay products). Such signal events can be observed in the near detector such as ATLAS with *e.g.* the prompt lepton accompanying the production of M_1. The long-lived sterile neutrinos decay at a macroscopic distance, where the displaced vertex (DV) is reconstructed if at least two tracks are observed stemming from the same DV inside the detector.

We do not study the production of the sterile neutrinos from the decay of lighter mesons such as $\pi^\pm$ and kaons as these are only relevant for very light sterile neutrinos, and their simulation in Pythia 8 [220, 221] is insufficiently validated in the forward direction, which is relevant for the FASER experiments. In fact, even for $D^\pm$ and $B^\pm$ mesons, we will use FONLL [222–225] to correct the behavior of Pythia 8 in the very large pseudorapidity regime. Finally, we ignore the vector mesons decays into sterile neutrinos, as their decay width is typically many orders of magnitude larger than that of pseudoscalar mesons leading to tiny branching ratios for sterile neutrino production.

Instead of performing a detailed study considering different components of the detectors separately, for simplicity we will take the whole detector as the fiducial volume, and make a comparison between the various experiments. Since the ATLAS detector was not designed to look for

Experiment	SHiP	ATLAS	AL3X	ANUBIS	CODEX-b
Int. Lumi.	2×10^{20} POT	3000 fb^{-1}	100 or 250 fb^{-1}	3000 fb^{-1}	300 fb^{-1}
Angular Cov.	0.89%	100%	13.73%	1.79%	1%
Experiment	FASER	FASER2	MAPP1	MAPP2	MATHUSLA
Int. Lumi.	150 fb^{-1}	3000 fb^{-1}	30 fb^{-1}	300 fb^{-1}	3000 fb^{-1}
Angular Cov.	1.1×10^{-8}	1.1×10^{-6}	0.17%	0.68%	3.8%

Table 5.1: Summary of integrated luminosities for the various experiments. "POT" for SHiP stands for "Protons on Target". We also list the simple geometric coverage for each experiment.

neutral LLPs, we shall add an estimate for the efficiency factor based on existing neutral LLP searches, which, however, search for heavier candidates than considered here.

One potential issue relates to possible background events which, depending on the placement of the detector, may consist of long-lived SM hadron decays, cosmic rays, hadronic interaction with the detector material, etc. All the experiments considered in this study, except ATLAS, employ a far detector with a distance $5 - 500$ meters away from the IP. The space between the IP and the far detector is usually sufficiently large to allow for the installation of veto and shielding segments, as argued in Refs. [193, 194, 196, 197, 199, 200, 202, 226, 227]. For MATHUSLA the rock and shielding below ground should remove the SM background. As for cosmic rays, directional cuts will be applied. To assess and compare the sensitivities of different experiments, we show 3-event isocurves which correspond to 95% confidence level (C.L.) with zero background. This is not appropriate for the ATLAS detector which has an almost 4π coverage immediately around the IP, and a large irreducible SM background is expected. Depending on the signal type, the number of such background events may vary. Instead of performing an estimate of background events for each scenario, we shall implement an estimate for the efficiency, which we discuss below.

In addition, since the detector efficiency of the future experiments is unknown, in order to make a fair comparison, we assume a 100% reconstruction efficiency for all the experiments except ATLAS.

The search potential of these experiments, but also of other fixed-target experiments, has been investigated for example for neutralinos [228–232]. For various other theoretical scenarios, see Ref. [233] for a recent review.

We start with a brief introduction of the fixed-target experiment SHiP, as its beam setup is different from the other experiments, and then discuss the other experiments, which are all associated to either the ATLAS, CMS, or LHCb IP and the LHC accelerator[3]. Since these experiments differ in the projected integrated luminosity, we summarize them in Table 5.1.

5.5.1 SHiP

The SHiP facility was proposed to make use of the high-intensity CERN SPS beam of 400 GeV protons incident on a fixed target made of *e.g.* a hybrid material composed of (solid) molybdenum alloy and pure tungsten [203–205]. It has not been approved yet. With a center-of-mass energy of approximately 27 GeV, large production rates of D- and B-mesons are expected. The SHiP experiment is proposed to have a cylindrical detector downstream at roughly 70 m away from the

[3]We consider the LHC center-of-mass energy at 14 TeV for all experiments. We assume an LHC upgrade before the experiments are online. Changing it to 13 TeV would only have a small effect on our results.

IP. The experiment is specifically designed for detecting long-lived neutral particles, which are produced from *e.g.* charm or bottom meson rare decays, fly an extended length, and then decay inside the detector chamber downstream, especially if the lab-frame decay length of the LLP lies within the SHiP sensitivity range. For the lifetime of the SHiP project, a total of 2×10^{20} protons on target (POT) are planned.

At SHiP, the initial meson M_1 of sterile neutrinos is produced in a hadronic collision between the beam protons and the target material. The differential production cross section is strongly forward peaked, and the M_1 will have a significant forward boost. This will be passed onto the decay products, including N, the sterile neutrino. The active decay chamber is 68.8 m downstream of the target. It has a cyclindrical shape with a length of 60 m, where the first 5 m are to be used for placing background suppression vetoes. The front surface has an elliptical shape with semi-axes of 5 m and 2.5 m. The optimal sensitivity is for particles with

$$68.8\,\mathrm{m} < \beta_N^z \gamma_N c\tau_N < 123.8\,\mathrm{m}\,, \tag{5.10}$$

where β_N^z, γ_N are the relativistic speed along the beam axis and the Lorentz boost factor of N, respectively.

In order to study sterile neutrinos produced from the decays of D- and B-mesons, we need to know the total number of these mesons expected at SHiP in its 5 year lifetime: $N_{D^\pm}$, N_{D^0}, N_{D_s}, $N_{B^\pm}$, N_{B^0}, and N_{B_s}, respectively. These numbers can be estimated by following Ref. [212]. See also the earlier work in Ref. [230]. The $c\bar{c}$ ($b\bar{b}$) production rate is 1.7×10^{-3} (1.6×10^{-7}) per collision. After the fragmentation factors are taken into account, the numbers of the heavy-flavor mesons can be estimated and reproduced below from Ref. [212]:

$$N_{D^\pm}^{\texttt{SHiP}} = 1.4 \times 10^{17}, \quad N_{D^0}^{\texttt{SHiP}} = 4.3 \times 10^{17}, \quad N_{D_s}^{\texttt{SHiP}} = 6.0 \times 10^{16}, \tag{5.11}$$

$$N_{B^\pm}^{\texttt{SHiP}} = 2.7 \times 10^{13}, \quad N_{B^0}^{\texttt{SHiP}} = 2.7 \times 10^{13}, \quad N_{B_s}^{\texttt{SHiP}} = 7.2 \times 10^{12}. \tag{5.12}$$

We note that B_c mesons are in principle also produced and may extend the upper reach in m_N. However, given the much smaller production cross section, we do not take it into account. Similarly for the other LHC experiments, as discussed below.

5.5.2 Experiments at the LHC

For ATLAS and extended programs at the ATLAS/CMS/LHCb sites, we consider pp collisions at $\sqrt{s} = 14\,\mathrm{TeV}$ with equal beam energies. These experiments benefit from a beam energy that is orders of magnitude higher compared to SHiP. As a result, the mesons and the therefrom produced sterile neutrinos are much more boosted, leading to good sensitivities even for detectors that are to be installed hundreds of meters away from the IP.

To perform the sensitivity estimate for experiments at ATLAS/CMS/LHCb, it is necessary to know the inclusive production rate of the heavy-flavor mesons at the HL-LHC with up to $3\,\mathrm{ab}^{-1}$ integrated luminosity. To achieve this, we follow the procedure in Refs. [230,231,234]. The LHCb collaborations reported D-meson and B-meson production cross sections for a 13 TeV pp-collider, for certain kinematic range. Using the simulation tools FONLL [222–225] and Pythia 8 we can extrapolate these cross sections to the whole kinematic range. We find that for $3\,\mathrm{ab}^{-1}$ integrated luminosity over the full 4π solid angle the following list of numbers of the produced charm and bottom mesons:

$$N_{D^\pm}^{\text{HL-LHC}} = 2.04 \times 10^{16}, \quad N_{D^0}^{\text{HL-LHC}} = 3.89 \times 10^{16}, \quad N_{D_s}^{\text{HL-LHC}} = 6.62 \times 10^{15}, \tag{5.13}$$

$$N_{B^\pm}^{\text{HL-LHC}} = 1.46 \times 10^{15}, \quad N_{B^0}^{\text{HL-LHC}} = 1.46 \times 10^{15}, \quad N_{B_s}^{\text{HL-LHC}} = 2.53 \times 10^{14}. \tag{5.14}$$

For the estimate of $N_{D^\pm}^{\text{HL-LHC}}$, the decay branching ratio of $D^{*\pm}$ into $D^\pm$ is included, and for the number of B-mesons the corresponding fragmentation factors determined by `Pythia 8` are used. These numbers will be used not only for the evaluation at the `ATLAS` experiment, but also for all the extended programs discussed below with a possible overall re-scaling by the integrated luminosity.

1. At the `ATLAS` IP, the differential cross section for the production of GeV-scale mesons is strongly peaked at large pseudorapidities, *i.e.* close to the beam pipe in both directions. The production rate of light neutral LLPs, resulting from the decay of the mesons, should then also be peaked in the large pseudorapidity regime. A far detector known as `FASER` (Forward Search ExpeRiment) [194,195] has been proposed, which is designed to specifically make use of this feature. It has been officially approved by CERN and should be collecting data during Run 3 of the LHC. It is placed in the existing TI12 tunnel at a distance of 480 m from the `ATLAS` IP and has a cylindrical shape exactly aligned with the beam collision axis, but slightly off of the beam due to the curvature of the accelerator. The `FASER` detector has a cylindrical radius of 10 cm and a length of 1.5 m, and the expected integrated luminosity is $150\,\text{fb}^{-1}$. The corresponding angular coverage is $\eta \in [9.17, +\infty]$ in pseudorapidity and full 2π in the azimuthal angle.

   After Run 3 is finished, `FASER` is currently planned to be upgraded to a larger version known as `FASER2`, to be under operation during the HL-LHC era, collecting up to $3\,\text{ab}^{-1}$ of data [195], and located in the same place. Its geometry is specified as a cylinder with 1 m radius and 5 m length, which is 300x larger by volume, than `FASER`. The pseudorapidity coverage is correspondingly enlarged to $\eta \in [6.86, +\infty]$ while the azimuthal angle remains fully covered. Here we study the search potential of both `FASER` and `FASER2` for sterile neutrinos as neutral LLPs.

   As mentioned earlier and discussed in Ref. [231], `Pythia 8` is not well validated in the large pseudorapidity regime for the differential production cross section of charm and bottom mesons. To solve this issue, we re-scale the meson production cross section in `Pythia 8` at different ranges of the transverse momentum and pseudorapidity by using the more reliable results given by `FONLL`.

2. A much larger experiment called "`MATHUSLA`" (MAssive Timing Hodoscope for Ultra Stable neutraL pArticles) has been suggested to be constructed at the surface above the `CMS` experiment [196–198]. It is proposed to be built for the HL-LHC phase with $3\,\text{ab}^{-1}$ integrated luminosity. With a box shape, it has a base area of 100 m$\times$ 100 m and a height of 25 m. Relative to the `CMS` IP, the front edge of the detector should be horizontally shifted along the beam axis by 68 m, and vertically upwards by 60 m. Despite its huge size, the large distance of `MATHUSLA` from the IP still leads to a small geometric coverage. It corresponds to a solid angle or geometric coverage of about 3.8%. Nevertheless, it has been shown to be one of the far detectors at the LHC that may have the strongest reach in the very small active-sterile neutrino mixing at $|U_{e4}|^2 \sim 10^{-9}$, when only the weak interaction is considered [198].

3. It has recently been proposed [200] to construct a detector, named `ANUBIS` (AN Underground Belayed In-Shaft search experiment), in one of the service shafts just above the `ATLAS` or `CMS` IP. Consequently, a total of 3 ab^{-1} integrated luminosity from the LHC is projected. Similarly to the detectors discussed above, it also has a cylindrical shape however with the axis oriented in the vertical direction. The cyclinder diameter is 18 m and

the length is 56 m. The axis of the cylinder runs from the middle point of the bottom: $(x_b, y_b, z_b) = (0, 24\,\text{m}, 14\,\text{m})$ to the top $(x_t, y_t, z_t) = (0, 80\,\text{m}, 14\,\text{m})$, where z is along the beam axis, x is horizontally transverse, and y is vertically transverse, and the IP is at $(x, y, z) = (0, 0, 0)$. Please refer to Refs. [200, 211] for a sketch. MC integration finds the angular coverage of ANUBIS to be 1.79% [234].

4. An external detector extension has also been proposed at the IP8 of the LHCb experiment. CODEX-b (COmpact Detector for EXotics at LHCb) [193] is designed as a cubic box of dimensions $10\,\text{m} \times 10\,\text{m} \times 10\,\text{m}$. Occupying an empty space with a distance $\sim$25 m from the LHCb IP, it covers the pseudorapidity range of $\eta \in [0.2, 0.6]$ with the azimuthal angle coverage of $\sim 6.4\%$. The total geometric coverage of the solid-angle is about 1%.

5. MAPP (MoEDAL's Apparatus for Penetrating Particles) is proposed as one sub-detector of the MoEDAL experiment [201,202] at the IP8 of LHCb, and designed for searching for neutral LLPs. Similar to FASER, the MAPP experiment will have a significant upgrade in a second version. MAPP1 is a rather small detector of volume $\sim 130\,\text{m}^3$, currently under deployment and expected to collect data during LHC Run 3 with up to 30 fb^{-1} integrated luminosity. It is roughly 55 m from the IP8 at a polar angle 5° from the beam. During the HL-LHC era, the MAPP2 program is planned to be under operation at IP8 until the end of Run 5, accumulating up to $300\,\text{fb}^{-1}$ of data. It is designed to occupy almost the whole of the UGC8 gallery in the LHC tunnel complex, taking up a volume of about $430\,\text{m}^3$. With a larger integrated luminosity and a bigger volume, MAPP2 is predicted to have higher sensitivity. The two detectors cover about 0.17% and 0.68% of the total solid angle [234], respectively.

6. AL3X (A Laboratory for Long-Lived eXotics) was proposed in Ref. [199] to be built at the LHC IP2 where the ALICE experiment sits. Placed at a horizontal distance along the beam line of 5.25 m from the IP, the detector has a cylindrical shape aligned with and surrounding the beam line, corresponding to a full azimuthal coverage. The proposed inner (outer) radius is 0.85 m (5 m) with the length 12 m. This gives a pseudo-rapidity coverage of $\eta \in [0.9, 3.7]$. The authors of Ref. [199] proposed two values of the integrated luminosity, 100 fb^{-1} and 250 fb^{-1}, in order to accommodate practical concerns including the move of the IP, beam quality, and investigation of background events. Here we focus on the benchmark value of 250 fb^{-1} integrated luminosity.

7. We have discussed proposed new experiments which are specifically designed to look for long-lived particles. They are typically placed some distance away from the various IPs at the LHC or, in the case of SHiP, designed as a fixed-target experiment with a long decay path. In *e.g.* Ref. [230] some of us considered the search for light long-lived particles at ATLAS. ATLAS can study decays upto a length of about $\sqrt{11^2 + (43/2)^2} = 24\,\text{m}$, where 11 m is the cylindrical radius and 24 m is half the detector length. Over this length, as we discuss below in more detail, the fraction $1 - \exp[-24\,\text{m}/(\beta\gamma c\tau)]$ of the LLP's decay where τ and γ denote the LLP lifetime and boost factor, respectively, and β is the relativistic speed of the particle. However, ATLAS offers almost 4π in angular coverage, which is significantly larger than the other detectors at the LHC. In Ref. [230], we found that for 100% signal efficiency, an integrated luminosity of $250\,\text{fb}^{-1}$, and assuming zero background, ATLAS is competitive with or slightly better than SHiP for the LLPs produced from B-mesons decays, and was somewhat worse in the case of D-mesons.

   Here we describe in more detail the geometrical parameters we use for the fiducial volume of the ATLAS detector. It has a cylindrical shape with inner (outer) radius of 0.0505 m (11 m)

corresponding to the beginning of the inner detector (the end of the muon spectrometer), and a length of 43 m. In principle, even if a DV is inside the beam pipe, as long as its distance from the IP is larger than the detector spatial resolution and consists of displaced tracks, it can be reconstructed. However, to be more conservative, we choose to include only DVs that are located inside the detector volume. We take $3\,\mathrm{ab}^{-1}$ as the benchmark value for the integrated luminosity over the lifetime fo the HL-LHC.

As we have mentioned, all the above proposed new experiments are specifically designed to look for light long-lived particles. They are thus further away from the LHC IPs and shielded from many SM backgrounds generated at the IP. All the same they will all have separate background issues, depending on where they are located. `MATHUSLA` is to be installed on the ground and thus highly susceptible to cosmic rays. `ANUBIS` is in a shaft which has minimal overhead shielding. `FASER` is far down along the tunnel, but still close to the beam pipe. In order to compare these experiments we have for now assumed that they can tackle the issues concerning background, and assumed zero background for all. The precise design of these detectors is also not yet well-established, except for the first phase of `FASER`. We thus furthermore assume 100% signal efficiency.

All this does not hold for `ATLAS` (or `CMS`, of course). `ATLAS` is a well-established experiment, operating in the immediate vicinity of the IP. There is purposely no shielding, as *a priori* all events are of interest. With respect to light long-lived particles there are thus large backgrounds which must be dealt with. Any cuts which are imposed to reduce the background, will also affect the signal efficiency, most likely in a significant manner. In order to compare a search at `ATLAS` with the other experiments we must impose a realistic signal efficiency, to take this into account. To our knowledge at the moment, there is no dedicated study at `ATLAS` or `CMS` for the scenarios we are considering here. We discuss several related analyses and estimate a signal efficiency based on this.

In Ref. [235], `ATLAS` considered the following scenario proposed in Ref. [236]. A Higgs boson decays to two dark fermions, which in turn decay to one or two dark photons plus an invisible hidden lightest stable particle. The dark photons are the long-lived particles and decay either to a pair of muons, or a pair of electrons/pions (light hadrons). Dark photon masses between 0.4 and 3.5 GeV are considered, *i.e.* similar to our sterile neutrino mass range. However the Higgs boson masses are 125 or 800 GeV and thus the dark photons would have a much higher boost than our sterile neutrino's. For the lighter Higgs mass and the purely hadronic decay of the dark photon `ATLAS` finds a signal efficiency of at best $5{\cdot}10^{-5}$ for $c\tau \approx 35\,\mathrm{mm}$, and dropping off rapidly for smaller or larger $c\tau$.

In Ref. [237], `ATLAS` considered the following scenario. A Higgs boson decays to a pair of neutral long-lived scalars, which in turn each decay to 2 jets, one in the inner detector and one in the muon spectrometer, thus utilizing different parts of the `ATLAS` detector. For the lightest mass scenario the Higgs boson is 125 GeV and the scalar is 8 GeV. A detector efficiency of $3{\cdot}10^{-5}$ is found, similar to the other analysis. In Ref. [238] `ATLAS` considered a related scenario with scalar masses down to 5 GeV. For a Higgs boson of 125 GeV, and a scalar of 5 GeV with a decay length of 75 cm they find a signal efficiency of $7{\cdot}10^{-4}$, somewhat better than in the other studies.

In all these analyses, `ATLAS` searches for pairs of produced particles. This reduces background but also efficiency. Overall we have applied a from the `ATLAS` point of view somewhat optimistic flat signal efficiency factor of 10^{-3} to all the `ATLAS` searches. In addition we assume that the corresponding cuts reduces the background to zero.

5.5.3 Monte-Carlo simulation

We perform the MC simulation with the tool `Pythia 8.243` [220, 221], in order to extract the kinematics and to estimate the number of signal events. We express the number of sterile neutrinos, N, produced as

$$N_N^{\rm prod} = \sum_i N_{M_i} \cdot {\rm Br}(M_i \to N + X), \tag{5.15}$$

where M_i is summed over all mesons that can decay to N in a given scenario. "Br" stands for decay branching ratio. N_{M_i} is the number of initial mesons, M_i, produced in the initial collisions at the LHC or for `SHiP`.

The number of sterile neutrino decays in a detector volume $N_N^{\rm dec}$ can then be estimated by taking into account the boost factor and traveling direction of N, geometries of the detector, and the decay branching ratio of sterile neutrinos into the signal final-state particles. For the latter, we consider all the decay channels except for the fully invisible state, which contains solely three neutrinos, and is mediated by the SM weak interaction. We use the expressions

$$N_N^{\rm dec} = N_N^{\rm prod} \cdot \langle P[N \text{ in f.v.}] \rangle \cdot {\rm Br}(N \to \text{signal}), \tag{5.16}$$

$$\langle P[N \text{ in f.v.}] \rangle \equiv \frac{1}{N_N^{\rm MC}} \sum_{i=1}^{N_N^{\rm MC}} P[N_i \text{ in f.v.}], \tag{5.17}$$

where $\langle P[N \text{ in f.v.}] \rangle$ denotes the average probability of all the simulated sterile neutrinos to decay inside the fiducial volume ("f.v.") and $P[N_i \text{ in f.v.}]$ is the individual probability of the $i-$th simulated sterile neutrino to decay in the f.v., discussed in more detail below. $N_N^{\rm MC}$ is the total number of sterile neutrinos N generated in the simulation. For all the experiments except `MAPP1` and `MAPP2`, we use formulas for calculating the individual decay probability with the exponential decay distribution, extracted from existing references [211, 230–232]. As input we use the boosted decay length and the traveling direction of each simulated sterile neutrino, denoted by $\lambda_i = \beta_i \gamma_i c \tau_N$, where β_i is the speed and γ_i the boost factor.

For the `MoEDAL-MAPP` detectors, following Ref. [234] we implement a code which determines whether each simulated sterile neutrino travels in the direction pointing towards the detector and if so returns L_{1i} and L_{2i}, where L_{1i} denotes the distance from the IP to the position where the $i-$th sterile neutrino would enter the detector, and L_{i2} the distance the $i-$th sterile neutrino would travel across the detector, if it leaves the detector without having decayed. If the travel direction of the long-lived sterile neutrino points towards the detector, we compute $P[N_i \text{ in f.v.}]$ for the `MoEDAL-MAPP` detectors through

$$P[N_i \text{ in f.v.}] = e^{-L_{1i}/\lambda_i} \cdot (1 - e^{-L_{2i}/\lambda_i}). \tag{5.18}$$

We use the modules "`HardQCD:hardccbar`" and "`HardQCD:hardbbbar`" of `Pythia 8` to simulate the production of the charm and bottom mesons, respectively, including the processes $q\bar{q}, gg \to c\bar{c}/b\bar{b}$. For each benchmark scenario, we simulate 10^6 events of the corresponding process, and fix the initial-state mesons to decay to the various channels, mediated by both the SM weak interaction and the EFT operators, with the corresponding decay branching ratios. From the MC simulation with `Pythia 8`, we obtain the average decay probability from which we calculate $N_N^{\rm dec}$ in Eq. (5.16).

We emphasize that for the partial decay widths of the heavy mesons into N and of the N into light mesons, we take into account the weak interaction via active-sterile neutrino mixing, the EFT operator(s), and also the interference between them. The computation for the production and decay processes of sterile neutrinos are presented in Sect. 5.2 and 5.3 and in the appendices.

5.6 Numerical results

To present the results of this collider study in a compact and representative manner we consider a subset of possible EFT operators and focus on the three scenarios described in Sect. 5.4. For scenario 1, the minimal scenario, there is no EFT operator involved, and we consider the full standard model charged- and neutral-currents mediated via the active-sterile neutrino mixing. For scenarios 2 and 3, which involve EFT operators, we must specify their flavor. In these scenarios we consider 5 different flavor assignments. Each assignment involves two EFT operators of different quark flavors. All EFT operators are dimension-6, and we drop the (6) superscript in the following. First, we fix the production mode via the "production operator" $(C_{\rm P})_{ij}$, with associated Wilson coefficients. We shall consider two cases for the indices ij, which indicate the up- and down-type quark generations considered in a flavor benchmark, respectively. The choices of the flavors should lead to charm and bottom meson decays:

$$\text{Sterile Neutrino Production Modes}: \quad \begin{cases} (C_{\rm P})_{21}: & D \to N + e\,(+X), \\ (C_{\rm P})_{13}: & B \to N + e\,(+X). \end{cases} \tag{5.19}$$

Here X indicates a potential final state meson. See examples below. Second, we simultaneously turn on another EFT operator the "decay operator" $(C_{\rm D})_{ij}$, which leads to the decay of sterile neutrinos via semi-leptonic processes. Here, the ij indicate the flavor content of the final state meson. We shall consider several decay modes

$$\text{Sterile Neutrino Decay Modes}: \quad \begin{cases} (C_{\rm D})_{11}: & N \to \pi^{\pm} + e^{\mp},\ \rho^{\pm} + e^{\mp}\,, \\ (C_{\rm D})_{12}: & N \to K^{\pm} + e^{\mp},\ K^{*\pm} + e^{\mp}\,, \\ (C_{\rm D})_{21}: & N \to D^{\pm} + e^{\mp},\ D^{*\pm} + e^{\mp}\,. \end{cases} \tag{5.20}$$

Both the production and decay will be induced by various operators with associated Wilson coefficients, which we discuss in detail below. For all scenarios we include the production and decay of sterile neutrinos via the SM weak interaction (see Sect. 5.4 for details) and the corresponding interference terms with the EFT operators. For the theoretical scenarios 2 and 3 we impose the type-I Seesaw relation to include weak interaction contributions through minimal mixing, see Sect. 5.4.

As indicated in Eq. (5.19), we only include sterile neutrino production via B and D decays, also for lighter sterile neutrinos with masses $m_N < m_K$, m_π, the kaon and pion masses, respectively. We do not include possible production via kaon or pion decays for the following reasons. Despite the larger production rates of these mesons, the simulation of soft pions is not well validated in quick MC simulation tools. Furthermore, the kaons are long-lived, leading to further complications. Finally, sterile neutrinos produced from pions and kaons are necessarily light, resulting in limited sensitivity reach in m_N. To summarize, while we show results for light sterile neutrinos in the following, these must be taken as conservative as we underestimate the number of the produced sterile neutrinos from pion and kaon decays both via the SM weak interaction as well as via the "decay operator" $C_{\rm D}$.

5.6.1 The minimal scenario

In the minimal scenario, the interactions are purely mediated by the W- and Z-bosons via the active-sterile neutrino mixing. Using the analytical expressions given in the previous sections for the production and decay of the sterile neutrino, we estimate the sensitivity reach of the experiments discussed in Sect. 5.5. We present the results in Fig. 5.6, shown in the plane $|U_{e4}|^2$

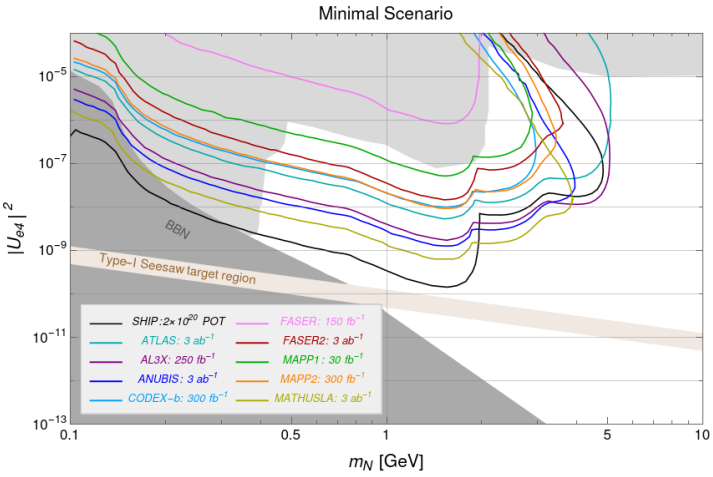

Figure 5.6: Results for the minimal scenario with the sterile neutrino mixed solely with the electron neutrino.

vs. m_N. Here, we lift the requirement of the type-I seesaw relation $|U_{e4}|^2 \simeq m_{\nu_e}/m_N$, and treat the mixing angle and the sterile neutrino mass as two independent free parameters. The light gray area shows the present bounds obtained by various experiments including the searches from `CHARM` [239], `PS191` [240], `JINR` [241], and `DELPHI` [242]. The dark gray area corresponds to the part excluded by big bang nucleosynthesis (BBN) [243,244]. We also show a brown band of "Type-I Seesaw target region" for m_{ν_e} between 0.05 eV and 0.12 eV with the relation $|U_{e4}|^2 \simeq m_{\nu_e}/m_N$. These two limits are derived from neutrino oscillation and cosmological observations, respectively. The former finds that there is at least one active neutrino mass eigenstate of mass at least 0.05 eV [245] while the latter imposed an upper limit of 0.12 eV for the sum of the active neutrino masses [246].

The sensitivity reaches of the various experiments have been determined in the literature [128, 195, 197, 211, 232, 247], except for the `MAPP1` and `MAPP2` experiments, for which we present the estimate for the sensitivity reach for the first time. Our estimate for the `ATLAS` experiment considers an integrated luminosity of $3\,\text{ab}^{-1}$ and takes 3000 signal events *before* taking into account an universal efficiency factor 10^{-3} as the 95% C.L. exclusion limit. To the best of our knowledge, a similar estimate for sterile neutrinos in the minimal scenario produced from heavy-flavor mesons rare decays has not been conducted for `ATLAS`. See Ref. [248] for a related study within the minimal model, with the sterile neutrino produced from W-decays, however with promptly decaying sterile neutrinos. Furthermore, in Ref. [249] `ATLAS` investigated a sterile neutrino mixing with ν_μ and with a delayed decay, *i.e.* a displaced vertex, as well as a promptly decaying sterile neutrino, which mixes with ν_e however only for $m_N \gtrsim 6\,\text{GeV}$. For the other experiments, we assume zero background and 100% detector efficiency. Hence we take 3 signal events as the 95% C.L. exclusion limit. Comparing the sensitivity reach of the experiments shown in Fig. 5.6 with those from the literature, we find a good agreement in most cases. For the `ANUBIS` exclusion limits, our results shown in Fig. 5.6 are inferior by a factor ~ 3.5, to those given in Ref. [211]. This difference is due to a corrected meson-production-rate and sterile-neutrino-decay-width calculation.

Given the general agreement with the existing results in the literature, we proceed to evaluate the sensitivities of these experiments to a set of benchmark scenarios, where the sterile neutrino interactions with the SM particles are enhanced by heavy new physics, encoded by EFT operators. There are a large number of possibilities for the flavor structure of the EFT operators. Here we

	Flavor benchmark 1.2	Flavor benchmark 1.3
production operator: $C_{\rm P}$	$C^{21}_{\rm SRR} = 4C^{21}_{\rm TRR}$	$C^{21}_{\rm VLR}$
decay operator: $C_{\rm D}$	$C^{11}_{\rm SRR} = 4C^{11}_{\rm TRR}$	$C^{11}_{\rm VLR}$
production process via $C_{\rm P}$	$D^{\pm}/D^0/D_s \to N + e^{\pm}(+X)$	
decay process via $C_{\rm D}$	$N \to \pi^{\pm} + e^{\mp},\ \rho^{\pm} + e^{\mp}$	

Table 5.2: Summary of flavor benchmark 1 for the theoretical scenarios 2 and 3 of Sect. 5.4, respectively. X denotes any additional final state particles.

consider a few representative flavor choices, to get an understanding of the general features and the sensitivity reach of various experiments. The calculations can easily be repeated for other flavor choices, for instance those inspired from specific UV-complete scenarios.

We note that in the following EFT flavor benchmarks, with the choice of the canonical type-I Seesaw relation, $m_N \lesssim 1$ GeV appears to be disfavored by BBN considerations. However, the inclusion of the EFT operator $C_{\rm D}$ can reduce the lifetime of the sterile neutrinos, possibly circumventing BBN constraint and leading to a potential lower bound on the EFT Wilson coefficients. Different flavor assignments result in different final-state particles, affecting the primordial helium and deuterium abundances to different extents. A detailed study is necessary to investigate the limits that can be set from BBN consideration on EFT operators and we do not present BBN exclusion bands below.

5.6.2 Flavor benchmark 1

We consider the theoretical scenarios 2 and 3 of Sect. 5.4 for a specific flavor choice. We focus on sterile neutrino production through decay of D-mesons, and thus consider the production operator $(C_{\rm P})_{21}$. For scenario 2, the leptoquark scenario, for $C_{\rm P}$ and $C_{\rm D}$ we consider scalar and tensor operators that are related through $C_{\rm SRR} = 4C_{\rm TRR}$. For scenario 3 corresponding to anomalous vector interactions, the production and decay operators are both $C_{\rm VLR}$. The following decays then produce sterile neutrinos

$$D^{\pm} \to e^{\pm} + N, \quad D^{\pm} \to \pi^0 + e^{\pm} + N, \quad D^{\pm} \to \rho^0 + e^{\pm} + N, \tag{5.21}$$

$$D^0 \to \pi^{\pm} + e^{\mp} + N, \quad D^0 \to \rho^{\pm} + e^{\mp} + N, \quad D_s \to K^{(*)0} + e^{\pm} + N\,. \tag{5.22}$$

We are sensitive to sterile neutrino masses $m_N < m_D - m_e$. For the decay operator we choose $(C_{\rm D})_{11}$ resulting in the decays

$$N \to e^{\pm} + \pi^{\mp}\,, \quad \text{and} \quad N \to e^{\pm} + \rho^{\mp}\,. \tag{5.23}$$

The essential features of this benchmark are summarized in Table 5.2. In addition, we include production and decay modes via minimal mixing which extends both the upper and lower reach in m_N.

Fig. 5.7 presents the sensitivity reach of all considered experiments for the flavor benchmark 1. The left panels correspond to theory scenario 2 (leptoquark) and the right panels to scenario 3 (anomalous vector interactions). In the upper row we plot the value of the decay operator $C_{\rm D}$ vs. the production operator $C_{\rm P}$ for a fixed sterile neutrino mass $m_N = 1$ GeV. In the bottom row we have fixed $C_{\rm D} = C_{\rm P}$ and show the dependence of the sensitivity of the experiments on $C_D = C_P$ and the sterile neutrino mass. Both the top and bottom panels show that the sensitivity reach

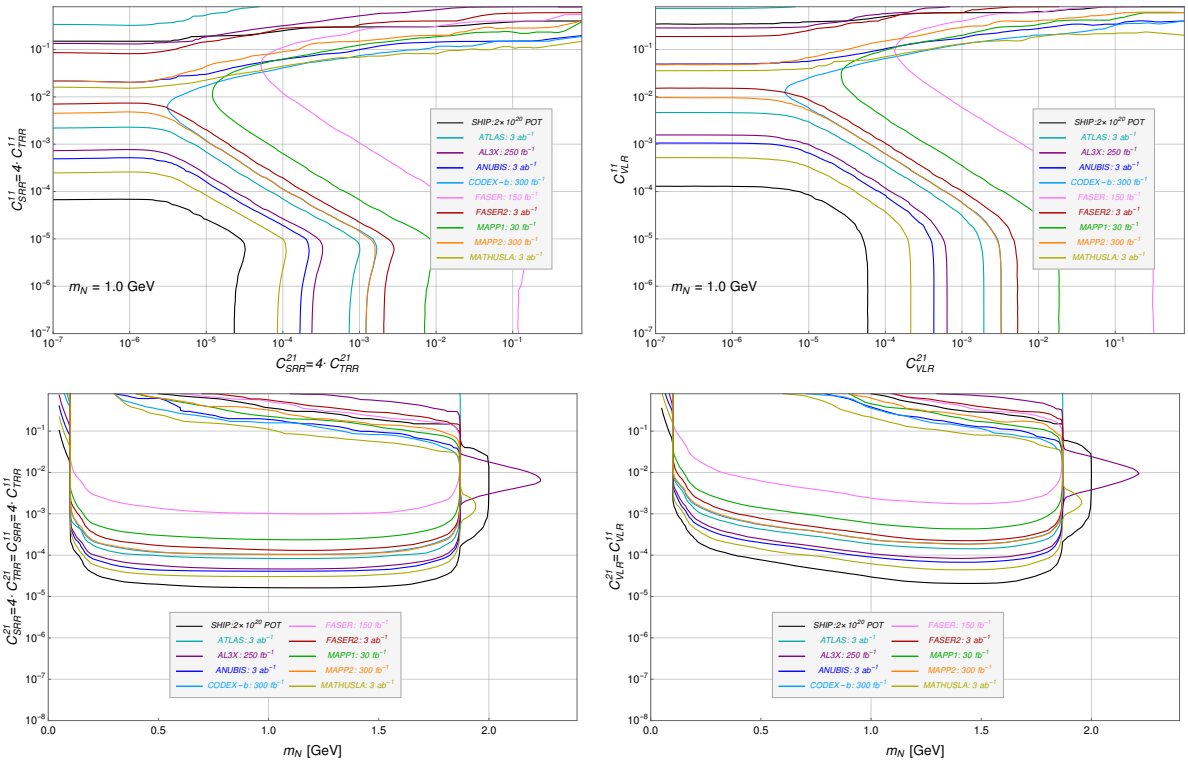

Figure 5.7: Results for the sensitivity reach for flavor benchmark 1. On the left we have the leptoquark-like case, and on the right the VLR case. For each case the upper figure shows C_{D} vs. C_{P}, where as the lower case is for $C_{\mathrm{P}} = C_{\mathrm{D}}$ and shows C_{P} vs. m_N. The color code for the various experiments is shown in each figure.

in scenarios 2 and 3 are rather similar, indicating that the specific Lorentz structure of the EFT interactions does not greatly affect the overall sensitivity. In the upper-left and lower-right part of the top plots the curves become horizontal and vertical, respectively. In this part of the parameter space either the production (horizontal, upper left) or decay (vertical, lower right) of sterile neutrinos through EFT operators becomes sub-leading with respect to the contributions from minimal mixing. This roughly happens for couplings $C_{\mathrm{P,D}} \leq 10^{-5}$, indicating that EFT operators can dominate over minimal interactions for a new physics scale of $\Lambda \sim \sqrt{v^2/C_{\mathrm{P,D}}} = \mathcal{O}(80)$ TeV. This scale does not include possible small dimensionless couplings or loop suppressions of the EFT operators and is thus only indicative of the sensitivity range.

For some experiments (`CODEX-b`, `MAPP1`, and `FASER`), there is no sensitivity in the upper left corner (small C_{P} and large C_{D}). This is caused by the rather weak detector acceptance of these experiments for the light sterile neutrinos produced from D-mesons decays.

In the lower set of plots, we assume equal $C_{\mathrm{P}} = C_{\mathrm{D}}$, and vary the sterile neutrino mass m_N and jointly the Wilson coefficients. The plots for scenario 2 and 3 look rather similar although in scenario 2, the sensitivity to smaller sterile neutrino masses is a bit better. The most sensitive experiment would clearly be `SHiP`, which reaches roughly $C_{\mathrm{P}} = C_{\mathrm{D}} \sim 2 \cdot 10^{-5}$ in the range $0.5\,\mathrm{GeV} < m_N < 1.8\,\mathrm{GeV}$. For couplings at this level, both the production and decay of sterile neutrinos are still dominated by the EFT operators and minimal mixing plays a sub-leading role. The sensitivity then depends a lot on the experimental setup under consideration. `FASER` reaches couplings at the 10^{-3} level (corresponding to scales of roughly 8 TeV in Λ). Next in sensitivity

	Flavor benchmark 2.2	Flavor benchmark 2.3
production operator: C_{P}	$C^{21}_{\mathrm{SRR}} = 4C^{21}_{\mathrm{TRR}}$	C^{21}_{VLR}
decay operator: C_{D}	$C^{12}_{\mathrm{SRR}} = 4C^{12}_{\mathrm{TRR}}$	C^{12}_{VLR}
production process via C_{P}	$D^{\pm}/D^0/D_s \to N + e^{\pm}(+X)$	
decay process via C_{D}	$N \to K^{\pm} + e^{\mp},\ K^{*\pm} + e^{\mp}$	

Table 5.3: Summary of flavor benchmark 2.

is MAPP1 at $3 \cdot 10^{-4}$, and then FASER2, MAPP2, CODEX-b, and ATLAS at roughly the 10^{-4} level. MATHUSLA, ANUBIS, and AL3X, should be sensitive to couplings down to around $5 \cdot 10^{-5}$, and finally SHiP at the aforementioned $C_{\mathrm{P,D}} \leq 2 \cdot 10^{-5}$ level. The hierarchy in sensitivity reach shown by the various experiments is essentially the same in scenarios 2 and 3, and is very similar to the hierarchy in the minimal scenario (see Fig. 5.6) for masses $m_N < m_D$.

Again, the sensitivity reach in m_N goes beyond the kinematical thresholds set by the pion and D-meson masses. For $m_N < m_\pi$, sterile neutrinos can still decay leptonically via the weak interaction. Thus larger C_{P} values can still lead to detectable rates of sterile neutrino production. We stress again that for $m_N < m_\pi$, we underestimate the production of sterile neutrinos by omitting production via pions and kaons. For $m_N > m_D$, sterile neutrinos for this benchmark can still be produced from the B-meson decays via the weak current. If C_{P} and C_{D} are large enough, sufficiently many sterile neutrinos are produced. Furthermore, specifically for AL3X, and SHiP, and to a lesser extent MATHUSLA, the boosted decay lengths of these sterile neutrinos can fall into the respective geometric sensitivity ranges. This corresponds to the extended sensitive parameter regions, as shown on the right-hand side of the two lower plots of Fig. 5.7.

5.6.3 Flavor benchmark 2

In flavor benchmark 2 we choose a different flavor-structure for the decay Wilson coefficient. For the production operator we take again $(C_{\mathrm{P}})_{21}$ but for the decay now set $(C_{\mathrm{D}})_{12}$. This leads to sterile neutrino decay processes

$$N \to e^{\pm} + K^{\mp}\,, \quad \text{and} \quad N \to e^{\pm} + K^{*\mp}\,. \tag{5.24}$$

Table 5.3 summarizes the details of this scenario.

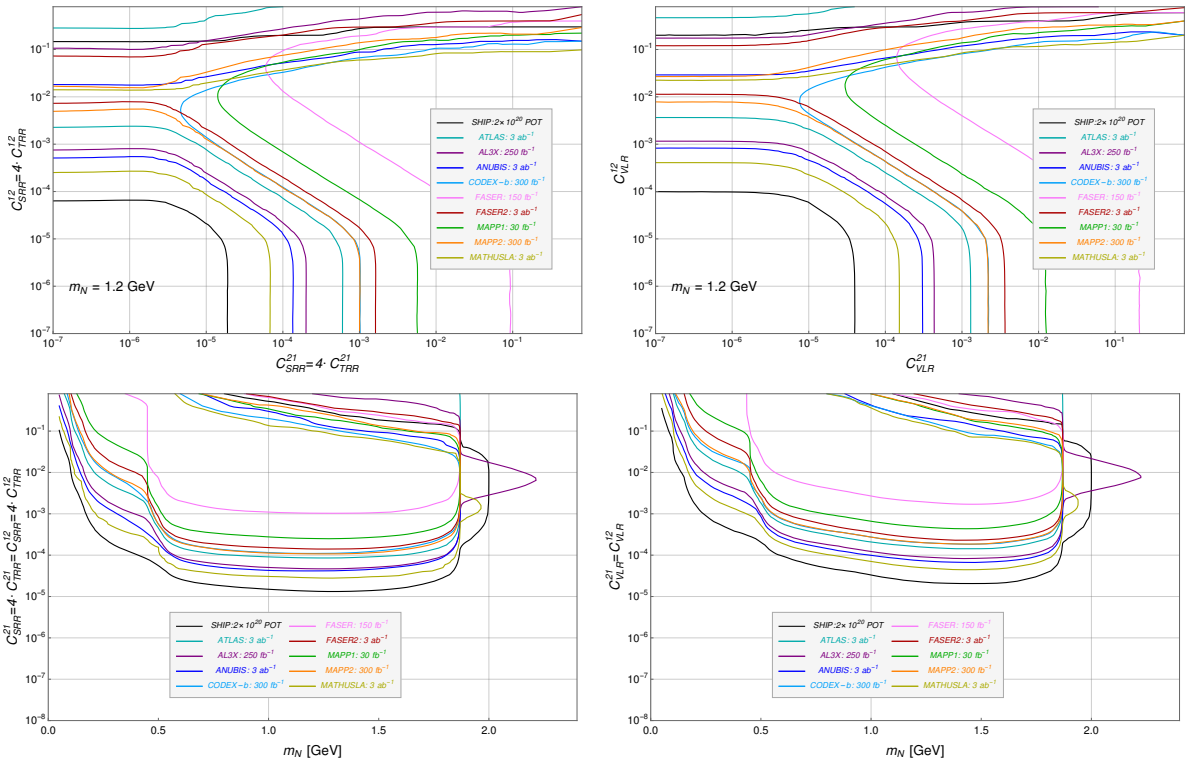

Figure 5.8: Results for flavor benchmark 2. The format is the same as in Fig. 5.7.

The sensitivity limits for this scenario are shown in Fig. 5.8 with the same format as in Fig. 5.7. On the left we consider $C_{\rm P} = C^{21}_{\rm SRR} = 4C^{21}_{\rm TRR}$, and on the right $C_{\rm P} = C^{21}_{\rm VLR}$. Similarly for the decay we have on the left $C_{\rm D} = C^{12}_{\rm SRR} = 4C^{12}_{\rm TRR}$ and on the right $C_{\rm D} = C^{12}_{\rm VLR}$. In the upper row, we show plots in the plane $C_{\rm D}$ vs. $C_{\rm P}$ with m_N at 1.2 GeV. Similar features as in the previous scenario are observed and there seems hence to be little sensitivity in the event rates to the specific final-state meson.

The hierarchy in sensitivity of the different experiments is also very similar. In the lower panels we see some differences compared to flavor benchmark 1. The sensitivity to lighter m_N is reduced due to the need to produce a heavier kaon in the final state. For $m_N < m_K$ the EFT operators no longer contribute to the decay rate and the SM weak interaction becomes the only mechanism for sterile neutrinos to decay and be detected. This leads to a further reduction in sensitivity. We stress again that our results in this regime are conservative as we have not considered sterile neutrino production via kaon decays.

5.6.4 Flavor benchmark 3

We proceed to study a scenario where sterile neutrinos are mainly produced through decays of B-mesons. Compared to flavor benchmark 1, we keep the same flavor structure for the decay Wilson coefficient, but turn on $C^{13}_{\rm P}$. This leads to the sterile neutrino production via the decay processes

$$B^\pm \to e^\pm + N, \qquad B^\pm \to \pi^0 + e^\pm + N, \qquad B^\pm \to \rho^0 + e^\pm + N, \tag{5.25}$$

$$B^0 \to \pi^\pm + e^\mp + N, \qquad B^0 \to \rho^\pm + e^\mp + N, \qquad B_s \to K^{(*)\pm} + e^\mp + N. \tag{5.26}$$

The relevant information is summarized in Table 5.4.

	Flavor benchmark 3.2	Flavor benchmark 3.3
production operator: C_{P}	$C^{13}_{\mathrm{SRR}} = 4C^{13}_{\mathrm{TRR}}$	C^{13}_{VLR}
decay operator: C_{D}	$C^{11}_{\mathrm{SRR}} = 4C^{11}_{\mathrm{TRR}}$	C^{11}_{VLR}
production process via C_{P}	$B^{\pm}/B^0/B_s \to N + e^{\pm}(+X)$	
decay process via C_{D}	$N \to \pi^{\pm} + e^{\mp},\ \rho^{\pm} + e^{\mp}$	

Table 5.4: Summary of flavor benchmark 3.

Our results for the sensitivity reach for this benchmark are shown in Fig. 5.9. The two top panels show results for the leptoquark (left) and C_{VLR} (right) scenarios in the C_{P}-C_{D} plane for fixed $m_N = 2.6$ GeV. The resulting curves are rather different from the scenarios, where sterile neutrinos are produced via D-meson decays. In the earlier flavor benchmarks, C_{P} can be turned off and sufficient sterile neutrinos will be produced via minimal mixing to still detect sterile neutrinos, as long as C_{D} is sufficiently large to ensure sterile neutrinos decay in the respective detector volumes. This feature has disappeared in this benchmark scenario and for $C_{\mathrm{P}} < 10^{-7}$ no detection is possible in any of the experiments, even for large C_{D}. This lack of sensitivity is explained by the fact that the production rates of B-mesons are smaller than that of D-meson by roughly a factor ~ 20 at 14 TeV pp collisions and by a factor ~ 3000 at SHiP.

The two lower panels in Fig. 5.9 assume $C_{\mathrm{P}} = C_{\mathrm{D}}$ and show sensitivity curves as a function of the sterile neutrino mass. In the previous flavor benchmarks SHiP showed the strongest sensitivity, but here it performs worse than MATHUSLA, ANUBIS, and AL3X. The reason is twofold. First, the ratio between the number of B-mesons produced and that of D-mesons is much smaller at SHiP than at the 14 TeV $pp-$collision experiments. Second, given their larger masses, the B-mesons, are less boosted in the very forward direction, leading to weakened acceptance of the SHiP detector for the long-lived sterile neutrinos. The hierarchies in sensitivity of the other experiments is the same as in the minimal scenario and the other flavor benchmarks. However, the overall reach is increased over the previous flavor benchmarks with the MATHUSLA sensitivity to couplings at the impressive $5 \cdot 10^{-6}$ level, corresponding to scales of $\mathcal{O}(100)$ TeV.

5.6.5 Flavor benchmark 4

	Flavor benchmark 4.2	Flavor benchmark 4.3
production operator: C_{P}	$C^{13}_{\mathrm{SRR}} = 4C^{13}_{\mathrm{TRR}}$	C^{13}_{VLR}
decay operator: C_{D}	$C^{12}_{\mathrm{SRR}} = 4C^{12}_{\mathrm{TRR}}$	C^{12}_{VLR}
production process via C_{P}	$B^{\pm}/B^0/B_s \to N + e^{\pm}(+X)$	
decay process via C_{D}	$N \to K^{(*)\pm} + e^{\mp}$	

Table 5.5: Summary of flavor benchmark 4.

For flavor benchmark 4 the production primarily proceeds via B-meson decay, as for the previous benchmark, but here sterile neutrinos decay to a kaon through C^{12}_{D}. The relevant information is summarized in Table 5.5.

Fig. 5.10 shows the numerical results for this benchmark. In the two top panels we show plots in the C_{P}-C_{D} plane for fixed $m_N = 2.8$ GeV. In general these plots show very similar features as

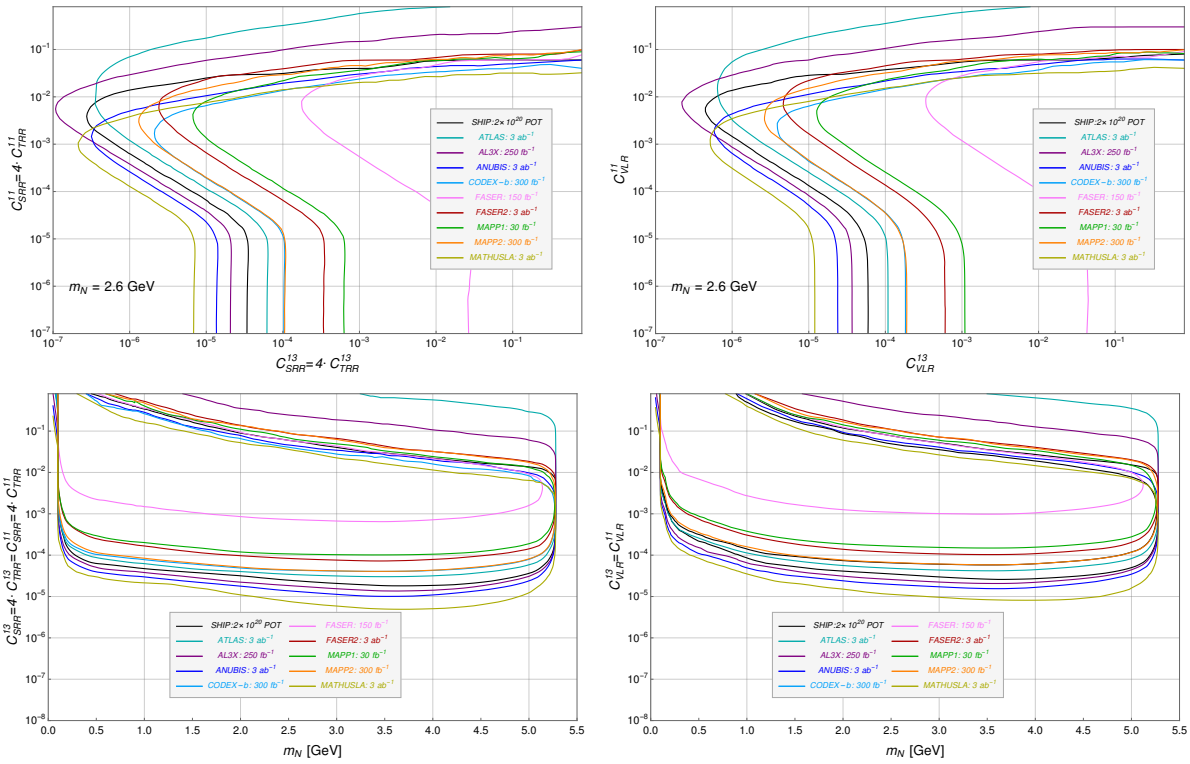

Figure 5.9: Results for flavor benchmark 3. The the scenarios and the labeling are as in Fig. 5.7.

their counterparts in Fig. 5.9, except for an overall small reduction in the reach of $C_{\rm P}$ because of the choice for a slightly larger mass of the sterile neutrino. The two lower plots show sensitivity curves in the plane $C_{\rm P} = C_{\rm D}$ vs. m_N. Compared to the lower panels of Fig. 5.9, they show similar exclusion limits for $m_N \gtrsim m_K$. However, for lighter sterile neutrinos, since only the decay modes via the weak current and active-sterile neutrino mixing are open, the sensitivity is significantly reduced. The hierarchies of the various experiments is the same as in the previous benchmark for both EFT scenarios.

5.6.6 Flavor benchmark 5

	Flavor benchmark 5.2	Flavor benchmark 5.3
production operator: $C_{\rm P}$	$C^{13}_{\rm SRR} = 4C^{13}_{\rm TRR}$	$C^{13}_{\rm VLR}$
decay operator: $C_{\rm D}$	$C^{21}_{\rm SRR} = 4C^{21}_{\rm TRR}$	$C^{21}_{\rm VLR}$
production process via $C_{\rm P}$	$B^{\pm}/B^0/B_s \to N + e^{\pm}(+X)$	
production process via $C_{\rm D}$	$D^{\pm}/D^0/D_s \to N + e^{\pm}(+X)$	
decay process via $C_{\rm D}$	$N \to D^{(*)\pm} + e^{\mp}$	

Table 5.6: Summary of flavor benchmark 5.

In flavor benchmark 5, we turn on the operators $C^{13}_{\rm P}$ and $C^{21}_{\rm D}$. In this case, the decay operator also leads to production of sterile neutrinos, but the resulting sterile neutrinos are restricted to

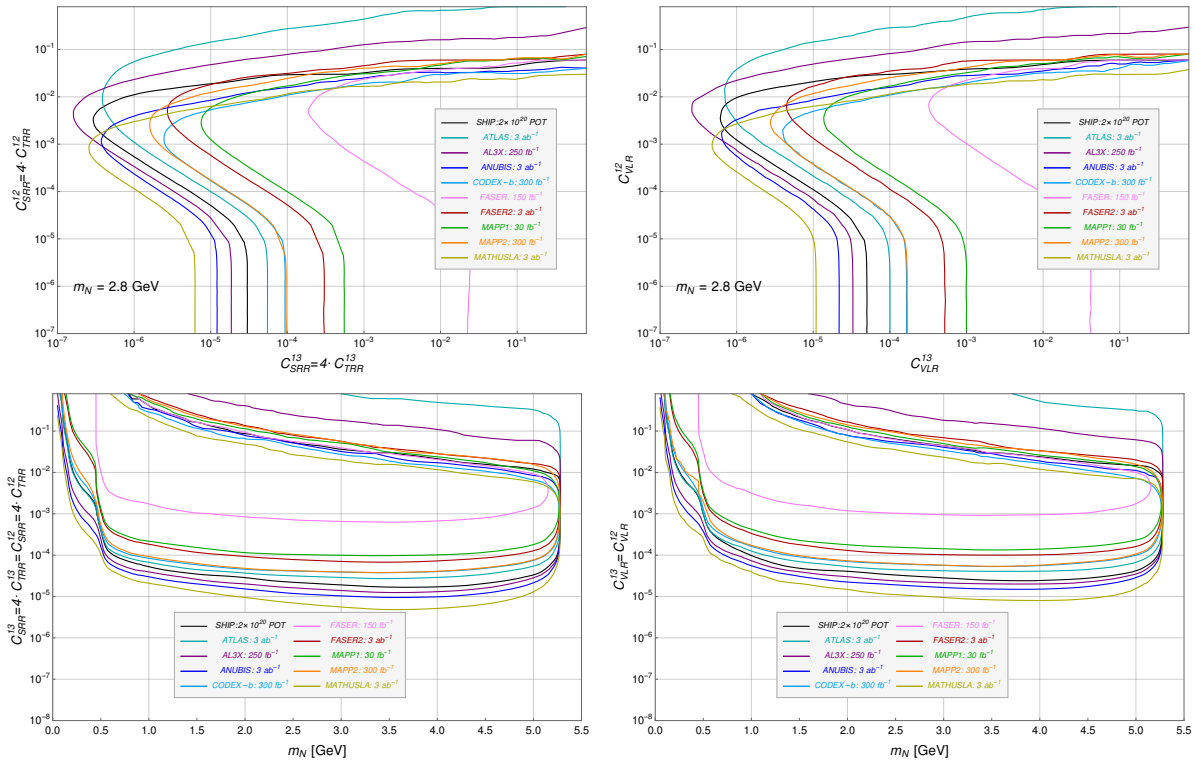

Figure 5.10: Results for flavor benchmark 4. The plot format is the same as in Fig. 5.7.

a mass range where they can only decay via minimal mixing. We summarize the benchmark features in Table 5.6. Fig. 5.11 shows the resulting sensitivity reach. In the upper row we fix the sterile neutrino mass at 3.5 GeV. In general the absolute and relative sensitivities to C_{P} and C_{D} are comparable to the previous flavor benchmark, but the sensitivity in the bottom panel drops a bit for $m_N < m_D$. In this case sterile neutrinos only decay via minimal mixing. The exception is `SHiP` for which the sensitivity grows for $m_N < m_D$, where `SHiP` becomes the most sensitive experiment in fact, because the production cross section difference between D- and B-mesons is much larger at `SHiP` than at the other experiments.

5.7 Discussion

Our results indicate that proposed experiments to detect long-lived particles are very sensitive to higher-dimensional operators in the νSMEFT Lagrangian. In the mass range $m_K < m_N < m_B$ the sensitivity curves are rather stable with respect to different EFT operators in Eq. (5.1) and the particular flavor configuration, as long as the sterile neutrino can be produced via the decay of D- or B-mesons, and the sterile neutrino can, in turn, decay semi-leptonically. While each particular choice of EFT operators and flavor assignment requires a detailed study, we find that `FASER` is sensitive to Wilson coefficient couplings of about $\sim 10^{-3}$ (this is extended to $\sim 10^{-4}$ for `FASER2`), while experiments such as `MATHUSLA`, `ANUBIS`, `AL3X`, and `SHiP` can reach down to coupling strengths of $\sim 5 \cdot 10^{-6}$. We see that such limits can be used to constrain the νSMEFT operators $C^{(6)}_{H\nu e}$, $C^{(6)}_{du\nu e}$, $C^{(6)}_{L\nu Qd}$, $C^{(6)}_{LdQ\nu}$, and $C^{(6)}_{Qu\nu L}$. Assuming a scaling of these Wilson coefficients as $\sim v^2/\Lambda^2$, the sensitivities range from $\Lambda \sim 8\,\mathrm{TeV}$ for `FASER` up to $\Lambda \sim 100\,\mathrm{TeV}$ for the larger experiments.

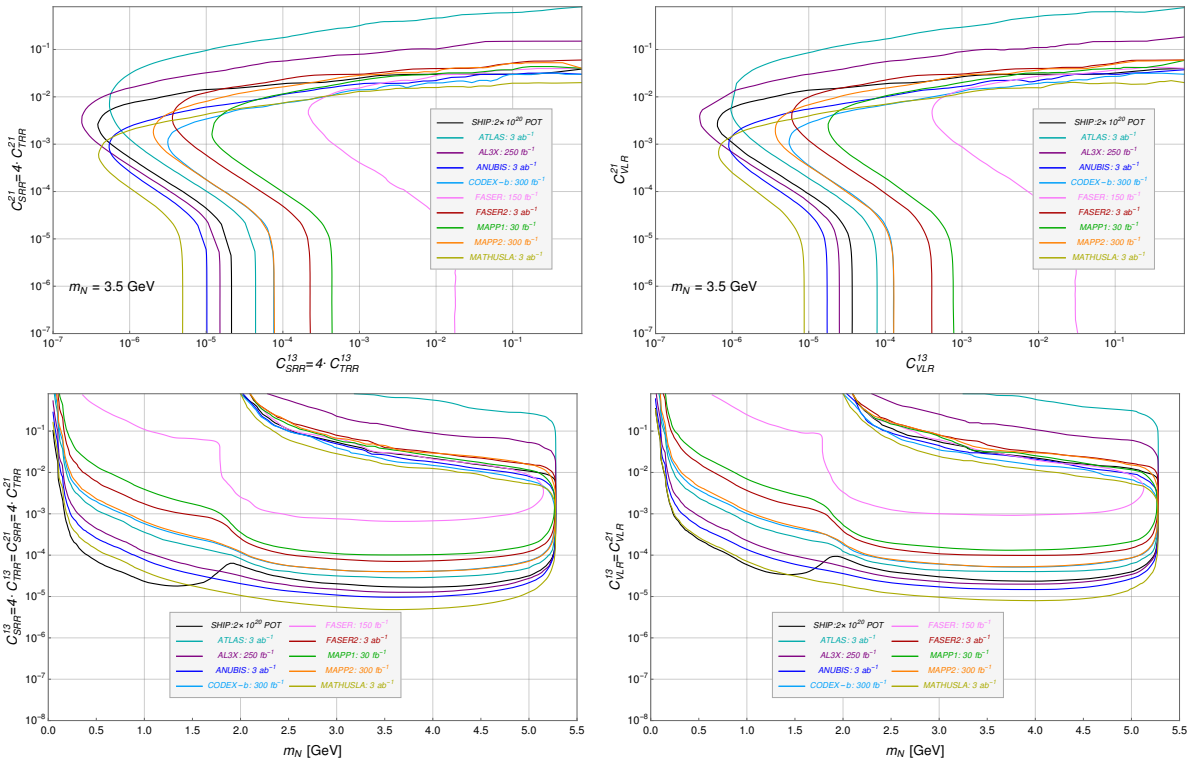

Figure 5.11: Results for flavor benchmark 5. The format is the same as in Fig. 5.7.

In this chapter we have focused on Majorana neutrinos (although our sensitivity curves are not affected dramatically if we had considered Dirac neutrinos instead) for which strong constraints can be set from $0\nu\beta\beta$ experiments. In Ref. [78] some of us developed a framework to calculate $0\nu\beta\beta$ decay rates in the presence of light sterile neutrinos and the νSMEFT Lagrangian. In particular, we investigated the reach of current and future experiments to probe scenario 2: the $3+1$ leptoquark model. As sterile neutrinos appear as virtual states, $0\nu\beta\beta$ experiments are sensitive to a broad range of neutrino masses with a peak sensitivity at $m_N \simeq 100\,\text{MeV}$, which drops off for larger or smaller masses. To make a comparison, we consider the case $y^{\overline{LR}}_{11} y^{RL*}_{11} = y^{\overline{LR}}_{21} y^{RL*}_{11} = 1$ and $y^{\overline{LR}}_{11} y^{RL*}_{11} = y^{\overline{LR}}_{11} y^{RL*}_{31} = 1$ and vanishing couplings for other flavors. We can then compare flavor benchmarks 1 and 3 to the sensitivity of $0\nu\beta\beta$ experiments, which only depend on sterile neutrino couplings to first-generation quarks and leptons.

For these choices of couplings, we can calculate $0\nu\beta\beta$ decay rates and determine the LHC and `SHiP` sensitivity curves as a function of m_N and m_{LQ} ($0\nu\beta\beta$ rates have a very small dependence on phases appearing in the $3+1$ neutrino mixing matrix and we neglect this dependence here for simplicity). The results are shown in Fig. 5.12. We stress that the uncertainties associated with hadronic and nuclear matrix elements for $0\nu\beta\beta$ decay rates are sizable and not included in the plot, for details we refer to Sect. 3.7.3. For flavor benchmark 1 (left panel of Fig. 5.12), the limits from $0\nu\beta\beta$ are somewhat stronger than the prospected sensitivity of `FASER2` and `MATHUSLA`, chosen as representative experiments, in the relevant mass range. For flavor benchmark 3 the prospected `MATHUSLA` overtake current $0\nu\beta\beta$ limits for masses between 1 and 5 GeV.

We stress that the bounds from $0\nu\beta\beta$ decay experiments are only valid for Majorana neutrinos and final-state electrons. However, the sensitivity curves for the various LHC experiments discussed here are (roughly) valid for (pseudo-)Dirac neutrinos, and in the appropriate mass range

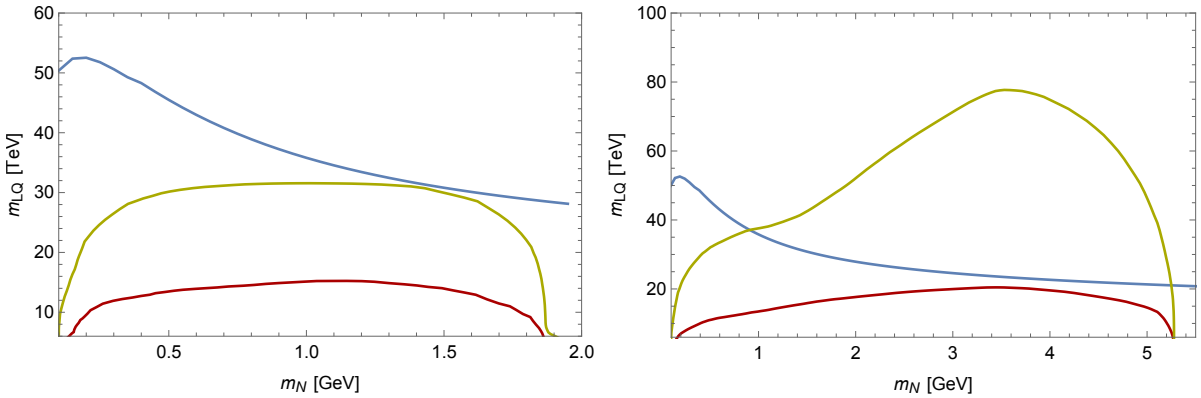

Figure 5.12: Comparison between constraints from neutrinoless double beta decay of ^{136}Xe (blue) [38] and projected sensitivity of FASER2 (red) and MATHUSLA (yellow) for the leptoquark scenario. In the left (right) panel we turned on LQ couplings corresponding to flavor benchmark 1 (3). See text for more details.

also for couplings to muons and, to lesser extent, taus instead of electrons, and in general to a broader range of quark flavors. They are thus more general than $0\nu\beta\beta$ limits albeit in a much small sterile neutrino mass range.

5.8 Conclusions

The possibility of sterile neutrinos provides one of the main motivations for the search for long-lived particles (LLPs). Sterile neutrinos provide compelling solutions to major problems in particle physics and cosmology, such as active neutrino masses and the baryon asymmetry of the Universe. Sterile neutrinos are in fact predicted in a variety of theoretical models, ranging from the minimal scenario where they interact with Standard Model (SM) particles through minimal mixing with active neutrinos, to more exotic scenarios involving new fields with masses well above the electroweak scale such as left-right symmetric models or grand unified theories.

In this chapter, we focused on relatively light sterile neutrinos with masses at the GeV scale, down to about 100 MeV. This mass range is interesting, as it is linked to low-scale leptogenesis and opens up the possibility of efficiently producing sterile neutrinos through the decays of pseudoscalar mesons, which are copiously produced in collider experiments. In particular at CERN, besides the ATLAS and CMS LHC collaborations, various proposed experiments are presently under discussion specifically targeting the detection of LLPs, such as the fixed-target experiment SHiP and a number of so-called far detectors at various pp-collision interaction points *e.g.* FASER and MATHUSLA. A large number of mesons are expected to be produced at the interaction points of these experiments, which in turn can decay to sterile neutrinos. We focused on sterile neutrinos which can be produced from bottom and charm meson decays in hadronic collisions, and investigated the sensitivity reach of present and future LHC experiments, and SHiP to detect sterile neutrinos.

We performed Monte-Carlo simulations to evaluate the sensitivity reach of the considered experiments: ATLAS, CODEX-b, FASER, MATHUSLA, AL3X, ANUBIS, MoEDAL-MAPP, and SHiP. For the minimal scenario, the obtained sensitivity curves are in agreement with existing results with minimal discrepancies, while we obtained sensitivity curves for the two MoEDAL-MAPP experiments for the first time. For the EFT scenarios we consider active-sterile neutrino mixing, the EFT

operators, and their interference terms simultaneously. For each EFT scenario, we considered a series of different flavor benchmarks, where the EFT operators induce either D- or B-meson decays into sterile neutrinos, and the sterile neutrinos decay to an electron and various mesons, $N \to e + M_{ij}$, *cf.* Tables 5.2-5.6. For the D-meson benchmarks, we found that `SHiP` and `MATHUSLA` have the most extensive sensitivity reach. They are sensitive to dimensionless Wilson coefficients at the 10^{-5} level, for most of the kinematically allowed sterile neutrino mass range. For such values of couplings, the production and decay of sterile neutrinos is dominated by the higher-dimensional operators with minimal sterile-active mixing playing a subleading role. Apart from dimensionless couplings and potential loop suppressions, the dimensionless Wilson coefficients scale as v^2/Λ^2, where Λ is the high-energy scale where the νSMEFT operators are generated. The sensitivity drops at the edges of the allowed mass range, but does not disappear completely, even for sterile neutrinos with masses above m_D, because of the contributions from SM weak interactions and active-sterile mixing. Assuming a v^2/Λ^2 scaling, `SHiP` and `MATHUSLA` could probe scales around 80 TeV. This scale is lowered to 8 TeV for `FASER` and 25 TeV for `FASER2`, which are much smaller experiments.

For our B-meson benchmarks, because of its much smaller B-meson production rates and a weaker acceptance, `SHiP` does not show the best performance. Instead, we found that `MATHUSLA` and `ANUBIS` would be sensitive to Wilson coefficients at the $5 \cdot 10^{-6}$ level. The sensitivity curves appear to be fairly independent of the Lorentz structure and the exact flavor configuration of the EFT operators, as long as sterile neutrinos can be produced through D- or B-meson decays and sterile neutrinos can decay semi-leptonically.

For our `ATLAS` study we applied an overall flat efficiency factor of 10^{-3}. Of all the experiments we have studied here only `ATLAS` is operational. Thus we strongly encourage our colleagues at `ATLAS` and `CMS` collaborations to perform a proper full analysis of the scenarios we have presented and investigated here. This should put our approximations on a much firmer footing.

Chapter 6

Long-lived sterile neutrinos at Belle II in effective field theory

In this chapter[1], we focus on the B-factory experiment `Belle II`, which is in operation in Japan. At `Belle II`, an electron beam of energy 7 GeV collides with a positron beam of energy 4 GeV, reaching the CM energy 10.58 GeV, *i.e.* at the $\Upsilon(4S)$ resonance. With a projected integrated luminosity of 50 ab^{-1}, this results in a very large number of $B\bar{B}$ events. Besides, `Belle II` is estimated to generate a large number of τ-pair production events, allowing for the study of rare τ decays to an unprecedented precision. This includes studying lepton flavor violation [250–254] and LLPs [252, 255–265]. In particular, Ref. [256] has studied the `Belle II` exclusion limits for long-lived sterile neutrinos which mix dominantly with ν_τ, by considering τ decays. Here, we propose a displaced-vertex search strategy similar to that discussed in Ref. [256], reproducing the minimal-scenario results, as well as extending the physics coverage to several scenarios in the νSMEFT, where one single EFT operator can lead to both production and decay of the sterile neutrinos. We consider the dim-6 operators in Table 2.3 and one fully leptonic operator $\mathcal{O}_{L\nu Le}$, which is $(\bar{L}\nu_R)\epsilon(\bar{L}e_R)$. After EWSB, these operators together with the SM weak interactions result in charged and neutral currents.

6.1 Theoretical scenarios

In this section, we study various possible channels for the production and decay of sterile neutrinos at `Belle II`. We extend the SM by adding a Majorana sterile neutrino ν_R, as well as the non-renormalizable interactions discussed in previous section. The sterile neutrino is produced by the decay of τ leptons either from the mixing between active and sterile neutrinos, or from the new higher-dimensional operators.

6.1.1 The minimal scenario

We first consider the minimal model, where a sterile neutrino interacts with SM particles only through the mixing between the active tau-neutrino ν_τ and the sterile neutrino. The active neutrinos ν_α can be expressed in terms of neutrino mass eigenstates ν_i

$$\nu_\alpha = U_{\alpha i}\nu_i \,, \tag{6.1}$$

[1] This chapter is based on G. Zhou, J. Y. Günther, Z. S. Wang, J. de Vries, and H. K. Dreiner JHEP 04 (2022) 057.

$\tau^- \to \nu_R\,(\bar{\nu}_R) + X_1$ & $\nu_R \to X_2$	X_1	X_2
Minimal scenario	$\pi^-, \rho^-, K^-, K^{*-}$, $e^- + \bar{\nu}_e\,, \mu^- + \bar{\nu}_\mu$	$(\pi^0, \rho^0, \eta, \eta', \omega, \phi$, $\bar{\nu}_e + \nu_e\,, \bar{\nu}_\mu + \nu_\mu\,, \bar{\nu}_\tau + \nu_\tau$, $e^- + e^+\,, \mu^- + \mu^+) + \nu_\tau$
Scenario $\mathcal{O}_{L\nu Qd}^{3\nu_R 11}$	π^-	$(\pi^0\,, \eta\,, \eta'\,, K^0) + \nu_\tau$
Scenario $\mathcal{O}_{Qu\nu L}^{11\nu_R 3}$	$\pi^-\,, K^-$	$(\pi^0\,, \eta\,, \eta') + \nu_\tau$
Scenario $\mathcal{O}_{H\nu e}^{\nu_R 1}$	$e^- + \nu_\tau\,(+\bar{\nu}_R)$	$(\,\pi^+, \rho^+, K^+, K^{*+}$, $e^+ + \nu_e\,, \mu^+ + \nu_\mu) + e^-$
Scenario $\mathcal{O}_{du\nu e}^{11\nu_R 3}$ & $\mathcal{O}_{du\nu e}^{11\nu_R 1}$	$\pi^-\,, \rho^-$	$(\pi^+\,, \rho^+) + e^-$
Scenario $\mathcal{O}_{L\nu Le}^{1\nu_R 31}$	$e^- + \bar{\nu}_e$	$e^- + \nu_\tau + e^+$
Scenario $\mathcal{O}_{LdQ\nu}^{311\nu_R}$	$\pi^-\,, \rho^-$	$(\pi^0\,, \rho^0\,, \omega\,, \eta\,, \eta'\,, K^0\,, K^{*0}) + \nu_\tau$

Table 6.1: All possible production, X_1, and decay, X_2, modes of a sterile neutrino ν_R at `Belle II`. The charge conjugate modes are implied.

where $\alpha = e, \mu, \tau$ and $i = 1, 2, 3, 4$. We only consider the mixing between ν_τ and the sterile neutrino proportional to $U_{\tau 4}$ as the mixing matrix elements U_{e4} and $U_{\mu 4}$ are severely constrained from other observables, see *e.g.* Refs. [212, 266]. We neglect the masses of the active neutrinos. As a result of the small mixing $U_{\tau 4}$, ν_R is approximately equivalent to ν_4, and we hence refer to both of them as the sterile neutrino. The production and decay rates depend on two independent parameters, the mixing matrix element $U_{\tau 4}$ and the mass of the sterile neutrino m_N. We list all the possible resulting production and decay channels in the minimal scenario in the second row of Table 6.1. For instance, with $X_1 = K^-$ and $X_2 = e^- + e^+ + \nu_\tau$, we have the decay chain,

$$\tau^- \to \nu_R + K^-, \qquad \text{followed by,} \qquad \nu_R \to e^- + e^+ + \nu_\tau\,. \tag{6.2}$$

The branching ratios of the production and decay channels are displayed in Fig. 6.1 and Fig. 6.2, as functions of m_N. As explained in Sect. 6.2, we do not consider all the decay channels of ν_R as visible. Therefore, in Fig. 6.2 only the visible channels are shown. The resulting proper decay length of the sterile neutrino times $|U_{\tau 4}|^2$ is presented in Fig. 6.3. For a discussion of the expression of the decay rates, we refer to Appendix C.

6.1.2 Scenarios from higher-dimensional operators

We now discuss scenarios with the SM extended by one of the operators listed in Table 2.3, possibly with more than one index structure. Here, we assume the type-I seesaw relation, so that the effects from the active-sterile neutrino mixing are negligible.[2] We consider the following operators in turn: $\mathcal{O}_{Qu\nu L}$, $\mathcal{O}_{L\nu Qd}$, $\mathcal{O}_{L\nu Le}$, $\mathcal{O}_{H\nu e}$ and $\mathcal{O}_{LdQ\nu}$. While we refrain from specifying a UV-complete model, which is not necessary for the low-energy phenomenology we are after, it is worthwhile to mention that these operators can easily be obtained in leptoquark models ($\mathcal{O}_{LdQ\nu}$), models with Z' bosons ($\mathcal{O}_{Qu\nu L}$, $\mathcal{O}_{L\nu Qd}$, $\mathcal{O}_{L\nu Le}$), and left-right symmetric models ($\mathcal{O}_{H\nu e}$).

The above operators are special in the sense that each of them can induce both the production and decay of sterile neutrinos by turning on only one flavor configuration. For example, with $\mathcal{O}_{Qu\nu L}^{11\nu_R 3}$, we can have the decay chains,

$$\tau^- \to \nu_R + (\pi^-, K^-), \qquad \nu_R \to \nu_\tau + (\pi^0\,, \eta\,, \eta')\,, \tag{6.3}$$

[2] That is, here we practically neglect the interactions of the minimal model discussed in the previous subsection.

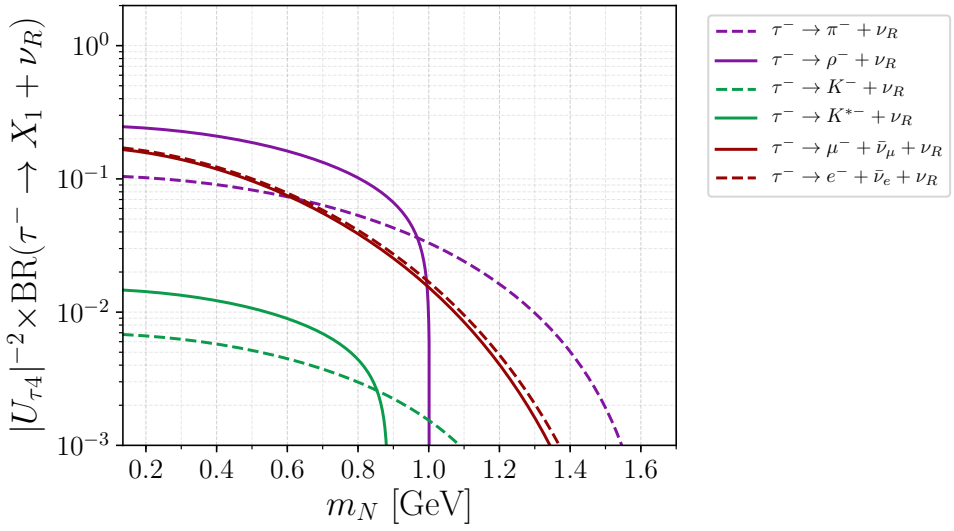

Figure 6.1: Tau decay branching ratios into a sterile neutrino in the minimal scenario.

where the production of the sterile neutrino from τ^- decays can be associated with a K^-, because the left-handed down-type quarks d_L are not in their mass eigenstates. In choosing the flavor combinations, we focus exclusively on first-generation quarks.

For the operator $\mathcal{O}_{duνe}$, one single flavor setting cannot account for the production and decay of the sterile neutrino simultaneously. Hence, we choose $\mathcal{O}_{duνe}^{11\nu_R 3}$ for the production and $\mathcal{O}_{duνe}^{11\nu_R 1}$ for the decay, and assume that $C_{duνe}^{11\nu_R 3} = C_{duνe}^{11\nu_R 1}$. All the possible modes are listed in Table 6.1.

For each dimension-six operator in Table 2.3, we suppose their Wilson coefficients are given by $1/\Lambda^2$. The production and decay rates are thus proportional to $1/\Lambda^4$ and are functions of both m_N and Λ. In Fig. 6.4 and Fig. 6.5, we present respectively the τ decay branching ratios into a sterile neutrino plus anything and the proper decay lengths, $c\tau_N$, of the sterile neutrino, as functions of m_N, for a fixed value of $\Lambda = 1$ TeV. All the EFT scenarios summarized in Table 6.1 are included. Further, we show the branching ratios of the visible decay modes of the sterile neutrino in Fig. 6.6. The branching ratio of the signature decay mode in the scenario with the operator $\mathcal{O}_{LνLe}^{1\nu_R 31}$ is not included here, as it is 100%.

6.2 Experiment and simulation

`Belle II` is an ongoing experiment at the SuperKEKB accelerator, which is an electron-positron collider operated at a relatively low center-of-mass energy $\sqrt{s} = 10.58\,\mathrm{GeV}$, *i.e.* at the $\Upsilon(4s)$ resonance. At `Belle II` an electron beam of energy 7 GeV collides asymmetrically with a positron beam of energy 4 GeV. With a projected 50 ab^{-1} integrated luminosity, besides the large number of B-mesons, `Belle II` is expected to produce inclusively 4.6×10^{10} tau pairs, via $e^- e^+ \to \tau^- \tau^+$. These events can be easily tagged, if one of the two τ's decays into one prong. Given the clean environment and the large production rates of the τ's, `Belle II` provides an ideal avenue for studying rare τ-decays.

For the purpose of this chapter, we study rare τ decays into a sterile neutrino, associated with either a charged meson or a charged lepton, plus missing energy from an escaping active neutrino. For the minimal scenario, the sterile neutrino is considered to be mixed with the ν_τ only, while for the EFT scenarios with higher-dimensional operators the sterile neutrino is assumed to have

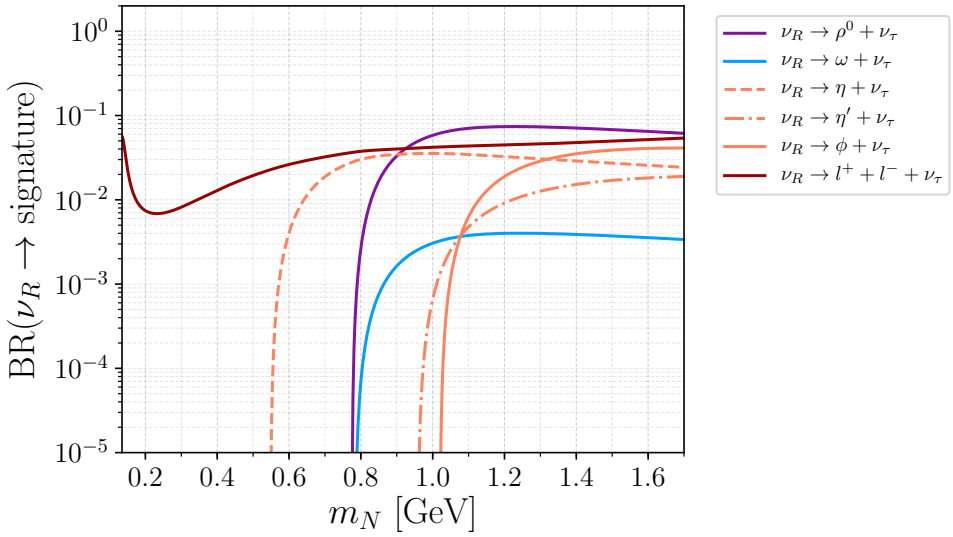

Figure 6.2: Branching ratios of visible decay modes in the minimal scenario.

four-fermion interactions with at least one third-generation lepton at the low-energy scale. We focus on the case that the sterile neutrinos are long-lived and decay to lighter mesons or leptons, disconnected from the production vertex, but within the tracker. We propose a displaced-vertex (DV) search strategy for these reactions, which requires at least two charged final-state particles for the signature. More concretely, the two displaced tracks can stem either directly from the decay of the long-lived sterile neutrino, or from the subsequent *prompt* decay of a meson, such as ρ^0 and η, produced from the sterile neutrino's decay.

We now explain the event selections we impose for this search. We define a fiducial volume of the `Belle II` detector by $10\,\mathrm{cm} < r < 80\,\mathrm{cm}$ and $-40\,\mathrm{cm} < z < 120\,\mathrm{cm}$, where r and z are the transverse and longitudinal distances to the IP, respectively. The positive z direction is defined to be on the side of the incoming positron beam. The choice of $r > 10\,\mathrm{cm}$ ensures that the background events from K_S decays, prompt tracks, as well as detector material interactions are removed. The sterile neutrino is required to decay inside the fiducial volume. Second, in general we expect the tracking efficiency to deteriorate with increasing (transverse) distance from the IP inside the tracker. To parameterize this effect, we apply a naive linear function to interpolate the displaced-tracking efficiency, ranging from 100% at $r = 10\,\mathrm{cm}$ to 0% at $r = 80\,\mathrm{cm}$; see also Refs. [252, 262].

The efficiency to reconstruct a DV relies on the final-state tracks. For the case of two tracks stemming from a DV, we follow Ref. [258] to take this DV reconstruction efficiency to be 12%. With any π^0, K^0, or photon *additional* to the two tracks in the sterile neutrino decay products, the DV reconstruction efficiency is further multiplied with 70%. Similarly, for any additional pair of charged pions, the efficiency is modified by a factor of 85%. [3] [4]

[3] These efficiencies are conservative estimates based on track finding efficiency investigations of the B-factory experiment BABAR (see Ref. [267, 268]). With the help of various Monte-Carlo event generators the efficiencies of reconstructing processes such as $e^+e^- \to \tau^+\tau^-$, $e^+e^- \to \pi^+\pi^-(\pi^+\pi^-)\gamma_{ISR}$, where γ_{ISR} is a high energetic photon emitted from an initial lepton, and hadronic decay modes are evaluated and compared to data of each BABAR run.

[4] To apply the analysis to reduce background events described in the following paragraph, the final state must be reconstructed as detailed as possible. Due to the unobservable neutrino in the final state we can not fully reconstruct it, but every other charged particle should be tracked.

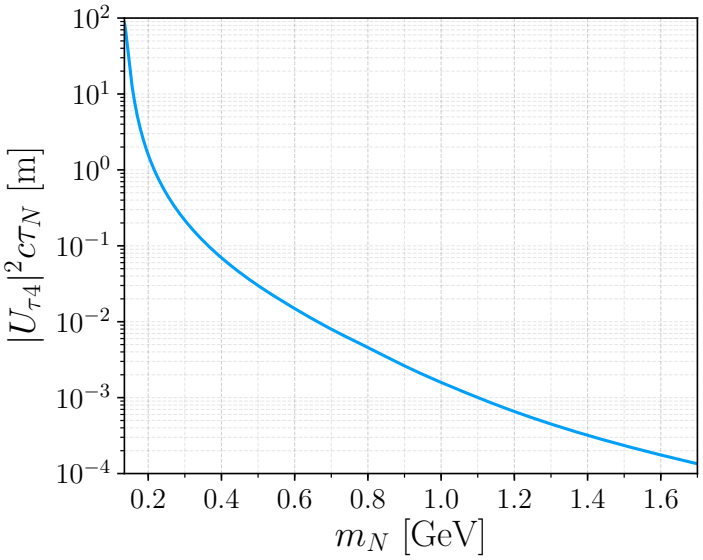

Figure 6.3: Proper decay length of the sterile neutrino times $|U_{\tau 4}|^2$ in the minimal scenario.

On top of all these cuts and efficiencies, we expect that a more detailed analysis including all detector effects can remove the remaining SM background events, while retaining about 75% of the signal events. We therefore apply an overall efficiency of 75% on top of the previously mentioned factors. This estimate is inspired by Ref. [256], where the authors showed that by computation with the four-momenta of the final-state particles it is possible to derive the τ energy and the LLP mass up to a two-fold ambiguity at `Belle II`. By comparing their distributions it is possible to remove the entire background events while keeping $\gtrsim 75\%$ of all the signal events.

The final expected signal-event number can thus be computed as:

$$N_S = 2 \cdot N_{\tau\bar{\tau}} \cdot \mathrm{BR}(\tau \to 1 \text{ prong}) \cdot \mathrm{BR}(\tau \to \nu_R + X_1) \cdot \epsilon \cdot \mathrm{BR}(\nu_R \to \text{visible}) \,, \tag{6.4}$$

where $N_{\tau\bar{\tau}} = 4.6 \times 10^{10}$, $\mathrm{BR}(\tau \to 1 \text{ prong}) \approx 85\%$, and ϵ denotes the final event selection efficiency. The factor 2 arises because in each signal event two τ's are produced, which can potentially each decay into a sterile neutrino. $\mathrm{BR}(\nu_R \to \text{visible})$ is the decay branching ratio of the sterile neutrino into at least two charged particles. This excludes final states X_2 (see Table 6.1) consisting of neutrinos only, involving π^0, which decays mostly into two photons, or involving K^0 (*i.e.* K_S or K_L), which is itself also long-lived and hence predominantly escapes the detector's fiducial volume.

We perform Monte-Carlo simulations with `Pythia8.245`, in order to numerically determine the event selection efficiencies ϵ for each benchmark scenario. `Pythia8` can generate $e^-e^+ \to \tau^-\tau^+$ events including the effects of ISR (initial state radiation) and FSR (final state radiation). The simulated τ's are all exclusively set to decay to $\nu_R + X_1$, according to the computed branching ratios of $\mathrm{BR}(\tau \to \nu_R + X_1)$ for different candidates of X_1, *cf.* Table 6.1. With `Pythia8` providing the kinematics of each simulated sterile neutrino, we estimate its decay probability inside the fiducial volume folded with the linear displaced-tracking efficiency. The DV reconstruction efficiencies which depend on the final state particles are then multiplied with the cutflow efficiency, according to the various sterile neutrino decay branching ratios. At the end, we include the final overall efficiency 75% for removing the background events.

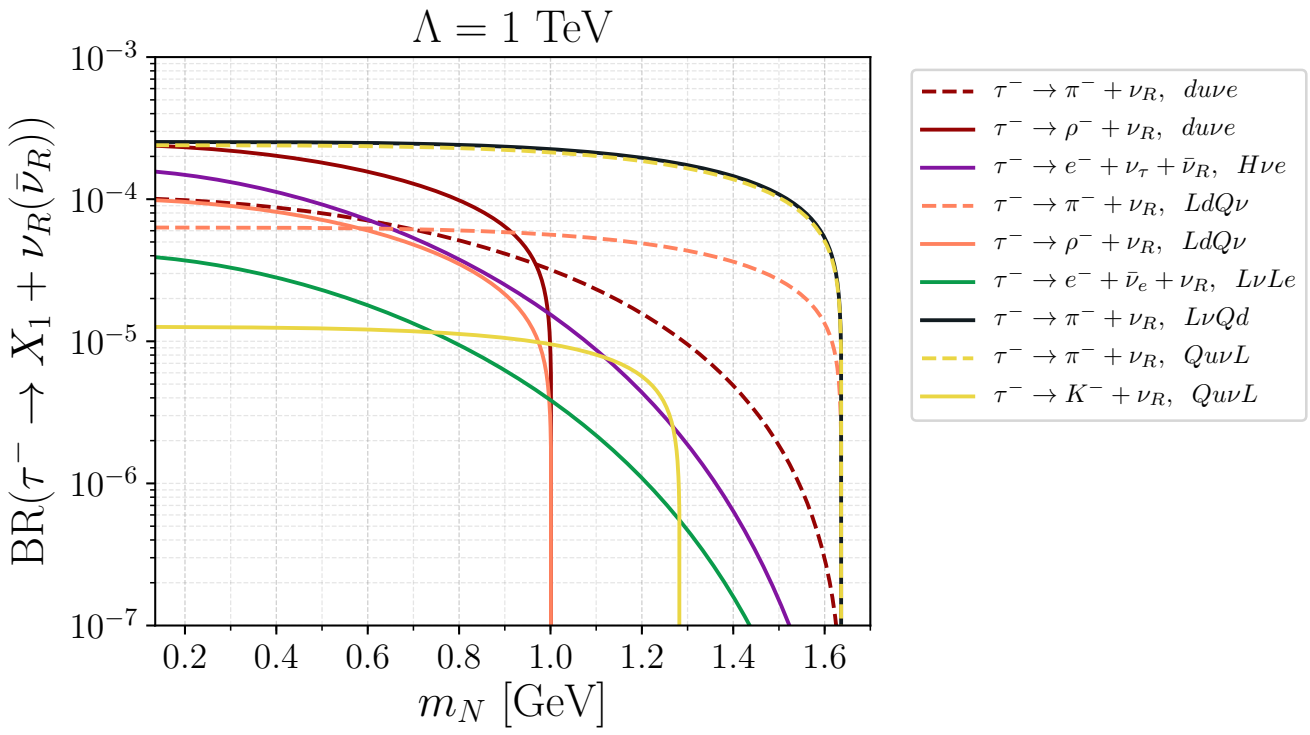

Figure 6.4: Tau decay branching ratios into a sterile neutrino for $\Lambda = 1$ TeV.

6.3 Numerical results

As discussed in Sect. 6.2, with the proposed search strategy, and for 50 ab^{-1} integrated luminosity, we expect vanishing background at `Belle II`. In our numerical results, we show three-signal-event isocurves as the exclusion limits at 95% confidence level, and also as a measure of sensitivity of the experiment to the ν_R-models.

In Fig. 6.7, we present the sensitivity limits for the minimal scenario, *cf.* Sect. 6.1.1, shown in the plane $|U_{\tau 4}|^2$ vs. m_N. We find general agreement with the exclusion limits obtained in Ref. [256]. We also compare our limits with existing bounds (marked dark gray) obtained by the `CHARM` [270, 271] and `DELPHI` [269], experiments, respectively. Moreover, recently Ref. [272] has performed a re-analysis of the CHARM search results [270, 273], obtaining updated bounds on $|U_{\tau 4}|^2$ in the sterile neutrino mas range 290 MeV $< m_N <$ 1.6 GeV. We have included these exclusion limits in Fig. 6.7, shown in light gray. We find most of the parameter space that `Belle II` is sensitive to has now been excluded, except a relatively limited region at 1.2 GeV $\lesssim m_N \lesssim$ 1.7 GeV for $|U_{\tau 4}|^2 \sim \mathcal{O}(10^{-4})$. For values of $|U_{\tau 4}|^2$ smaller than the `Belle II` limits, the production rates of the sterile neutrinos become too small and the sterile neutrinos are too long-lived to decay inside the detector fiducial volume, resulting in fewer than three signal events predicted. The left and right ends of the exclusion limits are determined by kinematical thresholds. At $m_N \sim 1.0$ GeV the isocurve displays a kink. This is due to the threshold of a τ-decay mode into a sterile neutrino and a rho-meson.

The `Belle II` exclusion limits for the various EFT operators listed in Table 2.3 are presented in Fig. 6.8, in the plane Λ vs. m_N. The left plot collects results for operators that are sensitive to neutrino masses below $\sim m_\eta$ as they induce sterile neutrino decays into pions or charged

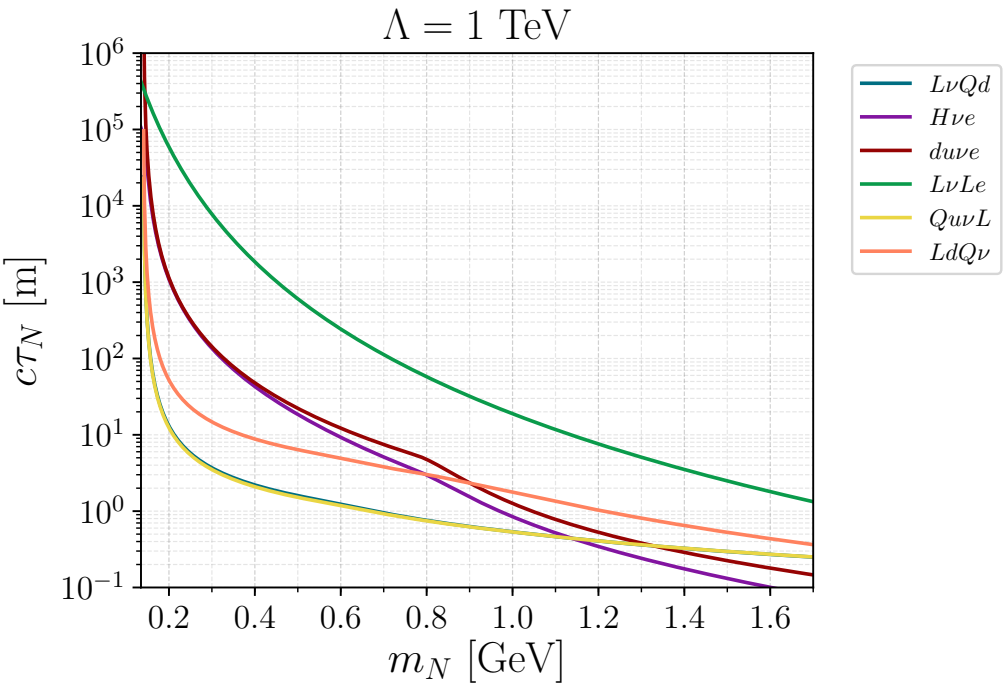

Figure 6.5: Proper decay lengths of the sterile neutrino in various EFT scenarios for $\Lambda = 1$ TeV.

leptons. The right plot displays operators that are insensitive to sterile neutrino masses below $\sim m_\eta$. We find the $C_{L\nu Qd}$ (black) and $C_{Qu\nu L}$ (yellow) sensitivities are almost identical, because the production and decay rates of the sterile neutrinos are similar. In general, we find all the six considered operators can be probed up to $\sim 1 - 3$ TeV in Λ across the sensitive mass ranges in the long-lived regime (large Λ). For even larger Λ values, the sterile neutrino lifetime would become so long that they decay only after traversing the detector and their production rates are also reduced too much, while for $\Lambda \lesssim 100$ GeV they decay before reaching the fiducial volume. For such small values of Λ the νSMEFT framework is inapplicable. For the same reason as in the minimal scenario (see Fig. 6.7) we observe a kink at m_N about 1.0 GeV in the long-lived regime for the $\mathcal{O}_{du\nu e}$ and $\mathcal{O}_{LdQ\nu}$ operators. For $LdQ\nu$ the kink is not as pronounced as in $du\nu e$ or the minimal scenario. Comparing the $\tau \to \nu_R + (\pi, \rho)$ branching ratios (see Fig. 6.4) for the EFT operators, we see that the rho branching ratio of $du\nu e$ quickly dominates the $m_N \lesssim 1$ GeV region over the pion branching ratio, whereas for $LdQ\nu$ the rho only overtakes for $m_N \lesssim 0.6$ GeV. Thus, the kink is less pronounced in this scenario.

In general UV-complete scenarios, several EFT operators can be induced simultaneously. In such scenarios the limits could change somewhat from our results here. While a general scan is not very useful, we have estimated what happens in a specific scenario where we have independent couplings for the production and decay of the sterile neutrino. In Fig. 6.8 we show constraints as a function of m_N for the choice $C_{duve}^{11\nu_R 3} = C_{duve}^{11\nu_R 1}$, where the first (second) coupling dominates the production (decay) of the sterile neutrino. We label the corresponding $\Lambda's$ by Λ_P (for production) and Λ_D (for decay). In Fig. 6.9 we investigated what happened if we freely vary the two couplings for a fixed sterile neutrino mass of $m_N = 0.8$ GeV. We observe that in the window where $\Lambda_{P,D} \geq 1$ TeV (where the EFT is valid) the constraints on the individual couplings can be strengthened by roughly a factor of 3, at the cost of a reduced sensitivity to the other coupling. With the expected sensitivities we therefore do not expect a significant difference in sensitivity

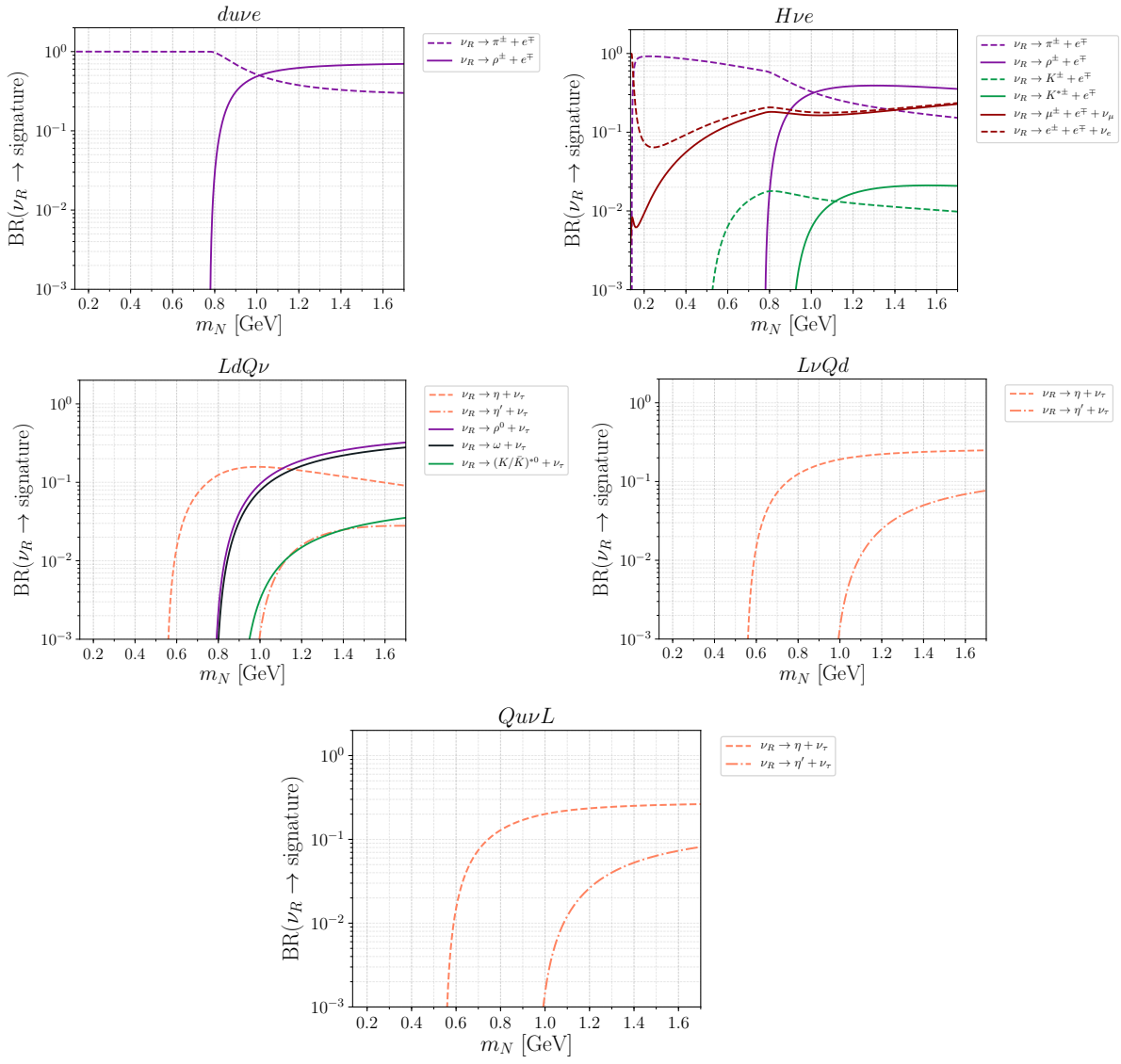

Figure 6.6: Branching ratios of visible decay modes for the sterile neutrino in νSMEFT scenarios.

for scenarios with more EFT couplings. Of course, specific UV-complete models can be studied in detail by matching to our EFT operators.

6.4 Conclusions

At Belle II, $10^{10} - 10^{11}$ tau leptons are predicted to be produced with an integrated luminosity of 50 ab^{-1} over the whole experiment lifetime, making it possible to search for rare τ decays. We have proposed a strategy based on displaced vertex at Belle II, to search for long-lived sterile neutrinos produced from τ decays. The search includes a requirement on the fiducial volume consisting of the tracker and a linear displaced-tracking efficiency. Further, to reconstruct the displaced vertices, we apply realistic efficiency factors depending on the final states of the sterile neutrino decays. Finally, based on existing literature [256, 258], an overall factor of 75% is imposed to account for removing the remaining background events.

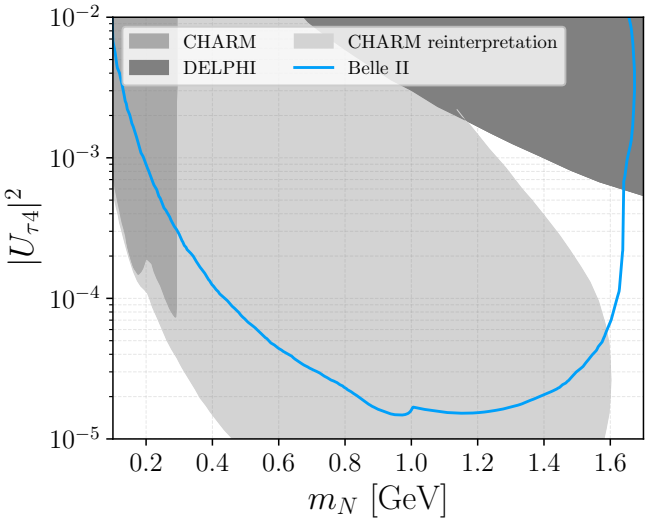

Figure 6.7: Expected sensitivity limits on the mixing matrix element squared, $|U_{\tau 4}|^2$, as function of the sterile neutrino mass, for the minimal scenario. The dark and medium gray areas correspond to the parameter regions currently excluded by DELPHI [269] and CHARM [270, 271], respectively. A recent re-interpretation [272] of the CHARM experiment results [270, 273] further excludes the light gray parameter region. The kink at $m_N \sim 1\,\text{GeV}$ is due to the ρ-threshold in the τ-decay.

We have not only considered the minimal scenario where the sterile neutrinos are produced and decaying via the same mixing parameter, $|U_{\tau 4}|^2$, but also worked in the framework of the Standard Model Effective Field Theory extended with sterile neutrinos encoding the effects of heavy new physics into non-renormalizable operators with dimensions up to six. Following the proposed search strategy, we obtained the sensitivity limits of Belle II to these theoretical scenarios. In the minimal scenario, our results are in general agreement with those obtained in Ref. [256]. For the EFT scenarios, we switch on one EFT operator at a time, and assume the type-I seesaw relation allowing us to disregard the weak interactions with the mixing parameter which is too small to affect the phenomenology. We find that with our search strategy for the various νSMEFT operators considered, Belle II can probe the new-physics scale up to about 3 TeV, assuming unity Wilson coefficients, in the kinematically allowed mass range, proving Belle II has unique sensitivities to νSMEFT interactions with third-generation leptons.

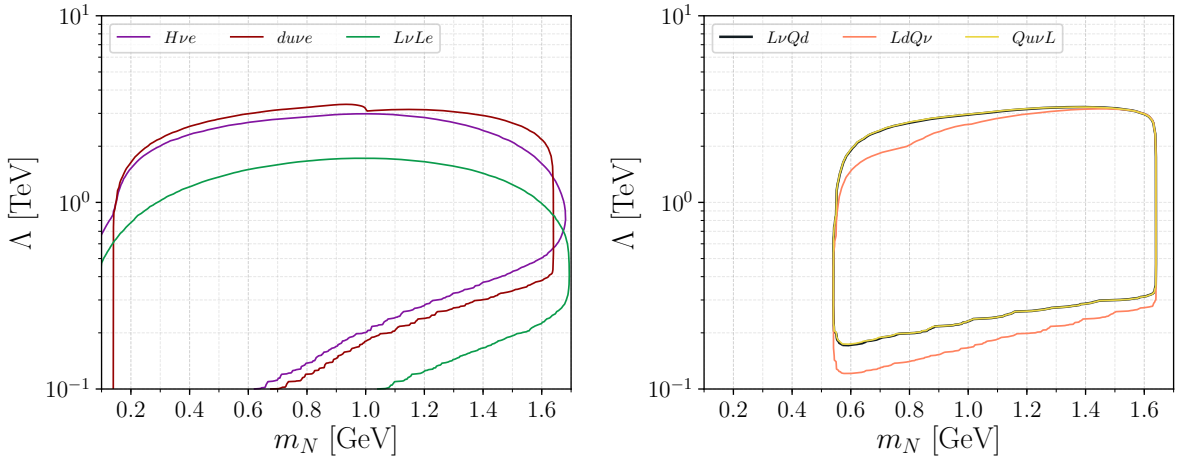

Figure 6.8: Sensitivity limits for the various EFT scenarios. We fix the Wilson coefficients at 1 and show projected bounds on the new-physics scale, Λ, as functions of m_N.

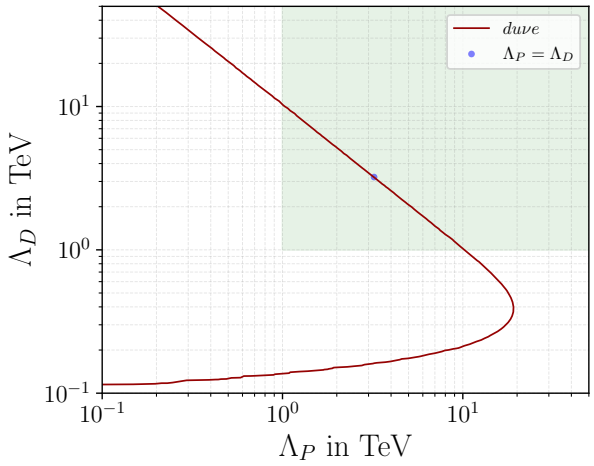

Figure 6.9: Sensitivity limits for the $du\nu e$ scenario for a fixed neutrino mass $m_N = 0.8$ GeV. The respective Wilson coefficients are fixed to 1, allowing to show projected bounds on the new physics scales Λ_P and Λ_D responsible for production and decay of the neutrino, respectively. Further included are a green area marking the parameter region $\Lambda_{P/D} \geq 1$ TeV, for which the νSMEFT framework is applicable, and a blue dot depicting the limit for $\Lambda_P = \Lambda_D$ corresponding to the limit of Fig. 6.8 at 0.8 GeV.

Chapter 7

Summary and outlook

The Standard Model is very successful and has passed a lot of stringent experimental tests involving a wide range of energy scales. But there are still motivations to search for beyond-the-Standard-Model physics both from observational evidence (dark matter, massive neutrinos and the dominance of matter over antimatter) as well as theoretical motivations (e.g. the strong-CP and the hierarchy problem). Since the discovery of the Higgs boson, the absence of evidence for BSM physics at the LHC indicates that the SM is valid up to energy scales somewhere above the electroweak scales indicating that, unless it is very well hidden, BSM particles have masses well above the EW scale. This implies we can consider the SM as the renormalizable part of a more general effective field theory, the so-called SM effective field theory (SMEFT). The SMEFT Lagrangian consisting of SM fields can be expanded in inverse powers of Λ, the energy scale of BSM physics, and obeys the SM Lorentz and gauge symmetries.

In this thesis we add right-handed neutrinos to the SM, which is the simplest BSM model. Sterile neutrinos are a well-motivated solution to the problems mentioned above. If sterile neutrinos are light, they cannot be integrated out and the SMEFT framework is not applicable. We therefore consider the neutrino-extended SMEFT (νSMEFT). Within this framework, we investigate the effect of sterile neutrinos on various experiments from high-energy colliders to low-energy high-precision $0\nu\beta\beta$ experiments.

Neutrinos are the only charge-neutral particles in the SM and could have a Majorana mass, which violates the lepton number by two units. We did a systematic study on lepton number violation in $0\nu\beta\beta$ and LNV kaon decays $K^- \to \pi^+ l^- l^-$. The higher-dimensional operators of νSMEFT are evolved step by step to an energy level of $\mathcal{O}(1)$ MeV for $0\nu\beta\beta$ and of $\mathcal{O}(100)$ MeV for LNV kaon decays. The decay rates are expressed in terms of the Wilson coefficients and low energy constants, and thus can be used to constrain higher-dimensional operators. Our results show that the $0\nu\beta\beta$ experiments can probe the scale of BSM physics around $\mathcal{O}(100)$ TeV. Current experimental results on the LNV kaon decays are too weak to give a meaningful BSM energy scale due to the small data samples. But this case can be changed when a sterile neutrino lies in the resonance region as the LNV decay rates are then significantly enhanced. In this case, we find a very strong limit around $\mathcal{O}(30)$ TeV on the BSM energy scale.

The long-lived sterile neutrinos at the collider are also investigated. Their decays lead to displaced vertices which can be reconstructed in detectors e.g. LHC and `Belle II`. Sterile neutrinos can be produced via rare mesonic decays that are copiously produced at the LHC interaction points and via the decays of tau leptons produced at `Belle II`. We consider a broad range of experiments at the LHC, the proposed fixed-target experiment `SHiP`, and `Belle II`. The νSMEFT corrections to sterile neutrino production and decay processes are calculated and we perform simulations for various detectors to estimate their sensitivity reaches. The LHC

experiments could probe BSM physics up to a hundred TeV while `Belle II` can only probe interactions related with tau leptons up to a few TeV.

In conclusion, we have probed the effects of higher-dimensional operators on several experiments and find that non-standard interactions involving sterile neutrinos have a dramatic impact on the phenomenology of LNV and sterile neutrino searches . We could use these experiments to probe BSM physics to a very high scale e.g. $\mathcal{O}(100)$ TeV. While we have worked in an effective field theory setup, the framework can readily be applied to explicit scenarios of BSM physics. In fact, this has already been done in the literature [158, 274–278] where a wide range of models is matched is to the EFT framework and, for instance, the neutrinoless double beta decay rates can be read off immediately to determine the feasibility of the particular model under consideration.

We can extend the work of this thesis in several directions. In the case of light sterile neutrinos we can consider the contributions from ultrasoft-neutrino exchange, which can dominate those contributions from potential neutrino exchange. We are already working out the formalism to include these corrections but the computations are not ready to be presented in this thesis. Another direction is to compute the various LECs associated to hard-neutrino exchange by generalizing the strategy of Refs. [106,107] to get more accurate predictions for LNV observables.

The LNV kaon decays can only give strong limits on the mixing angle or new physics scale in a small sterile neutrino mass range, however we can consider the LNV decays of heavier mesons including D- and B-type mesons and get a broader sterile neutrino mass range. For the displaced-vertex probe, we can consider sterile neutrinos mixing with other type of active neutrinos or study higher-dimensional operators with different flavor configurations. In the minimal model, the mixing angle between ν_L and ν_R is very small due to the strong constraint from $0\nu\beta\beta$. However the LHC can only give very weak constraint on the mixing angle for sterile neutrinos with mass above the GeV level. If the sterile neutrino is found at the collider, it means there are at least two kinds of sterile neutrinos with degenerate masses so that their contributions to $0\nu\beta\beta$ can cancel each other to satisfy current $0\nu\beta\beta$ experimental result. Thus it is interesting to probe sterile neutrinos heavier than GeV level at the LHC and combine the result from $0\nu\beta\beta$.

We can also generalize the idea of sterile neutrinos, and in particular the νSMEFT framework, to cosmology. For instance, N_{eff}, the number of relativistic species, has been calculated in the SM precisely. The higher-dimensional operators in νSMEFT with light sterile neutrinos would affect neutrino decoupling and thus modify N_{eff}. We can also probe the effect of sterile neutrinos on big-bang nucleosynthesis and leptogenesis. Sterile neutrinos might be a candidate of dark matter and they could be detected when scattering off nuclei. We can use the EFT framework to calculate the cross section for sterile neutrinos in dark matter direct detection experiments. With the work in this thesis and future developments, we will understand sterile neutrinos better by a systematic combination of cosmological observations and data obtained from low-energy precision experiments to high-energy colliders.

Appendix A

Derivative contributions to four-quark two-lepton operators

Integrating out a heavy neutrino induces operators involving four-quark fields, two-lepton fields, and a derivative, in addition to the contributions discussed in Sects. 3.1 and 4.1. These terms can be generated through dim-6 operators, proportional to $\bar{m}_\nu^{-2}$, or through dim-7 interactions, $\propto \bar{m}_\nu^{-1}$. When such operators are matched onto Chiral Perturbation Theory, they will give rise to interactions that come with new, unknown, LECs.

We first discussion derivative contributions in the case of $0\nu\beta\beta$. For the dimension-6 contributions one expects the derivative operators to be suppressed by m_q/m_ν compared to the operators of Sect. 3.1 [1]. However, there are several Wilson coefficients for which the contributions in Sect. 3.1 scale as $\sim v^4/\Lambda^4$, while the derivative couplings can be induced by interfering with the SM coupling, $C^{(6)}_{\rm VLL}$. This implies that there is a regime, $1 \lesssim \frac{\Lambda^2 m_q}{v^2 m_\nu}$, where the derivative interactions are important. Here we will refrain from constructing the full set of derivative interactions that are induced in this way. The reason being that these interactions are only relevant in fairly specific scenarios and regimes of parameter space. In addition, their construction would lead to a sizable number of new operators all of which will come with unknown LECs, meaning that we cannot do better than an order-of-magnitude estimates in this regime. We therefore restrict ourselves to listing the contributions can be captured by the usual dim-9 interactions, i.e. the terms that, through the equations of motions, can be written as $m_q \times \mathcal{O}^{(9)}$. The $\sim m_q$ terms resulting from interference with the SM-like vector operators are given by

$$
\begin{aligned}
\delta C^{(9)}_{1\,L} &= -4v m_d\, C^{(6)}_{\rm VLL} \bar{m}_\nu^{-2} C^{(6)\,T}_{\rm TRR}\,, \qquad \delta C^{(9)\prime}_{1\,L} = -4v m_u\, C^{(6)}_{\rm VRL} \bar{m}_\nu^{-2} C^{(6)\,T}_{\rm TRR}\,,\\
\delta C^{(9)}_{2\,L} &= v\left(m_u C^{(6)}_{\rm VLL} - m_d C^{(6)}_{\rm VRL}\right) \bar{m}_\nu^{-2} C^{(6)\,T}_{\rm SLR}\,, \qquad \delta C^{(9)\prime}_{2\,L} = v\left(m_u C^{(6)}_{\rm VRL} - m_d C^{(6)}_{\rm VLL}\right) \bar{m}_\nu^{-2} C^{(6)\,T}_{\rm SRR}\,,\\
\delta C^{(9)}_{4\,L} &= -4v\left(m_d C^{(6)}_{\rm VRL} + m_u C^{(6)}_{\rm VLL}\right) \bar{m}_\nu^{-2} C^{(6)\,T}_{\rm TRR},\\
\delta C^{(9)}_{5\,L} &= -\frac{v}{2}\left[\left(m_u C^{(6)}_{\rm VLL} - m_d C^{(6)}_{\rm VRL}\right) \bar{m}_\nu^{-2} C^{(6)\,T}_{\rm SRR} + \left(m_u C^{(6)}_{\rm VRL} - m_d C^{(6)}_{\rm VLL}\right) \bar{m}_\nu^{-2} C^{(6)\,T}_{\rm SLR}\right]\,.
\end{aligned}
\tag{A.1}
$$

These $\sim m_q$ terms are expected to contribute at the same order as the original derivative couplings. Although NDA counts a derivative as a factor of $\sim \Lambda_\chi \gg m_q$ when matching onto ChiPT, the insertion of m_q allows for a chirality flip which changes the chiral symmetry properties of the operators. In the above cases this allows one to trade derivative operators that do not induce $\pi\pi$ terms at LO, for interactions that do induce $\pi\pi$ terms proportional to m_q. As a result,

[1] This estimate holds when the interactions in Sect. 3.1 induce $\pi\pi$ couplings at LO, while the corresponding derivative terms do not. This is the case for both the scalar and tensor dimension-6 operators.

	$C^{(6)}_{\mathrm{VLR,ud}}$	$C^{(6)}_{\mathrm{VRR,ud}}$	$C^{(6)}_{\mathrm{SRR,ud}}$	$C^{(6)}_{\mathrm{SLR,ud}}$	$C^{(6)}_{\mathrm{TRR,ud}}$
$C^{(6)}_{\mathrm{VLL,us}}$	$\frac{1}{2}m_d\mathcal{O}^{\mu}_{6,\mathrm{usud}}E_\mu$ $-\frac{1}{2}m_u\mathcal{O}^{\mu}_{8,\mathrm{usud}}E_\mu$ $+m_l\mathcal{O}_1E_L$	$\frac{1}{2}m_d\mathcal{O}^{\mu}_{8,\mathrm{usud}}E_\mu$ $-\frac{1}{2}m_u\mathcal{O}^{\mu}_{6,\mathrm{usud}}E_\mu$ $-2m_l\mathcal{O}'_5E_L$	$m_u\mathcal{O}'_4E_L$ $-m_s\mathcal{O}'_2E_L$ $-\frac{1}{2}m_l\mathcal{O}^{\mu}_{6,\mathrm{usud}}E_\mu$	$m_u\mathcal{O}_2E_L$ $-m_s\mathcal{O}_4E_L$ $-\frac{1}{2}m_l\mathcal{O}^{\mu}_{8,\mathrm{usud}}E_\mu$	$8m_u\mathcal{O}'_5E_L$ $-4m_d\mathcal{O}_1E_L$
$C^{(6)}_{\mathrm{VRL,us}}$	$\frac{1}{2}m_d\mathcal{O}^{\mu'}_{8,\mathrm{usud}}E_\mu$ $-\frac{1}{2}m_u\mathcal{O}^{\mu'}_{6,\mathrm{usud}}E_\mu$ $-2m_l\mathcal{O}_5E_L$	$\frac{1}{2}m_d\mathcal{O}^{\mu'}_{6,\mathrm{usud}}E_\mu$ $-\frac{1}{2}m_u\mathcal{O}^{\mu'}_{8,\mathrm{usud}}E_\mu$ $+m_l\mathcal{O}'_1E_L$	$m_u\mathcal{O}'_2E_L$ $-m_s\mathcal{O}'_4E_L$ $-\frac{1}{2}m_l\mathcal{O}^{\mu'}_{8,\mathrm{usud}}E_\mu$	$m_u\mathcal{O}_4E_L$ $-m_s\mathcal{O}_2E_L$ $-\frac{1}{2}m_l\mathcal{O}^{\mu'}_{6,\mathrm{usud}}E_\mu$	$8m_d\mathcal{O}_5E_L$ $-4m_u\mathcal{O}'_1E_L$
$C^{(6)}_{\mathrm{SRL,us}}$	$-m_d\mathcal{O}'_2E_R$ $+m_u\mathcal{O}_4E_R$ $\frac{1}{2}m_l\mathcal{O}^{\mu}_{6,\mathrm{udus}}E_\mu$	$-m_d\mathcal{O}_4E_R$ $+m_u\mathcal{O}'_2E_R$ $\frac{1}{2}m_l\mathcal{O}^{\mu'}_{8,\mathrm{udus}}E_\mu$	$m_l\mathcal{O}'_2E_R$	$m_l\mathcal{O}_4E_R$	$-2m_d\mathcal{O}^{\mu}_{6,\mathrm{udus}}E_\mu$ $-2m_u\mathcal{O}^{\mu'}_{8,\mathrm{udus}}E_\mu$
$C^{(6)}_{\mathrm{SLL,us}}$	$-m_d\mathcal{O}'_4E_R$ $+m_u\mathcal{O}_2E_R$ $\frac{1}{2}m_l\mathcal{O}^{\mu}_{8,\mathrm{udus}}E_\mu$	$-m_d\mathcal{O}_2E_R$ $+m_u\mathcal{O}'_4E_R$ $\frac{1}{2}m_l\mathcal{O}^{\mu'}_{6,\mathrm{udus}}E_\mu$	$m_l\mathcal{O}'_4E_R$	$m_l\mathcal{O}_2E_R$	$-2m_d\mathcal{O}^{\mu}_{8,\mathrm{udus}}E_\mu$ $-2m_u\mathcal{O}^{\mu'}_{6,\mathrm{udus}}E_\mu$
$C^{(6)}_{\mathrm{TLL,us}}$	$-4m_u\mathcal{O}_1E_R$ $+8m_s\mathcal{O}_5E_R$	$-4m_s\mathcal{O}'_1E_R$ $+8m_u\mathcal{O}'_5E_R$	$2m_s\mathcal{O}'_{8,\mathrm{usud}}E_\mu$ $+2m_u\mathcal{O}_{6,\mathrm{usud}}E_\mu$	$2m_u\mathcal{O}_{8,\mathrm{usud}}E_\mu$ $+2m_s\mathcal{O}'_{6,\mathrm{usud}}E_\mu$	$-8m_s(2\mathcal{O}'_{9,\mathrm{udus}}+\mathcal{O}'_{8,\mathrm{usud}})E_\mu$ $+8m_u(2\mathcal{O}_{7,\mathrm{usud}}+\mathcal{O}_{6,\mathrm{usud}})E_\mu$

Table A.1: The dim-9 interactions induced by integrating a heavy neutrino between two dim-6 operators involving neutrinos of different chiralities (the coefficients have been divided by $\frac{1}{v^4}\frac{1}{m_\nu^2}$ and the corresponding two dim-6 WCs).

one expects the relative scaling of $\Lambda_\chi \sim (4\pi)^2 m_q$ for the derivative and m_q terms, respectively, allowing us to use the latter as an order-of-magnitude estimate for the total.

We can derive similar $\sim m_q$ terms for the interference of $C^{(6)}_{\mathrm{VLR}}$ with $C^{(6)}_{\mathrm{VLL}}$. However, in this case a chirality flip does not lead to chiral enhancement (the induced operators are dim-9 vector operators which do not induce $\pi\pi$ terms at LO), implying that the m_q terms cannot be used to estimate the derivative pieces in this case. If such interference terms are important we would have to construct the derivative terms to obtain an order-of-magnitude estimate.

In principle we should give all the derivative contributions in the case of LNV kaon decays, because this LNV process is caused by two different interactions with different flavor configurations. In Table A.1 we give the matching conditions only for interactions, which via the equations of motions can be written as $m_q \times \mathcal{O}^{(9)}$ or $m_l \times \mathcal{O}^{(9)}$ with m_q being the light quark mass and m_l the mass of charged lepton. The remaining terms contain a derivative and are of dim-10, which result in unknown LECs when matched onto Chiral Perturbation Theory. Thus we neglect them here. To make the expressions in a compact form, we have removed an overall factor $\frac{1}{v^4}\frac{1}{m_\nu^2}$ and the dim-6 WCs, and we also use $E_\mu = \bar{e}\gamma_\mu\gamma_5 C\bar{e}^T$ and $E_{L,R} = \bar{e}_{L,R}C\bar{e}^T_{L,R}$. Dim-9 interactions are also induced by terms, *e.g.* $C^{(6)}_{\mathrm{VLR,us}} \times C^{(6)}_{\mathrm{VLL,ud}}$. We can easily get the dim-9 interactions induced by $C^{(6)}_{\mathrm{VLR,us}} \times C^{(6)}_{\mathrm{VLL,ud}}$ via a replacement $d \leftrightarrow s$ on the dim-9 interactions induced by $C^{(6)}_{\mathrm{VLL,us}} \times C^{(6)}_{\mathrm{VLR,ud}}$.

Appendix B

Matching and interpolation formulae for the leptoquark scenario

As discussed in Sect. 3.7.3, right below the electroweak scale we can match the leptoquark model of Eq. (3.128) to the dim-6 operators involving the first-generation quarks and charged leptons

$$\mathcal{L}^{(6)}_{\Delta L=0} = \frac{2G_F}{\sqrt{2}}\left[\bar{c}^{(6)}_{\substack{\mathrm{SR}\\ea}}\ \bar{u}_L d_R \bar{e}_L \nu_{Ra} + \bar{c}^{(6)}_{\substack{\mathrm{T}\\ea}}\ \bar{u}_L \sigma^{\mu\nu} d_R \bar{e}_L \sigma^{\mu\nu} \nu_{Ra}\right], \tag{B.1}$$

where

$$\bar{c}^{(6)}_{\substack{\mathrm{SR}\\ea}} = 4\bar{c}^{(6)}_{\substack{\mathrm{T}\\ea}} = \frac{v^2}{2m^2_{\mathrm{LQ}}} y^{\overline{LR}}_{1a} y^{RL*}_{1e}\,, \tag{B.2}$$

and a runs from 1 to n. For simplicity we neglect the evolution to lower energies and simply give the matching to the operators in Eq. (2.23). We obtain

$$\left(C^{(6)}_{\mathrm{VLL}}\right)_{ei} = -2V_{ud}U_{ei}\,, \qquad \left(C^{(6)}_{\mathrm{SRR}}\right)_{ei} = 4\left(C^{(6)}_{\mathrm{TRR}}\right)_{ei} = \sum_{a=1}^{n} \bar{c}^{(6)}_{\substack{\mathrm{SR}\\ea}} U^*_{3+a,i}\,. \tag{B.3}$$

With these nonzero Wilson coefficients the $0\nu\beta\beta$ decay rate can be directly read from the master formula. For mass eigenstates $m_i < \Lambda_\chi$, the interactions only introduce contributions to the subamplitude $\mathcal{A}_L(m_i)$ which is given by

$$\begin{aligned}
\mathcal{A}_L(m_i) \;=\; & -\frac{m_i}{4m_e}\Bigg\{ \left[\mathcal{M}_V(m_i) + \mathcal{M}_A(m_i)\right]\left(C^{(6)}_{\mathrm{VLL}}\right)^2_{ei} \\
& \quad + \left[\mathcal{M}_S(m_i) + \mathcal{M}_{PS}(m_i)\frac{B^2}{m_\pi^2}\right]\left(C^{(6)}_{\mathrm{SRR}}\right)^2_{ei} - \mathcal{M}_T(m_i)\left(C^{(6)}_{\mathrm{TRR}}\right)^2_{ei}\Bigg\} \\
& + \frac{1}{4m_e}\left[2B\mathcal{M}_{PS}(m_i)\left(C^{(6)}_{\mathrm{SRR}}\right)_{ei} - m_N\mathcal{M}_{TV}(m_i)\left(C^{(6)}_{\mathrm{TRR}}\right)_{ei}\right]\left(C^{(6)}_{\mathrm{VLL}}\right)_{ei} \\
& + \frac{m_\pi^2}{m_e v}\Bigg[\left(\frac{m_i v}{m_\pi^2 F_\pi^2} c_{iL}^{\nu\pi\pi} + \frac{v}{\Lambda_\chi} c_{iL}^{\prime\pi\pi}\right)\mathcal{M}_{PS,sd} \\
& + \frac{1}{2}\left(c_{iL}^{\pi N} - \frac{v}{\Lambda_\chi} c_{iL}^{\prime\pi\pi}\right)\left(M^{AP}_{GT,sd} + M^{AP}_{T,sd}\right) - \frac{2}{g_A^2} C_{iL}^{NN} M_{F,sd}\Bigg].
\end{aligned} \tag{B.4}$$

The first three lines arise from the exchange of potential neutrinos while the last two lines arise from hard-neutrino exchange. The couplings are given by

$$
\begin{aligned}
c_{iL}^{\nu\pi\pi} &= -2g_{\mathrm{S1}}^{\pi\pi}(m_i)\left(C_{\mathrm{SRR}}^{(6)}\right)_{ei}^2 - 2g_{\mathrm{TT}}^{\pi\pi}(m_i)\left(C_{\mathrm{TRR}}^{(6)}\right)_{ei}^2 ,\\
c_{iL}^{\prime\pi\pi} &= \left[g_{\mathrm{S,VLL}}^{\pi\pi}(m_i)\left(C_{\mathrm{SRR}}^{(6)}\right)_{ei} - \frac{1}{4}g_{\mathrm{T,VLL}}^{\pi\pi}(m_i)\left(C_{\mathrm{TRR}}^{(6)}\right)_{ei}\right]\left(C_{\mathrm{VLL}}^{(6)}\right)_{ei}\\
c_{iL}^{\pi N} &= \frac{v}{\Lambda_\chi}\left[g_{\mathrm{S,VLL}}^{\pi N}(m_i)\left(C_{\mathrm{SRR}}^{(6)}\right)_{ei} - \frac{1}{2}g_{\mathrm{T,VLL}}^{\pi N}(m_i)\left(C_{\mathrm{TRR}}^{(6)}\right)_{ei}\right]\left(C_{\mathrm{VLL}}^{(6)}\right)_{ei} ,\\
C_{iL}^{NN} &= \frac{v}{\Lambda_\chi}\left[g_{\mathrm{S,VLL}}^{NN}(m_i)\left(C_{\mathrm{SRR}}^{(6)}\right)_{ei} - \frac{1}{2}g_{\mathrm{T,VLL}}^{NN}(m_i)\left(C_{\mathrm{TRR}}^{(6)}\right)_{ei}\right]\left(C_{\mathrm{VLL}}^{(6)}\right)_{ei}\\
&\quad + m_i v\left[\frac{1}{4}g_{\nu}^{NN}(m_i)\left(C_{\mathrm{VLL}}^{(6)}\right)_{ei}^2 + \frac{1}{4}g_{\mathrm{S1}}^{NN}(m_i)\left(C_{\mathrm{SRR}}^{(6)}\right)_{ei}^2 + \frac{1}{4}g_{\mathrm{TT}}^{NN}(m_i)\left(C_{\mathrm{TRR}}^{(6)}\right)_{ei}^2\right] .
\end{aligned}
\tag{B.5}
$$

Mass eigenstates with $m_i > \Lambda_\chi$ are integrated out at the quark level and induce dim-9 operators. From Eqs. (3.9) and (A.1) we find the following contributions

$$
C_{1L}^{(9)} = -\frac{v}{2m_i}\left(C_{\mathrm{VLL}}^{(6)}\right)_{ei}^2 - \frac{4m_d v}{m_i^2}\left(C_{\mathrm{VLL}}^{(6)}\right)_{ei}\left(C_{\mathrm{TRR}}^{(6)}\right)_{ei} \tag{B.6}
$$

$$
C_{2L}^{(9)\prime} = \frac{v}{m_i}\left[\frac{1}{2}\left(C_{\mathrm{SRR}}^{(6)}\right)_{ei}^2 + 8\left(C_{\mathrm{TRR}}^{(6)}\right)_{ei}^2\right] - \frac{m_d v}{m_i^2}\left(C_{\mathrm{VLL}}^{(6)}\right)_{ei}\left(C_{\mathrm{SRR}}^{(6)}\right)_{ei} , \tag{B.7}
$$

$$
C_{3L}^{(9)\prime} = \frac{16v}{m_i}\left(C_{\mathrm{TRR}}^{(6)}\right)_{ei}^2 , \tag{B.8}
$$

$$
C_{4L}^{(9)} = -\frac{4m_u v}{m_i^2}\left(C_{\mathrm{VLL}}^{(6)}\right)_{ei}\left(C_{\mathrm{TRR}}^{(6)}\right)_{ei} , \tag{B.9}
$$

$$
C_{5L}^{(9)} = -\frac{m_u v}{2m_i^2}\left(C_{\mathrm{VLL}}^{(6)}\right)_{ei}\left(C_{\mathrm{SRR}}^{(6)}\right)_{ei} , \tag{B.10}
$$

The resulting amplitude $\mathcal{A}_L^{(9)}$ is

$$
\mathcal{A}_L^{(9)} = \frac{m_\pi^2}{m_e v}\left[\left(\frac{c_L^{\pi\pi}}{m_\pi^2} + c_L^{\prime\pi\pi}\right)\mathcal{M}_{PS,sd} + \frac{1}{2}\left(c_L^{\pi N} - c_L^{\prime\pi\pi}\right)\left(M_{GT,sd}^{AP} + M_{T,sd}^{AP}\right) - \frac{2}{g_A^2}c_L^{NN}M_{F,sd}\right] ,
$$

with $c_L^{\pi\pi}$, $c_L^{\prime\pi\pi}$, $c_L^{\pi N}$, and c_L^{NN} defined in Eqs. (3.31), (3.33), and (3.34).

We introduce interpolation formulae for the LECs appearing in Eqs. (B.5) along the lines of Sect. 3.6.1. For the pionic terms we use

$$
\begin{aligned}
g_{\mathrm{S1}}^{\pi\pi}(m_i) &= g_{\mathrm{S1}}^{\pi\pi}(0)\frac{1}{1 + 8\frac{m_i^2}{F_\pi^2}g_{\mathrm{S1}}^{\pi\pi}(0)\left[g_2^{\pi\pi}(m_0) - B^2\right]^{-1}} ,\\
g_{\mathrm{TT}}^{\pi\pi}(m_i) &= g_{\mathrm{TT}}^{\pi\pi}(0)\frac{1}{1 + \frac{m_i^2}{F_\pi^2}g_{\mathrm{TT}}^{\pi\pi}(0)\left[4g_3^{\pi\pi}(m_0) + 2g_2^{\pi\pi}(m_0)\right]^{-1}} ,\\
g_{\mathrm{S,VLL}}^{\pi\pi}(m_i) &= g_{\mathrm{S,VLL}}^{\pi\pi}(0)\frac{1}{1 - \frac{2m_i^2}{\Lambda_\chi}g_{\mathrm{S,VLL}}^{\pi\pi}(0)\left[B + \frac{1}{2m_\pi^2}\left[-2m_d g_2^{\pi\pi}(m_0) + m_u g_5^{\pi\pi}(m_0)\right]\right]^{-1}} ,\\
g_{\mathrm{T,VLL}}^{\pi\pi}(m_i) &= g_{\mathrm{T,VLL}}^{\pi\pi}(0)\frac{1}{1 + \frac{m_i^2 m_\pi^2}{8\Lambda_\chi}g_{\mathrm{T,VLL}}^{\pi\pi}(0)\left[m_u g_4^{\pi\pi}(m_0) + \frac{5}{3}m_d m_\pi^2 g_1^{\pi\pi}(m_0)\right]^{-1}} .
\end{aligned}
\tag{B.11}
$$

The pion-nucleon interpolation formula is

$$\begin{aligned} g^{\pi N}_{\rm S,VLL}(m_i) &= g^{\pi\pi}_{\rm S,VLL}(m_i)\,, \\ g^{\pi N}_{\rm T,VLL}(m_i) &= g^{\pi N}_{\rm T,VLL}(0)\frac{1}{1+\frac{m_i^2 m_\pi^2}{4\Lambda_\chi} g^{\pi N}_{\rm T,VLL}(0)\left[m_u g_4^{\pi\pi}(m_0)+2m_d m_\pi^2 g_1^{\pi N}(m_0)\right]^{-1}}\,. \end{aligned} \tag{B.12}$$

A similar formula can be written down for $g^{\pi N}_{\rm S,VLL}(m_i)$ once four-quark operators involving derivatives are explicitly included, see Appendix A. The nucleon-nucleon interpolation formulae become

$$\begin{aligned} g^{NN}_{\rm S1}(m_i) &= g^{NN}_{\rm S1}(0)\frac{1}{1+m_i^2 g^{NN}_{\rm S1}(0)\left[2g_2^{NN}(m_0)-\frac{1}{2}g_S^2\right]^{-1}}\,, \\ g^{NN}_{\rm TT}(m_i) &= g^{NN}_{\rm TT}(0)\frac{1}{1+m_i^2 g^{NN}_{\rm TT}(0)\left[32g_2^{NN}(m_0)+64g_3^{NN}(m_0)-24g_T^2\right]^{-1}}\,, \\ g^{NN}_{\rm S,VLL}(m_i) &= g^{NN}_{\rm S,VLL}(0)\frac{1}{1-\frac{m_i^2}{\Lambda_\chi} g^{NN}_{\rm S,VLL}(0)\left[m_d\, g_2^{NN}(m_0)+\frac{1}{2}m_u\, g_5^{NN}(m_0)\right]^{-1}}\,, \\ g^{NN}_{\rm T,VLL}(m_i) &= g^{NN}_{\rm T,VLL}(0)\frac{1}{1+\frac{m_i^2}{8\Lambda_\chi} g^{NN}_{\rm T,VLL}(0)\left[m_d\, g_1^{NN}(m_0)+m_u\, g_4^{NN}(m_0)\right]^{-1}}\,. \end{aligned} \tag{B.13}$$

In all the above relations we use the matching scale $\mu = m_0 = 2$ GeV. With some effort the relations can be RGE improved as we did for $g^{\pi\pi}_{\rm LR}(m_i)$, $g^{NN}_{\rm LR}(m_i)$, and $g^{NN}_{\nu}(m_i)$ in Sect. 3.6.1. This is more complicated for scalar and tensor interactions because scalar and tensor quark bilinears have non-vanishing anomalous dimensions in contrast to the vector case. Given the large uncertainties, and in order not to clutter up the expressions, we refrain from explicitly including the RGE corrections in the interpolation formula.

Appendix C

Two-body sterile neutrino production and decay processes

C.1 Charged currents

Sterile neutrinos can decay into a charged meson and a charged lepton by the weak interaction or EFT operators. Pseudoscalar mesons can decay into a two-body final state for pseudoscalar and axial-vector currents, while vector mesons can decay into a two-body final state via vector or tensor currents. For pseudoscalar mesons containing an anti-quark $\bar{q}_i$ and a quark q_j, we define meson decay constants via

$$\langle 0|\bar{q}_i\gamma^\mu\gamma^5 q_j|M(q)\rangle \equiv iq^\mu f_M\,, \tag{C.1}$$

where $|M(q)\rangle$ is a pseudoscalar meson with momentum q. Current-algebra or leading-order chiral perturbation theory gives

$$\langle 0|\bar{q}_i\gamma^5 q_j|M(q)\rangle = i\frac{m_M^2}{m_{q_i}+m_{q_j}}f_M \equiv if_M^S \tag{C.2}$$

for the pseudoscalar current. The vector and tensor currents only induce two-body final states for vector mesons. We define

$$\begin{aligned}\langle 0|\bar{q}_i\gamma^\mu q_j|M^*(q,\epsilon)\rangle &\equiv if_M^V m_{M^*}\epsilon^\mu\,,\\ \langle 0|\bar{q}_i\sigma^{\mu\nu} q_j|M^*(q,\epsilon)\rangle &\equiv -f_M^T(q^\mu\epsilon^\nu - q^\nu\epsilon^\mu)\,,\end{aligned} \tag{C.3}$$

where $|M^*(q,\epsilon)\rangle$ denotes a vector meson M^* with mass m_{M^*}, momentum q and polarization ϵ^μ. Heavy-quark symmetry relates $f_M^T \simeq f_M^V$. All decay constants are given below in Appendix E.

Armed with these decay constants, we calculate the production and decay rates of neutrino mass eigenstates starting from Eq. (5.1). We begin with neutrino production via the decay of pseudoscalar mesons $M_{ij}^- \to l_k^- + \nu_l$, and the corresponding decay $\nu_l \to M_{ij}^+ + l_k^-$ where ij denotes the generation of quark flavors that make up the meson (we drop these indices below for notational convenience), k the charged lepton generation, and $l = \{1,\ldots,\bar{n}\}$ the neutrino mass eigenstate. For the decay of the neutrino mass eigenstate we also include the decay to the charge-conjugate final state which is equally likely due to the Majorana nature of ν_l.

We obtain for the summed-over-spins squared amplitudes for sterile neutrino (N) production

$$\begin{aligned}\sum_{\text{spins}} |\mathcal{M}(M^- \to N + l_k^-)|^2 &= \frac{G_F^2}{2}\Bigg\{ f_M^2 \left[\left| C^{(6)}_{\text{VLL}} \right|^2 + \left| C^{(6)}_{\text{VLR}} - C^{(6)}_{\text{VRR}} \right|^2 \right] f_{VV,1} \\ &\quad + f_M^2 \text{Re}\left[C^{(6)}_{\text{VLL}} (C^{(6)}_{\text{VLR}} - C^{(6)}_{\text{VRR}})^* \right] f_{VV,2} \\ &\quad + (f_M^S)^2 \left| C^{(6)}_{\text{SLR}} - C^{(6)}_{\text{SRR}} \right|^2 f_{SS} \\ &\quad + f_M f^S_{M_{ij}} \text{Re}\left[C^{(6)}_{\text{VLL}} (C^{(6)}_{\text{SLR}} - C^{(6)}_{\text{SRR}})^* \right] f_{VS,1} \\ &\quad + f_M f^S_{M_{ij}} \text{Re}\left[(C^{(6)}_{\text{VLR}} - C^{(6)}_{\text{VRR}}) (C^{(6)}_{\text{SLR}} - C^{(6)}_{\text{SRR}})^* \right] f_{VS,2} \Bigg\},\end{aligned} \tag{C.4}$$

where all Wilson coefficients carry flavor indices $ijkl$ and we defined the functions

$$\begin{aligned} f_{VV,1} &\equiv m_M^2 (m_k^2 + m_N^2) - (m_k^2 - m_N^2)^2 , \\ f_{VV,2} &\equiv -4 m_M^2 m_k m_N , \\ f_{SS} &\equiv m_M^2 - m_k^2 - m_N^2 , \\ f_{VS,1} &\equiv -2 m_N (m_M^2 + m_k^2 - m_N^2) , \\ f_{VS,2} &\equiv 2 m_k (m_M^2 - m_k^2 + m_N^2). \end{aligned} \tag{C.5}$$

For sterile neutrino decay, we include the charge-conjugated final states leading to an additional factor 2 compensating the additional 1/2 from initial-spin averaging. We then obtain

$$2 \times \frac{1}{2} \sum_{\text{spins}} |\mathcal{M}(N \to M + l_k)|^2 = \sum_{\text{spins}} |\mathcal{M}(M \to N + l_k)|^2 \Big|_{f_{ab,i} \to g_{ab,i}} , \tag{C.6}$$

where $ab = \{VV, SS, VS\}$, $i = \{1, 2\}$, and $g_{ab,i} = -f_{ab,i}$.

Similarly, for processes involving vector mesons we find

$$\begin{aligned}\frac{1}{3} \sum_{\text{spins}} |\mathcal{M}(M^{*-} \to N + l_k^-)|^2 &= \frac{G_F^2}{6}\Bigg\{ (f^V_{M^*})^2 \left[\left| C^{(6)}_{\text{VLL}} \right|^2 + \left| C^{(6)}_{\text{VLR}} + C^{(6)}_{\text{VRR}} \right|^2 \right] f^*_{VV,1} \\ &\quad + (f^V_{M^*})^2 \text{Re}\left[C^{(6)}_{\text{VLL}} (C^{(6)}_{\text{VLR}} + C^{(6)}_{\text{VRR}})^* \right] f^*_{VV,2} \\ &\quad + (f^T_{M^*})^2 \left| C^{(6)}_{\text{TRR}} \right|^2 f^*_{TT} \\ &\quad + f^V_{M^*} f^T_{M^*} \text{Re}\left[C^{(6)}_{\text{VLL}} C^{(6)\,*}_{\text{TRR}} \right] f^*_{VT,1} \\ &\quad + f^V_{M^*} f^T_{M^*} \text{Re}\left[(C^{(6)}_{\text{VLR}} + C^{(6)}_{\text{VRR}}) C^{(6)\,*}_{\text{TRR}} \right] f^*_{VT,2} \Bigg\},\end{aligned} \tag{C.7}$$

where

$$\begin{aligned} f^*_{VV,1} &\equiv 2 {m_{M^*}}^4 - m^2_{M^*_{ij}} (m_k^2 + m_N^2) - (m_k^2 - m_N^2)^2 , \\ f^*_{VV,2} &\equiv 12 m^2_{M^*} m_k m_N , \\ f^*_{TT} &\equiv 16 \left(m^4_{M^*} + m^2_{M^*_{ij}} (m_k^2 + m_N^2) - 2 (m_k^2 - m_N^2)^2 \right) , \\ f^*_{VT,1} &\equiv -24 m_N (m^2_{M^*} + m_k^2 - m_N^2) , \\ f^*_{VT,2} &\equiv -24 m_k (m^2_{M^*} - m_k^2 + m_N^2) . \end{aligned} \tag{C.8}$$

For sterile neutrino decay

$$2 \times \frac{1}{2} \sum_{\text{spins}} |\mathcal{M}(N \to M^* + l_k)|^2 \;=\; \sum_{\text{spins}} |\mathcal{M}(M^* \to N + l_k)|^2 \Big|_{f^*_{ab,i} \to g^*_{ab,i}} , \tag{C.9}$$

where $ab = \{VV, TT, VT\}$, $i = \{1, 2\}$, and $g^*_{VV,i} = -f^*_{VV,i}$, $g^*_{TT} = -f^*_{TT}$, $g^*_{VT,i} = f^*_{VT,i}$.

The expression for the decay rates is given by

$$\Gamma = \frac{\sqrt{\lambda(m_1, m_2, m_3)}}{16\pi m_1^3} \frac{1}{n} \sum_{\text{spins}} |\mathcal{M}|^2 \tag{C.10}$$

where n is the appropriate spin-averaging factor, m_1 is the mass of the decaying particle, and m_2 and m_3 are the masses of the final-state particles.

C.2 Sterile neutrino decays into neutral pseudoscalar mesons via weak interaction

We follow Ref. [212] and write the neutral weak axial current as

$$J^A_{Z,\mu} = -\frac{1}{\sqrt{2}}(j^A_{3,\mu} + \frac{1}{\sqrt{3}} j^A_{8,\mu} - \frac{1}{\sqrt{6}} j^A_{0,\mu} + \frac{1}{\sqrt{2}} j^A_{\eta_c,\mu} + \cdots) , \tag{C.11}$$

where

$$\begin{aligned} j^A_{3,\mu} &= \frac{1}{\sqrt{2}}(\bar{u}\gamma_\mu\gamma_5 u - \bar{d}\gamma_\mu\gamma_5 d) , \\ j^A_{8,\mu} &= \frac{1}{\sqrt{6}}(\bar{u}\gamma_\mu\gamma_5 u + \bar{d}\gamma_\mu\gamma_5 d - 2\bar{s}\gamma_\mu\gamma_5 s) , \\ j^A_{0,\mu} &= \frac{1}{\sqrt{3}}(\bar{u}\gamma_\mu\gamma_5 u + \bar{d}\gamma_\mu\gamma_5 d + \bar{s}\gamma_\mu\gamma_5 s) \\ j^A_{\eta_c,\mu} &= \bar{c}\gamma_\mu\gamma_5 c . \end{aligned} \tag{C.12}$$

We define

$$\langle 0|j^A_{Z,\mu}|M^0_{a,P}(q)\rangle \equiv -i\frac{f_M}{\sqrt{2}} q_\mu , \qquad \langle 0|j^A_{a,\mu}|M^0_{a,P}(q)\rangle \equiv i f^a_M q_\mu , \tag{C.13}$$

for $a = \{0, 3, 8, \eta_c\}$ and the M subscript labels the final-state pseudoscalar meson. Clearly we have

$$f_M = f^3_M + \frac{1}{\sqrt{3}} f^8_M - \frac{1}{\sqrt{6}} f^0_M + \frac{1}{\sqrt{2}} f^{\eta_c}_M . \tag{C.14}$$

To clarify the notation: for neutral pions $f^0_{\pi^0} = f^8_{\pi^0} = f^{\eta_c}_{\pi^0} = 0$ and $f_{\pi^0} = f^3_{\pi^0} = f_{\pi^\pm}$. For η and η' mesons, we have $f^3_{\eta^{(\prime)}} = f^{\eta_c}_{\eta^{(\prime)}} = 0$ (neglecting isospin breaking), but we do need to take into account η-η' mixing. We use the phenomenological parametrization in terms of two mixing angles

$$\begin{pmatrix} f^8_\eta & f^0_\eta \\ f^8_{\eta'} & f^0_{\eta'} \end{pmatrix} = \begin{pmatrix} f_8 \cos\theta_8 & -f_0 \sin\theta_0 \\ f_8 \sin\theta_8 & f_0 \cos\theta_0 \end{pmatrix} , \tag{C.15}$$

where the values of $\theta_{0,8}$ and $f_{0,8}$ are given in Table E.2. We then obtain

$$f_\eta = \frac{f_8 \cos\theta_8}{\sqrt{3}} + \frac{f_0 \sin\theta_0}{\sqrt{6}} , \qquad f_{\eta'} = \frac{f_8 \sin\theta_8}{\sqrt{3}} - \frac{f_0 \cos\theta_0}{\sqrt{6}} . \tag{C.16}$$

The decay width of $N \to \nu_e + M_P^0$ can now be written as

$$\Gamma(N \to \nu_e M_P^0) = 2 \times \frac{G_F^2 f^2 m_N^3 |U_{e4}|^2}{32\pi}(1 - \frac{{m_P^0}^2}{m_N^2})^2 \,, \tag{C.17}$$

where we add a 2 to account for the Majorana nature of sterile neutrinos, f is given by f_η, $f_{\eta'}$, $f_{\eta_c}/\sqrt{2}$ or $f_{\pi^\pm}$, and m_P^0 is the mass of M_P^0.

C.3 Sterile neutrino decays into neutral vector mesons via weak interaction

We write the vector component of the neutral weak current as

$$j^V_{Z,\mu} = \left(\frac{1}{2} - \frac{4}{3}\sin^2\theta_w\right)(\bar{u}\gamma_\mu u + \bar{c}\gamma_\mu c) + \left(-\frac{1}{2} + \frac{2}{3}\sin^2\theta_w\right)\left(\bar{d}\gamma_\mu d + \bar{s}\gamma_\mu s\right) \,, \tag{C.18}$$

where θ_w is the Weinberg angle. We define the currents

$$\begin{aligned} j^V_{\rho^0,\mu} &= \frac{1}{\sqrt{2}}(\bar{u}\gamma_\mu u - \bar{d}\gamma_\mu d) \,, \\ j^V_{\omega,\mu} &= \frac{1}{\sqrt{2}}(\bar{u}\gamma_\mu u + \bar{d}\gamma_\mu d) \,, \\ j^V_{\phi,\mu} &= \bar{s}\gamma_\mu s \,, \\ j^V_{\mathrm{J},\mu} &= \bar{c}\gamma_\mu c \,, \end{aligned} \tag{C.19}$$

which correspond to the neutral vector mesons ρ^0, ω, ϕ, and J/Ψ, respectively. We rewrite

$$j^V_{Z,\mu} = \frac{1}{\sqrt{2}}(1 - 2\sin^2\theta_w) j^V_{\rho^0,\mu} - \frac{\sqrt{2}}{3}\sin^2\theta_w j^V_{\omega,\mu} + \left(-\frac{1}{2} + \frac{2}{3}\sin^2\theta_w\right) j^V_{\phi,\mu} + (\frac{1}{2} - \frac{4}{3}\sin^2\theta_w) j^V_{\mathrm{J}/\Psi,\mu} \,. \tag{C.20}$$

The hadronic matrix elements are defined as

$$\langle 0|j^V_{a,\mu}|M^0_{a,V}(q,\epsilon)\rangle = i f_a \epsilon_\mu \,, \tag{C.21}$$

where $a = \rho^0, \omega, \phi, \mathrm{J}/\Psi$. The decay width becomes

$$\Gamma(N \to \nu_e M^0_{a,V}) = 2 \times \frac{G_F^2 f_a^2 g_a^2 |U_{e4}|^2 m_N^3}{32\pi {m_a}^2}\left(1 + 2\frac{{m_a}^2}{m_N^2}\right)\left(1 - \frac{{m_a}^2}{m_N^2}\right)^2 \,, \tag{C.22}$$

where f_a and g_a are listed in Table E.3 and m_a is the mass of $M^0_{a,V}$.

C.4 Sterile neutrino decays into neutral mesons via higher-dimensional operators

In the work of `Belle II`, sterile neutrinos could decay into neutral pseudoscalar or vector mesons via the higher-dimensional operators. To compute the corresponding decay rates, we work in the $SU(3)$ chiral perturbation theory, following the calculation procedure as detailed in Ref. [279]. We

first write down the leading-order chiral Lagrangian containing the Lorentz- and chiral-invariant terms with the lowest number of derivatives,

$$\mathcal{L}_{\pi,K} = \frac{F^2}{4}\mathrm{Tr}\left[(D_\mu U)^\dagger (D^\mu U)\right] + \frac{F^2}{4}\mathrm{Tr}\left[U^\dagger\chi + U\chi^\dagger\right] , \tag{C.23}$$

where $D_\mu U = \partial_\mu U - i l_\mu U + i U r_\mu$ and $\chi = 2B(M + s - ip)$. l_μ, r_μ, s, p are external sources and $M = \mathrm{diag}(m_u, m_d, m_s)$ is a diagonal 3×3 quark mass matrix. U is given by

$$U(x) = \exp\left(\frac{i\sqrt{2}\Pi(x)}{F}\right) , \qquad \Pi(x) = \begin{pmatrix} \frac{\pi^0}{\sqrt{2}} + \frac{\eta_8}{\sqrt{6}} + \frac{\eta_0}{\sqrt{3}} & \pi^+ & K^+ \\ \pi^- & -\frac{\pi^0}{\sqrt{2}} + \frac{\eta_8}{\sqrt{6}} + \frac{\eta_0}{\sqrt{3}} & K^0 \\ K^- & \bar{K}^0 & -\sqrt{\frac{2}{3}}\eta_8 + \frac{\eta_0}{\sqrt{3}} \end{pmatrix} . \tag{C.24}$$

η_8 and η_0 are in the singlet-octet basis and their relations with the physical states η and η' are

$$\begin{pmatrix} \eta \\ \eta' \end{pmatrix} = \frac{1}{F}\begin{pmatrix} F_8\cos\theta_8 & -F_0\sin\theta_0 \\ F_8\sin\theta_8 & F_0\cos\theta_0 \end{pmatrix}\begin{pmatrix} \eta_8 \\ \eta_0 \end{pmatrix} . \tag{C.25}$$

The values of the relevant parameters are [279, 280]

$$\begin{aligned} F &= 92.2\,\mathrm{MeV}\,, \qquad F_0 = 118.1\,\mathrm{MeV}\,, \qquad F_8 = 133.8\,\mathrm{MeV}\,, \\ \theta_0 &= -11.0^\circ\,, \qquad\qquad \theta_8 = -26.7^\circ\,. \end{aligned} \tag{C.26}$$

By using the external source field method and expand U to leading order we obtain the decay rates of the sterile neutrino.

The neutral tensor current leads to the decay of the sterile neutrino into a vector meson. We define the following matrix element:

$$\langle 0|\bar{q}_1\sigma^{\mu\nu}d|M_V^0(q,\epsilon)\rangle \equiv -f_M^T(q^\mu\epsilon^\nu - q^\nu\epsilon^\mu)\,, \tag{C.27}$$

where q_1 can be a down or strange quark, d is a down quark, and $M_V^0 = \rho^0\,, \omega\,, K^{*0}$. The tensor decay constants f_M^T are related to the vector decay constants by $f_{\rho^0}^T = f_{\rho^\pm}/\sqrt{2}$, $f_\omega^T = f_\omega/\sqrt{2}$, and $f_{K^{*0}}^T = f_{K^{*\pm}}$.

Appendix D

Definition of three-body decay form factors

A sterile neutrino N can be produced via the decay of a pseudoscalar meson, M_P, with mass M

$$M_P \to M'_{P/V} + e^{\pm} + N\,, \tag{D.1}$$

where $M'_{P/V}$ is a pseudoscalar or vector meson with mass m. For a final-state pseudoscalar meson, we require the following form factors:

$$\begin{aligned}
\langle M'_P(p')|\bar{q}_1\gamma^\mu q_2|M_P(p)\rangle &= f_+(q^2)\left[(p+p')^\mu - \frac{M^2-m^2}{q^2}q^\mu\right] + f_0(q^2)\frac{M^2-m^2}{q^2}q^\mu\,,\\
\langle M'_P(p')|\bar{q}_1 q_2|M_P(p)\rangle &= f_S(q^2)\,,\\
\langle M'_P(p')|\bar{q}_1\sigma^{\mu\nu} q_2|M_P(p)\rangle &= \frac{2i}{M+m}[p^\mu p'^\nu - p^\nu p'^\mu]f_T(q^2)\,,
\end{aligned} \tag{D.2}$$

where $q^\mu = p^\mu - p'^\mu$. Applying the equations of motion, the scalar form factor becomes

$$f_S(q^2) = f_0(q^2)\frac{M-m}{m_1-m_2}\,, \tag{D.3}$$

where m_1 and m_2 denote the mass of q_1 and q_2, respectively. A similar trick for the tensor form factor gives

$$f_T(q^2) = \frac{(M+m)^2}{q^2}\left[f_+(q^2) - f_0(q^2)\right]\,. \tag{D.4}$$

When a vector meson is produced additional form factors are required

$$\begin{aligned}
\langle M'_V(p',\epsilon)|\bar{q}_1\gamma^\mu q_2|M_P(p)\rangle &= ig(q^2)\epsilon^{\mu\nu\alpha\beta}\epsilon^*_\nu P_\alpha q_\beta\,,\\
\langle M'_V(p',\epsilon)|\bar{q}_1\gamma^\mu\gamma^5 q_2|M_P(p)\rangle &= f(q^2)\epsilon^{*\mu} + a_+(q^2)P^\mu\epsilon^*\cdot p + a_-(q^2)q^\mu\epsilon^*\cdot p\,,\\
\langle M'_V(p',\epsilon)|\bar{q}_1\sigma^{\mu\nu} q_2|M_P(p)\rangle &= g_+(q^2)\epsilon^{\mu\nu\alpha\beta}\epsilon^*_\alpha P_\beta + g_-(q^2)\epsilon^{\mu\nu\alpha\beta}\epsilon^*_\alpha q_\beta + g_0(q^2)\epsilon^{\mu\nu\alpha\beta}p_\alpha p'_\beta p\cdot\epsilon^*\,,\\
\langle M'_V(p',\epsilon)|\bar{q}_1\gamma^5 q_2|M_P(p)\rangle &= f_{PS}\epsilon^*\cdot p\,,
\end{aligned} \tag{D.5}$$

where $\epsilon^{*\mu}$ is the polarization vector of the vector meson, and $P^\mu = p^\mu + p'^\mu$. The pseudo-scalar form factor is given by

$$f_{PS} = \frac{1}{m_1+m_2}\left[f(q^2) + a_+(q^2)(M^2-m^2) + a_-(q^2)q^2\right]\,. \tag{D.6}$$

We refer Ref. [266] for a detailed discussion on the form factors.

Appendix E

Physical parameters and decay constants

The values of relevant CKM matrix elements are extracted from Ref. [132]

$$\begin{aligned} |V_{cd}| &= 0.218, \quad |V_{ud}| = 0.974, \quad |V_{us}| = 0.224, \\ |V_{cs}| &= 0.997, \quad |V_{ub}| = 0.00394, \quad |V_{cb}| = 0.0422. \end{aligned} \tag{E.1}$$

We use the quark masses at a renormalization scale of $\mu = 2$ GeV in $\overline{\text{MS}}$

$$\begin{aligned} m_u &= 2.2\,\text{MeV}\,, \quad m_d = 4.7\,\text{MeV}\,, \quad m_s = 93\,\text{MeV}\,, \\ m_c &= 1.27\,\text{GeV}\,, \quad m_b = 4.18\,\text{GeV}\,. \end{aligned} \tag{E.2}$$

Decay constants for pseudoscalar and vector mesons are given in Table E.1. Parameters to calculate decay constants for the neutral pseudoscalar and vector mesons are given in Tables E.2 and E.3, respectively.

meson M_P	f_M [MeV]	meson M_V	f_M^V [MeV]
$D^{\pm}$	212 [281]	$D^{*\pm}$	266 [282]
$D_s^{\pm}$	249 [281]	$D_s^{*\pm}$	308 [282]
$B^{\pm}$	187 [281]	$K^{*\pm}$	230 [283]
$B_c^{\pm}$	434 [284]	$\rho^{\pm}$	209 [285]
$K^{\pm}$	155.6 [281]		
$\pi^{\pm}$	130.2 [281].		

Table E.1: Decay constants for charged pseudoscalar and vector mesons.

f_0	0.148 GeV [286]
f_8	0.165 GeV [286]
f_{η_c}	0.335 GeV [287]
θ_0	-6.9° [286]
θ_8	-21.2° [286]

Table E.2: Decay constants and angles for η, η' and η_c.

meson M	f_a [GeV^2]	g_a
ρ^0 [213]	0.171	$1 - 2\sin^2\theta_w$
ω [213]	0.155	$-\frac{2}{3}\sin^2\theta_w$
ϕ [213]	0.232	$\sqrt{2}(-\frac{1}{2} + \frac{2}{3}\sin^2\theta_w)$
J [288]	1.29	$\sqrt{2}(\frac{1}{2} - \frac{4}{3}\sin^2\theta_w)$

Table E.3: Decay constants and g_a of neutral vector mesons.

Nederlandse Samenvatting

Het standaardmodel (SM) is zeer succesvol en heeft veel strenge experimentele testen doorstaan met een breed scala aan energieschalen. Maar er zijn nog steeds motivaties om te zoeken naar fysica die verder gaat dan het standaardmodel vanwege het observationele bewijs (donkere materie, massieve neutrino's en de dominantie van materie over antimaterie) en de theoretische motivaties (de sterke CP en het hiërarchieprobleem). Sinds de ontdekking van het Higgs-deeltje geeft de afwezigheid van bewijs voor BSM-fysica ("Beyond the Standard Model", dus natuurkunde die verder gaat dan het standaard model) bij de LHC aan dat het SM geldig is tot energieschalen ergens boven de elektrozwakke schaal en dat de BSM-fysica ruim boven de EW-schaal ligt. Daarom zouden we het SM kunnen beschouwen als het renormaliseerbare deel van een algemenere effectieve veldentheorie. De SMEFT Lagrangian bestaande uit SM velden kan worden geëxpandeerd in inverse machten van Λ, de energieschaal van BSM fysica, en is symmetrisch in de Lorentz en ijksymetriën.

In dit proefschrift voegen we rechtshandige neutrino's toe aan het SM, wat het eenvoudigste BSM-model is. Steriele neutrino's zijn een goed gemotiveerde oplossing voor de bovengenoemde problemen. Als steriele neutrino's niet kunnen worden geïntegreerd omdat ze licht zijn, is de SMEFT niet van toepassing. We moeten dan een standaardmodel overwegen, uitgebreid met een effectieve theorie die ook steriele neutrino's bevat. In dit proefschrift onderzoeken het effect van steriele neutrino's en het neutrino-uitgebreide effectieve Standard Model op verschillende experimenten, van deeltjesversnellers werkende op een hoge energie schaal tot hoge-precisie experimenten op een laag energieniveau, bijvoorbeeld neutrinoloos dubbelzwak verval ($0\nu\beta\beta$).

Neutrino's zijn de enige ladingsneutrale deeltjes in het SM en zouden een Majorana-massa kunnen hebben, die het leptongetal met twee eenheden schendt. We hebben een systematische studie gedaan naar schending van het leptongetal in $0\nu\beta\beta$ en LNV kaon vervalkanalen $K^- \to \pi^+ l^- l^-$. De hoger-dimensionale operatoren van νSMEFT worden stap voor stap geëvolueerd naar een energieniveau van $\mathcal{O}(1)$ MeV voor $0\nu\beta\beta$ en van $\mathcal{O}(100)$ MeV voor LNV kaon verval. De vervalsnelheden worden uitgedrukt in termen van de Wilson-coëfficiënten en lage energieconstanten, en kunnen dus worden gebruikt om hoger-dimensionale operatoren te beperken. Onze resultaten laten zien dat de $0\nu\beta\beta$ experimenten de schaal van BSM-fysica rond $\mathcal{O}(100)$ TeV kunnen onderzoeken. De huidige experimentele resultaten van de LNV-kaonverval zijn te zwak om een zinvolle BSM-energieschaal te geven vanwege het geringe beschikbaarheid van experimentele data. Maar dit geval kan worden veranderd wanneer een steriele neutrino in het resonantiegebied ligt, aangezien de LNV-vervalsnelheden aanzienlijk worden verhoogd. We vinden een zeer sterk limiet rond $\mathcal{O}(30)$ TeV op de BSM-energieschaal.

Ook de langlevende steriele neutrino's bij de versneller worden onderzocht. Hun verval leidt tot verplaatste vervalpunten die kunnen worden gereconstrueerd in detectoren, b.v. LHC en `Belle II`. Steriele neutrino's kunnen worden geproduceerd via een zeldzaam mesonische verval dat overvloedig wordt geproduceerd op de LHC-interactiepunten en via het verval van tauleptonen, geproduceerd in `Belle II`. We beschouwen een breed scala aan experimenten bij de

LHC, het voorgestelde statisch-doel experiment `SHiP` en `Belle II`. De νSMEFT-correcties voor steriele neutrinoproductie- en vervalprocessen worden berekend en we voeren simulaties uit voor verschillende detectoren om hun zoekgevoeligheden in te schatten. De LHC-experimenten kunnen de BSM-fysica onderzoeken tot honderd TeV, terwijl `Belle II` alleen interacties kan onderzoeken die verband houden met tau-leptonen tot een paar TeV.

Concluderend hebben we de effecten van hoger-dimensionale operatoren op verschillende experimenten onderzocht en ontdekten we dat niet-standaard interacties met steriele neutrino's een dramatische impact hebben op de hierboven genoemde fenomenologie. We zouden deze experimenten kunnen gebruiken om BSM-fysica op een zeer hoge schaal te onderzoeken, b.v. $\mathcal{O}(100)$ TeV. Hoewel we in een effectieve veldtheorie hebben gewerkt, kan het raamwerk gemakkelijk worden gebruikt in expliciete BSM-fysica modellen. In feite is dit al gedaan in de literatuur [158, 274–278] waar een breed scala aan modellen is afgestemd op de EFT raamwerk en bijvoorbeeld de neutrinolose dubbele bètavervalsnelheden $0\nu\beta\beta$ kunnen onmiddellijk worden afgelezen om de haalbaarheid van het betreffende model in kwestie te bepalen.

We kunnen het werk van dit proefschrift in verschillende richtingen uitbreiden. In het geval van lichte steriele neutrino's kunnen we de bijdragen van "ultra-softe" neutrino-uitwisseling beschouwen, die de genoemde bijdragen van potentiële neutrino-uitwisseling kunnen domineren. We zijn al bezig met het formalisme om deze correcties op te nemen, maar de berekeningen zijn nog niet klaar om in dit proefschrift te worden gepresenteerd. Een andere richting is het berekenen van de verschillende LEC's die verband houden met de uitwisseling van "harde" neutrino's door de strategie van Refs. [106, 107] te generaliseren om nauwkeurigere voorspellingen voor Lepton-number-schendende (LNV) waarnemingen te krijgen.

Het LNV-kaonverval kan alleen sterke limieten geven aan de menghoek of nieuwe fysica-schaal in een klein steriel neutrino-massabereik, maar we kunnen het LNV-verval van zwaardere mesonen, waaronder D- en B-type mesonen, beschouwen en een breder bereik van steriele neutrino-massa's. Voor de experimenten met verplaatste vervalpunten kunnen we overwegen om steriele neutrino's te mengen met andere soorten actieve neutrino's of hoger-dimensionale operatoren met verschillende smaakconfiguraties te bestuderen. In het minimale model is de menghoek tussen ν_L en ν_R erg klein vanwege de sterke beperking van $0\nu\beta\beta$. De LHC kan echter slechts een zeer zwakke beperking geven aan de menghoek voor steriele neutrino's met een massa boven het GeV-niveau. Als het steriele neutrino wordt gevonden bij de versneller, betekent dit dat er minstens twee soorten steriele neutrino's zijn met bijna gelijke massa, zodat hun bijdragen aan $0\nu\beta\beta$ elkaar kunnen opheffen om te voldoen aan het huidige $0\nu\beta\beta$ experimentele resultaat. Het is dus interessant om steriele neutrino's zwaarder dan GeV-niveau op de LHC te onderzoeken en het resultaat van $0\nu\beta\beta$te combineren.

We kunnen het idee van steriele neutrino's, en in het bijzonder het νSMEFT-raamwerk, ook generaliseren naar de kosmologie. Zo is N_{eff}, het aantal relativistische soorten, nauwkeurig berekend in het SM. De hoger-dimensionale operatoren in νSMEFT met lichte steriele neutrino's zouden de ontkoppeling van neutrino's beïnvloeden en dus N_{eff} wijzigen. We kunnen ook het effect van steriele neutrino's op big-bang-nucleosynthese en leptogenese onderzoeken. Steriele neutrino's kunnen een kandidaat zijn voor donkere materie en ze kunnen worden gedetecteerd wanneer ze van kernen worden verstrooid. We kunnen het EFT-raamwerk gebruiken om de effectieve botsingsdoorsnede voor steriele neutrino's in directe detectie-experimenten van donkere materie te berekenen. Met het werk in dit proefschrift en in de toekomst zullen we steriele neutrino's beter begrijpen door middel van systematische werken opererend op schalen van de kosmologie tot de fysica in de deeltjesversnellers en precisie-experimenten met lage energie.

Acknowledgements

Here I want to thank the people who helped me in physics and daily life during the past five years in Amherst and Amsterdam.

First of all, I would like to thank Jordy de Vries, who is my PhD supervisor. I still remember our first conversation. It was you who brought me in contact with real physics research. You helped me quite a lot and we often discussed our physics problems. You are always willing to answer my questions, no matter whether they were easy or difficult. I really appreciate that you helped me so much with my post-doc applications. I've always felt happy and respected while working with you during these four years. Time flies! I hope we can still collaborate in the future!

Then I would like to thank Haolin Li. I really enjoyed our discussions. I have asked you so many questions since our first talk. I'm always impressed by your wide knowledge of physics.

I want to say thanks to my collaborators Wouter Dekens, Emanuele Mereghetti, Kaori Fuyuto, Herbi Dreiner, Zeren Wang and Julian Günther. I fondly remember our discussions and zoom meetings.

Yao Wu is the first person I met when I arrived at UMASS 5 years ago. You helped me really really a lot in daily life and social activities. Thank you for helping me with driving and traveling. I will not forget our visits to New York and Boston and our road trips.

I would like to say thanks to the nice and humorous people in my office.

Thanks to the US and the Netherlands, as this PhD work is my first job with actual income. Thanks to China, I had the opportunity to get a good education with nearly zero tuition. This gave me the opportunity to pursue my PhD at the UvA.

I would like to thank my parents for their support during these years, and thank those cute friends for their friendship. Finally I thank Huan for accompanying me during these years. I cannot believe that it has been more than five years since the first time we met.

Bibliography

[1] G. Aad *et al.* [ATLAS Collaboration], Phys. Lett. B **716**, 1 (2012), [arXiv:1207.7214 [hep-ex]].

[2] L. S. Kisslinger and D. Das, Int. J. Mod. Phys. A **34**, 1930013 (2019), [arXiv:1908.00612 [physics.gen-ph]].

[3] P. A. Zyla *et al.* [Particle Data Group], PTEP **2020**, 083C01 (2020).

[4] A. D. Sakharov, Pisma Zh. Eksp. Teor. Fiz. **5**, 32 (1967).

[5] N. S. Manton, Phys. Rev. D **28**, 2019 (1983).

[6] F. R. Klinkhamer and N. S. Manton, Phys. Rev. D **30**, 2212 (1984).

[7] A. I. Bochkarev and M. E. Shaposhnikov, Mod. Phys. Lett. A **2**, 417 (1987).

[8] M. Dine and A. Kusenko, Rev. Mod. Phys. **76**, 1 (2003), [arXiv:hep-ph/0303065].

[9] T. Aaltonen *et al.* [CDF Collaboration], Science **376**, 170 (2022).

[10] B. Abi *et al.* [Muon g-2 Collaboration], Phys. Rev. Lett. **126**, 141801 (2021), [arXiv:2104.03281 [hep-ex]].

[11] J. P. Lees *et al.* [BaBar Collaboration], Phys. Rev. D **88**, 072012 (2013), [arXiv:1303.0571 [hep-ex]].

[12] S. Hirose *et al.* [Belle Collaboration], Phys. Rev. Lett. **118**, 211801 (2017), [arXiv:1612.00529 [hep-ex]].

[13] R. Aaij *et al.* [LHCb Collaboration], Phys. Rev. Lett. **120**, 171802 (2018), [arXiv:1708.08856 [hep-ex]].

[14] P. Minkowski, Phys. Lett. **67B**, 421 (1977).

[15] M. Gell-Mann, P. Ramond, and R. Slansky, Conf. Proc. **C790927**, 315 (1979), [arXiv:1306.4669 [hep-th]].

[16] R. N. Mohapatra and G. Senjanovic, Phys. Rev. **D23**, 165 (1981).

[17] M. Drewes, Int. J. Mod. Phys. E **22**, 1330019 (2013), [arXiv:1303.6912 [hep-ph]].

[18] A. Kusenko, Phys. Rept. **481**, 1 (2009), [arXiv:0906.2968 [hep-ph]].

[19] M. Drewes *et al.*, JCAP **1701**, 025 (2017), [arXiv:1602.04816 [hep-ph]].

[20] A. Boyarsky, M. Drewes, T. Lasserre, S. Mertens, and O. Ruchayskiy, Prog. Part. Nucl. Phys. **104**, 1 (2019), [arXiv:1807.07938 [hep-ph]].

[21] S. Davidson, E. Nardi, and Y. Nir, Phys. Rept. **466**, 105 (2008), [arXiv:0802.2962 [hep-ph]].

[22] R. Mohapatra and J. C. Pati, Phys. Rev. D **11**, 2558 (1975).

[23] J. C. Pati and A. Salam, Phys. Rev. D **10**, 275 (1974), [Erratum: Phys.Rev.D 11, 703–703 (1975)].

[24] M. Bando and K. Yoshioka, Prog. Theor. Phys. **100**, 1239 (1998), [arXiv:hep-ph/9806400].

[25] C.-W. Chiang, G. Cottin, A. Das, and S. Mandal, JHEP **12**, 070 (2019), [arXiv:1908.09838 [hep-ph]].

[26] I. Doršner, S. Fajfer, A. Greljo, J. F. Kamenik, and N. Košnik, Phys. Rept. **641**, 1 (2016), [arXiv:1603.04993 [hep-ph]].

[27] F. del Aguila, S. Bar-Shalom, A. Soni, and J. Wudka, Phys. Lett. **B670**, 399 (2009), [arXiv:0806.0876 [hep-ph]].

[28] Y. Liao and X.-D. Ma, Phys. Rev. D **96**, 015012 (2017), [arXiv:1612.04527 [hep-ph]].

[29] C. Arnaboldi *et al.*, Phys. Lett. **B557**, 167 (2003), [arXiv:hep-ex/0211071].

[30] S. Umehara *et al.*, Phys. Rev. **C78**, 058501 (2008), [arXiv:0810.4746 [nucl-ex]].

[31] A. S. Barabash and V. B. Brudanin [NEMO Collaboration], Phys. Atom. Nucl. **74**, 312 (2011), [arXiv:1002.2862 [nucl-ex]].

[32] A. Gando *et al.* [KamLAND-Zen Collaboration], Phys. Rev. Lett. **110**, 062502 (2013), [arXiv:1211.3863 [hep-ex]].

[33] M. Agostini *et al.* [GERDA Collaboration], Phys. Rev. Lett. **111**, 122503 (2013), [arXiv:1307.4720 [nucl-ex]].

[34] J. B. Albert *et al.* [EXO-200 Collaboration], Nature **510**, 229 (2014), [arXiv:1402.6956 [nucl-ex]].

[35] S. Andringa *et al.* [SNO+ Collaboration], Adv. High Energy Phys. **2016**, 6194250 (2016), [arXiv:1508.05759 [physics.ins-det]].

[36] R. Arnold *et al.* [NEMO-3 Collaboration], Phys. Rev. **D92**, 072011 (2015), [arXiv:1506.05825 [hep-ex]].

[37] R. Arnold *et al.* [NEMO-3 Collaboration], Phys. Rev. **D93**, 112008 (2016), [arXiv:1604.01710 [hep-ex]].

[38] A. Gando *et al.* [KamLAND-Zen Collaboration], Phys. Rev. Lett. **117**, 082503 (2016), [arXiv:1605.02889 [hep-ex]], [Addendum: Phys.Rev.Lett. 117, 109903 (2016)].

[39] S. R. Elliott *et al.*, J. Phys. Conf. Ser. **888**, 012035 (2017), [arXiv:1610.01210 [nucl-ex]].

[40] R. Arnold *et al.* [NEMO-3 Collaboration], Phys. Rev. **D94**, 072003 (2016), [arXiv:1606.08494 [hep-ex]].

[41] R. Arnold *et al.* [NEMO-3 Collaboration], Phys. Rev. **D95**, 012007 (2017), [arXiv:1610.03226 [hep-ex]].

[42] M. Agostini *et al.*, [arXiv:1703.00570 [nucl-ex]], [Nature544,47(2017)].

[43] C. E. Aalseth *et al.* [Majorana Collaboration], Phys. Rev. Lett. **120**, 132502 (2018), [arXiv:1710.11608 [nucl-ex]].

[44] J. B. Albert *et al.* [EXO Collaboration], Phys. Rev. Lett. **120**, 072701 (2018), [arXiv:1707.08707 [hep-ex]].

[45] C. Alduino *et al.* [CUORE Collaboration], Phys. Rev. Lett. **120**, 132501 (2018), [arXiv:1710.07988 [nucl-ex]].

[46] M. Agostini *et al.* [GERDA Collaboration], Phys. Rev. Lett. **120**, 132503 (2018), [arXiv:1803.11100 [nucl-ex]].

[47] O. Azzolini *et al.*, [arXiv:1802.07791 [nucl-ex]].

[48] R. Arnold *et al.*, Eur. Phys. J. **C78**, 821 (2018), [arXiv:1806.05553 [hep-ex]].

[49] D. Q. Adams *et al.* [CUORE Collaboration], [arXiv:1912.10966 [nucl-ex]].

[50] S. I. Alvis *et al.* [Majorana Collaboration], Phys. Rev. **C100**, 025501 (2019), [arXiv:1902.02299 [nucl-ex]].

[51] K. Tetsuno, "Status of 48Ca double beta decay search and its future prospect in CANDLE," TAUP2019, September 9-13, 2019, Toyama, Japan .

[52] M. Agostini *et al.* [GERDA Collaboration], Science **365**, 1445 (2019), [arXiv:1909.02726 [hep-ex]].

[53] O. Azzolini *et al.* [CUPID Collaboration], Phys. Rev. Lett. **123**, 032501 (2019), [arXiv:1906.05001 [nucl-ex]].

[54] V. Alenkov *et al.*, Eur. Phys. J. **C79**, 791 (2019), [arXiv:1903.09483 [hep-ex]].

[55] G. Anton *et al.* [EXO-200 Collaboration], Phys. Rev. Lett. **123**, 161802 (2019), [arXiv:1906.02723 [hep-ex]].

[56] T. Iida *et al.*, Nucl. Part. Phys. Proc. **273-275**, 2633 (2016).

[57] N. Abgrall *et al.* [LEGEND Collaboration], AIP Conf. Proc. **1894**, 020027 (2017), [arXiv:1709.01980 [physics.ins-det]].

[58] C. Patrick and F. Xie, "Status of the SuperNEMO $0\nu\beta\beta$ experiment," in *Proceedings, Prospects in Neutrino Physics (NuPhys2016): London, UK, December 12-14, 2016*. 2017. arXiv:1704.06670 [physics.ins-det].

[59] A. Salvio and F. Sannino, eds., *From the Fermi Scale to Cosmology*. Frontiers, 2019. http://www.desy.de/~schwenn/9782889632053-1.PDF.

[60] [CUORE Collaboration], D. Q. Adams *et al.*, "Update on the recent progress of the CUORE experiment," in *28th International Conference on Neutrino Physics and Astrophysics (Neutrino 2018) Heidelberg, Germany, June 4-9, 2018*. 2018. arXiv:1808.10342 [nucl-ex]. https://doi.org/10.5281/zenodo.1286904.

[61] [SNO+ Collaboration], J. Paton, "Neutrinoless Double Beta Decay in the SNO+ Experiment," in *Prospects in Neutrino Physics (NuPhys2018) London, United Kingdom, December 19-21, 2018*. 2019. arXiv:1904.01418 [hep-ex].

[62] J. B. Albert *et al.* [nEXO Collaboration], Phys. Rev. **C97**, 065503 (2018), [arXiv:1710.05075 [nucl-ex]].

[63] J. J. Gomez-Cadenas, "Status and prospects of the NEXT experiment for neutrinoless double beta decay searches," 2019. arXiv:1906.01743 [hep-ex].

[64] [PandaX-III Collaboration], K. Han, "PandaX-III: Searching for Neutrinoless Double Beta Decay with High Pressure Gaseous Time Projection Chambers," in *15th International Conference on Topics in Astroparticle and Underground Physics (TAUP 2017) Sudbury, Ontario, Canada, July 24-28, 2017*. 2017. arXiv:1710.08908 [physics.ins-det].

[65] W. R. Armstrong *et al.* [CUPID Collaboration], [arXiv:1907.09376 [physics.ins-det]].

[66] L. Si *et al.*, [arXiv:2205.12809 [nucl-ex]].

[67] S. Abe *et al.* [KamLAND-Zen Collaboration], [arXiv:2203.02139 [hep-ex]].

[68] E. Cortina Gil *et al.* [NA62 Collaboration], [arXiv:2202.00331 [hep-ex]].

[69] E. Cortina Gil *et al.* [NA62 Collaboration], Phys. Lett. B **797**, 134794 (2019), [arXiv:1905.07770 [hep-ex]].

[70] R. Appel *et al.*, Phys. Rev. Lett. **85**, 2877 (2000), [arXiv:hep-ex/0006003].

[71] V. Cirigliano, W. Dekens, J. de Vries, M. Graesser, and E. Mereghetti, JHEP **12**, 097 (2018), [arXiv:1806.02780 [hep-ph]].

[72] G. 't Hooft, Phys. Rev. Lett. **37**, 8 (1976).

[73] P. B. Arnold and L. D. McLerran, Phys. Rev. D **36**, 581 (1987).

[74] Y. Kwon and P. Panigrahi, Phys. Rev. D **37**, 1702 (1988).

[75] B. Grzadkowski, M. Iskrzynski, M. Misiak, and J. Rosiek, JHEP **10**, 085 (2010), [arXiv:1008.4884 [hep-ph]].

[76] L. Lehman, Phys. Rev. **D90**, 125023 (2014), [arXiv:1410.4193 [hep-ph]].

[77] Y. Liao and X.-D. Ma, JHEP **11**, 043 (2016), [arXiv:1607.07309 [hep-ph]].

[78] W. Dekens, J. de Vries, K. Fuyuto, E. Mereghetti, and G. Zhou, JHEP **06**, 097 (2020), [arXiv:2002.07182 [hep-ph]].

[79] G. Zhou, [arXiv:2112.00767 [hep-ph]].

[80] J. Schechter and J. W. F. Valle, Phys. Rev. **D22**, 2227 (1980).

[81] A. Kobach, Phys. Lett. **B758**, 455 (2016), [arXiv:1604.05726 [hep-ph]].

[82] V. Cirigliano, W. Dekens, J. de Vries, M. L. Graesser, and E. Mereghetti, JHEP **12**, 082 (2017), [arXiv:1708.09390 [hep-ph]].

[83] M. L. Graesser, JHEP **08**, 099 (2017), [arXiv:1606.04549 [hep-ph]].

[84] G. Prézeau, M. Ramsey-Musolf, and P. Vogel, Phys. Rev. **D68**, 034016 (2003), [arXiv:hep-ph/0303205].

[85] Y. Liao, X.-D. Ma, and H.-L. Wang, JHEP **01**, 127 (2020), [arXiv:1909.06272 [hep-ph]].

[86] S. Weinberg, Physica **A96**, 327 (1979).

[87] J. Gasser and H. Leutwyler, Annals Phys. **158**, 142 (1984).

[88] E. E. Jenkins and A. V. Manohar, Phys. Lett. **B255**, 558 (1991).

[89] V. Bernard, N. Kaiser, and U.-G. Meißner, Int. J. Mod. Phys. **E4**, 193 (1995), [arXiv:hep-ph/9501384].

[90] A. Manohar and H. Georgi, Nucl. Phys. **B234**, 189 (1984).

[91] H. W. Hammer, S. König, and U. van Kolck, [arXiv:1906.12122 [nucl-th]].

[92] M. Pavon Valderrama and D. R. Phillips, Phys. Rev. Lett. **114**, 082502 (2015), [arXiv:1407.0437 [nucl-th]].

[93] V. Cirigliano, W. Dekens, J. De Vries, M. L. Graesser, E. Mereghetti, S. Pastore, and U. Van Kolck, Phys. Rev. Lett. **120**, 202001 (2018), [arXiv:1802.10097 [hep-ph]].

[94] V. Cirigliano, W. Dekens, J. De Vries, M. L. Graesser, E. Mereghetti, S. Pastore, M. Piarulli, U. Van Kolck, and R. B. Wiringa, Phys. Rev. **C100**, 055504 (2019), [arXiv:1907.11254 [nucl-th]].

[95] V. Cirigliano, W. Dekens, E. Mereghetti, and A. Walker-Loud, Phys. Rev. **C97**, 065501 (2018), [arXiv:1710.01729 [hep-ph]], [Erratum: Phys. Rev.C100,no.1,019903(2019)].

[96] Y. F. Li and S.-s. Liu, Phys. Lett. **B706**, 406 (2012), [arXiv:1110.5795 [hep-ph]].

[97] A. de Gouvea and W.-C. Huang, Phys. Rev. **D85**, 053006 (2012), [arXiv:1110.6122 [hep-ph]].

[98] J. Gasser and H. Leutwyler, Nucl. Phys. **B250**, 465 (1985).

[99] M. González-Alonso and J. Martin Camalich, Phys. Rev. Lett. **112**, 042501 (2014), [arXiv:1309.4434 [hep-ph]].

[100] A. Nicholson *et al.*, [arXiv:1805.02634 [nucl-th]].

[101] T. Bhattacharya, V. Cirigliano, S. Cohen, R. Gupta, H.-W. Lin, and B. Yoon, Phys. Rev. **D94**, 054508 (2016), [arXiv:1606.07049 [hep-lat]].

[102] R. Gupta, Y.-C. Jang, B. Yoon, H.-W. Lin, V. Cirigliano, and T. Bhattacharya, Phys. Rev. **D98**, 034503 (2018), [arXiv:1806.09006 [hep-lat]].

[103] S. Aoki *et al.* [Flavour Lattice Averaging Group Collaboration], [arXiv:1902.08191 [hep-lat]].

[104] H. Monge-Camacho *et al.*, PoS **LATTICE2018**, 263 (2019), [arXiv:1904.12055 [hep-lat]].

[105] C. Patrignani *et al.* [Particle Data Group], Chin. Phys. **C40**, 100001 (2016).

[106] V. Cirigliano, W. Dekens, J. de Vries, M. Hoferichter, and E. Mereghetti, JHEP **05**, 289 (2021), [arXiv:2102.03371 [nucl-th]].

[107] V. Cirigliano, W. Dekens, J. de Vries, M. Hoferichter, and E. Mereghetti, Phys. Rev. Lett. **126**, 172002 (2021), [arXiv:2012.11602 [nucl-th]].

[108] R. Wirth, J. M. Yao, and H. Hergert, Phys. Rev. Lett. **127**, 242502 (2021), [arXiv:2105.05415 [nucl-th]].

[109] R. Mertig, M. Bohm, and A. Denner, Comput. Phys. Commun. **64**, 345 (1991).

[110] V. Shtabovenko, R. Mertig, and F. Orellana, Comput. Phys. Commun. **207**, 432 (2016), [arXiv:1601.01167 [hep-ph]].

[111] M. Horoi and A. Neacsu, [arXiv:1706.05391 [hep-ph]].

[112] S. Stoica and M. Mirea, Phys. Rev. **C88**, 037303 (2013), [arXiv:1307.0290 [nucl-th]].

[113] J. Kotila and F. Iachello, Phys. Rev. **C85**, 034316 (2012), [arXiv:1209.5722 [nucl-th]].

[114] D. Stefanik, R. Dvornicky, F. Simkovic, and P. Vogel, Phys. Rev. **C92**, 055502 (2015), [arXiv:1506.07145 [hep-ph]].

[115] J. Hyvärinen and J. Suhonen, Phys. Rev. **C91**, 024613 (2015).

[116] J. Menéndez, J. Phys. **G45**, 014003 (2018).

[117] J. Barea, J. Kotila, and F. Iachello, Phys. Rev. **C91**, 034304 (2015), [arXiv:1506.08530 [nucl-th]].

[118] J. Barea, private communication .

[119] M. Blennow, E. Fernandez-Martinez, J. Lopez-Pavon, and J. Menendez, JHEP **07**, 096 (2010), [arXiv:1005.3240 [hep-ph]].

[120] J. Barea, J. Kotila, and F. Iachello, Phys. Rev. **D92**, 093001 (2015), [arXiv:1509.01925 [hep-ph]].

[121] V. Cirigliano, Z. Davoudi, T. Bhattacharya, T. Izubuchi, P. E. Shanahan, S. Syritsyn, and M. L. Wagman [USQCD Collaboration], Eur. Phys. J. **A55**, 197 (2019), [arXiv:1904.09704 [hep-lat]].

[122] C. Drischler, W. Haxton, K. McElvain, E. Mereghetti, A. Nicholson, P. Vranas, and A. Walker-Loud, "Towards grounding nuclear physics in QCD," 2019. arXiv:1910.07961 [nucl-th].

[123] X. Feng, L.-C. Jin, X.-Y. Tuo, and S.-C. Xia, Phys. Rev. Lett. **122**, 022001 (2019), [arXiv:1809.10511 [hep-lat]].

[124] X.-Y. Tuo, X. Feng, and L.-C. Jin, Phys. Rev. **D100**, 094511 (2019), [arXiv:1909.13525 [hep-lat]].

[125] W. Detmold and D. Murphy, PoS **LATTICE2018**, 262 (2019), [arXiv:1811.05554 [hep-lat]].

[126] J. Barry, W. Rodejohann, and H. Zhang, JHEP **07**, 091 (2011), [arXiv:1105.3911 [hep-ph]].

[127] K. N. Abazajian *et al.*, [arXiv:1204.5379 [hep-ph]].

[128] J. C. Helo, M. Hirsch, and Z. S. Wang, JHEP **07**, 056 (2018), [arXiv:1803.02212 [hep-ph]].

[129] M. Chrzaszcz, M. Drewes, T. E. Gonzalo, J. Harz, S. Krishnamurthy, and C. Weniger, [arXiv:1908.02302 [hep-ph]].

[130] P. D. Bolton, F. F. Deppisch, and P. S. B. Dev, [arXiv:1912.03058 [hep-ph]].

[131] D. A. Bryman and R. Shrock, Phys. Rev. **D100**, 073011 (2019), [arXiv:1909.11198 [hep-ph]].

[132] M. Tanabashi *et al.* [Particle Data Group], Phys. Rev. D **98**, 030001 (2018).

[133] C. Giunti and T. Lasserre, Ann. Rev. Nucl. Part. Sci. **69**, 163 (2019), [arXiv:1901.08330 [hep-ph]].

[134] A. Donini, P. Hernandez, J. Lopez-Pavon, M. Maltoni, and T. Schwetz, JHEP **07**, 161 (2012), [arXiv:1205.5230 [hep-ph]].

[135] U. Mahanta, Phys. Rev. D **62**, 073009 (2000), [arXiv:hep-ph/9909518].

[136] D. Aristizabal Sierra, M. Hirsch, and S. Kovalenko, Phys. Rev. D **77**, 055011 (2008), [arXiv:0710.5699 [hep-ph]].

[137] K. Babu, P. B. Dev, S. Jana, and A. Thapa, JHEP **03**, 006 (2020), [arXiv:1907.09498 [hep-ph]].

[138] A. Aguilar-Arevalo *et al.* [LSND Collaboration], Phys. Rev. **D64**, 112007 (2001), [arXiv:hep-ex/0104049].

[139] A. A. Aguilar-Arevalo *et al.* [MiniBooNE Collaboration], Phys. Rev. Lett. **102**, 101802 (2009), [arXiv:0812.2243 [hep-ex]].

[140] A. A. Aguilar-Arevalo *et al.* [MiniBooNE Collaboration], Phys. Rev. Lett. **110**, 161801 (2013), [arXiv:1303.2588 [hep-ex]].

[141] A. A. Aguilar-Arevalo *et al.* [MiniBooNE Collaboration], Phys. Rev. Lett. **121**, 221801 (2018), [arXiv:1805.12028 [hep-ex]].

[142] M. Dentler, Á. Hernández-Cabezudo, J. Kopp, P. A. N. Machado, M. Maltoni, I. Martinez-Soler, and T. Schwetz, JHEP **08**, 010 (2018), [arXiv:1803.10661 [hep-ph]].

[143] K. Abazajian, G. M. Fuller, and M. Patel, Phys. Rev. **D64**, 023501 (2001), [arXiv:astro-ph/0101524].

[144] L. Canetti, M. Drewes, and M. Shaposhnikov, Phys. Rev. Lett. **110**, 061801 (2013), [arXiv:1204.3902 [hep-ph]].

[145] A. M. Sirunyan *et al.* [CMS Collaboration], Phys. Rev. **D99**, 052002 (2019), [arXiv:1811.01197 [hep-ex]].

[146] M. Aaboud *et al.* [ATLAS Collaboration], Eur. Phys. J. **C79**, 733 (2019), [arXiv:1902.00377 [hep-ex]].

[147] M. Aaboud *et al.* [ATLAS Collaboration], JHEP **01**, 016 (2019), [arXiv:1809.11105 [hep-ex]].

[148] M. Shaposhnikov, Nucl. Phys. **B763**, 49 (2007), [arXiv:hep-ph/0605047].

[149] M. Mitra, G. Senjanovic, and F. Vissani, Nucl. Phys. **B856**, 26 (2012), [arXiv:1108.0004 [hep-ph]].

[150] C. Giunti and E. M. Zavanin, JHEP **07**, 171 (2015), [arXiv:1505.00978 [hep-ph]].

[151] V. Cirigliano, M. González-Alonso, and M. L. Graesser, JHEP **02**, 046 (2013), [arXiv:1210.4553 [hep-ph]].

[152] Y. Liao, X.-D. Ma, and H.-L. Wang, JHEP **03**, 120 (2020), [arXiv:2001.07378 [hep-ph]].

[153] I. Bischer and W. Rodejohann, Nucl. Phys. B **947**, 114746 (2019), [arXiv:1905.08699 [hep-ph]].

[154] P. D. Bolton, F. F. Deppisch, L. Gráf, and F. Šimkovic, Phys. Rev. D **103**, 055019 (2021), [arXiv:2011.13387 [hep-ph]].

[155] T. Li, X.-D. Ma, and M. A. Schmidt, JHEP **10**, 115 (2020), [arXiv:2007.15408 [hep-ph]].

[156] B. Dasgupta and J. Kopp, Phys. Rept. **928**, 63 (2021), [arXiv:2106.05913 [hep-ph]].

[157] W. Dekens, J. de Vries, and T. Tong, JHEP **08**, 128 (2021), [arXiv:2104.00140 [hep-ph]].

[158] V. Cirigliano, W. Dekens, J. de Vries, K. Fuyuto, E. Mereghetti, and R. Ruiz, JHEP **08**, 103 (2021), [arXiv:2105.11462 [hep-ph]].

[159] Y. Liao, X.-D. Ma, and H.-L. Wang, Chin. Phys. C **45**, 073102 (2021), [arXiv:2102.03491 [hep-ph]].

[160] C. Dib, V. Gribanov, S. Kovalenko, and I. Schmidt, Phys. Lett. B **493**, 82 (2000), [arXiv:hep-ph/0006277].

[161] G. Cvetic, C. Dib, S. K. Kang, and C. S. Kim, Phys. Rev. D **82**, 053010 (2010), [arXiv:1005.4282 [hep-ph]].

[162] A. Atre, T. Han, S. Pascoli, and B. Zhang, JHEP **05**, 030 (2009), [arXiv:0901.3589 [hep-ph]].

[163] J. C. Helo, S. Kovalenko, and I. Schmidt, Nucl. Phys. B **853**, 80 (2011), [arXiv:1005.1607 [hep-ph]].

[164] V. Gribanov, S. Kovalenko, and I. Schmidt, Nucl. Phys. B **607**, 355 (2001), [arXiv:hep-ph/0102155].

[165] J. Mejia-Guisao, D. Milanés, N. Quintero, and J. D. Ruiz-Alvarez, Phys. Rev. D **97**, 075018 (2018), [arXiv:1708.01516 [hep-ph]].

[166] G. Cvetic and C. S. Kim, Phys. Rev. D **96**, 035025 (2017), [arXiv:1705.09403 [hep-ph]], [Erratum: Phys.Rev.D 102, 019903 (2020), Erratum: Phys.Rev.D 102, 039902 (2020)].

[167] D. Milanes, N. Quintero, and C. E. Vera, Phys. Rev. D **93**, 094026 (2016), [arXiv:1604.03177 [hep-ph]].

[168] R. M. Godbole, S. P. Maharathy, S. Mandal, M. Mitra, and N. Sinha, Phys. Rev. D **104**, 095009 (2021), [arXiv:2008.05467 [hep-ph]].

[169] V. Cirigliano, W. Dekens, M. Graesser, and E. Mereghetti, Phys. Lett. **B769**, 460 (2017), [arXiv:1701.01443 [hep-ph]].

[170] M. J. Savage, Phys. Rev. **C59**, 2293 (1999), [arXiv:nucl-th/9811087].

[171] N. Carrasco, P. Dimopoulos, R. Frezzotti, V. Lubicz, G. C. Rossi, S. Simula, and C. Tarantino [ETM Collaboration], Phys. Rev. **D92**, 034516 (2015), [arXiv:1505.06639 [hep-lat]].

[172] V. Bertone *et al.* [ETM Collaboration], JHEP **03**, 089 (2013), [arXiv:1207.1287 [hep-lat]], [Erratum: JHEP 07, 143 (2013)].

[173] B. J. Choi *et al.* [SWME Collaboration], Phys. Rev. D **93**, 014511 (2016), [arXiv:1509.00592 [hep-lat]].

[174] P. A. Boyle, N. Garron, and R. J. Hudspith [RBC, UKQCD Collaboration], Phys. Rev. **D86**, 054028 (2012), [arXiv:1206.5737 [hep-lat]].

[175] N. Garron, R. J. Hudspith, and A. T. Lytle [RBC/UKQCD Collaboration], JHEP **11**, 001 (2016), [arXiv:1609.03334 [hep-lat]].

[176] T. Blum *et al.*, Phys. Rev. D **91**, 074502 (2015), [arXiv:1502.00263 [hep-lat]].

[177] T. Blum *et al.*, Phys. Rev. D **86**, 074513 (2012), [arXiv:1206.5142 [hep-lat]].

[178] J. M. Butterworth, M. Chala, C. Englert, M. Spannowsky, and A. Titov, Phys. Rev. D **100**, 115019 (2019), [arXiv:1909.04665 [hep-ph]].

[179] B. C. Canas, O. G. Miranda, A. Parada, M. Tortola, and J. W. F. Valle, Phys. Lett. B **753**, 191 (2016), [arXiv:1510.01684 [hep-ph]], [Addendum: Phys.Lett.B 757, 568–568 (2016)].

[180] G. Zhou, J. Y. Günther, Z. S. Wang, J. de Vries, and H. K. Dreiner, [arXiv:2111.04403 [hep-ph]].

[181] J. De Vries, H. K. Dreiner, J. Y. Günther, Z. S. Wang, and G. Zhou, JHEP **03**, 148 (2021), [arXiv:2010.07305 [hep-ph]].

[182] G. Cvetic and C. S. Kim, Phys. Rev. D **94**, 053001 (2016), [arXiv:1606.04140 [hep-ph]], [Erratum: Phys.Rev.D 95, 039901 (2017)].

[183] E. J. Chun, A. Das, S. Mandal, M. Mitra, and N. Sinha, Phys. Rev. D **100**, 095022 (2019), [arXiv:1908.09562 [hep-ph]].

[184] T. Asaka and H. Ishida, Phys. Lett. B **763**, 393 (2016), [arXiv:1609.06113 [hep-ph]].

[185] G. Zhang and B.-Q. Ma, Phys. Rev. D **103**, 033004 (2021), [arXiv:2101.05566 [hep-ph]].

[186] C. Dib and C. S. Kim, Phys. Rev. D **89**, 077301 (2014), [arXiv:1403.1985 [hep-ph]].

[187] G. J. Feldman and R. D. Cousins, Phys. Rev. D **57**, 3873 (1998), [arXiv:physics/9711021].

[188] R. Shrock, Phys. Lett. B **96**, 159 (1980).

[189] R. E. Shrock, Phys. Rev. D **24**, 1232 (1981).

[190] J. Alwall, R. Frederix, S. Frixione, V. Hirschi, F. Maltoni, O. Mattelaer, H. S. Shao, T. Stelzer, P. Torrielli, and M. Zaro, JHEP **07**, 079 (2014), [arXiv:1405.0301 [hep-ph]].

[191] G. Aad *et al.* [ATLAS Collaboration], JINST **3**, S08003 (2008).

[192] S. Chatrchyan *et al.* [CMS Collaboration], JINST **3**, S08004 (2008).

[193] V. V. Gligorov, S. Knapen, M. Papucci, and D. J. Robinson, Phys. Rev. D **97**, 015023 (2018), [arXiv:1708.09395 [hep-ph]].

[194] J. L. Feng, I. Galon, F. Kling, and S. Trojanowski, Phys. Rev. D **97**, 035001 (2018), [arXiv:1708.09389 [hep-ph]].

[195] A. Ariga *et al.* [FASER Collaboration], Phys. Rev. D **99**, 095011 (2019), [arXiv:1811.12522 [hep-ph]].

[196] J. P. Chou, D. Curtin, and H. Lubatti, Phys. Lett. B **767**, 29 (2017), [arXiv:1606.06298 [hep-ph]].

[197] D. Curtin *et al.*, Rept. Prog. Phys. **82**, 116201 (2019), [arXiv:1806.07396 [hep-ph]].

[198] C. Alpigiani *et al.* [MATHUSLA Collaboration], [arXiv:2009.01693 [physics.ins-det]].

[199] V. V. Gligorov, S. Knapen, B. Nachman, M. Papucci, and D. J. Robinson, Phys. Rev. D **99**, 015023 (2019), [arXiv:1810.03636 [hep-ph]].

[200] M. Bauer, O. Brandt, L. Lee, and C. Ohm, [arXiv:1909.13022 [physics.ins-det]].

[201] J. L. Pinfold, Universe **5**, 47 (2019).

[202] J. L. Pinfold, Phil. Trans. Roy. Soc. Lond. A **377**, 20190382 (2019).

[203] M. Calviani, M. Battistin, R. Betemps, J.-L. Grenard, D. Horvath, A. Perillo Marcone, A. J. Rakai, R. Rinaldesi, S. Sgobba, C. C. Strabel, V. Venturi, H. Vincke, A. P. Perez, and A. Pacholek [SHiP collaboration Collaboration].

[204] M. Anelli *et al.* [SHiP Collaboration], [arXiv:1504.04956 [physics.ins-det]].

[205] C. Ahdida *et al.* [SHiP Collaboration], JINST **14**, P03025 (2019), [arXiv:1810.06880 [physics.ins-det]].

[206] J. Ghiglieri and M. Laine, JHEP **05**, 132 (2017), [arXiv:1703.06087 [hep-ph]].

[207] P. Hernández, M. Kekic, J. López-Pavón, J. Racker, and J. Salvado, JHEP **08**, 157 (2016), [arXiv:1606.06719 [hep-ph]].

[208] E. K. Akhmedov, V. A. Rubakov, and A. Yu. Smirnov, Phys. Rev. Lett. **81**, 1359 (1998), [arXiv:hep-ph/9803255].

[209] T. Asaka, S. Blanchet, and M. Shaposhnikov, Phys. Lett. **B631**, 151 (2005), [arXiv:hep-ph/0503065].

[210] T. Asaka and M. Shaposhnikov, Phys. Lett. **B620**, 17 (2005), [arXiv:hep-ph/0505013].

[211] M. Hirsch and Z. S. Wang, Phys. Rev. D **101**, 055034 (2020), [arXiv:2001.04750 [hep-ph]].

[212] K. Bondarenko, A. Boyarsky, D. Gorbunov, and O. Ruchayskiy, JHEP **11**, 032 (2018), [arXiv:1805.08567 [hep-ph]].

[213] P. Coloma, E. Fernández-Martínez, M. González-López, J. Hernández-García, and Z. Pavlovic, [arXiv:2007.03701 [hep-ph]].

[214] L. M. Johnson, D. W. McKay, and T. Bolton, Phys. Rev. D **56**, 2970 (1997), [arXiv:hep-ph/9703333].

[215] D. Gorbunov and M. Shaposhnikov, JHEP **10**, 015 (2007), [arXiv:0705.1729 [hep-ph]], [Erratum: JHEP 11, 101 (2013)].

[216] K. Aamodt *et al.* [ALICE Collaboration], JINST **3**, S08002 (2008).

[217] B. B. Abelev *et al.* [ALICE Collaboration], Int. J. Mod. Phys. A **29**, 1430044 (2014), [arXiv:1402.4476 [nucl-ex]].

[218] J. Alves, A.Augusto *et al.* [LHCb Collaboration], JINST **3**, S08005 (2008).

[219] R. Aaij *et al.* [LHCb Collaboration], Int. J. Mod. Phys. A **30**, 1530022 (2015), [arXiv:1412.6352 [hep-ex]].

[220] T. Sjostrand, S. Mrenna, and P. Z. Skands, JHEP **05**, 026 (2006), [arXiv:hep-ph/0603175].

[221] T. Sjostrand, S. Mrenna, and P. Z. Skands, Comput. Phys. Commun. **178**, 852 (2008), [arXiv:0710.3820 [hep-ph]].

[222] M. Cacciari, M. Greco, and P. Nason, JHEP **05**, 007 (1998), [arXiv:hep-ph/9803400].

[223] M. Cacciari, S. Frixione, and P. Nason, JHEP **03**, 006 (2001), [arXiv:hep-ph/0102134].

[224] M. Cacciari, S. Frixione, N. Houdeau, M. L. Mangano, P. Nason, and G. Ridolfi, JHEP **10**, 137 (2012), [arXiv:1205.6344 [hep-ph]].

[225] M. Cacciari, M. L. Mangano, and P. Nason, Eur. Phys. J. C **75**, 610 (2015), [arXiv:1507.06197 [hep-ph]].

[226] G. Aielli *et al.*, [arXiv:1911.00481 [hep-ex]].

[227] S. Alekhin *et al.*, Rept. Prog. Phys. **79**, 124201 (2016), [arXiv:1504.04855 [hep-ph]].

[228] H. Dreiner, G. Polesello, and M. Thormeier, [arXiv:hep-ph/0207160].

[229] A. Dedes, H. K. Dreiner, and P. Richardson, Phys. Rev. D **65**, 015001 (2001), [arXiv:hep-ph/0106199].

[230] J. de Vries, H. K. Dreiner, and D. Schmeier, Phys. Rev. **D94**, 035006 (2016), [arXiv:1511.07436 [hep-ph]].

[231] D. Dercks, J. De Vries, H. K. Dreiner, and Z. S. Wang, Phys. Rev. D **99**, 055039 (2019), [arXiv:1810.03617 [hep-ph]].

[232] D. Dercks, H. K. Dreiner, M. Hirsch, and Z. S. Wang, Phys. Rev. D **99**, 055020 (2019), [arXiv:1811.01995 [hep-ph]].

[233] J. Alimena *et al.*, [arXiv:1903.04497 [hep-ex]].

[234] H. K. Dreiner, J. Y. Günther, and Z. S. Wang, [arXiv:2008.07539 [hep-ph]].

[235] G. Aad *et al.* [ATLAS Collaboration], Eur. Phys. J. C **80**, 450 (2020), [arXiv:1909.01246 [hep-ex]].

[236] A. Falkowski, J. T. Ruderman, T. Volansky, and J. Zupan, JHEP **05**, 077 (2010), [arXiv:1002.2952 [hep-ph]].

[237] G. Aad *et al.* [ATLAS Collaboration], Phys. Rev. D **101**, 052013 (2020), [arXiv:1911.12575 [hep-ex]].

[238] M. Aaboud *et al.* [ATLAS Collaboration], Eur. Phys. J. C **79**, 481 (2019), [arXiv:1902.03094 [hep-ex]].

[239] F. Bergsma *et al.* [CHARM Collaboration], Phys. Lett. **166B**, 473 (1986).

[240] G. Bernardi *et al.*, Phys. Lett. **B203**, 332 (1988).

[241] S. A. Baranov *et al.*, Phys. Lett. **B302**, 336 (1993).

[242] P. Abreu *et al.* [DELPHI Collaboration], Z. Phys. **C74**, 57 (1997), [Erratum: Z. Phys.C75,580(1997)].

[243] N. Sabti, A. Magalich, and A. Filimonova, JCAP **11**, 056 (2020), [arXiv:2006.07387 [hep-ph]].

[244] A. Boyarsky, M. Ovchynnikov, O. Ruchayskiy, and V. Syvolap, Phys. Rev. D **104**, 023517 (2021), [arXiv:2008.00749 [hep-ph]].

[245] L. Canetti and M. Shaposhnikov, JCAP **09**, 001 (2010), [arXiv:1006.0133 [hep-ph]].

[246] N. Aghanim *et al.* [Planck Collaboration], Astron. Astrophys. **641**, A6 (2020), [arXiv:1807.06209 [astro-ph.CO]].

[247] C. Ahdida *et al.* [SHiP Collaboration], JHEP **04**, 077 (2019), [arXiv:1811.00930 [hep-ph]].

[248] G. Aad *et al.* [ATLAS Collaboration], [arXiv:2008.07949 [hep-ex]].

[249] G. Aad *et al.* [ATLAS Collaboration], JHEP **10**, 265 (2019), [arXiv:1905.09787 [hep-ex]].

[250] J. Heeck and W. Rodejohann, Phys. Lett. B **776**, 385 (2018), [arXiv:1710.02062 [hep-ph]].

[251] F. Tenchini, M. Garcia-Hernandez, T. Kraetzschmar, P. K. Rados, E. De La Cruz-Burelo, A. De Yta-Hernandez, I. Heredia de la Cruz, and A. Rostomyan, PoS **ICHEP2020**, 288 (2021).

[252] K. Cheung, A. Soffer, Z. S. Wang, and Y.-H. Wu, [arXiv:2108.11094 [hep-ph]].

[253] J. T. Daub, H. K. Dreiner, C. Hanhart, B. Kubis, and U. G. Meissner, JHEP **01**, 179 (2013), [arXiv:1212.4408 [hep-ph]].

[254] H. K. Dreiner, K. Nickel, F. Staub, and A. Vicente, Phys. Rev. D **86**, 015003 (2012), [arXiv:1204.5925 [hep-ph]].

[255] C. S. Kim, Y. Kwon, D. Lee, S. Oh, and D. Sahoo, Eur. Phys. J. C **80**, 730 (2020), [arXiv:1908.00376 [hep-ph]].

[256] C. O. Dib, J. C. Helo, M. Nayak, N. A. Neill, A. Soffer, and J. Zamora-Saa, Phys. Rev. D **101**, 093003 (2020), [arXiv:1908.09719 [hep-ph]].

[257] M. Duerr, T. Ferber, C. Hearty, F. Kahlhoefer, K. Schmidt-Hoberg, and P. Tunney, JHEP **02**, 039 (2020), [arXiv:1911.03176 [hep-ph]].

[258] S. Dey, C. O. Dib, J. Carlos Helo, M. Nayak, N. A. Neill, A. Soffer, and Z. S. Wang, JHEP **02**, 211 (2021), [arXiv:2012.00438 [hep-ph]].

[259] M. Duerr, T. Ferber, C. Garcia-Cely, C. Hearty, and K. Schmidt-Hoberg, JHEP **04**, 146 (2021), [arXiv:2012.08595 [hep-ph]].

[260] A. Filimonova, R. Schäfer, and S. Westhoff, Phys. Rev. D **101**, 095006 (2020), [arXiv:1911.03490 [hep-ph]].

[261] X. Chen, Z. Hu, Y. Wu, and K. Yi, Phys. Lett. B **814**, 136076 (2021), [arXiv:2001.04382 [hep-ph]].

[262] E. Bertholet, S. Chakraborty, V. Loladze, T. Okui, A. Soffer, and K. Tobioka, [arXiv:2108.10331 [hep-ph]].

[263] D. W. Kang, P. Ko, and C.-T. Lu, JHEP **04**, 269 (2021), [arXiv:2101.02503 [hep-ph]].

[264] M. Acevedo, A. Blackburn, N. Blinov, B. Shuve, and M. Stone, [arXiv:2105.12744 [hep-ph]].

[265] S. Dreyer *et al.*, [arXiv:2105.12962 [hep-ph]].

[266] J. De Vries, H. K. Dreiner, J. Y. Günther, Z. S. Wang, and G. Zhou, JHEP **03**, 148 (2021), [arXiv:2010.07305 [hep-ph]].

[267] T. Allmendinger *et al.*, Nucl. Instrum. Meth. A **704**, 44 (2013), [arXiv:1207.2849 [hep-ex]].

[268] B. Aubert *et al.* [BaBar Collaboration], Nucl. Instrum. Meth. A **729**, 615 (2013), [arXiv:1305.3560 [physics.ins-det]].

[269] P. Abreu *et al.* [DELPHI Collaboration], Z. Phys. C **74**, 57 (1997), [Erratum: Z.Phys.C 75, 580 (1997)].

[270] F. Bergsma *et al.* [CHARM Collaboration], Phys. Lett. B **166**, 473 (1986).

[271] J. Orloff, A. N. Rozanov, and C. Santoni, Phys. Lett. B **550**, 8 (2002), [arXiv:hep-ph/0208075].

[272] I. Boiarska, A. Boyarsky, O. Mikulenko, and M. Ovchynnikov, [arXiv:2107.14685 [hep-ph]].

[273] F. Bergsma *et al.* [CHARM Collaboration], Phys. Lett. B **128**, 361 (1983).

[274] G. Li, M. Ramsey-Musolf, and J. C. Vasquez, Phys. Rev. Lett. **126**, 151801 (2021), [arXiv:2009.01257 [hep-ph]].

[275] M. Drewes, Y. Georis, and J. Klarić, Phys. Rev. Lett. **128**, 051801 (2022), [arXiv:2106.16226 [hep-ph]].

[276] G. Li, M. J. Ramsey-Musolf, S. Su, and J. C. Vasquez, [arXiv:2109.08172 [hep-ph]].

[277] P. D. Bolton, F. F. Deppisch, and P. S. B. Dev, JHEP **03**, 152 (2022), [arXiv:2112.12658 [hep-ph]].

[278] G. Li, M. J. Ramsey-Musolf, and J. C. Vasquez, [arXiv:2202.01789 [hep-ph]].

[279] X.-W. Gu, C.-G. Duan, and Z.-H. Guo, Phys. Rev. D **98**, 034007 (2018), [arXiv:1803.07284 [hep-ph]].

[280] Y.-H. Chen, Z.-H. Guo, and B.-S. Zou, Phys. Rev. D **91**, 014010 (2015), [arXiv:1411.1159 [hep-ph]].

[281] J. L. Rosner, S. Stone, and R. S. Van de Water, [arXiv:1509.02220 [hep-ph]].

[282] N. Dhiman and H. Dahiya, Eur. Phys. J. Plus **133**, 134 (2018), [arXiv:1708.07274 [hep-ph]].

[283] H. K. Dreiner, M. Kramer, and B. O'Leary, Phys. Rev. **D75**, 114016 (2007), [arXiv:hep-ph/0612278].

[284] B. Colquhoun, C. Davies, R. Dowdall, J. Kettle, J. Koponen, G. Lepage, and A. Lytle [HPQCD Collaboration], Phys. Rev. D **91**, 114509 (2015), [arXiv:1503.05762 [hep-lat]].

[285] D. Ebert, R. Faustov, and V. Galkin, Phys. Lett. B **635**, 93 (2006), [arXiv:hep-ph/0602110].

[286] R. Escribano, S. Gonzàlez-Solís, P. Masjuan, and P. Sanchez-Puertas, Phys. Rev. D **94**, 054033 (2016), [arXiv:1512.07520 [hep-ph]].

[287] K. Edwards *et al.* [CLEO Collaboration], Phys. Rev. Lett. **86**, 30 (2001), [arXiv:hep-ex/0007012].

[288] D. Bečirević, G. Duplančić, B. Klajn, B. Melić, and F. Sanfilippo, Nucl. Phys. B **883**, 306 (2014), [arXiv:1312.2858 [hep-ph]].